Etude et optimisation des capteurs solaires photovoltaïques thermiques hybrides et de leur intégration dans des systèmes énergétiques de petite taille destinés aux prosommateurs

Ioana-Mădălina Barbu

Thèse présentée pour obtenir le grade de

Docteur de l'université de Strasbourg

École doctorale MSII

Laboratoire ICUBE – Département Mécanique (D-M)

Discipline / Spécialité: ÉNERGETIQUE

Etude et optimisation des capteurs solaires photovoltaïques thermiques hybrides et de leur intégration dans des systèmes énergétiques de petite taille destinés aux prosommateurs

---

Par: **Ioana-Mădălina BARBU**

THÈSE dirigée par:

Monica SIROUX	Professeur, Laboratoire ICUBE, INSA de Strasbourg
George DARIE	Professeur, Université POLITECHNICA Bucharest

RAPPORTEURS:

Patrick SALAGNAC	Professeur, Université de la Rochelle
Rodica FRUNZULICĂ	Professeur, Université Technique de Construction Bucarest

EXAMINATEURS:

Horia NECULA	Professeur, Université POLITECHNICA Bucharest
George DARIE	Directeur de thèse, Professeur, Université POLITECHNICA Bucharest
Monica SIROUX	Directeur de thèse, Laboratoire ICUBE, INSA de Strasbourg

Date de soutenance : **23 septembre 2021**

Declaration of Authorship

I, Ioana-Madalina MANOLE (BARBU), declare that this thesis titled, “Etude et optimisation des capteurs solaires photovoltaïques thermiques hybrides et de leur intégration dans des systèmes énergétiques de petite taille destinés aux prosommateurs” and the work presented in it are my own. I hereby certify that, to the best of my knowledge, the content of this thesis is original and the result of my own work. All of the assistance I received and the sources I used have been properly acknowledged.

Résumé

Dans le contexte énergétique actuel, le développement des technologies d'énergies renouvelables est crucial. À long terme, les énergies renouvelables commenceront à dominer le mix énergétique mondial au détriment des combustibles fossiles. En raison de leur intermittence, les sources d'énergies renouvelables devront être combinées pour répondre à l'éventail complet de la demande énergétique. L'énergie solaire est une source abondante, facilement disponible presque partout dans le monde, et elle a donc un grand potentiel pour prendre en charge une grande partie du mix d'énergies renouvelables à l'avenir, combinée à d'autres énergies renouvelables telles que l'éolien et la biomasse. En théorie, il y a suffisamment de rayonnement solaire dans le monde pour satisfaire 10 000 fois la consommation énergétique mondiale.

L'énergie solaire fait partie des sources d'énergie les plus abondantes et les plus prometteuses, avec un fort potentiel pour le développement durable. Les deux technologies classiques de conversion de l'énergie solaire en énergie utile sont les capteurs photovoltaïques et les capteurs solaires thermiques. Pour améliorer la compétitivité du marché et augmenter le taux de conversion de l'énergie solaire en énergie utile, des panneaux de cogénération photovoltaïque-thermique (PVT) ont été développés (Figure 1). Il s'agit d'équipements hybrides qui intègrent les deux technologies conventionnelles (panneaux solaires et thermiques), produisant simultanément de l'électricité et de la chaleur dans un système de micro-cogénération.

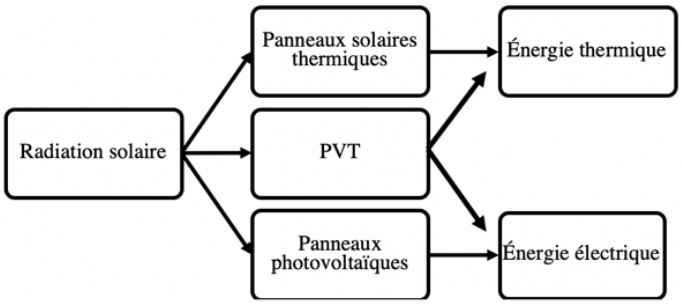

FIGURE 1: Technologies classiques de conversion de l'énergie solaire en énergie utile

Les systèmes PVT sont particulièrement avantageux dans les endroits où l'espace est limité, comme les zones urbaines, car ils augmentent le taux de conversion de l'énergie

solaire par mètre carré. De plus, la conversion de l'énergie thermique entraîne le refroidissement du système, ce qui présente l'avantage supplémentaire d'augmenter l'efficacité des cellules photovoltaïques, car elles sont affectées par la surchauffe. L'efficacité des cellules PV diminue avec l'augmentation de la température de fonctionnement. Au fur et à mesure que la cellule chauffe, la puissance électrique produite par le circuit diminue. De plus, l'énergie thermique extraite du capteur peut être utilisée pour diverses applications (résidentielles ou industrielles) et ainsi une efficacité énergétique globale plus élevée de l'ensemble du système énergétique peut être obtenue en combinant les deux composants.

Dans la première partie, une analyse bibliographique a permis de recueillir et de synthétiser des informations sur les principes de fonctionnement des panneaux PVT, leurs applications, leurs forces et leurs faiblesses. Elle a également mis en évidence les dernières recherches sur le sujet et a identifié les domaines qui nécessitent un examen plus approfondi : un modèle numérique explicite qui peut être facilement adapté à n'importe quelle configuration de panneau et régime de fonctionnement ; une analyse paramétrique de l'ensemble du système PVT, et pas seulement du panneau autonome, l'impact de la demande du consommateur sur l'efficacité du système PVT et du panneau, des données expérimentales réelles sur les performances du système PVT. Ces domaines ont été abordés dans la suite de cette recherche.

Un système photovoltaïque thermique (PVT) hybride est un module dans lequel la couche photovoltaïque (PV) ne produit pas seulement de l'électricité mais sert également d'absorbeur thermique. De cette façon, la chaleur et l'électricité sont produites simultanément. Les deux composants d'un système hybride (collecteur thermique et cellule photovoltaïque) ont généralement les mêmes principes de fonctionnement que des équipements séparés. Le module PV a pour rôle de convertir l'énergie solaire en électricité grâce à des cellules PV interconnectées et encapsulées dans du verre ou des polymères pour la protection. Le rôle des capteurs thermiques est de capter l'énergie solaire sous forme d'énergie thermique, et de transférer cette chaleur à un agent thermique circulant à travers un système de tuyaux ou de canaux. Une coupe transversale typique d'un collecteur PVT est illustrée à la Figure 2.

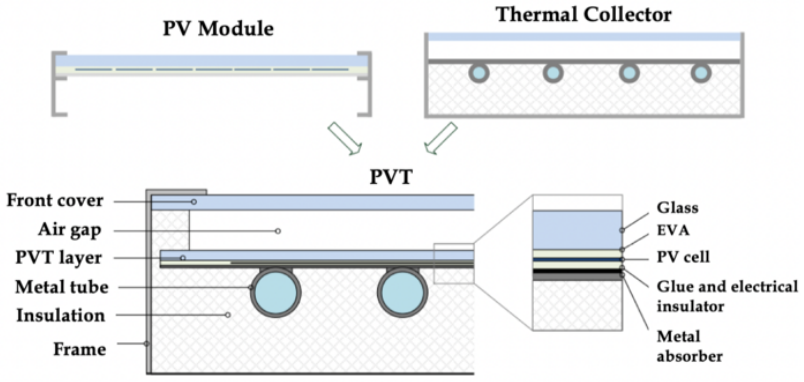

FIGURE 2: Système photovoltaïque thermique (PVT) hybride

Les performances d'un système thermique photovoltaïque hybride dépendent de multiples paramètres : conditions climatiques, propriétés thermo-physiques, géométriques et électriques. Dans la deuxième partie un modèle numérique explicite amélioré d'un collecteur PVT basé sur les équations du bilan thermique du système est proposé (Figure 3). Le modèle permet d'établir les températures du capteur à tout moment, en fonction des données externes : température ambiante, irradiation solaire et vitesse du vent. Le modèle numérique est développé et résolu dans MatLAB. Le modèle a été validé par rapport à un prototype expérimental de la littérature (Figure 4).

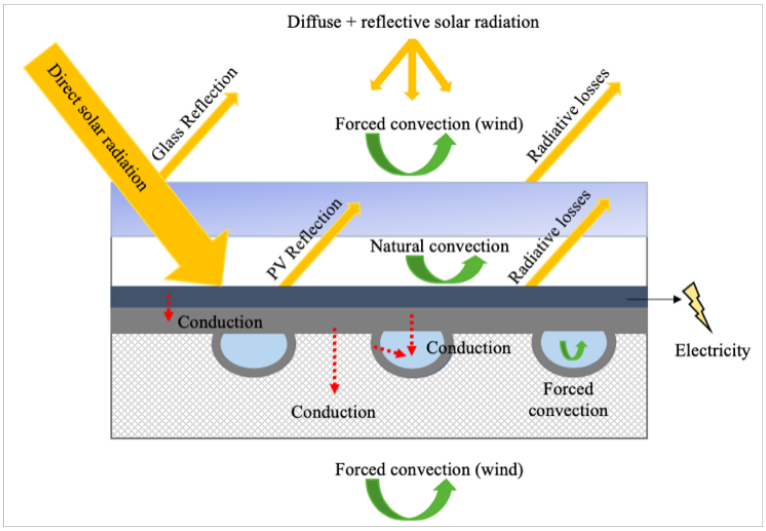

FIGURE 3: Echanges de chaleur dans un système photovoltaïque thermique (PVT) hybride

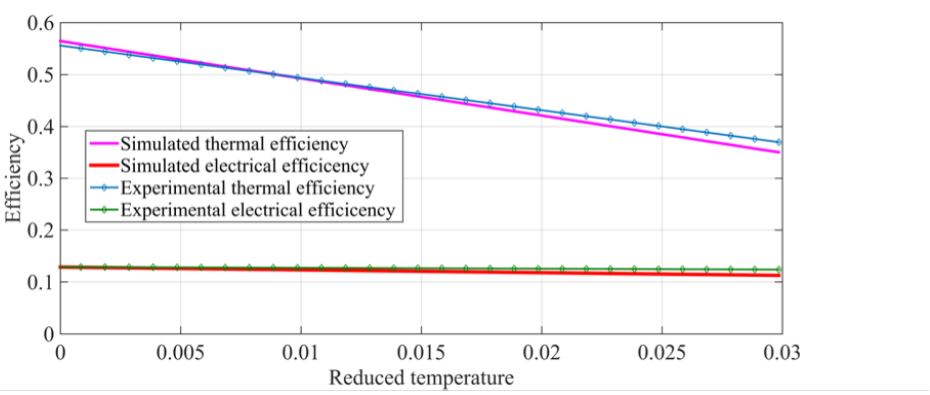

FIGURE 4: Comparaison des résultats de la simulation et des résultats expérimentaux

Ensuite, le modèle a été appliqué pour deux études de cas pour les climats de Bucarest, en Roumanie, et de Strasbourg, en France. L'entrée du modèle se compose de la température ambiante, de la vitesse du vent et de l'irradiance globale, qui ont été obtenues pour les deux emplacements à partir de la base de données Meteonorn. Les simulations ont été effectuées pour des journées d'été et d'hiver représentatives, de 8h00 à 20h00. Les résultats montrent la température de chaque couche à un moment donné, et on peut observer une température légèrement plus élevée du fluide de travail à Bucarest pendant l'été, et à Strasbourg pendant l'hiver (Figure 5 et Figure 6).

Les analyses paramétriques de l'OFAT réalisées dans cette étude ont montré dans la plupart des cas un compromis entre les performances électriques et thermiques du système PVT. En termes de vitesse du vent et d'isolation, il a été observé que les avantages thermiques d'un vent faible et d'une isolation élevée compensent la diminution de l'efficacité électrique. Pour une conception optimale, l'épaisseur de l'isolation doit être maximisée et la vitesse du vent minimisée, ce qui peut être obtenu par un placement stratégique des panneaux dans des zones protégées du vent. Le facteur de remplissage s'est avéré optimal lorsqu'il est maximisé, car les avantages électriques sont plus importants que les avantages thermiques. La largeur des canaux de l'échangeur de chaleur doit également être maximisée dans la mesure où cela est technologiquement possible pour obtenir les meilleures performances. Le débit doit également être maximisé, mais en gardant à l'esprit l'augmentation de la quantité d'énergie utilisée pour le pompage.

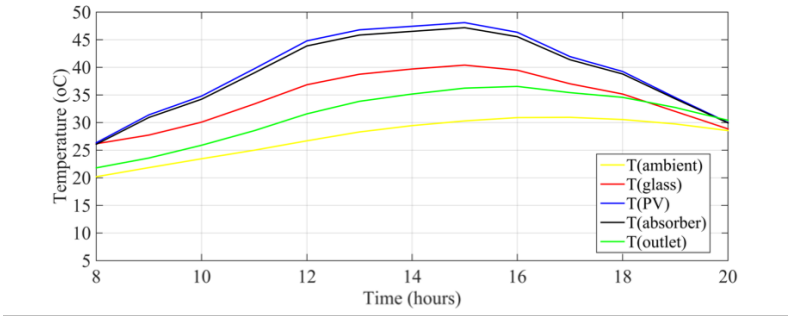

(A)

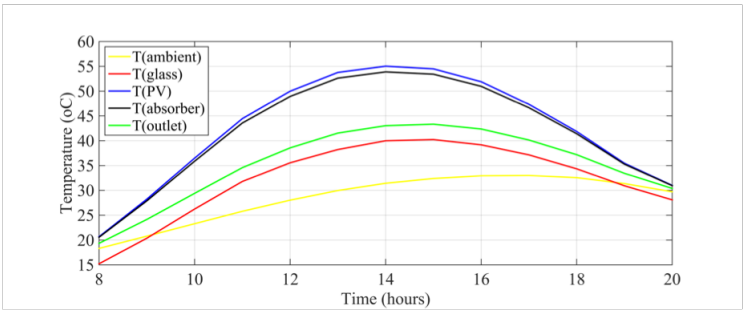

(B)

FIGURE 5: Température du PVT en fonction du temps pendant une journée d'été à Strasbourg (A) et Bucarest (B)

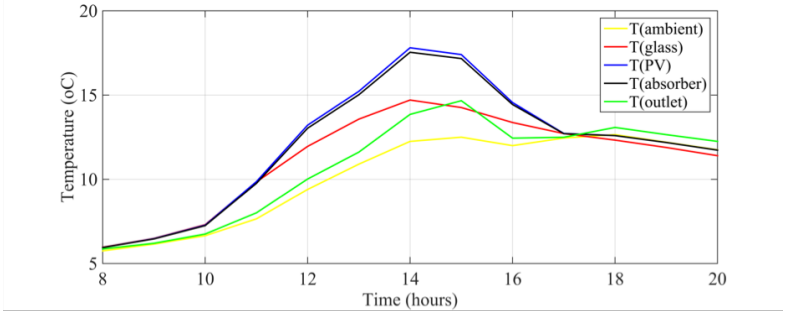

(A)

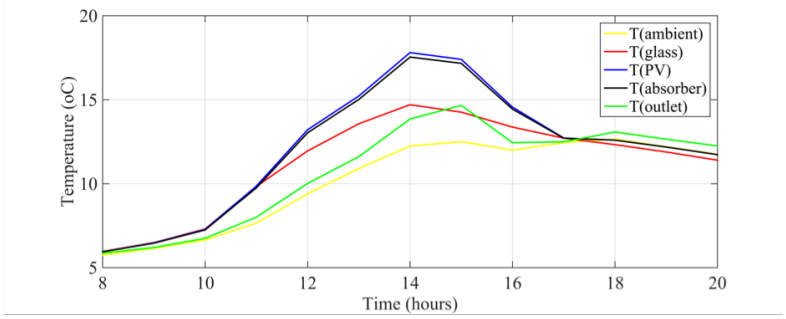

(B)

FIGURE 6: Température du PVT en fonction du temps pendant une journée d'hiver à Strasbourg (A) et Bucarest (B)

Le panneau PVT peut être optimisé afin de maximiser la production d'énergie thermique ou électrique, selon la portée et les applications du bâtiment. Il peut être à commande électrique - maximisant l'efficacité électrique, thermique - maximisant l'efficacité thermique, ou une solution de compromis - maximisant l'efficacité globale. Sur la base des résultats de l'analyse paramétrique, une recommandation technique a été proposée pour chacun des modes de fonctionnement.

Dans la section suivante, un système PVT est proposé pour un consommateur domestique résidentiel à Strasbourg et à Bucarest avec les conditions météorologiques variables correspondant aux deux emplacements différents (Figure 7). Le système PVT et le consommateur couplé sont modélisés dans TRNSYS (v17, Thermal Energy System Specialists, Madison, USA). Une analyse des performances est réalisée afin d'établir la production d'énergie instantanée quotidienne et la production d'énergie annuelle.

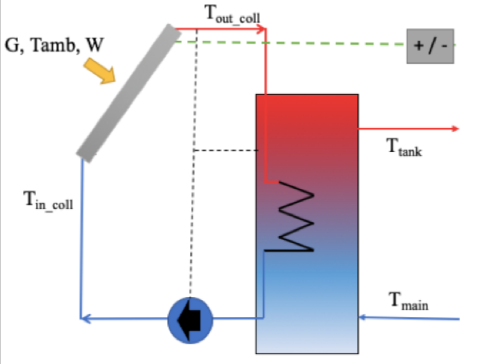

FIGURE 7: Schéma simplifié d'un système PVT couplé à un réservoir de stockage

Les résultats indiquent une performance supérieure de 10 à 12 % à Bucarest par rapport à Strasbourg en raison de conditions météorologiques légèrement meilleures (Figure 8). L'efficacité du système a été évaluée par différentes méthodes (efficacité énergétique et économie d'énergie primaire). Selon la méthode utilisée, le lieu et la période de l'année, les résultats varient de 15 % pour le rendement énergétique à 90 % pour le rendement d'économie d'énergie primaire. La méthode d'évaluation de l'efficacité la plus appropriée pour cette étude s'est avérée être la méthode d'économie d'énergie, car elle prend en compte les différences régionales dans la production d'énergie. Cette étude conclut que le marché roumain du PVT a un bon potentiel d'adoption de la technologie, d'autant plus qu'il est actuellement moins mature qu'en France. L'analyse transitoire

d'un système PVT connecté à un consommateur réel a montré que la moitié de la demande annuelle d'énergie électrique et thermique pouvait être satisfaite par un système PVT simple et peu coûteux soutenu par des solutions de secours (respectivement un banc de batteries et un chauffage auxiliaire).

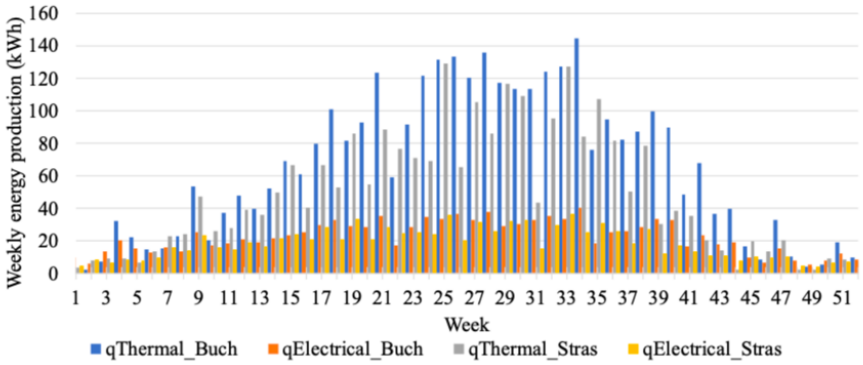

FIGURE 8: Comparaison des performances des systèmes PVT pour Bucarest et Strasbourg

Dans l'ensemble, il semble que le PVT à petite échelle soit une solution prometteuse pour une exploitation maximale de l'énergie solaire, en particulier dans les secteurs résidentiels et urbains. Une sensibilisation du public et des projets de démonstration fournissant la preuve du concept sont nécessaires pour introduire cette technologie sur le marché grand public.

Dans tous les systèmes de cogénération, un équilibre doit être atteint entre la chaleur et l'électricité produites. Il est donc important d'établir l'interconnexion et la relation entre les deux. Cette recherche étudie l'impact de la variation d'un certain nombre de paramètres thermiques sur la production électrique d'un capteur PVT.

Une analyse OFAT est effectuée pour les paramètres suivants : débit de sortie du réservoir, taille du réservoir, température principale de l'eau froide et courbe de demande du consommateur. L'analyse est effectuée sur une simulation transitoire d'un système PVT modélisé dans TRNSYS. L'impact le plus important sur le rendement électrique (d'environ 6,8 %) est causé par la variation du débit de sortie vers le consommateur. La taille du réservoir a un impact de 4,7 %. De plus, il a été observé que le pic d'efficacité électrique se produit en même temps que le pic de demande du consommateur, donc faire correspondre la courbe de demande avec la courbe de production est

également un aspect important. Un autre aspect étudié dans cette partie est la variation instantanée de la puissance thermique et électrique du système en fonction de la température d'entrée du PVT. Cette analyse paramétrique du système PVT a montré un certain nombre de faits intéressants. Tout d'abord, plus la température de l'eau froide du réseau est basse, meilleur est le rendement électrique de la cellule. De même, plus le réservoir de stockage d'eau est grand, meilleur est le rendement électrique de la cellule, mais il y a une perte de qualité de l'énergie thermique. Plus la demande en eau des consommateurs est élevée, meilleur est le rendement électrique des cellules, car celles-ci sont refroidies plus rapidement. Lorsqu'il y a un pic dans la demande d'eau chaude du consommateur, l'efficacité électrique de la cellule atteint également un pic. L'impact des différents paramètres sur les performances du système est illustré à la Figure 9. Ces conclusions sont utiles pour concevoir des systèmes d'énergie renouvelable à petite échelle à haut rendement et pour fournir une performance maximale pour un consommateur donné.

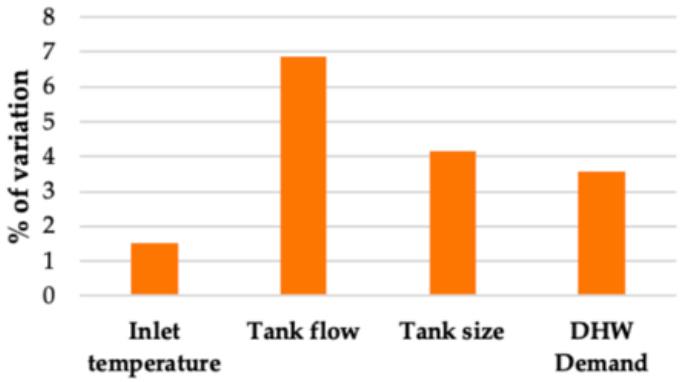

FIGURE 9: L'impact des différents paramètres sur les performances du système

L'introduction de l'énergie solaire décentralisée à petite échelle est un élément essentiel du bouquet énergétique du futur. La production sur place de chaleur et d'électricité renouvelables est bénéfique pour de multiples raisons : moins de pollution, moins de pertes thermiques/électriques dues au transport, fiabilité accrue du système. Un système solaire hybride, comprenant des panneaux solaires thermiques (ST), des panneaux photovoltaïques (PV) et des panneaux photovoltaïques-thermiques (PVT), a été mis en place dans une école maternelle de Bucarest, en Roumanie (Figure 10 et Figure 11). Le

système est décrit en détail, avec tous les composants techniques et les auxiliaires. Quatre types de jours représentatifs ont été analysés : jour nuageux de printemps, jour clair de printemps, jour nuageux d'été, jour clair d'été. Ce système a été analysé en termes de puissance instantanée, de températures instantanées en différents points du système et de production d'énergie quotidienne et mensuelle. Les efficacités thermique et électrique ont également été analysées.

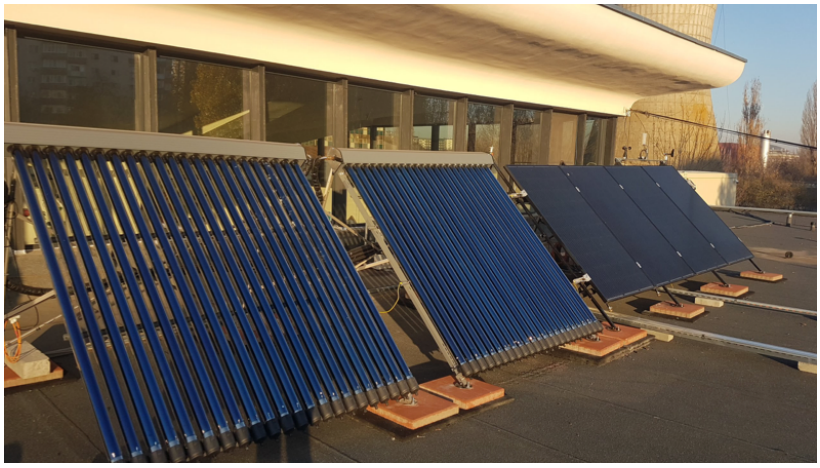

FIGURE 10: Photo du dispositif expérimental

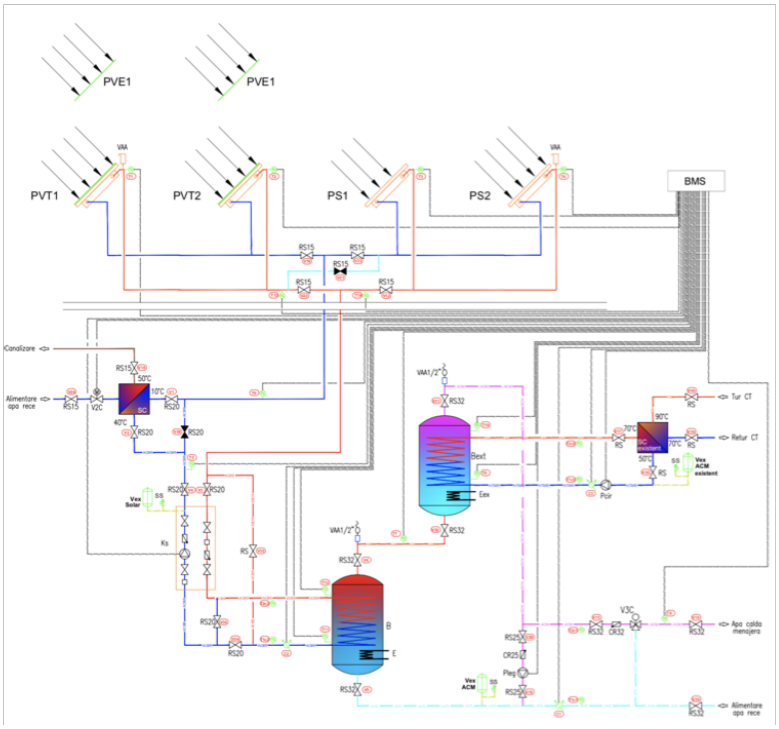

FIGURE 11: Photo du dispositif expérimental

L'analyse quotidienne de quatre jours représentatifs a montré que la meilleure performance thermique du système se produit les jours clairs et chauds, tandis que la meilleure performance électrique se produit pendant les jours nuageux plus froids. Il existe un compromis entre la production électrique et thermique du système. Afin d'améliorer le rendement électrique pendant les journées très chaudes, une dissipation suffisante de la chaleur du ballon est nécessaire, sinon l'énergie thermique s'accumule et le système n'est plus refroidi. Dans l'ensemble, le capteur PVT a produit plus d'énergie au cours de la période analysée de quatre mois (Figure 12).

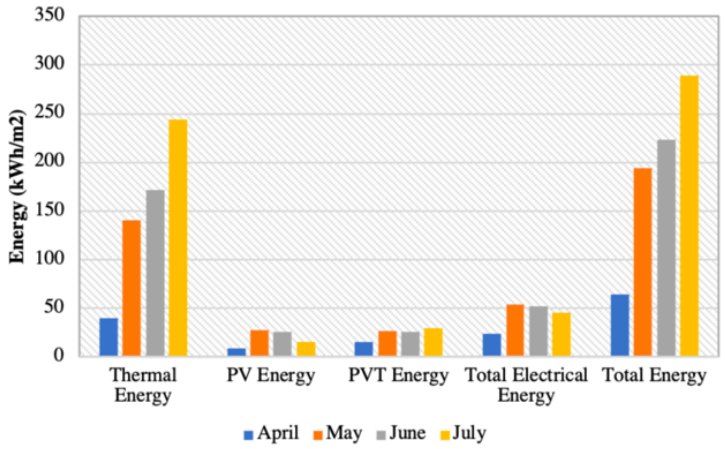

FIGURE 12: Energie totale collectée par la station expérimentale pendant 4 mois

De la comparaison des panneaux PV et PVT, il a été conclu que le PVT fonctionne mieux les jours où il n'y a pas d'excès d'accumulation de chaleur dans le réservoir ; en revanche, le PV est légèrement plus performant les jours où l'énergie thermique du réservoir n'est pas dissipée. En tant que recommandation technique, les capteurs PVT ne conviennent que dans les systèmes qui ont une source de dissipation de chaleur à proximité, soit vers un consommateur, soit en stockage thermique.

Les résultats confirment la pertinence d'un système PVT hybride pour couvrir les besoins énergétiques des petits consommateurs d'énergie. Ce type de consommateur en particulier, un jardin d'enfants, convient à un système d'énergie solaire car le pic de demande se produit à la mi-journée, généralement simultanément au pic de rayonnement solaire et à la température ambiante.

Enfin, l'aperçu économique du marché des systèmes hybrides PVT et des subventions disponibles a révélé qu'il y a un manque de normalisation au niveau européen,

et un manque de clarté concernant la classification des capteurs PVT dans les technologies de l'énergie solaire. En termes d'évaluation économique, les subventions sont un paramètre important pour établir les bénéfices de l'investissement. Trois scénarios ont été étudiés, avec une subvention élevée, moyenne et sans subvention, et les résultats ont montré une période de retour de l'investissement entre 7 et 15 ans, ce qui est comparable aux technologies solaires traditionnelles (Figure 14). Il a été observé, à partir de l'analyse économique, que l'investissement dans les capteurs PVT n'est pas rentable financièrement à petite échelle en raison du prix actuel élevé du PVT par rapport aux capteurs PV et ST (solaire thermique) standard (Figure 13). Cependant, pour une capacité installée plus importante et avec un système de subvention approprié en place, la solution de cogénération devient rentable, l'investissement est récupéré rapidement et la VAN pendant la durée de vie de l'équipement est élevée. Ainsi, on peut conclure que, dans les conditions actuelles du marché, les collecteurs PVT ne sont rentables qu'à plus grande échelle et uniquement avec des programmes de subvention en place. De plus, si l'espace disponible est limité, l'investissement en PVT est également justifié par rapport aux standards PV et ST pour maximiser la conversion solaire.

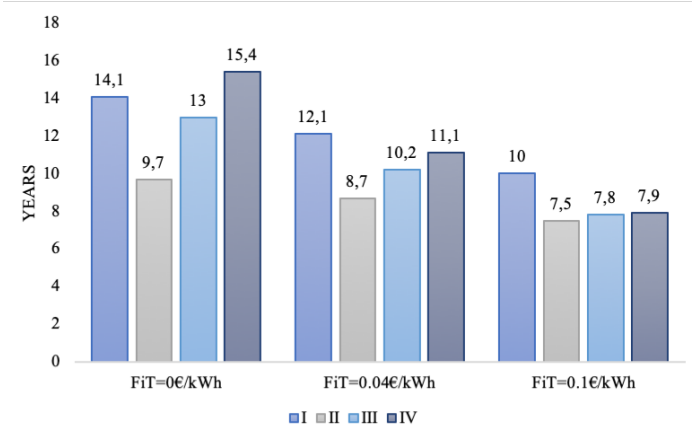

FIGURE 13: Période de retour de l'investissement pour les trois scénarios étudiés

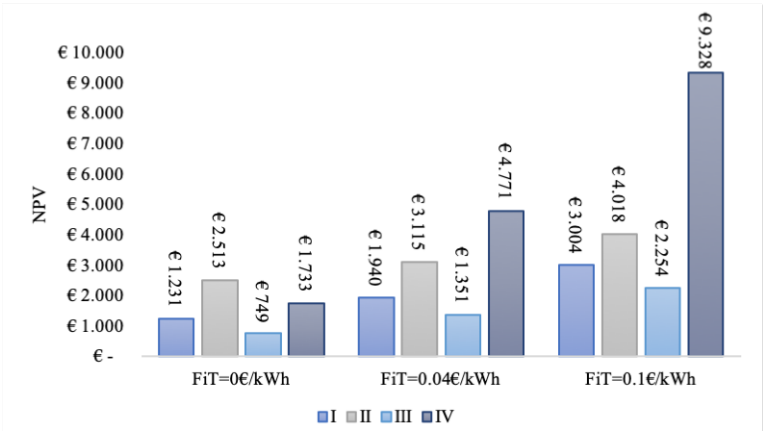

FIGURE 14: Etude économique pour les trois scénarios étudiés

À la suite de ce projet, plusieurs pistes de recherche ont été identifiées. Un domaine important est la combinaison et l'hybridation de diverses technologies d'énergie renouvelable, parmi lesquelles les capteurs PVT, pour fournir les systèmes énergétiques fiables et autosuffisants du futur. Ces technologies comprennent - le solaire, la biomasse, les pompes à chaleur, pour fournir de la chaleur, de l'électricité et aussi du refroidissement. Dans de nombreuses zones urbaines, le refroidissement intérieur et la climatisation sont une source majeure de consommation d'énergie, la trigénération solaire est donc un domaine de recherche important. Une enquête plus approfondie sur les matériaux et revêtements PVT pour maximiser l'efficacité thermique sans affecter la production électrique serait également bénéfique pour faire avancer la technologie sur le marché et démontrer son potentiel. Un prototype expérimental est prévu pour être développé au laboratoire l'INSA Strasbourg ICube.

Dans le cadre de cette thèse une analyse complète des capteurs PVT a été réalisée pour différents régimes de fonctionnement. Les avantages de l'énergie solaire (combustible gratuit, pas de bruit, pas d'émissions, fonctionnement sûr) sont renforcés par un autre ensemble d'avantages fournis par l'intégration de capteurs photovoltaïques et thermiques (meilleure efficacité photovoltaïque due à une température de fonctionnement plus basse, meilleure utilisation de l'espace, plus de conversion solaire, production sur site pour les deux types de besoins énergétiques). Bien que d'une manière générale, la courbe de demande du consommateur corresponde aux heures de fonctionnement des capteurs PVT, l'énergie solaire a encore un caractère aléatoire, à la fois prévisible (cycle jour-nuit) et imprévisible (donné par nébulosité). Actuellement, l'utilisation

de capteurs solaires thermiques hybrides photovoltaïques est conditionnée par la combinaison de la source solaire avec une autre source auxiliare ou des systèmes de stockage externes.

Les capteurs PVT sont encore une nouvelle technologie, qui n'a pas encore complètement pénétrée sur le marché, avec peu de données de performance fiables disponibles pour les concepteurs et les planificateurs. En termes de technologie et d'économie, les deux industries distinctes (PV et solaire thermique) doivent converger davantage, et un effort interdisciplinaire de l'industrie et du milieu universitaire est requis afin d'accélérer le développement des capteurs PVT et d'atteindre un marché concurrentiel prix qu'il est accessible à la grande masse des prosommateurs.

Publications and Conferences

1. 'Numerical model and parametric analysis of a liquid based hybrid photovoltaic thermal (PVT) collector' - Madalina Barbu, Monica Siroux, George Darie – Energy Reports 2021, Impact Factor 6.87.

2. 'A parametric study of a hybrid photovoltaic thermal (PVT) system coupled with a domestic hot water (DHW) storage tank' - Madalina Barbu, George Darie, Monica Siroux – Energies 2020, 13(24), 6481, Impact Factor: 3.

3. 'Analysis of a Residential Photovoltaic-Thermal (PVT) System in Two Similar Climate Conditions' - Madalina Barbu, George Darie, Monica Siroux – Energies 2019 12(19):3595, Impact Factor: 3.

4. 'A technical-economical analysis of the implementation of hybrid solar energy systems in small energy prosumer applications' -Madalina Barbu, Roxana Patrascu, George Darie, Diana Tutica - Quality - Access to Success 2019, 20(169), 134-138, Impact Factor 0.580.

5. 'Optimizing the non-reheat steam cycle of concentrated solar power plants with molten salt'- Victor-Eduard Cenusa, Mihaela Norisor, Florin-Niculae Alexe, Madalina Barbu, Marian Gioanta - Rev. Roum. Sci. Techn.– Electrotechn. et Energ. Vol. 64, 3, pp. 281–286, Bucarest, 2019, Impact Factor 0,760.

6. 'Assessment of the quota of recuperative cooling of the compressed gas at turbocharged Reciprocating Internal Combustion Engines' - Victor-Eduard Cenusa, Mihaela Norisor, Florin-Niculae Alexe, Madalina Barbu - TEM Journal 2019 8(1), 3-11, Impact Factor 0.51.

7. 'Analysing the Heat and Exergy Transfer in Steam Generators of Nuclear Power Plants with Pressurized Light Water Reactors' - Cenusa Victor-Eduard, Florin-Niculae Alexe, Mihaela Norisor, Madalina Barbu – Conference Proceedings: 2019 International Conference on ENERGY and ENVIRONMENT (CIEM).

8. 'Assessment of reciprocating engines performances starting from manufacturers' data'- Cenusa Victor-Eduard, Florin-Niculae Alexe, Mihaela Norisor, Madalina

Barbu, Roxana Patrascu, George Darie - Conference Proceedings: 2019 International Conference on ENERGY and ENVIRONMENT (CIEM)

9. 'Dynamic modelling and sensibility analysis of a hybrid photovoltaic-thermal (PVT) system' – Madalina Barbu, George Darie, Monica Siroux - 7th Eur. Conf. Ren. Energy Sys. 10 June 2019, Madrid, Spain

10. 'Cogeneration in solar energy systems: Hybrid Photovoltaic Thermal (PV/T) Panels' -Madalina Barbu, George Darie - 14th WEC Central and Eastern Europe Regional Energy Forum - FOREN 2018, Costinesti, Romania.

Abstract

In the current global context of pollution, depletion of resources and climate change, the development of renewable energy technologies is crucial. Solar energy is among the most abundant and most promising energy sources, with high potential for sustainable development. The two conventional technologies for converting solar energy into useful energy are photovoltaic and solar thermal collectors. To improve the market competitiveness and to increase the conversion rate of solar energy into useful energy, photovoltaic-thermal (PVT) panels have been developed. These are hybrid equipments that incorporate the two conventional technologies (solar and thermal panels), generating simultaneously both electricity and heat in a micro-cogeneration equipment. PVT systems are in particular beneficial in locations where space is limited, such as urban areas, as they increase the rate of conversion of solar energy per square meter. Moreover, the conversion of thermal energy leads to the cooling of the system which brings an additional advantage of increasing the efficiency of the photovoltaic cells, as they are impacted negatively by overheating.

A hybrid photovoltaic thermal (PVT) collector is a module in which the photovoltaic (PV) layer is not only producing electricity but also serves as a thermal absorber. As a result, power and heat are produced simultaneously. The performance of a hybrid photovoltaic thermal collector is dependent on multiple parameters: climate conditions, thermo-physical, geometrical and electrical properties. In this research, a dynamic numerical model is proposed to simulate the heat exchange in the layers of the PVT panel. The model consists of a system of simultaneous equations solved in MATLab, and it can evaluate the temperature in each of the layers of the collector at any given time. The model was applied to two different climatic conditions: Bucharest, Romania and Strasbourg, France, in order to assess and compare their behaviour. The results show the temperature of each layer at any particular time, and a slightly higher temperature of the working fluid can be observed in Bucharest during the summer, and in Strasbourg during the winter. The model is validated and can be applied to any climatic conditions and adapted for any geometrical or thermo-physical configuration. Next, a one-factor-at-a-time parametric analysis is carried out in order to assess the impact of

various parameters on the electrical, thermal and global efficiency. Based on this analysis, a number of technical recommendations have been proposed.

A transient simulation of a small sized domestic household system was carried out in TRNSYS, comparing the system performance in Bucharest and Strasbourg. The results indicated a slightly better yearly performance in Bucharest. Overall, the yearly energy production of electricity and heat, both supported by back-up solutions (auxiliary heater and battery bank respectively) indicates that the energy demand of an average single family house could be covered to about 50% over one year, with a slightly better performance in the Bucharest climate compared to Strasbourg. This was expected due to the slightly better meteorological conditions.

In all co-generation systems there is an equilibrium that needs to be achieved between the produced heat and power. Thus, establishing the inter-connection and relationship between the two is important. This research investigated the impact of the variation of a number of thermal parameters on the electrical output of a PVT collector. An OFAT analysis is performed for the following parameters: tank outlet flow, tank size, consumer demand curve and the temperature of the cold water main. The analysis is done on a transient simulation of a PVT system modelled in TRNSYS. The most significant impact on the electrical efficiency (6.8%) is caused by variation of the flow rate to the consumer. The size of the tank has an impact of 4.7%. Also, it was noted that the peak electrical efficiency is simultaneous with the peak consumer demand, thus matching the demand curve with the production curve is also an important aspect. Another aspect investigated in this section is the instantaneous variation of the electrical and thermal power of the system as a function of the PVT inlet temperature.

An experimental study of a demo system from the UPB campus was carried out. The daily analysis of four representative days (spring cloudy day, spring clear day, summer cloudy day, summer clear day) showed that the best thermal performance of the system occurs on the warm clear days, while the best electrical performance occurs during the colder cloudy days, and generally there is a tradeoff between the electrical and thermal performance. When comparing PV and PVT collectors, it was concluded that PVT performs better in the days when there is no excess of heat accumulation in the tank; on the other hand, the PV performs slightly better during the days when the tank thermal

energy is not dissipated. As a technical recommendation, PVT collectors are only appropriate in systems that have a nearby source of heat dissipation, either to a consumer or in thermal storage.

The economic overview of the PVT market and the available subsidies revealed the fact that there is still a lack of standardisation at a European level, and lack of clarity regarding the classification of PVT collectors in the solar energy technologies. In terms of economical evaluation, subsidies are an important parameter for establishing the benefits of the investment. Three scenarios were investigated, with high, medium and no subsidy, and the results showed a payback period of the investment between 7 and 15 years, which is comparable to the traditional solar technologies.

Overall, small scale PVT technology appears to be a promising solution for maximum solar energy conversion, with some significant benefits over the standard PV and thermal collectors, especially in the residential and urban sectors. Additional demonstrative projects, consumer awareness, standardisation and proof of concept are required to push this technology further on the mainstream market.

Acknowledgements

I would like to take this opportunity to express my gratitude towards my supervisors, prof. Monica Siroux and prof. George Darie for their support and guidance in this uncharted journey. I would also like to thank the members of our department, prof. Roxana Patrascu, prof. Eduard Minciuc, prof. Florin Alexe, prof. Constantin Ionescu, sl. Diana Ban, sl. Mihaela Norisor, for their valuable advice, as well as for the opportunity to work with them in multiple projects where I gained valuable knowledge. My thanks also go to prof. Radu Porumb for his help with the experimental data. And not last, to my colleague Stefan-Dominic Voronca, who went through a similar journey and to who I could always go to for information and moral support.

My family has always been my number one supporter on my academic journey. Thank you mom, dad and sisters!

Saving the best for last, I would like to thank my husband Pompiliu for his unconditional support, help, and encouragement, without which I would not have been able to finalise this doctoral thesis. And my two wonderful boys, Horia and Cezar, my source of inspiration and energy, to whom I dedicate this work. I love you.

Contents

List of Figures

List of Tables

Chapter 1

Introduction

1.1 Current Status of Solar Energy

Since the 1990s, electricity consumption in the European Union has increased by about 1% every year. It only started to show a decrease since 2017 ($\pm$ 0.3%), when significant measures have been applied in order to increase energy efficiency in all sectors of activity. It is estimated that without the introduction of new energy efficiency policies, the annual increase in consumption will continue to tend to 1% by 2050 [1].

Even in the situation of stagnant growth of electricity demand, there are two essential factors that stir great interest in renewable energy production: the technological factor, related to the fact that most of the energy equipment in large conventional power plants are reaching the end of their life cycle, and closely related to this, the climate factor and implicitly the direction of the strategies of the EU member states to increase the share of renewables in the energy mix by 2030 to 32%. Almost 80% of total greenhouse gas emissions come from the use of fossil fuels in the energy sector [2]. Increasing the share of renewable energy is expected to help the EU achieve its goal of reducing greenhouse gas emissions by 40% by 2030 [3] and by 80-95% by 2050 [4]. In addition, greater use of renewable energy sources to meet the energy demand will reduce the EU's dependence on fossil fuels [1].

As a result of the global energy policies that are being put in place for the future, the development of renewable energy technologies is essential for achieving these goals. In the long run, renewable energy will start to dominate the world energy mix in the detriment of fossil fuels. Due to their intermittence, renewable sources will have to be combined together to provide the full spectrum of energy demand. Solar energy is an

abundant source, easily available mostly everywhere in the world, and thus it has a great potential of taking over a large share of the renewable energy mix in the future, combined with other renewables such as wind and biomass. In theory, there is enough solar radiation around the world to supply 10,000 times the global energy demand [5].

In the last ten years, solar energy has become one of the most popular forms of renewable energy, both globally and in Europe. It is playing an increasingly important role in terms of environmental protection and preservation, and in terms of the economic efficiency given by the latest solar technologies. In addition to ensuring self-production and self-consumption of energy among individual consumers, solar and photovoltaic panels also have significant industrial and agricultural potential. Figure 1.1 shows the development of global installed capacity of solar thermal heat, photovoltaics and wind energy between 2010 and 2019.

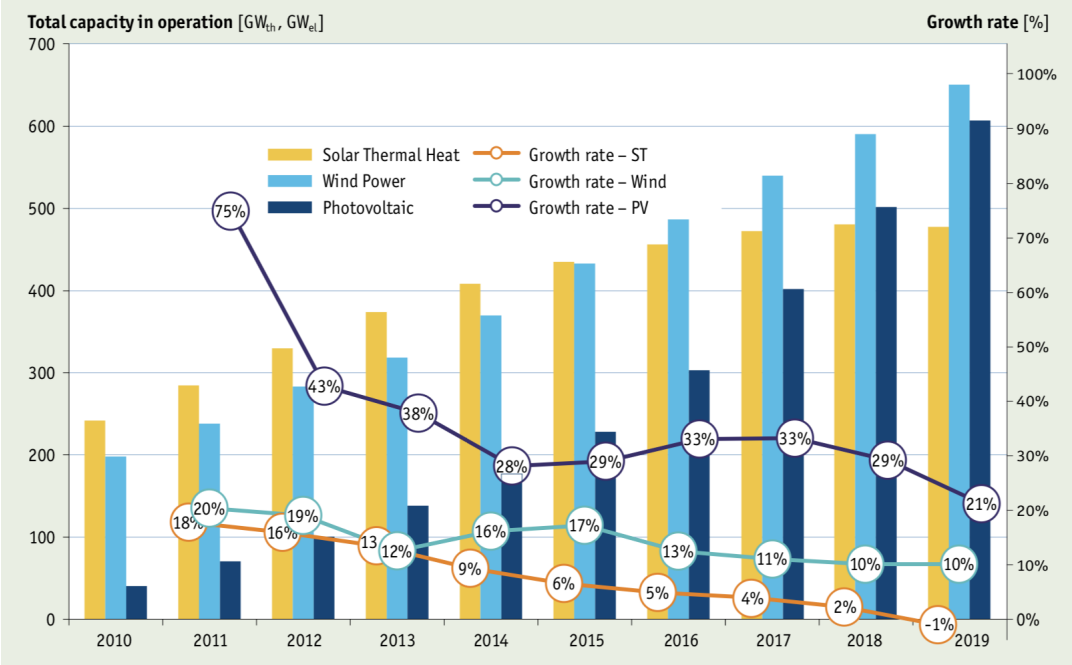

FIGURE 1.1: Global capacity in operation and market growth rates between 2010 and 2019 (reproduced from [6])

In the face of global warming, the public has started to gain more and more confidence in solar energy. A study conducted by the European Social Survey (ESS) on the attitude of European citizens towards climate change and various forms of energy showed that solar energy is the most popular among renewable energies, with nine out of ten people considering it is the most appropriate technology to achieve the EU's decarbonisation targets by 2050 [7].

The report on "Costs of electricity production", published by IRENA in 2019, shows a considerable decrease in costs related to the manufacture of photovoltaic panels, up to 96% in the period 2010-2019 [8] (Figure 1.2). The report also predicts that by 2024 prices will continue to drop by 15% to 35%. Also, a report on the solar energy market, published by Solar Power Europe, shows that currently solar energy is more economical than any fossil or nuclear fuel, with typical prices below 0.04 Euro/kWh [9].

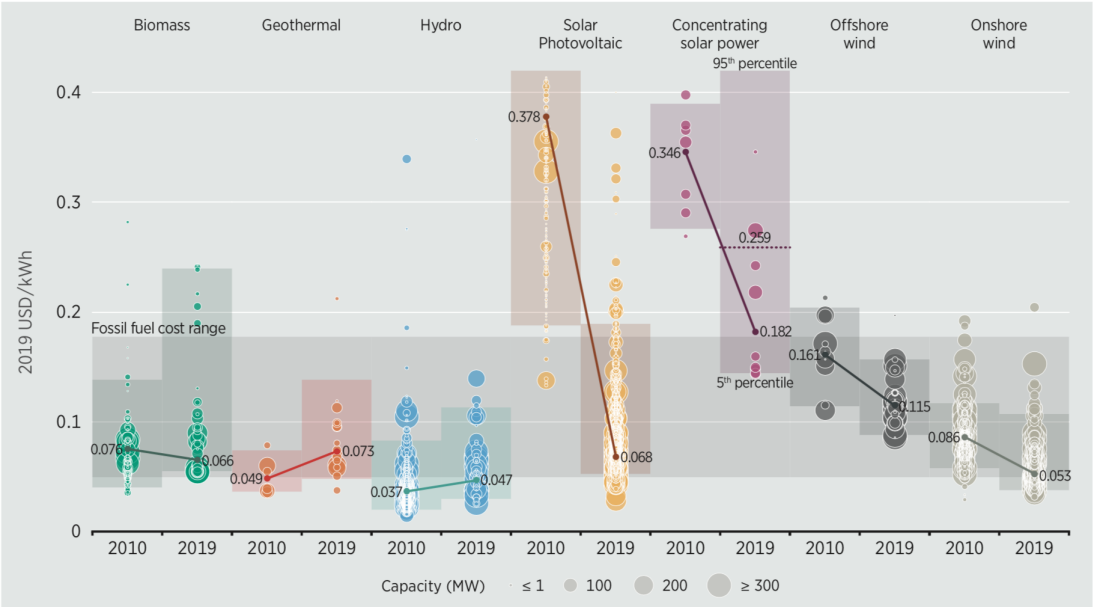

FIGURE 1.2: Global levelised cost of electricity from newly built utility-scale renewable energy technologies for 2010-2019 (reproduced from [8])

Romania, as an EU member state, pursues the same directions of promoting renewable sources and encouraging investments in the solar energy sector. The maturation of technologies and the continuous gain of experience of current users in Romania lead to the idea that solar energy has a great potential for further implementation. The market penetration is a long process that requires the continuation and extension of support policies for such investments, such as the Casa Verde Plus program of Feed-in Tariffs.

1.2 Motivation for research topic

In line with the current global trends of energy efficiency are the novel photovoltaic-thermal (PVT) collectors which produce simultaneously heat and electricity. These collectors have a high potential for being adopted in the domestic sector for on site small scale thermal and electrical production. PVT collectors make use of limited roof and

facade space, which is essential in the large overcrowded urban areas, and are suitable for buildings which have a combined demand of electricity and heat.

Currently, the PVT panels market is limited and they are scarcely adopted worldwide. This is due to limited performance data, no standardisation, and few producers with limited marketing possibilities, which leads to limited end-user awareness regarding the product.

A survey carried out by SHC Task 60 identified in 2019 a total installed PVT collector area of 1 166 888 m^2 (606 MW_{th}, 208 MW_{peak}), with 567 MW_{th} and 194 MW_{peak} of the total installed capacity. A significant share is in Europe (675 427 m^2) followed by Asia excluding China (281 104 m^2) and China (133 942 m^2). The distribution is shown in Figure 6.4.

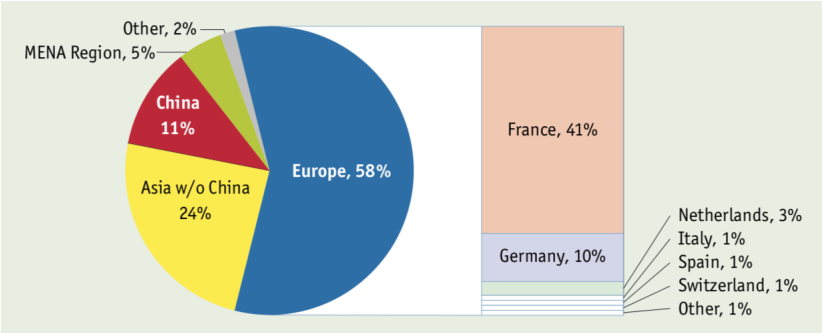

FIGURE 1.3: Distribution of the total installed PVT area by location in 2019 [6])

The installed capacity of PVT panels is considerably small compared to the solar thermal and PV collectors separately, which is a direct result of their novelty and limited demonstration. However, they are gaining momentum in the EU and provide an area of active research.

The motivation of this thesis is to contribute towards the development of the PVT collectors, in terms of improving their efficiency and evaluating the best methods of integration into the small scale energy mix. The topics researched in this project give a better understanding on their operation, sensibility to various parameters, and suitability for various types of consumers.

1.3 Aim and Objectives

This doctoral thesis is an in-dept, multi-dimensional study of the novel PVT collectors. The overall aim is to gain a deep understanding and to perform a thorough and systematic analysis of PVT micro-cogeneration collectors and systems in order to improve their efficiency and evaluate the best possibilities for integrating them into the energy mix of small consumers (prosumers). Various methods of predicting the efficiency and performance of PVT systems given realistic meteorological data and functioning parameters are presented and their reliability is evaluated.

The novelty of this study lies in the multiple methods of analysis that look at the PVT panels in a well-rounded manner, in multiple situations: a singular panel modelled numerically both in steady-state and dynamic state, a transient simulation of a system of PVT panels with real consumer demand curves (domestic prosumer, school, kindergarten, hotel), a system of PVT panels integrated in the local district heating system. In addition, the analysis is carried out from multiple perspectives, looking at their thermal, electrical and overall efficiency and how they are influenced by various parameters, as well as economical and technological.

This project investigates liquid based flat plate PVT panels and proposes reliable methodologies for modelling their behaviour.

In order to achieve the aforementioned aim, the following objectives have been achieved:

- Carry out a comprehensive literature review on the current knowledge and research on PVT panels and systems;
- Develop and validate a numerical 3D model that can be easily adapted for various PVT configurations;
- Carry out a sensibility analysis of various constructive and operative parameters of a PVT panel in order to improve their efficiency;
- Investigate the system integration of PVT panels for various domestic and commercial consumers;
- Perform a sensibility OFAT analysis on the thermal parameters of a system for improving the efficiency of their integration;

- Perform data analysis on an experimental system installed at the University Politehnica of Bucharest;
- Investigate the techno-economic potential of PVT collectors.

1.4 Thesis outline

The work has been structured as follows:

Chapter 2: Background understanding of the subject (solar radiation, photovoltaic effect, semiconductor physics, heat transfer phenomena, the effect of temperature on the functioning of photovoltaic cells) - Classification of existing PVT systems - Study of relevant literature - Identification of possible optimization parameters - Evaluation of existing modelling tools - Identify possible configurations of integration at the consumer level.

Chapter 3: Development of a numerical model for evaluating the temperatures inside the panel -Implementation and evaluation in MatLAB - Application of the model in different climatic conditions: Bucharest and Strasbourg - Validation of the model with data from the literature - Sensibility one factor at at time (OFAT) analysis for various parameters and discussion of results.

Chapter 4: Designing a PVT system for a household consumer - Implementation in TRNSYS coupled to a realistic consumer - Identification of methods for evaluating the energy performance of a PVT system - Weekly and annual simulations of the system performance - Evaluation of simulation results - Parametric OFAT study of the thermal components of the system - Summary and discussion of results.

Chapter 5: Overview of an experimental demonstrative installation at the University Politehnica of Bucharest - Description of installed equipment - Collection and analysis of relevant data- Discussion of results - Reproduction of the system using TRNSYS software for validation.

Chapter 6: Evaluation of the current PVT market and available subsidies in various countries - A brief economic analysis of PVT panels compared to traditional solar thermal and PV side by side for various subsidy scenarios - A SWOT analysis of the strengths, weaknesses, opportunities and threats of the technology.

Chapter 7: Conclusions of the current research and directions for future work.

Chapter 2

Background

2.1 Solar Energy

2.1.1 Solar radiation

The sun is a hot gas sphere with an internal temperature of 20 x 106 K. Its internal energy is transferred by convection to the external layer of the Sun (photosphere), and is subsequently emitted as radiation to the Earth, which, at the entrance into the atmosphere, receives about 1366 W / m^2 of solar radiation, or a total power of 1.7 x 1014 kW, with a annual yield of of 1.5 x 1018 kWh. However, not all solar radiation has the same quality, varying according to the wavelength (λ) of the photons emitted. The sun emits radiation in a wide range of wavelengths, from cosmic rays to long-range radio waves (Figure 2.1). The visible spectrum is in the wavelength range of 400-700 nm.

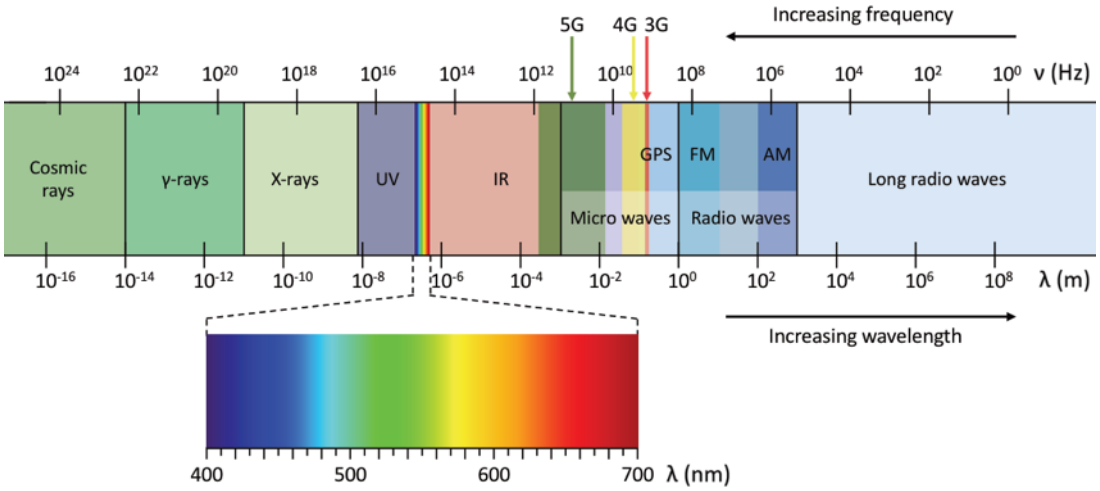

FIGURE 2.1: Solar radiation spectrum as a function of wavelength and frequency [10]

The distribution of solar radiation reaching the Earth is illustrated qualitatively, as a function of the photon wavelength, in Figure 2.3. The radiation is described by the parameter called spectral emissivity ($P(\lambda)$), which is measured in power over the surface and over the wavelength unit. AM (air mass) is the distance traveled by the solar radiation to reach the Earth's surface, shown in Figure 2.2 and is defined as:

$$AM = \frac{1}{cos\theta} \tag{2.1}$$

where θ is the angle between the direction of the sun at a given time and the direction perpendicular to the earth's surface (Figure 2.2). An air mass AM of 1.5, the equivalent of an angle of 48.2°, is used for the reference calculations.

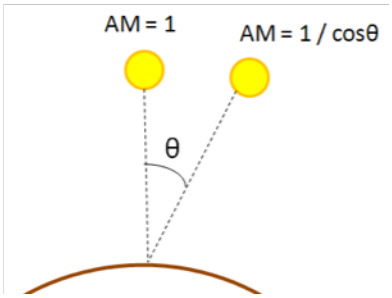

FIGURE 2.2: Air mass diagram

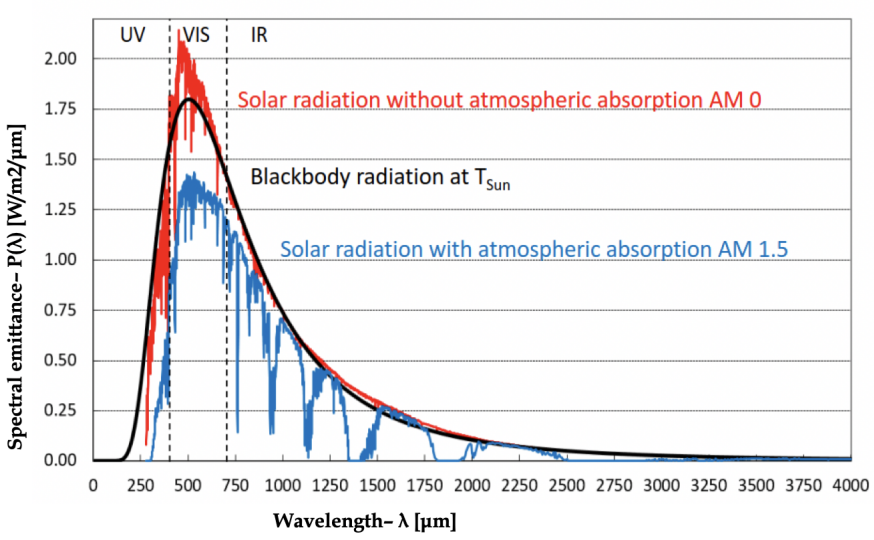

FIGURE 2.3: Solar radiation distribution as a function of wavelength [10]

In Figure 2.3, the red line represents the solar radiation emitted by the Sun's photosphere that can be observed upon entering the Earth's atmosphere (AM = 0), and the

blue line is the reference solar radiation, through an air mass of 1.5 (AM = 1.5). An idealised black body with a temperature of 6000K emits the radiation described by the black curve; it can be seen that it approximates quite well the curve of solar radiation at AM = 0.

2.1.2 Photovoltaic effect

Solar radiation can be converted into electrical energy through the photovoltaic effect, discovered by physicist A.E. Becquerel in 1839. The basic components of a photovoltaic cell are: a semiconductor material, with a negative charge part (N), and a positive one (P), separated by an n-p junction, and two electrodes (Figure 2.4). The physical phenomena that take place within the cell are:

1. Capturing incident solar radiation;
2. Generation of charge carriers - electron pairs and gaps;
3. Separation of load carriers;
4. The appearance of a potential difference between electrodes that leads to the movement of electrons through the external circuit.

These processes are schematically illustrated in Figure 2.4.

From the total solar radiation incident on a PV cell, only a fraction can be captured and converted into electricity. This is primarily due to the specific properties of the semiconductor material, especially the distance between the valence band and the conduction band, called the band-gap. Any photon of light with an energy less than this distance fails to excite the electron in a higher state (to move it from the valence band to the conduction band), so the photon passes without being captured, and the phenomenon is called non-absorption. In addition, photons with a higher energy than the band-gap manage to excite the electrons with all their energy, but later the electrons return to their default level of the conduction band, and the excess energy is transformed into heat and lost. This phenomenon is called thermal relaxation or thermalization, and leads to the heating of the photovoltaic cell, which has negative effects on their operation, as will be explained in the next section.

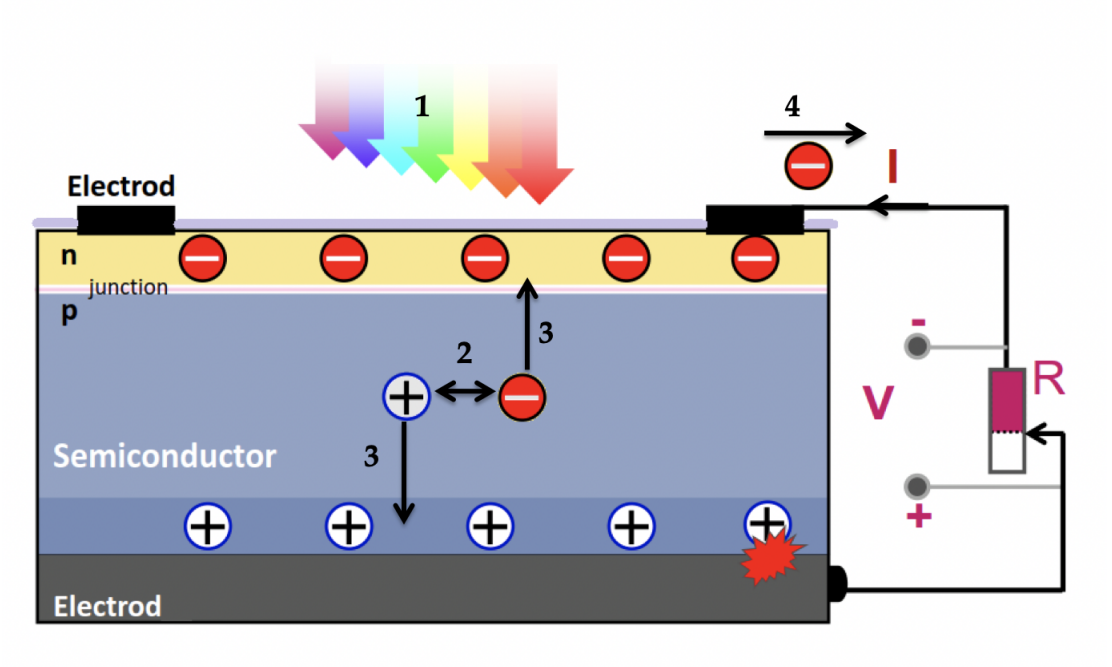

FIGURE 2.4: Schematic diagram of how a PV cell works [10]

Figure 2.5 illustrates the share of incident solar radiation that can be extracted in the form of electricity from a silicon cell. The green area represents the excess energy of the photons, which leads to thermalization, and the gray area illustrates the non-absorption, i.e. photons with too long a wavelength, so with insufficient energy to excite the electrons. The red line indicates the specific band-gap, which in this case silicon is 1.12 eV, which corresponds to a wavelength of λ Si = 1107 μm.

In addition to the intrinsic losses of semiconductor material, there are a number of other factors that contribute to decreased PV cell efficiency [11]:

- Light reflection at the surface of the module;
- Recombination of electron-gap pairs before they are separated;
- Serial resistances of the circuit, Joule effect;
- Shading caused by electrodes and conductive bars;
- Degradation caused by environmental conditions - high temperatures, wind, humidity.

The next section will investigate the main reason for the decrease in the electrical efficiency of the PV cell, namely the increase in operating temperature.

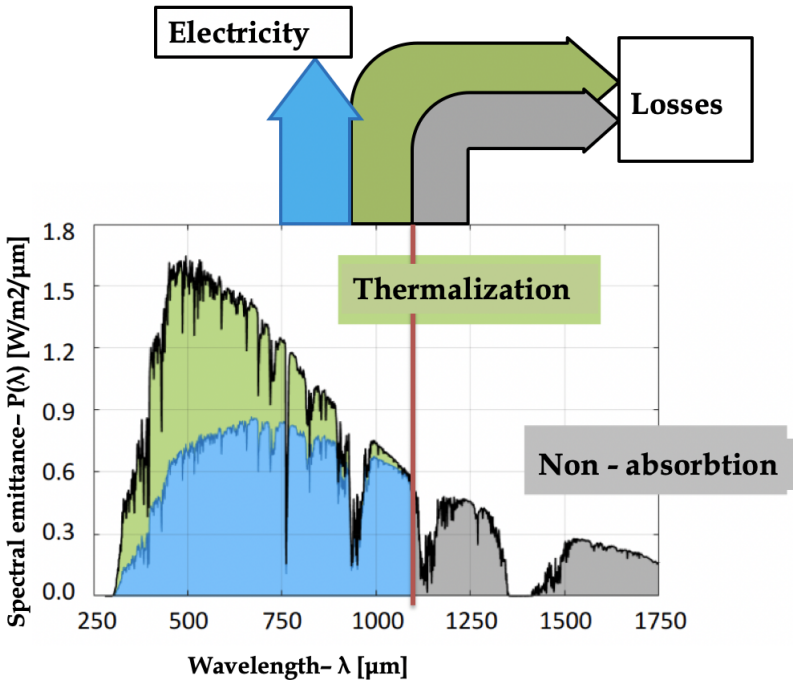

FIGURE 2.5: Sankey diagram for a PV cell

2.1.3 The influence of high temperatures on the PV cell

The operating temperature is one of the most important parameters and closely related to the electrical efficiency of the PV panel. The most important feature of hybrid PVT systems is the cooling capacity of photovoltaic cells. To better understand the benefits of PV panel cooling, it is important to establish the relationship between operating temperature and system efficiency.

In a PV cell, in addition to high ambient temperatures, heat is also produced by internal physical phenomena, as follows [11] [10]:

- Non-absorption of photons with less energy than the band-gap of the material;
- Radiative or Auger recombination of electron-pair pairs;
- Joule effect on the current passing through the resistance at the junction p-n.

The electrical efficiency of PV cells decreases with increasing operating temperature. In other words, while the material is heating up, the production of electricity in the circuit is reduced. Numerous analytical models have been proposed to express the dependence of electrical efficiency as a function of operating temperature. A comprehensive

review was carried out by Dubey and Sarvaiya (2014) [12]. One of the first correlations between efficiency and temperature, still used today, was proposed by Evans and Florschuetz in 1977 [13], and is presented in Equation 2.2.

$$\eta_{el} = \eta_{ref}[1 - \beta_r(T_c - T_r) \tag{2.2}$$

where η_{el} is the electrical efficiency of the cell at temperature T_c, η_{ref} is the reference electrical efficiency of the cell evaluated at the reference temperature T_r, and β_r is the temperature coefficient.

The temperature coefficient β_r is has a specific value for each type of semiconductor material. For mono and poly crystalline silicone cells, both the experimental data in the literature ([14]–[17]) and the specifications of PV cell manufacturers indicate a temperature coefficient between 0.3% -0.9% above the standard operating temperature (25^{o}C). Another commonly used semiconductor is copper-indium gallium selenide (CIGS), which shows a decrease in efficiency of 0.29% -0.53% per degree Celsius ([14], [18]). Another study [19] on cadmium tellurium semiconductor (CdTe) indicates a decrease in efficiency of 0.17% per degree Celsius. These data are summarized in Table 2.1 below.

Semiconductor	**Temperature coefficient (%/^{o}C)**
Mono-c-SI	0.3-0.9
Multi-c-SI	0.3-0.9
a-Si	0.2
a-Si/μc-SI	0.26
CIGS	0.29-0.53
CdTe	0.17-0.25

TABLE 2.1: Temperature coefficients for various types of cells [14]–[16], [18]–[20]

The variation of the electrical parameters in a mono-crystalline silicon cell at different operating temperatures is illustrated in the graphs below. Figure 2.6 shows the variation of the IV curve at temperatures of -25^{o}C, 25^{o}C, 75^{o}C. A small increase in the intensity of the electric current (I) can be observed with the increase of the temperature. On the other hand, the voltage drop (V) is much more significant. In the case of electric power, Figure 2.7 illustrates the decrease of the maximum power of the system with the same temperature variation as previously.

To explain why the increase in operating temperature causes a decrease in power in

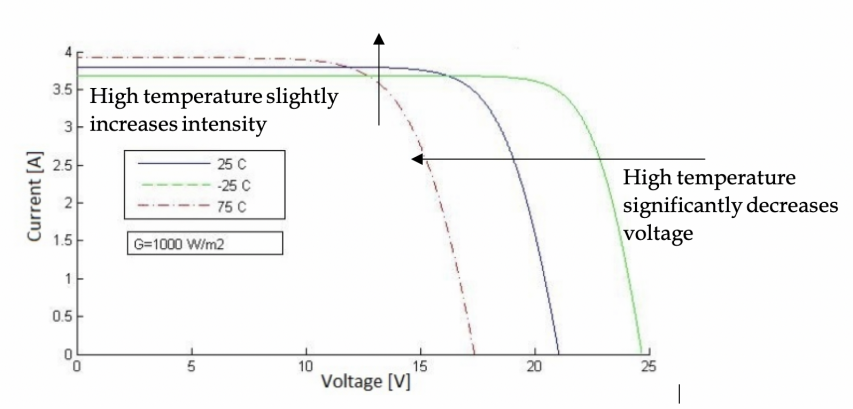

FIGURE 2.6: The effect of temperature on the IV curve

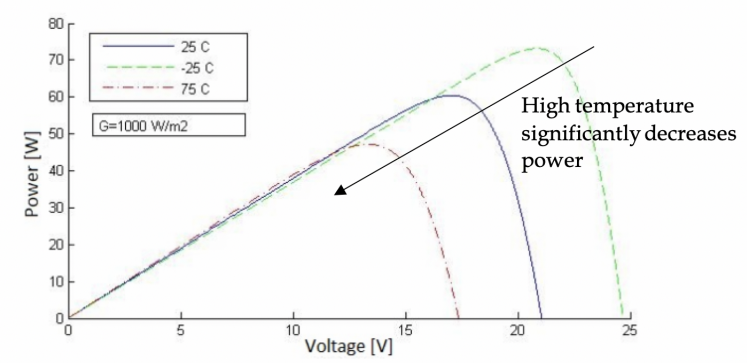

FIGURE 2.7: The effect of temperature on the PV curve

a PV cell, the physical phenomena that take place within the cell can be broken down into the following components:

1. Increased thermal vibrations in the semiconductor structure in the form of phonons, which leads to lateral dispersion of particles. This creates additional collisions between the load-bearing particles.

2. Decreased carrier mobility. Mobility (μ) is the ability of a load-bearing particle to move in an environment as an effect of an electric field, and is defined as the ratio between the average speed of the particle (v_p) and the intensity of the electric field (ξ):

$$\mu = \frac{v_p}{\xi} \tag{2.3}$$

Within the same material, the positive and negative particles have different values of mobility. At standard test temperature (25^{o}C), the negative particles (electrons) have mobility μ_n of 1360 cm^{2}V^{-1}s^{-1}, and the positive particles (gaps) μ_p of 450

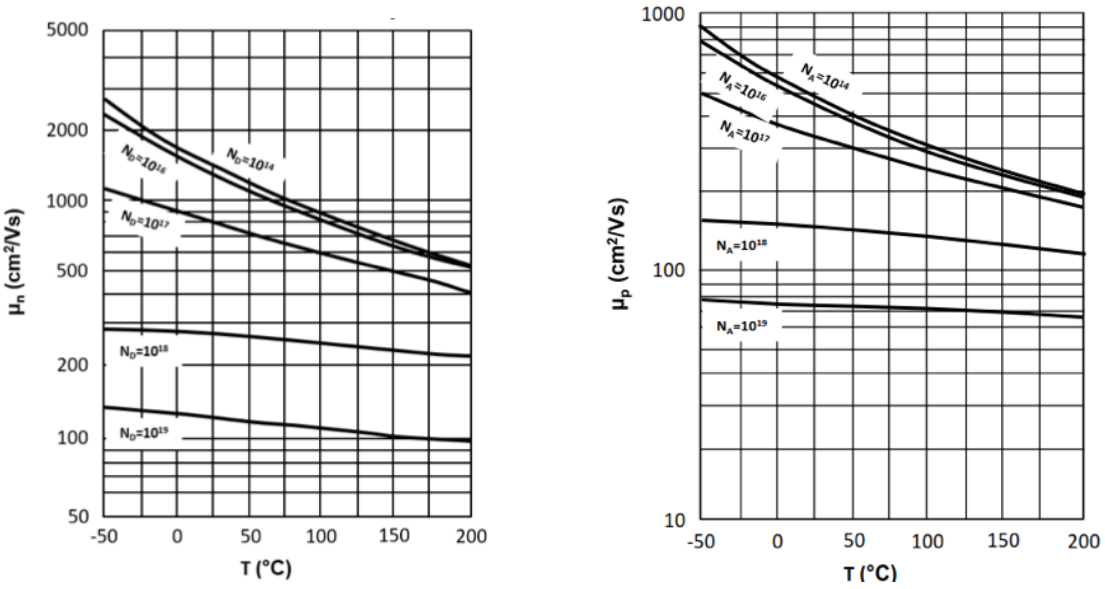

(A) The effect of temperature on the mobility of electrons

(B) The effect of temperature on the mobility of holes

FIGURE 2.8: The effect of temperature on the mobility for various doping concentrations [21]

cm2V-1s-1. The relationship between mobility and temperature is inversely proportional:

$$\mu \propto T^{-2/3} \tag{2.4}$$

This effect is illustrated in Figures 2.8a and 2.8b, where it can be observed that the influence of temperature varies depending on the level of particle doping. In other words, for a highly doped cell with a concentration of 10^{19} particles per cm^3, the effect of temperature on particle mobility is not significant.

3. The internal voltage at the p-n junction decreases, therefore the ability to separate the electrons from the gaps decreases, which leads to a smaller potential difference, and a weaker current generated.

In addition to the negative effect on power in the electrical circuit, discussed above, the high operating temperatures in a PV panel also has physical effects of wear on the component materials. An extensive experimental study on the damage mechanisms of PV panels, performed on 1740 panels [22] indicates that 39% of the damage phenomena are associated with high operating temperatures. Mainly, two recurring phenomena occur:

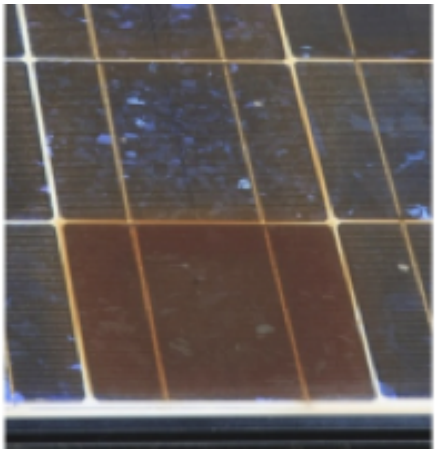

(A) Burning of metal contacts

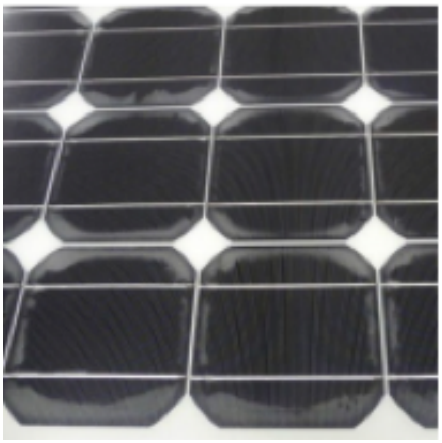

(B) Delamination of the semiconductor material

FIGURE 2.9: Effects of thermal stress in a PV cell

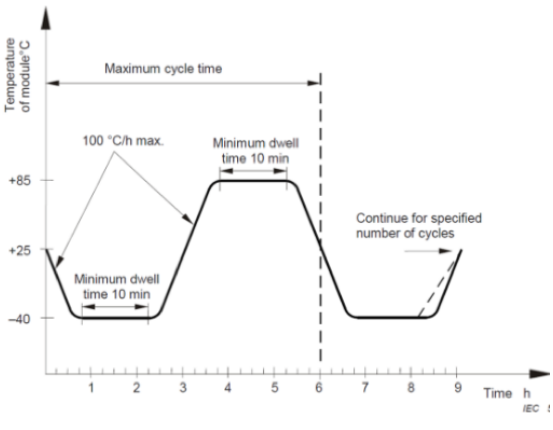

(A) Testing standards of PV panels

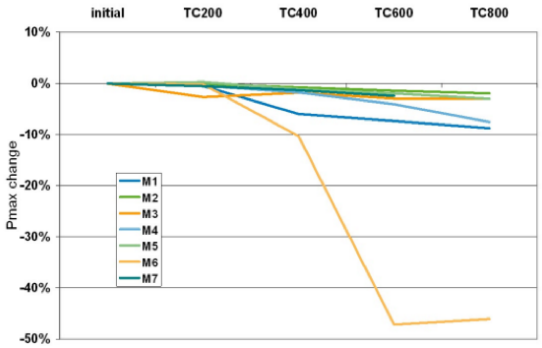

(B) The decrease of maximum power for different panels after a number of thermal cycles [22]

FIGURE 2.10: Thermal heating-cooling cycles

1. Local overheating of the components induces thermal stress and can lead to burning of metal contacts (Figure 2.9a) or delamination of the semiconductor material (Figure 2.9b);

2. The thermal heating-cooling cycles also induce thermo-mechanical stress in the components. Cyclic temperature tests are part of the testing standards of PV panels, and are defined by IEC 61215: 2005, Figure 2.10a. One study [22] shows that for 6 out of 7 panels, at 200, 400, 600 and 800 thermal cycles, the maximum power decreases between 3% and 9% (Figure 2.10b).

2.2 PVT collectors

There is already great interest and progress in the field of solar energy. Currently, the solar energy technologies can be broadly classified into solar thermal (ST) collectors and photovoltaic (PV) collectors. Solar thermal collectors convert solar radiation into useful heat, a concept that has been used for centuries for heating water. Photovoltaic systems employ the photovoltaic effect which was first discovered in 1839 [23], which consists in the generation of an electric potential in a material exposed to light radiation In this way, solar radiation is converted into electricity. Both of these technologies have already found popularity for a wide range of domestic and industrial applications. The solar thermal collectors can be employed for space heating and domestic hot water directly for the end user or integrated in district heating systems, solar assisted air conditioning (especially due to the incidence of high ambient temperatures with the need for cooling down inside homes), swimming pools heating or water desalination. PV systems can be used to produce electrical energy off grid, connected to the local electricity grid, or for storage (in batteries or fuel cells).

In order to take full advantage of both technologies, hybrid photovoltaic-thermal (PVT) equipments have been developed. They combine and maximize the benefits of the two traditional types of energy extraction technologies into one single equipment, producing simultaneously electrical and thermal energy (Figure 2.11). PVT panels can be labeled as micro-cogeneration technology.

FIGURE 2.11: Schematic diagram of PVT components

2.2.1 Main characteristics of PVT panels

Combining ST and PV technologies into a hybrid PVT panel has a number of advantages:

- First of all, significant heat losses occur during the photovoltaic reactions. Most commercial PV cells use silicone as the semi-conductor material, which is very convenient due to it being the second most abundant material in the Earth's mass. However, crystalline silicone has a band-gap of 1.1 eV. Any photon of light with less energy will not be able to move the electrons and energy cannot be produced. In addition, photons of light with higher energy than the bandgap would move the electrons but the surplus energy is lost, typically in the form of thermal energy. Thus, harvesting the thermal energy from the collectors leads to an increase the operation capacity of the solar collector and an improvemement the rate of solar energy conversion.

- The PV cells efficiency falls with the increase of the operating temperature, as discussed in a previous section. As the cell heats up, the electrical power released in the circuit decreases. Many analytical models have been proposed for quantifying the dependence of the power efficiency on the operating temperature of various cells, with a comprehensive review carried out by Dubey, Sarvaiya and Seshadri [12]. One simple example of correlation for the relationship between efficiency and temperature was proposed by Florschuetz [13] is shown in the Equation 2.2. Consequently, PV cells from PVT collectors have an electrical efficiency of about 4% -12% higher than the same cell in a standalone PVc ollector [24].

- The thermal energy extracted from the collector can be used for various applications (residential or industrial) and thus a higher global energy efficiency of the entire energy system can be obtained by combining the two components. The thermal efficiency of solar collectors η_{th} is defined by the equation below [25]:

$$\eta_{th} = \frac{Q_u}{G_{STC} A_c} \tag{2.5}$$

Where Q_u is the useful thermal energy obtained, $G_{STC}$is the solar radiation on the collector at STC and A_c is the area of the collector. η_{el} is the electrical efficiency of the PV collector at STC, shown in Equation 2.6. The standard test conditions STC are defined by: irradiance G=1000 W/m^2, cell temperature t=25^{o}C and air mass AM=1.5.

$$\eta_{el} = \frac{P_{STC}}{G_{STC} A_c} \tag{2.6}$$

where P_{STC} is the nominal power of the PV collector at STC, and it can be defined as the voltage V_{STC} times the current I_{STC} at the point of maximum power during the test. For the hybrid collector the global efficiency is η_{gl} and can be defined as the sum between the thermal and electrical efficiency:

$$\eta_{gl} = \eta_{el} + \eta_{th} \tag{2.7}$$

Thus, in the energy flow diagram of the hybrid system, shown in Figure 2.12, there is an additional thermal energy component, which did not exist in the diagram in Figure 2.5 of a simple PV system.

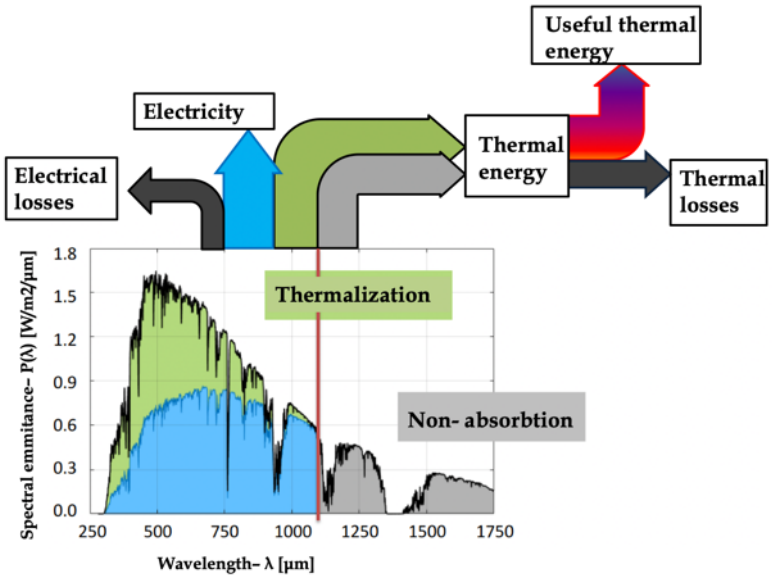

FIGURE 2.12: Sankey diagram for a PVT panel

- This technical solution is suitable for urban consumers where roof and facade space is limited, and where electricity and heat are required simultaneously.
- The installation time as well as the costs associated with installation and maintenance are significantly reduced by installing one piece of equipment as opposed to two separate ones.

The two components of a hybrid system (thermal collector and photovoltaic cell) generally have the same operating principles as separate equipment. The PV module has the role of converting solar energy into electricity through PV cells that are interconnected and encapsulated in glass or polymers for protection. The role of the thermal collectors is to capture solar energy in the form of thermal energy, and to transfer this heat to a thermal agent flowing through a system of pipes or channels. From a technical point of view, the joint can have multiple configurations. However, an essential element present in any installation is the PVT layer (Figure 2.13), which makes possible the heat transfer between the PV cell and the thermal agent.

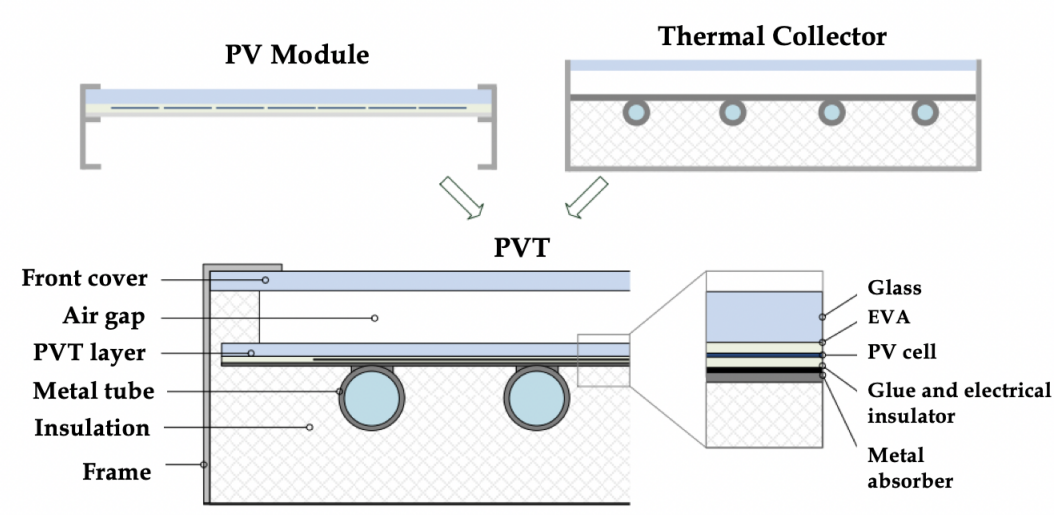

FIGURE 2.13: Schematic diagram of the components of a PVT collector [26]

2.2.2 Solar thermal component

Solar thermal collectors consist of a thermal absorber (a material with the capacity to collect solar energy), a system of pipes for the circulation of the thermal agent and an insulator material for thermal insulation. The thermal absorber is typically a thin sheet of aluminium, copper, steel, or a thermally stable polymers such as silicone, generally painted with a matte black coating in order to increase the quantity of absorbed solar radiation. The system of pipes can be circulated by air, water, an air and water mixtures, or other innovative thermal agents such as saline (brine) or refrigerants [27].

For PVT panels, liquid based collectors are the most suitable mostly due to the fact

that air collectors have as a main application space heating, which is usually not required in hot climates, except for particular applications such as hotels, hospitals, or industrial applications.[27]. The thermal efficiency of the ST ranges between 45% -80% [28] depending on the operating conditions and the constructive configuration, with a maximum value of about 97%, obtained in a large collector with concentrating mirrors [29]. A commercial flat plate solar collector has a typical thermal efficiency is 60-70%[30].

Solar thermal collectors can be classified according to various criteria:

1. According to the type of thermal agent:
   (a) Air-based
   (b) Liquid-based
   (c) Air-liquid mix
   (d) Phase-changing materials (PCM)

   Air-based systems can be natural or forced convection, the latter having a better heat transfer coefficient than natural convection, but have the disadvantage of requiring external energy for ventilation. In the literature, it has been found that the thermal efficiency of these systems varies between 38% and 75% [31]. The main application of air circulation systems is ventilation, room heating or hot water preheating systems.

   Liquid-based systems are generally more efficient than air-based systems, due to a considerably higher heat transfer coefficient and higher heat capacity. The liquid agent can be circulated by gravity or by pumping, and the power required for this is less than that for a fan in an air-based system [31]. The thermal agent may be water, salt water, or a mixture of glycol and water. There are also bi-fluid configurations, consisting of a water-air mixture, but they are not developed due to the high production costs. The thermal efficiency of liquid-based systems varies in the literature between 60% and 80% [28].

   A novelty in research is the use of phase change materials as a thermal agent, especially those with solid-liquid transformation, such as paraffin wax, calcium chloride hexahydrate, sodium sulfate decahydrate (Glauber's salt), or various nanofluids [32]. Although these materials are relatively affordable, technical difficulties in

processing, encapsulating and maintaining the systems to ensure proper operation lead to high costs [33].

2. According to the configuration of the cooling system:

   The solar thermal panel can be configured as a flat plate (Figure 2.14a), or with evacuated tubes (Figure 2.14b), depending on the purpose of the application and local conditions. The use of concentrating mirrors is also possible to amplify the solar ration in parabolic systems (Figure 2.14c).

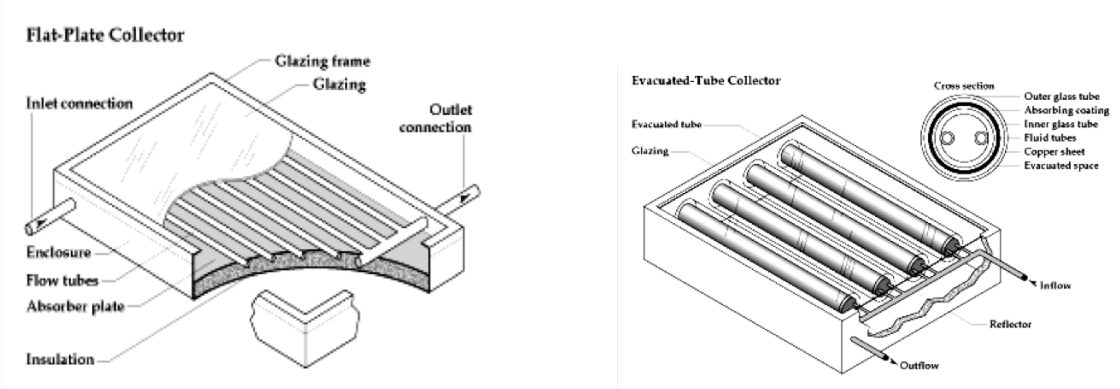

(A) Flat plate collector

(B) Evacuated tubes collector

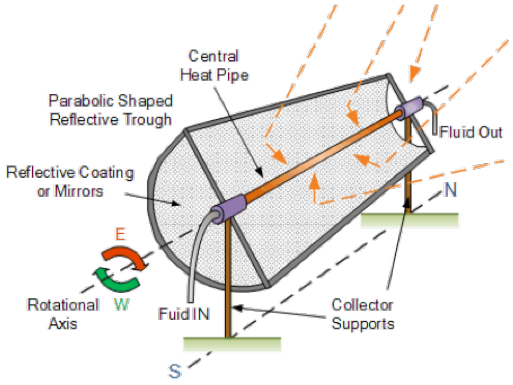

(C) Parabolic collector

FIGURE 2.14: Types of solar thermal collectors

3. According to the quality of thermal energy:

   (a) Low temperature - under 50^oC

   (b) Medium temperature - between 50^oC and 80^oC

   (c) High temperature - above 80^oC

For residential consumers, solar collectors reach medium temperatures, which can cover the need for domestic hot water for consumption, heating, or even cold generation for high-capacity systems (usually collectors with concentrating mirrors). Depending on the thermal level of the energy produced, industrial applications can be: technological processes in the agricultural field, product drying, water distillation, processing in the food industry, heating of industrial spaces. Figure 2.15 shows the possible applications of the heat produced by the solar thermal component of a PVT system depending on the temperature level.

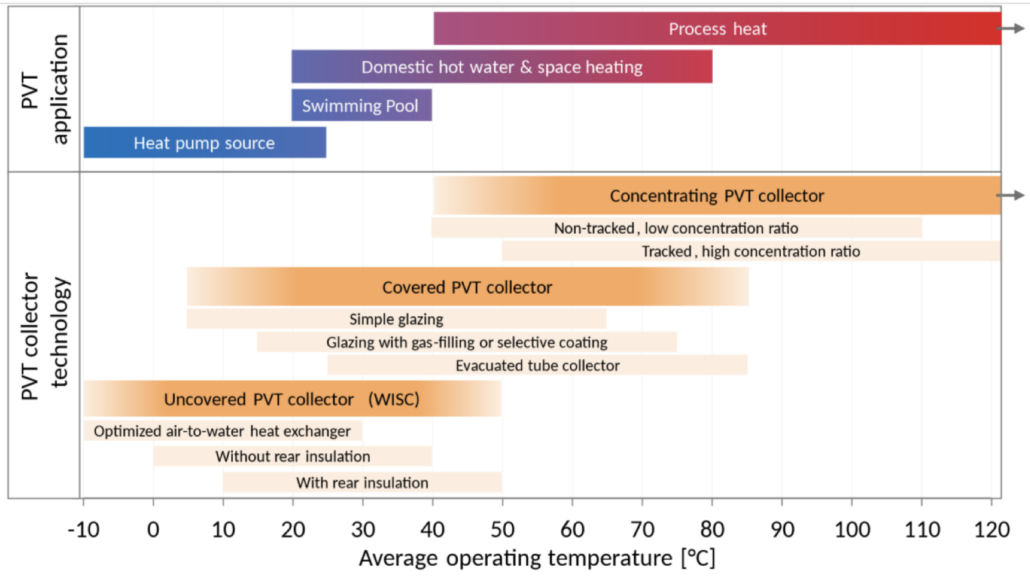

FIGURE 2.15: Temperature dependent applications [34]

At the end of 2016, the total installed solar thermal energy capacity globally was 456 GWth [30]. Production in the same year was 375 TWh, leading to a reduction in CO_2 emissions by 40.3 tonnes, compared to an equivalent production from fossil fuels [30]. A large part of the capacity is covered by individual consumers, up to 90%, but also large farms are being developed for central heating.

2.2.3 Photovoltaic component

The photovoltaic component comes in a wide variety of typologies and classifications. In terms of geometric configuration, the most common types of PV panels are flat, but there are other configurations, such as concentrated PV panels (CPV), which use

a system of mirrors to concentrate sunlight, and which are the most commonly recommended for arid or tropical climates where the solar intensity is constantly strong, to justify the high initial investment.

Traditionally, photovoltaic cells are made of silicon, either in monocrystalline, polycrystalline or amorphous form. These are predominant in the market, making up 95% of the total production of PV panels in 2020. The mono-crystalline cells cover about 66% of the total market (compared to 45% in 2018) [35]. A new generation of cells are made of a thin film with a thickness of a few micrometers, which has the advantage of being flexible and easily incorporated into various building materials (e.g. glass, facade). The third generation of cells uses either ink, special types of paint, plastic, or organic matter. The National Renewable Energy Laboratory has an extensive database, constantly updated to monitor the performance of the latest technologies. Figure 2.16 illustrates a graph of the efficiencies of different cell types over time; it can be seen that a record experimental efficiency of 48% was obtained by a tandem concentrator with 4 junctions [32].

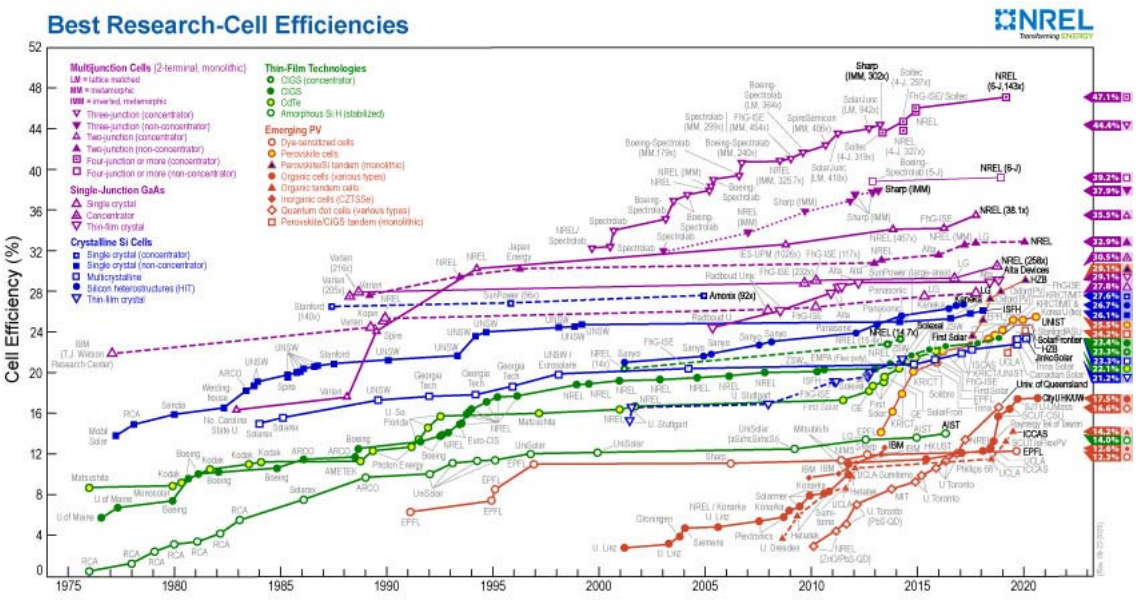

FIGURE 2.16: Best research PV cells efficiency [36]

Table 2.2 shows the most common and studied cell types, along with their theoretical performance in the laboratory and on the market, as well as the main fields of applicability. At the end of 2016, PV panels had an installed capacity of 586 GW [37], producing 1.8% of total global energy. The year 2019 also saw an increase of new installations of

798 GW, representing an increase of 20% compared to the previous year, which resulted in a significant decrease in the price of modules.

Cell	Theoretical efficiency	Lab efficiency	Real efficiency	Applications
m-SI	27%	24.7%	14-16%	Large sized roof and facade panels, low power appliances, aerospatial applications
p-SI	27%	19.8%	12-14%	Large sized roof and facade panels, appliances
a-Si	25%	13%	6-8%	Small sized roof and facade panels, low power appliances
GaAs	29%	27.5%	18-20%	Concentrated PV systems, aerospatial applications
CIGS	27.5%	18.2%	10-12%	Small sized roof and facade panels, low power appliances
CdTe	28.5%	16%	8%	Building integrated modules

TABLE 2.2: Efficiency and applications of PV cells

2.2.4 PVT classification and applications

The configuration of a PVT panel depends a number of factors, among which the most important are: the type of thermal agent, geometry and properties of the cooling system (materials, pipe diameter), photovoltaic cell type, presence / absence of antireflective layer (glazed / unglazed). Various reviews have been carried out in the literature on the possible types and configurations of PVT panels [28], [32], [38]. Generally, the final product is defined by the type of solar collector chosen and the type of PV cell, resulting in a large number of possible permutations. A non-exhaustive classification of the types of PVT systems is illustrated in Figure 2.17 below.

As with individual PV panels, c-Si cells are also most commonly used for PVT systems [26]. Mono-crystalline cells have a higher coefficient of solar absorption than poly-crystalline cells. Thin film technologies have a lower temperature coefficient, and are therefore suitable for high temperature applications [26]. For systems with solar concentration which operate at very high temperatures, cell cooling is essential, so PVT applications in this area are suitable.

Depending on the chosen application and the consumers' energy priorities, three PVT configuration can be identified. In the first instance, thermal energy can be considered as the main useful product for various applications (space heating, water, ventilation, etc.). Conventionally, solar thermal systems use external electricity to pump and

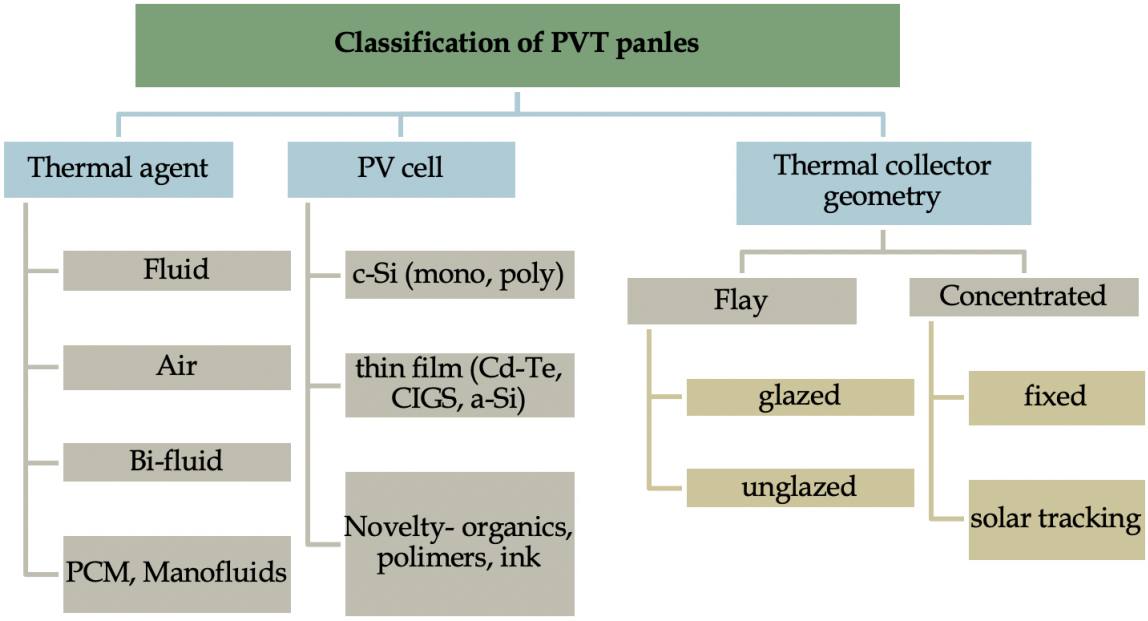

FIGURE 2.17: Classification of PVT panels [26]

circulate fluid through pipes. By integrating PV cells, the need to use an external source is eliminated, so the system is independent. In other applications, where electricity is the main useful product, the heating system can be installed for the sole purpose of cooling the mode and thus improving the efficiency of the cell. To maximize the benefits of the two technologies, it is possible to extract both thermal and electrical energy, and use both by consumers. This configuration is the most beneficial and is the main subject of this study.

In terms of applications, PVT panels are ideal in systems where electricity and heat can be used simultaneously. Unlike individual PV modules, which can be installed in large PV parks, PVT systems are more suitable close to the consumer, to avoid considerable losses. which take place in the process of thermal energy transportation. Thus, integration in the urban or industrial environment, directly to the consumer, is the most common.

2.2.5 Current research and technological development

Several studies have been conducted to analyze PVT systems compared to individual PV systems and solar collectors. Euh et al. [39] obtained for an experimental PVT system without transparent coating a 13% lower efficiency on the thermal side, but a 0.8%

higher electrical efficiency for electrical conversion compared to the two separate equipments. The total conversion efficiency of the system can increase by up to 40% [40]. The benefit of PV cell cooling has been studied experimentally through various cooling configurations, and an improvement in electrical efficiency has been obtained from 13.9% to 15.9% [41].

For a 3 bedroom family home, with 4 consumers, located in Great Britain, it was estimated that a 15 m^2 PVT system covers 36% of the hot water demand and 51% of the electricity [42], [43]. A dynamic simulation over one year was performed to compare the energy coverage for three types of collectors, unglazed, with a protective layer (glazed), or with two protective layers double glazed [44]. The results, illustrated in Figure 2.18, indicate a high thermal performance for double glazed collectors, and a coverage of up to 100% electrical demand of unglazed collectors.

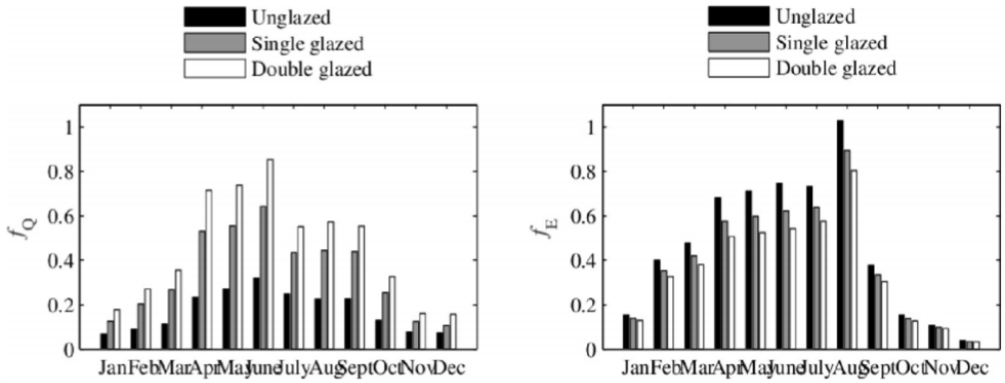

FIGURE 2.18: Electrical and thermal coverage of a PVT system in UK [44]

An extensive study [45] examines the environmental aspects of PVT systems, with reference to the energy recovery period required for their production, and the CO_2 emissions associated with the production process. The results indicate energy recovery periods used for their production between 1 and 14 years depending on the configuration (BAPVT, BIPVT, CPVT). Life cycle analysis - LCA (LCA) is also an important indicator, and is performed for different types of modules, illustrating a wide variety of levels of environmental impact depending on materials and production methods.

The research of PVT collectors first started in the 1970s [46]. Since then, significant progress has been made and important work has been dedicated towards increasing their performance by studying and optimising their constructive and operational parameters.

The weather condition (wind speed, solar radiation, ambient temperature), and the constructive parameters of the PVT collectors (channel type and width, insulation, packing factor, glazing) are some of the main factors that impact the performance. The choice of geometry in terms of widths and lengths is also an important factor influencing the energy output.

Major research has been dedicated to the evaluation of the impact of various geometrical configurations on the electrical and thermal output, and consequently the global energy performance [47], [48]. Various configurations of the piping system are possible (Figure 2.19), and the most commonly used are 'direct flow' (or 'harp design'), and 'serpentine flow'. A mathematical study [47] on a p-Si cell PVT panel indicates that the most thermally efficient design is the spiral configuration, with a thermal efficiency of 68%, and the lowest efficiency was observed to be 45% for the serpentine type design.

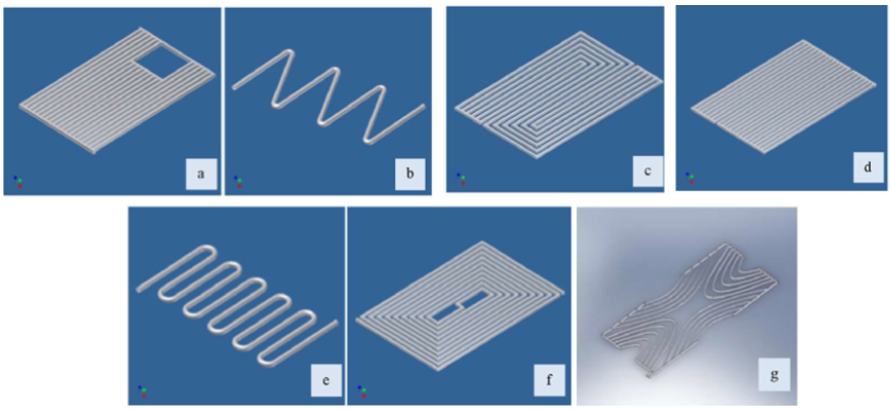

FIGURE 2.19: Types of pipe configurations a)direct flow b)serpentine design c)parallel serpentine design d)modified parallel serpentine design e)oscilatorry flow f)spiral flow g)web design [47]

The pressure loss that occurs with the thermal agent has an important impact on the overall efficiency of the system. A higher pressure drop means a higher pumping energy requirement for a given flow. Experimental tests were performed on aluminium collectors, comparing different classical harp and coil geometries with a new model, called Bionic configuration (Figure 2.20, right), and for the latter a pressure loss of 400% was obtained. than for serpentine, and 50% smaller than the harp [49]. The bionic model was created based on the concepts of fractal geometry, inspired by models in nature (the system of blood vessels or leaf veins), in order to obtain a uniform flow and minimize pressure losses.

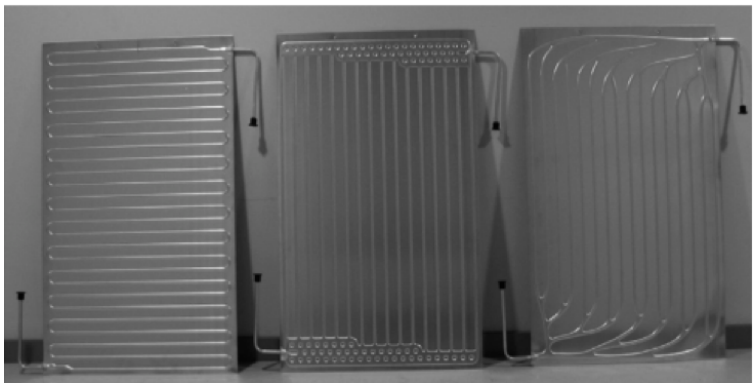

FIGURE 2.20: Experimentally tested configurations for assessing the pressure loss [49]

Fractal geometry has been studied and successfully applied in various heat exchangers [50], [51]. Fractal-type channels (Figure 2.21) can outperform the hydraulic performance of traditional coil or harp models due to uniform flow and lack of steep bifurcations. A review study [51] gathered multiple promising results, with up to 80% improvements in fractal heat exchangers compared to classical geometries. Most are based on theoretical and numerical studies, as the main disadvantage of fractal models is the difficulty of manufacturing the complex geometry. However, there is a growing interest in this area, especially in the future perspective of the commercial use of 3D printing methods.

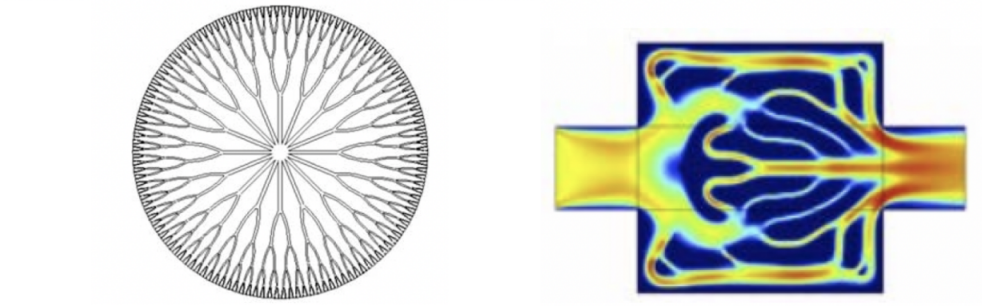

FIGURE 2.21: A)Circular fractal heat exchanger B)Optimized topology of a heat exchanger [52], [53]

The collector material is an important component, as it transfers solar thermal energy to the heating medium. The thermal conductivity of the material must be as high as possible to allow the passage of heat, and the specific heat must be low to allow rapid thermal reactions with changing operating conditions [28]. The most commonly used materials are illustrated in Table 2.3. Copper has the most suitable properties for this

application, and the older generations of solar collectors are made mainly of copper. However, due to the high price in recent years (an increase of about 400% between 2004 and 2012), aluminium is also used, having a cost 4 times lower [54].

Material	Thickness (mm)	Density (kg/m^2)	Thermal conductivity (W/mK)	Specific heat (J/kgK)
Copper	0.3	8920	380	350
Alluminium	1	2700	160	900
Steel	2	7860	50	450
Polymer	2-3	900-1500	0.2-0.8	1200-1800

TABLE 2.3: Thermal collector material properties

The section of the collector channels has also been studied, and is closely related to the manufacturing process and the choice of material. Three types of channels were studied and compared in a study by Aste et al. [28], illustrated in Figure 2.22, highlighting the advantages and disadvantages of each (Table 2.4).

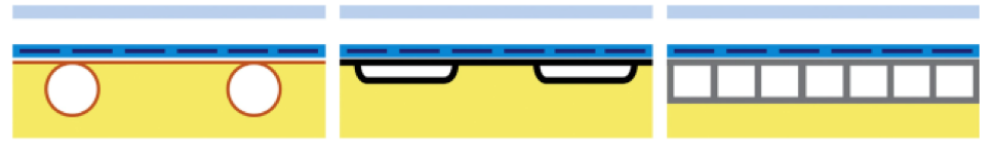

FIGURE 2.22: Tubular, trapezoidal and rectangular channel collector [28]

Configuration	Material (mm)	Geometry (kg/m^2)	Advantages (W/mK)	Disadvantages (J/kgK)
Sheet and tube	Copper, Aluminium	Serpentine, Harp	Easy fabrication Thin materials	Small contact surface Variable costs
Roll bond	Alluminium	Any	Geometric flexibility Thin materials	1mm thickness
Rectangular	Polymer	Harp	Large contact surface	Special components required

TABLE 2.4: Advantages and disadvantages of tubular, trapezoidal and rectangular channel collectors [28]

The entire panel can be in direct contact with the environment, without a protective layer (unglazed), or protected by one or more transparent layers (glazed). In the case of an uncovered collector, the incident radiation is higher, but simultaneously the thermal losses through convection and radiation are increased. That is why a transparent protective layer is usually used, most often glass, which acts as a unidirectional filter, being characterized by high transparency in the visible spectrum, and opacity for longer wavelengths, in the infrared area. Alternatives to glass are polymers such

as polycarbonate or polyvinyl fluoride, but which show considerable thermal and mechanical degradation over the life of the module [28].

An active study topic is the introduction of a low emissivity layer, which aims to reduce radiation losses, such as tin oxide, indium oxide, tin oxide and zinc. A detailed study on the effect of various types of low-e coatings [26] indicates, in most cases, a thermal gain at the expense of an electrical loss. Another study [55] on a low emissivity layer of SiO_2 indicates a decrease in emissivity from 80% to 20%. This, in combination with an antireflective layer, leads to an increase in both thermal and electrical production, although only by 1% in the latter.

In general, when introducing protective or low-emissivity layers, there is a trade-off between thermal and electrical efficiency. Figure 2.23 illustrates a comparison of gross electricity and heat production for climatic conditions in Würzburg, Germany [26] for five types of systems: simple PV systems, thermal collectors, and three types of PVT solutions, without external protection, with glass state and with a layer of glass and low-emissivity coating. It can be observed that, with the introduction of each layer, there is gain on the thermal side, but decreases the electricity production. This is due to an increased thermal and radiative insulation, respectively to the increase of the spectral losses by reflection at the surface of the module.

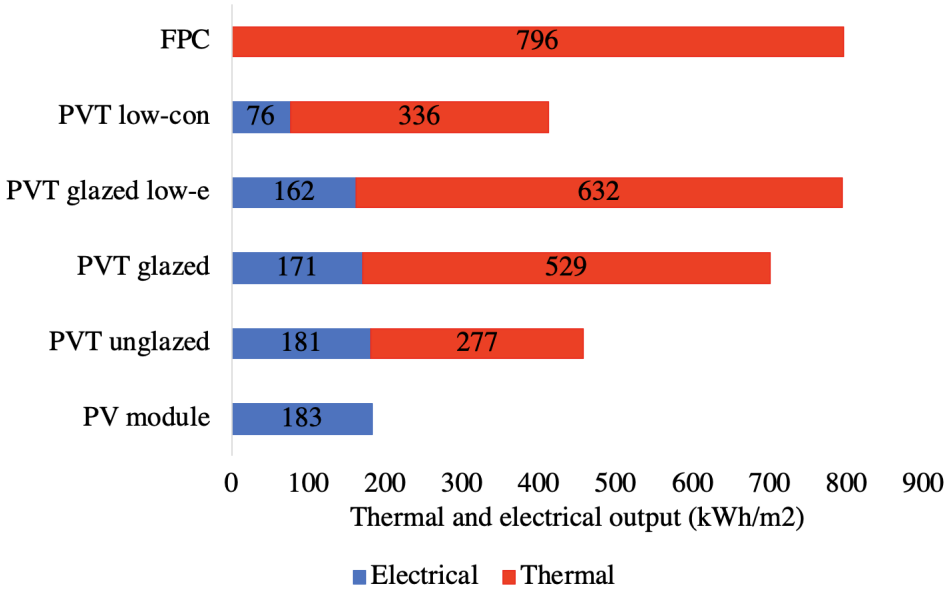

FIGURE 2.23: Thermal and electrical output for various collectors at a reference temperature of 25^{o}C [26]

The type of connection between the photovoltaic cell layer and the thermal collector

is also an important aspect to consider. The connection can be achieved by gluing with a thermo-conductive adhesive, which is resistant to high temperatures. When applying the adhesive by this method, air bubbles may appear, resulting in a non-homogeneous transfer surface, and at a low heat transfer coefficient [56]. Another solution is the lamination in a single component of all the elements (glass, PV layer, electrical insulation, thermal collector), and can bring a thermal improvement of 10% compared to the adhesive connection [57]. The disadvantages of lamination are the occurrence of possible deformations due to the different coefficients of expansion of the component elements, and the technological difficulty to achieve the lamination for sheet and tube type systems.

Other aspects that can be considered for optimizing the design of a hybrid solar collector are the flow of thermal agent, the type of electrical and thermal insulation, the diameter and distance between the collector tubes, the series or parallel connection of the cells, the level of cell doping . All these represent the optimization parameters with impact on the design and final performance of a PVT system.

Multiple parametric studies have been published in the literature on the topic of PVT collectors, varying some constructive parameters, such as the packing factor of the PV layer [58], the flow rate [59], tube spacing [60], tilt angle [58], glazing [44] and thickness of insulation [60]. Most studies indicate that the best performance is achieved with a compromise between the thermal performance and electrical performance. A study carried out a parametric analysis on a PV collector combined with a phase changing material (PCM), and showed that every 100 W/m^2 increase in solar radiation can lead to about a 5^oC increase in peak temperature. The results indicate that the melting point of the PCM should be higher than ambient temperature [61]. Another study by [62] carried out an optimization of a individual panel from the point of view of exergetic efficiency using a muti-objective optimization. This was done in terms of inlet temperature, air gap, mass flow rate, thickness and insulation thickness, and it found the optimum design for three PVT operational modes: Thermal exergy-driven Electric-driven and trade-off solution. These types of studies are generally based on a numerical model of standalone collectors.

Other important factors that impact the overall performance are the thermal parameters of the full PVT system, especially the temperature of the liquid at the inlet of the

collector, which has the role of cooling down the PV cell and collecting the excess heat, and which in turn is dependant on the temperature of the liquid at the outlet of the thermal storage tank. The thermal storage tank temperature is influenced several factors: type of tank and heat exchanger, volume of tank, water draw (which in turn is determined by the rate of domestic hot water consumption) and the cold water main temperature that replaces the water drawn from the tank [44]. An interesting parameter is the rate of consumption of the end user, not only in terms of total daily quantity, but also the distribution over the course of the day (also referred to as the demand curve). The daily demand curve can vary significantly depending on the type of consumer (offices, schools, household, industrial). The impact of the type of consumer on the efficiency of the system is one of the topics covered by this research.

An interesting paper [63] investigated the effects of the consumer behaviour on the efficiency of a solar thermal system located in South Africa. The results revealed that even small behavioural changes can cause a significant efficiency improvement. Another parametric study of a full system [64] investigates in terms of cost savings a solar-heating-and-cooling solution for a detached single-family household in hot climates. Another research [65] performed a parametric study of a solar-assisted house heating system coupled with a seasonal underground thermal energy storage tank, evaluating in terms of annual energy production the variation of some of the main system parameters, such as the insulation thickness of the tank and the size of the tank. A parametric study on a solar cooling system was carried out for Athens, Greece [66], and after optimisation it achieved a solar coverage ratio up to 89.85%. A PV system parametric was also carried out from a technical-economical point of view [67], and it investigates the impact of the weather, system cost, price of electricity, location, electrical specifications and feed-in tariffs on the economic feasibility of a grid-connected PV-battery systems.

As explained previously, an increase in he cell temperature T_c leads to a decrease in the electrical efficiency. On the other hand, a decrease in T_c results in an improved electrical efficiency. Thus, the main factors that influence the value of this temperature are an interesting topic of research. The relationship between the thermal and electrical performance is of importance in any cogeneration system. For example, in a combined heat and power (CHP) plant, the electrical energy production increases when there is

quantitatively suitable thermal energy dissipation source [68]. Similarly, in a PVT collector, if the recovered heat is not dissipated from the storage tank, the PV cell is not cooled down, and there is a significant drop in the electrical energy efficiency, up to 15% [69]. For traditional CHP systems the relationship between the electrical and thermal performance has been widely researched [70], there is limited research on this topic for PVT collectors.

2.2.6 Integration of PVT technology in small and medium prosumer energy systems

Both PV and thermal panels have a large global installed capacity. However, despite the popularity of these two technologies used separately, there are a limited number of installations of PVT reported worldwide. Due to their novelty, little centralized data is available except for some locations. For example, in the UK there are a only a few hundred installed equipments with very limited performance monitoring data, most of them installed by the company 'Newform Energy' [71]. In France, the start-up 'DualSun' has reported to install 180 equipments around the country, and monitoring data shows that the systems cover 65% of the hot water needs of a single family house [72]. A housing complex in Switzerland has 1000 m^2 of installed PVT panels, with a capacity of 190 MWh per year. In Europe there are around 56 manufacturers that produce and install PV/T system ([34].

Due to the global trend of reducing dependence on fossil fuels, many construction projects in recent years integrate solar energy systems directly from the design stage. Thus, instead of building applied PVT (BAPVT) as exemplified in Figure 2.24a, there are more and more examples of building integrated panels (BIPVT), which are used directly as building material in facades or roofs. As opposed to having the equipment installed on a standard roof, BIPVT utilizes the technology straight from the design stages of a building, integrating it as a building technology through roofing or façade materials. (Figure 2.24b). A review by Debbarma et al. [73] identified a number of case studies that successfully use BIPVT, and an experimental study by Kim et al. [74] indicates promising results.

(A) Building applied PVT (BAPVT)

(B) Building integrated PVT (BIPVT)

FIGURE 2.24: BAPVT vs BIPVT

A particularly important emerging market segment for renewable energy is the standalone self-consumers (either businesses, schools, households). Self-consumption simply means that the production and utilization of energy are both done on-site, and this is the most efficient use renewable sources. As a result, transportation costs and electrical/thermal losses associated with it are reduces, and the intermittence of injecting renewable sources in the electrical grid is avoided. An emerging name for these self-producers is 'prosumers', which is a combination of the terms 'producer' and 'consumer'. Historically, energy prosumption is not a novel concept and can be exemplified by biomass or wood combustion. However, the business model that has been established in the modern age between energy producers and consumers has been shaped into a one way production, from energy companies towards the paying user. Thus, the concept of 'prosumers' is gaining a fresh outlook and is also being enhanced by the 21st century increased social responsibility. More and more consumers prefer to produce their own clean renewable energy, driven by various motivations:

- Independence from the regulated grid and protection against the fluctuation of energy prices;
- Reduction of energy losses and transport costs;

- Financial benefits from various governmental subsidies (i.e Feed in Tariffs, green certificates).

The term 'energy prosumer' started gaining an increased scientific interest; while in 2010 there were only 12 published papers on Science Direct that contained the term 'energy prosumer', in 2020 this number increased to 1251 papers on "Web of Science Core Collection" [75]. This indicated the fact that introducing PVT technologies on the market can be regarded as a great potential niche. Some examples of particular scenarios where integrating PVT collectors as part of the energy mix can be highly recommended and yields most benefits are enumerated below:

- New builds (energy positive or energy neutral buildings) – For individual home owners, the outcome is a reduction of utility bills and enhancing the off-grid security, while for the residential investors and developers, renewable energy is a an important selling point, despite the higher initial cost,.
- Retrofitting - replacing outdated/ defective solar thermal or PV collectors – The space is already available and the energy yield can be increased significantly by using hybrid PVT collectors instead of separate PV and ST collectors.
- Social housing – Implementing PVT collectors can significantly reduce the tenants' bills
- Schools and office buildings – Renewable energy promote and raises awareness of social responsibility but also reduces the utility bills.
- Remote areas – Implementing renewable is highly beneficial where electrical grid and district heating connection is difficult and expensive.

Also, the modern 'prosumer' is not only concerned with the on-site energy production, but is also concerned of his carbon footprint and energy consumption, aiming to optimize the balance between their own needs and the impact on the environment. As a result, a demand side management movement is also emerging, with more and more people involved advocating towards the reducing of carbon footprints. Monitoring peak production times and attempting yo to synchronies it with peak production by means of better planning strategies would make the introduction of PVT collectors even

more successful among consumers. Many novel, state of the art ideas and technologies are constantly emerging in the scientific community; however, regardless of their ingenious solutions and high efficiencies, more often than none the economical feasibility test is decisive when it comes to market scalability and penetration. This also applies to the PVT technology, which needs to bring economical benefits for consumers to adopt it.

PVT panels can be integrated into energy systems in different configurations, depending on consumer needs, climatic conditions, and the local energetic system. The most simple configuration is illustrated in Figure 2.25, and consists of a heat exchanger connected directly to the domestic hot water consumption or heating system, or both.

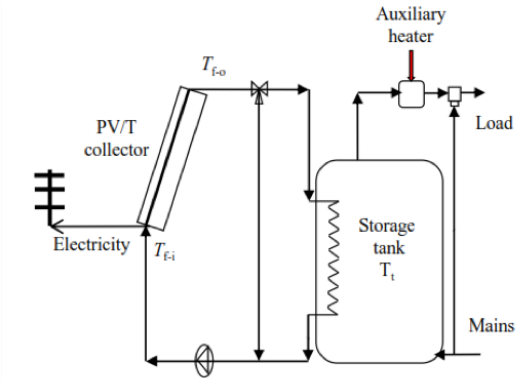

FIGURE 2.25: Basic PVT system connected through a coiled heat exchanger to the DHW/heating storage tank of a dwelling [31]

Another common solution is the coupling with a heat pump, where the solar collector acts as an evaporator (Figure 2.26). The system consists of a PVT collector, a compressor, a condenser, an expansion valve and a storage tank. The thermal agent is a coolant that evaporates from solar radiation [76]. An experimental study [77] evaluated a PVT-HP (Heat Pump) system (Figure 2.26) with 2.25 m^2 manifolds, a 150l storage tank, and R22 as coolant, and obtained a COP of 3.42 in January and 4.70 in July, weather conditions in Nanjing, China.

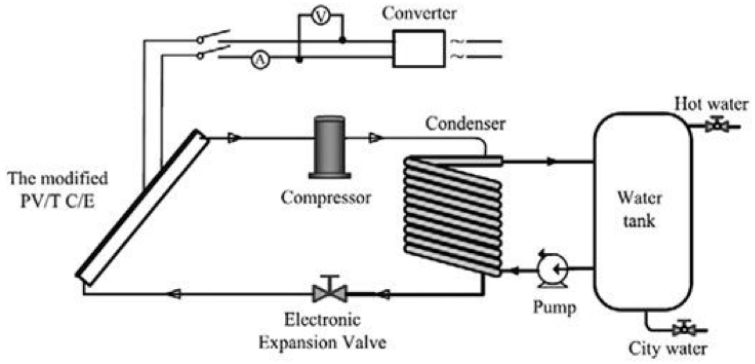

FIGURE 2.26: PVT system coupled with a heat pump [77]

In more complex systems, the geothermal source can also be introduced. This combination has the potential to reach higher temperatures and use a high percentage of renewable energy for the energy needs of a home. An example is illustrated in Figure 2.27. These systems are complex and expensive, but have the advantage of seasonal heat storage, ideal for locations with climatic variations throughout the year [78]. In this case, there is also the demand-control problem, i.e. the attempt to change the demand curve to maximize consumption during periods of production or low electricity prices. Salpakari and Lund [79] developed a non-linear energy cost optimization algorithm for a NYEB home in Helsinki, taking into account the geothermal source, the change in consumption and an integrated battery storage system, achieving an improvement in the consumption rate by 30% and reduced annual energy costs by 25%.

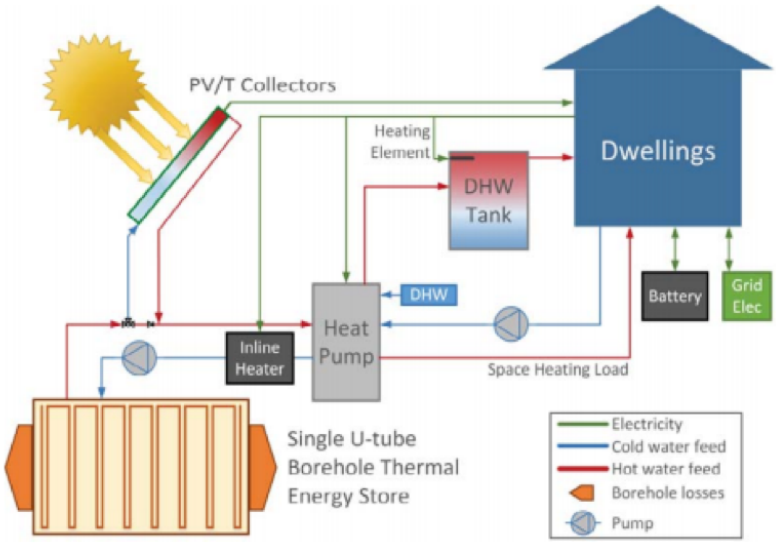

FIGURE 2.27: PVT system coupled with a geothermal source [79]

Another innovative application of PVT systems is the coupling with an organic

Rankine cycle (ORC) engine (Figure 2.28). A thermal energy storage tank (TES) acts as an interface between the ORC motor and the solar collectors, and is also an evaporator in the ORC cycle. The study was conducted on an engine with a rated power of $1kW_{el}$ combined with $15m^2$ of PVT collectors, and a storage requirement of 100L in Cyprus and 400L in the UK. Different energy storage media were investigated: phase-changed hydrated salt, oil, water, quartz, granite. Through this process, using hydrated salt, solar-electric conversion efficiencies of 4.4–6.4% were obtained in the UK climate, and 6.3–7.3% in Cyprus [80].

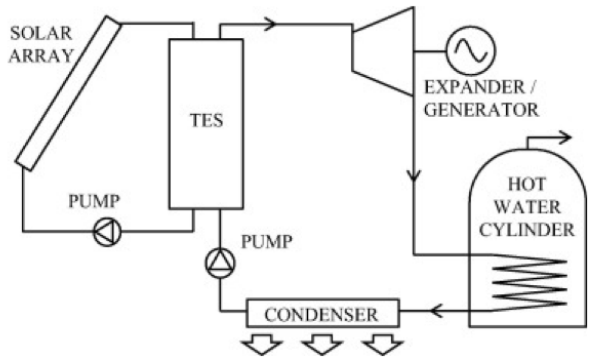

FIGURE 2.28: PVT system coupled with a ORC engine [80]

Integrating renewable sources directly with the consumer is an attractive solution, but can raise problems for the electricity and district heating network. Integration requires technical solutions such as centralized control, flexible operation of conventional exchanges, real-time monitoring and response. These barriers are less significant at a very small level, in the home or small community, where heat and electricity can be stored. Examples of market penetration of distributed electricity and heat production can be seen in countries such as Germany, Denmark, Sweden. An example of an interconnected system at the community level is shown in Figure 2.29.

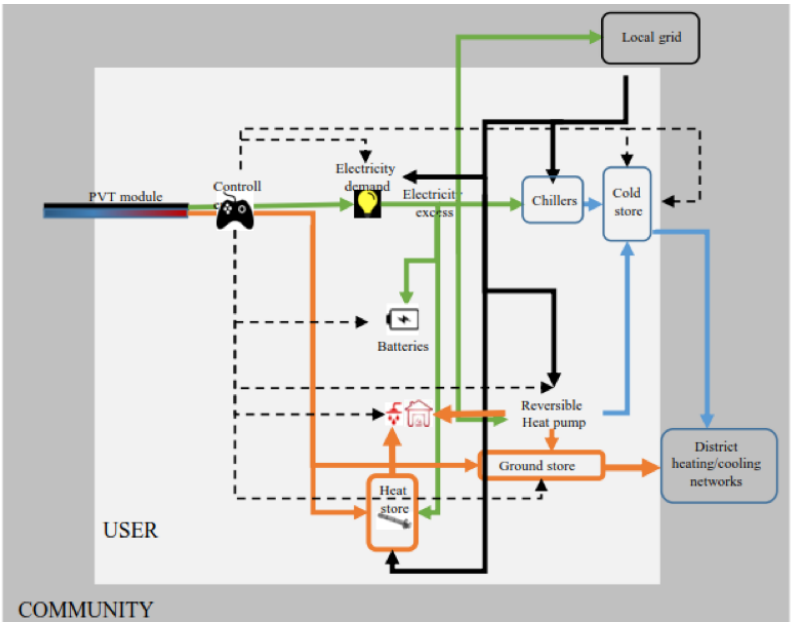

FIGURE 2.29: PVT system integrated in a community grid [31]

Chapter 3

Numerical model and parametric analysis of a PVT panel

This chapter presents an explicit dynamic numerical model of a PVT system for a Crystalline Silicon roll-bond collector and undertakes a sensibility analysis of its performance by running simulations for variable parameters in order to establish their impact on the overall collector performance. The proposed thermal model is able to evaluate the temperatures at each layer inside the collector, taking into account all the heat transfer processes between the layers or with the environment. Based on the output temperatures, the system performance indicators can then be assessed for various operational and fabrication parameters. The numerical model proposed here can be easily adapted for multiple configurations and operating conditions.

3.1 PVT configuration

The PVT system can take various configurations: liquid, air or dual liquid-air based, flat or concentrated. The thermal collector can also be of multiple geometries (direct flow, harp, fractal, spiral) and manufacturing methods (sheet and tube, roll bond, rectangular channels). A typical PVT system is obtained by coupling a solar thermal collector underneath a PV panel. [28] carries out a comprehensive review on the various thermophysical, geometrical and manufacturing technologies for PVT collectorss. One of the most common configurations, which was also used for this study, is described below.

The model is a liquid based PVT panel, with a direct flow geometry of the thermal absorber (Figure 4.1) and roll bond channels (Figure 4.2). The water based heat

exchanger was chosen due to a better heat transfer capacity compared to air collectors, and in order to provide the domestic hot water demand of the end user. The direct flow geometry of the channels was chosen due to its simplicity and good proved experimental performance [28]. The roll bond fabrication method is easy to achieve (technological know-how from the refrigeration industry), relatively inexpensive and very flexible in terms of geometry [28].

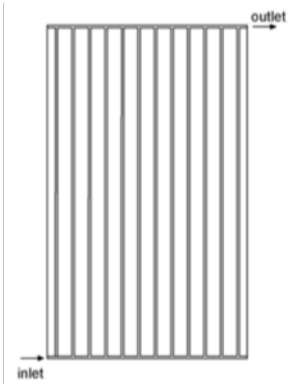

FIGURE 3.1: Direct flow collector geometry

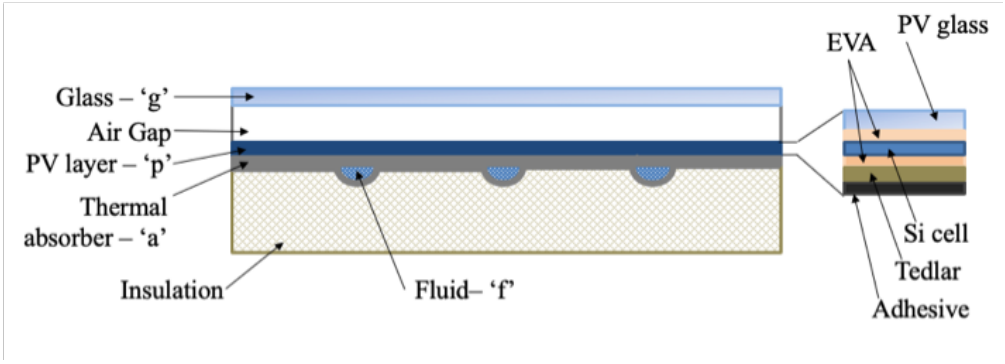

FIGURE 3.2: Cross section of the PVT collector

The PV cell is Crystalline Silicon, with a reference electrical efficiency (η_{STC}) of 15% at a reference operating temperature (T_{ref}) of 25°C and temperature coefficient (β_T) of 0.5 % K. The size of the panel is 1m x 2m, and the thickness of the channel is 0.008m. The collector fluid is a 30/70% glycol-water mix. Table 3.1 summarises the main thermophysical, geometrical and optical properties of the layers, which were adopted from the literature [48], [60], [81]. Most of the properties are constant, except for the thermal conductivity of the air and the fluid, which are variable with the temperature.

Property	Glass	Air Gap	PV	Thermal Absorber	Fluid	Insulation	Unit
Emissivity (ϵ)	0.9	-	0.96	-	-	-	-
Absorbance (α)	0.1	-	0.9	-	-	-	-
Transmittance (τ)	0.93	-	-	-	-	-	-
Thickness (H)	0.004	0.02	0.006	0.001	-	0.04	m
Density (ρ)	2200	-	2330	2699	1050	16	$\frac{kg}{m^3}$
Specific heat (c)	670	-	900	800	4000	1120	$\frac{J}{kgK}$
Thermal conductivity (k)	1.1	*	140	237	*	0.035	$\frac{W}{mK}$

TABLE 3.1: Optical, geometrical and thermo-physical properties of the PVT layers (* varies with temperature)

The thermal energy circulates through the layers of the PVT panel and to/from the exterior through three types of heat transfer processes: radiation, convection and conduction. Radiation is the process of heat transfer without any physical contact and it does not heats the transfer medium. Any physical body of a temperature greater than 0 K emits a level of radiation through electromagnetic waves. When radiation reaches a body, it can be either be absorbed, reflected or transmitted. Conduction is the movement of heat through a solid material or at the interface of two materials/layers that are in contact due to molecular collisions. Conduction that occurs on the solar panel is caused by the thermal gradients and its direction is from high temperature to low temperatures. Convection is the heat transfer in which energy moves within a fluid or gas through flow of matter from higher to lower temperature regions. It can be natural, occurring due to difference in densities, or forced by an external physical movement, such as a pump or the wind.

Various heat transfer processes take place inside a PVT panel and they are shown in Figure 3.3; radiation with a yellow arrow, convection in green and conduction in red. The glass layer receives direct and indirect solar radiation from the sun, a fraction of which is reflected, another part absorbed and the rest transmitted to the PV layer. It also receives reflected radiation and radiative losses from the PV layer. It loses some heat to the environment through the forced convection caused by the wind. The PV layer receives a part of the solar radiation, out of which some is reflected back to the glass

layer and some is absorbed. It also loses heat through the radiative process to the glass. In addition, in the air gap takes place a natural (free) convective heat transfer between the glass and the PV. Out of the incident radiation, a fraction is converted to electricity through the photovoltaic effect. The absorber layer exchanges heat with the PV layer, with the insulation and with the fluid through conduction, and the insulation loses heat to the environment through forced convection from the wind. The heat transfer in the fluid occurs also through forced convection generated by the pumping system.

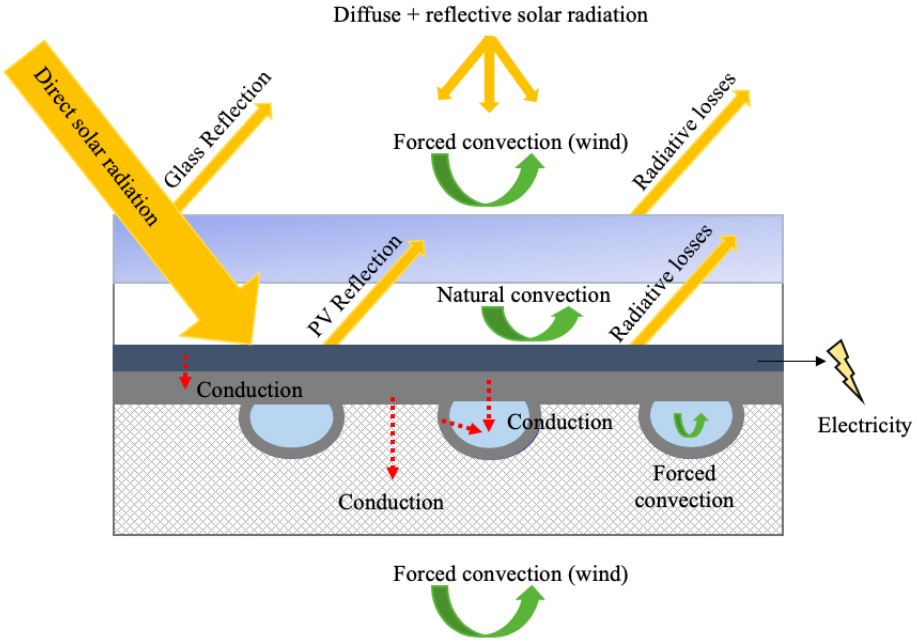

FIGURE 3.3: Schematic heat transfer processes in the layer of a PVT panel

3.2 Numerical model of the PVT collector

In order to develop the numerical model, it was assumed that:

- Edges are well insulated, thus no heat losses occur at the edges;
- The temperature of the PV cells is the same across all the layer at any given instant of time;
- Thermal conductivity is constant over each layer;
- Optical properties of materials are constant over the analysed spectrum of wavelengths;

- Vertical heat conduction in the layers is negligible, due to the fact that the layers are very thin;
- Heat losses from the PVT outlet to the tank inlet are negligible due to the fact that the pipes are short;
- The solar irradiance, ambient temperature and wind speed are constant across the surface of the collector at any given time;
- No dust or partial shading is considered;
- The flow rate of the fluid is constant, 0.05 kg/s, and the initial fluid inlet temperature at time t=0 is T_{i0}=15^{o}C;
- The initial fluid inlet temperature at time t=0 is T_{i0}=15^{o}C. At every consecutive time step, the new T_{fi} is the average value between T_{i0} (assumed to be the cold-water inlet main temperature) and T_{fo} from the previous time step (the temperature of the fluid at the outlet of the panel).

The analysed components are: glass, PV, thermal absorber, fluid and tank. Some models [59], [81] also analyse the behaviour of the air gap layer and the insulation layer, but those temperatures were found not to be relevant for the purpose of this study, and thus the model is simplified to only compute the four areas of interest.

3.2.1 Energy balance

A heat balance equation is developed for each of the significant layers of the system based on the equation for the variation of internal energy in a physical body:

$$Mc\frac{dT}{dt} = AH\rho c\frac{dT}{dt} = \frac{dU}{dt} \tag{3.1}$$

where M [kg] is the mass of the layer, c [J/K] is the specific heat capacity of the material, T [K] is the temperature, dt [s] is the chosen time step of the simulation, A [m^2] is the area of the layer, H [m] is the height of the layer, ρ [kg/m^3] is the density of the layer and dU [J] is the change in internal energy of the system.

Glass

The thermal balance of the glass layer considers the radiative and convective losses to the environment ($Q_{g-e,RD}$ and $Q_{g-e,CV}$), the radiative and convective heat transfer to the PV layer ($Q_{g-p,RD}$ and $Q_{g-p,CV}$) and the heat absorbed by the glass (Q_g).

$$M_g c_g \frac{dT_g}{dt} = Q_{g-p,CV} + Q_{g-p,RD} + Q_{g-p,CV} + Q_{g-p,RD} + Q_g \tag{3.2}$$

After expanding the terms, it becomes:

$$A_g H_g \rho_g c_g \frac{dT_g}{dt} = h_{g-e,CV} A_g (T_e - T_g) + h_{g-e,RAD} A_g (T_{sky} - T_g) + \\ + h_{gap} A_g (T_p - T_g) + h_{g-p,RAD} A_g (T_p - T_g) + A_g G_{irr} \alpha_g \tag{3.3}$$

Where $h_{g-e,CV}$ is the coefficient of forced convection between the glass and environment, A_g is the area of glass, T_e is the temperature of the environment, T_g is the temperature of the glass layer, $h_{g-e,RD}$ is the coefficient of radiative heat loss between the glass and environment, T_{sky} is the the equivalent radiative temperature of the sky, h_{gap} is the thermal coefficient of the gap, T_p is the temperature pf the PV layer, $h_{g-p,RD}$ is the coefficient of radiative heat loss between the glass and the PV layer, α_g is the absorbance of the glass and G_{irr} is the incident irradiation on the absorber.

The coefficient of heat transfer from the glass to the environment is in fact the forced convection coefficient due to wind h_w, and can be expressed through various empirical correlations, with multiple reviews carried out [60], [82], summarised in Figure 3.4.

Authors	Equations	Remarks
MacAdmas	$h_{wi} = 5.7 + 3.8V_{wi}$	$V_{wi} < 5$ m/s
	$h_{wi} = 6.47 + V_{wi}^{0.78}$	$V_{wi} > 5$ m/s
Watmuff et al.	$h_{wi} = 2.3 + 3V_{wi}$	$0 < V_{wi} < 7$ m/s
Kumar et al.	$h_{wi} = 10.03 + 4.687V_{wi}$	$0 < V_{wi} < 4$ m/s
Sharples and Charlesworth	$h_{wi} = 8.3 + 2.2V_{wi}$	$0.8 < V_{wi} < 6.5$ m/s for the collector titled at 0°
	$h_{wi} = 6.5 + 3.3V_{wi}$	$0.8 < V_{wi} < 6.5$ m/s for the collector titled at 90°

FIGURE 3.4: Convective heat transfer coefficient correlations [60]

The chosen correlation, by MacAdams, gives good agreement between experiment

and simulation, and covers wind speeds from 0 to 10 m/s. This correlation is widely used in the literature for numerical PVT models [26], [60].

$$h_{g-e,CV} = \begin{cases} 5.7 + 3.8u_w, & \text{if } u_w < 5m/s \\ 6.47u_w^{0.78}, & \text{if } u_w > 5m/s \end{cases} \tag{3.4}$$

The coefficient of radiative heat loss to the environment is calculated by using the equivalent radiative temperature of the sky T_{sky}, which can be expressed as a linear function of the ambient temperature and the sky cloud coverage in octaves (N) [48]. There are multiple equations available for defining the sky temperature, most commonly it can be expressed as a linear function of the ambient temperature (T_e) and the sky cloud coverage in octaves (N) [48].

$$h_{g-e,RAD} = \epsilon_g \sigma (T_g^2 + T_{sky}^2)(T_g + T_{sky}) \tag{3.5}$$

$$T_{sky} = 0.0552 T_e^{1.5} + 2.625N \tag{3.6}$$

If clear sky conditions are assumed or there is no data available on the cloud coverage, Eq. (6) can be further simplified to Eq. (7), with less that 1% effect on the thermal and electrical output of the system [31], [83]:

$$T_{sky} = 0.0552 T_e^{1.5} \tag{3.7}$$

The thermal coefficient of the air gap takes into account the conduction in the top layers of the PV sandwich (PV glass and EVA) and the convective heat transfer coefficient between the glass and the plate.

$$\frac{1}{h_{gap}} = \frac{H_{PVg}}{k_{PVg}} + \frac{H_{EVA}}{k_{EVA}} + \frac{1}{h_{g-p,CV}} \tag{3.8}$$

The convective heat transfer coefficient in an enclosed space is:

$$h_{g-p,CV} = \frac{Nu_{air} k_{air}}{H_{gap}} \tag{3.9}$$

Where H is the height of the layer (measured at the middle of the layer), k is the thermal conductivity and Nu_{air} is the Nusselt number for air.

The Nusselt number correlation for inclined plates for tilt angles from 0 to 60 degrees, is given by [84]:

$$Nu_{air} = 1 + 1.44\left[1 - \frac{1708}{Racos\phi}\right]^{+}\left[1 - \frac{(sin1.8\phi)^{1.6}1708}{Racos\phi}\right] + \left[\left(\frac{Racos\phi}{5830}\right)^{1/3} - 1\right]^{+} \tag{3.10}$$

Where ϵ_p is the emissivity of the PV layer and ϵ_g is the emissivity of the glass.

The radiative coefficient between the glass and the PV is expressed below:

$$h_{g-p,RAD} = \epsilon_{g-p}\sigma(T_g^2 + T_p^2)(T_g + T_p) \tag{3.11}$$

where ϵ_{g-p} is the equivalent glass-PV infrared emissivity:

$$\epsilon_p = \frac{1}{\frac{1}{\epsilon_g} + \frac{1}{\epsilon_p} - 1} \tag{3.12}$$

The behaviour of a transparent medium (reflection, transmission and absorption) depends on the properties of the material itself (thickness, extinction coefficient, refractive index) as well as on the incoming solar radiation. Duffie and Beckman [25] defined the numerical model which describes the radiation through a glass cover. In the case of glass, the material properties are assumed to be independent of the radiation wavelength. Also, the solar radiation becomes polarized when passing through the cover.

The reflection of unpolarized radiation passing through 2 media with different refractive index with a smooth surface is described by Fresnel's law. The perpendicular component is defined by Equation 3.13, and the parallel component is defined by Equation 3.14.

$$r_{\perp} = \frac{\sin^2(\vartheta_2 - \vartheta_1)}{\sin^2(\vartheta_2 + \vartheta_1)} \tag{3.13}$$

$$r_{\parallel} = \frac{\tan^2(\vartheta_2 - \vartheta_1)}{\tan^2(\vartheta_2 + \vartheta_1)} \tag{3.14}$$

where ϑ_1 and ϑ_2 are the angles of incidence and refraction respectively, and they are defined by Snell's law:

$$n_1 \sin \vartheta_1 = n_2 \sin \vartheta_2 \tag{3.15}$$

The total reflective index is the average of the two components:

$$r = \frac{1}{2} \left(r_\perp + r_\parallel \right) \tag{3.16}$$

The angular dependence of the transmittance of glass is also considered, as it is found to influence the thermal and electrical performance of the collector due to the fact that less light is transmitted at large incidence angles. The glass transmittance as a function of the incident angle is defined in Equation 3.17.

$$\tau \left(\theta_1 \right) = \frac{1}{2} \left[\frac{\tau_\alpha \left(\theta_1 \right) \left(1 - r_\perp \right)^2}{1 - \left(r_\perp \tau_\alpha \left(\theta_1 \right) \right)^2} + \frac{\tau_\alpha \left(\theta_1 \right) \left(1 - r_\parallel \right)^2}{1 - \left(r_\parallel \tau_\alpha \left(\theta_1 \right) \right)^2} \right] \tag{3.17}$$

where $\tau_\alpha \left(\theta_1 \right)$ is the fraction of transmitted irradiance trough the glass taking into account the absorption losses:

$$\tau_\alpha \left(\theta_1 \right) = \exp \left(\frac{-KL}{\cos \theta_2} \right) \tag{3.18}$$

where K is a proportionality constant with a value of 4 m^{-1} for glass [25] and L is the thickness of the glass.

PV Layer

The PV layer includes glass, two layers of encapsulant (EVA), the PV cell and Tedlar. The thermal balance of the PV layer considers the radiative and convective heat transfer to the glass layer ($Q_{p-g,RD}$ and $Q_{p-g,CV}$), the conductive heat transfer to the absorber layer ($Q_{p-a,CD}$), the heat absorbed by the PV layer (Q_p) from which the produced electricity (E) is substrcted.

$$M_p c_p \frac{dT_p}{dt} = Q_{p-g,CV} + Q_{p-g,RD} + Q_{p-a,CD} + Q_p - E \tag{3.19}$$

After expanding the terms, it becomes:

$$A_p H_p \rho_p c_p \frac{dT_p}{dt} = h_{gap} A_p (T_g - T_p) + h_{p-g,RD} A_p (T_g - T_p) + h_{p-a,CD} A_p (T_a - T_p) + A_p G_{irr} (\tau\alpha)_p - \eta_{EL(T)} A_p G_{irr} \quad (3.20)$$

Where A_p is the are of the PV layer, $h_{p-a,CD}$ is the conduction coefficient from the PV layer to the absorber, T_a is the temperature of the thermal absorber layer, and $\eta_{EL(T)}$ is the time dependent electrical efficiency of the cell.

The heat transfer coefficient of the air gap and the radiation coefficient are calculated in Eqs. 3.8 and 3.12. The conduction coefficient through the layers of EVA, Tedlar and adhesive is:

$$\frac{1}{h_{p-a,CD}} = \frac{H_{EVA}}{k_{EVA}} + \frac{H_{Ted}}{k_{Ted}} + \frac{H_{adh}}{k_{adh}} \quad (3.21)$$

The temperature dependant conversion efficiency of the cell decreases with the increase in the operating temperature T_p, as shown in the equation below. The temperature coefficient β_{PV} is a property of the type of cell.

$$\eta_{EL(T)} = \eta_{ref}[1 - \beta_{PV}(T_p - T_{ref})] \quad (3.22)$$

Thermal absorber

The thermal balance of the absorber layer takes into account the heat transfer to the fluid ($Q_{a-f,CD}$) the conductive heat transfer to the PV layer ($Q_{a-p,CD}$), and the heat lost to the insulation ($Q_{a-i,CD}$).

$$M_a c_a \frac{dT_p}{dt} = Q_{a-p,CD} + Q_{a-f,CD} + Q_{a-i,CD} \quad (3.23)$$

After expanding the terms, it becomes:

$$A_a H_a \rho_a c_a \frac{dT_a}{dt} = h_{a-p,CD} A_a (T_p - T_a) + h_f A_a (T_f - T_a) + h_{a-i,CD} A_a (T_i - T_a) \quad (3.24)$$

Where $h_{a-p,CD}$ is the heat transfer coefficient from the absorber to the PV layer, A_a is the area of the thermal absorber, h_{a-f} is the heat transfer coefficient of the fluid, T_f is

the temperature of the fluid, $h_{a-e,CD}$ is the conductive heat loss coefficient to the environment.

The heat transfer coefficient from the thermal absorber to the PV layer ($h_{a-p,CD}$) was previously defined in Eq. 3.21. The fluid heat transfer coefficient depends on the type of flow (turbulent or laminar), as shown in the equations below [85]:

$$h_f = \begin{cases} 4.36\frac{k_f}{D_H}, & \text{for } Re < 2300 \\ \frac{k_f}{D_H}0.023Re^{0.8}Pr^{0.4}, & \text{for } Re > 2300 \\ 2\frac{k_f}{D_H}, & \text{for } \dot{m} = 0kg/s \end{cases} \tag{3.25}$$

Where k_f is the thermal conductivity of the fluid, D_H is the hydraulic diameter, Re is the Reynolds number, Pr is the Prandtl number and m is the mass flow rate.

The heat transfer coefficient from the absorber to the insulation is:

$$h_{a-i,CD} = \frac{2k_i}{H_i} \tag{3.26}$$

Insulation

The thermal balance in the insulation layer takes into account the conductive heat transfer to the absorber layer ($Q_{i-a,CD}$) and the heat loss to the environment (Q_{i-e}).

$$M_i c_i \frac{dT_i}{dt} = Q_{i-a,CD} + Q_{i-e} \tag{3.27}$$

which becomes

$$A_i H_i \rho_i c_i \frac{dT_i}{dt} = h_{i-a,CD} A_i (T_a - T_i) + h_{i-e} A_i (T_e - T_i) \tag{3.28}$$

The heat transfer coefficient to the absorber layer ($h_{i-a,CD}$) is the same as in Eq. 3.26. For the calculation of the heat loss coefficient to the environment, the radiation and forced convection can be neglected, since the are is shaded and it can be assumed that there is no wind at the back of the panel.

$$h_{i-e} = \frac{2k_i}{H_i} \tag{3.29}$$

Fluid

The energy balance equation for the fluid takes into account the thermal energy coming from the absorber(Q_{f-a}) and the heat accumulated by the fluid (Q_f).

$$M_f c_f \frac{dT_f}{dt} = Q_{f-a} + Q_f \tag{3.30}$$

which becomes

$$V_f \rho_f c_f \frac{dT_f}{dt} = h_f \frac{\pi DL}{2}(T_a - T_f) + \dot{m} c_f (T_{f-i} - T_{f-o}) \tag{3.31}$$

The heat transfer coefficient of the fluid is calculated in Eq. 3.25, $\dot{m}$ is the mass flow rate of the fluid [kg/s] and the inlet and outlet temperatures are represented by T_{f-i} and T_{f-o} respectively.

$$T_f = \frac{T_{f-i} + T_{f-o}}{2} \tag{3.32}$$

3.2.2 System Performance

The energy performance of the system can be defined in terms of electrical, thermal and overall efficiencies (η_{EL}, η_{TH}, $\eta_{overall}$).

Electrical performance

The electrical efficiency is defined as the ratio between the electrical power generated output (P_{EL}) and the incident solar radiation on the collector (AG_{irr}):

$$\eta_{EL} = \frac{P_{EL}}{AG_{irr}} \tag{3.33}$$

Thermal performance

The standard equation for thermal efficiency is represented by the ratio between the amount of thermal energy generated by the system ($\dot{Q_{th}}$) and the solar radiation incident on the surface of the collector (AG_{irr}):

$$\eta_{TH} = \frac{\dot{Q_{th}}}{AG_{irr}} = \frac{\dot{m} c_f (T_{f-o} - T_{f-i})}{AG_{irr}} \tag{3.34}$$

An alternative definition for the thermal efficiency was given by [86]. It proposes a distinction between the thermal and electrical power of the system, therefore the electrical power output is subtracted from the total incident radiation. This way of defining the efficiency gives a more accurate comparison between the thermal performance of a PVT and a stand alone solar thermal system.

$$\eta_{TH}^{*} = \frac{\dot{Q}_{th}}{AG_{irr} - P_{EL}} = \frac{\dot{m}c_f(T_{f-o} - T_{f-i})}{AG_{irr} - P_{EL}} = \frac{\eta_{TH}}{1 - \eta_{EL}} \tag{3.35}$$

Overall performance

The global efficiency of the collector (η_{GL}) can be calculated as the sum of the thermal and electrical efficiencies from the point of view of the 1st law of thermodynamics. This is also known as the **first law efficiency**.

$$\eta_{GL} = \eta_{EL} + \eta_{TH} \tag{3.36}$$

A different approach would be to consider the quality / grade difference between the two types of energy: electrical energy is of higher quality compared to the thermal energy. Thus, due to the fact that a kW_{el} cannot be directly compared to a kW_{th}, some authors [28], [87] propose the **primary energy saving efficiency** (η_{PES}) as a more accurate way of assessing the efficiency of the collector:

$$\eta_{PES} = \eta_{TH} + \frac{\eta_{EL}}{\eta_{Tpower}} \tag{3.37}$$

where η_{Tpower} is the average efficiency of electrical energy production depending on the country of reference, assumed yo be 0.4 on average [28].

When assessing the primary energy saving efficiency, it's important to note that the conversion efficiency η_{Tpower} is dependant on the regional context. Furthermore, it is based on a quantitate assessment and not a qualitative one, as it does not take into account the temperature of the fluid at the outlet of the system. Another indicator used for determining the performance of the system, which can be applied irrespective of the location and considers the fluid temperature, is the **second law efficiency** [86]. In this case, the thermal energy is assessed by its capacity of being converted into work

through an ideal Lorentz Cycle:

$$\eta_{II} = \eta_{EL} + \eta_{TH} \cdot \eta_{ideal} \tag{3.38}$$

The outlet temperature of a PVT system is not constant, thus the ideal efficiency is calculated as follows:

$$\eta_{ideal} = 1 - \frac{T_{amb}}{T_{LMTD}} \tag{3.39}$$

where T_{LMTD} is the logarithmic mean temperature of the fluid.

Another useful way to describe the qualitative performance of a PVT system is through the **exergetic efficiency** [28], [88]. Exergy is the maximum amount of work that can be produced from the energy of a system in a set of reference environmental conditions. In a PVT system, the energetic efficiency can be defined as the ratio between the total exergy output (photovoltaic and thermal) and the total energy input (solar radiation).

$$\varepsilon_{pvt} = \frac{\int_{t_1}^{t_2}(A_c \cdot \dot{E_{\chi th}} + A_c \cdot \dot{E_{\chi el}})dt}{A_c \cdot \int_{t_1}^{t_2}(A_c \cdot \dot{E_{\chi sun}})dt} \tag{3.40}$$

where $\dot{E_{\chi th}}$ is the thermal exergy output per unit area of collector, $\dot{E_{\chi el}}$ is the electrical (photovoltaic) exergy output per unit area of PV, $\dot{E_{\chi sun}}$ is the exergy input of solar radiation, and $t_2 - t_1$ is the time duration of the calculation interval. The exergy outputs can be defined as a function of the energy outputs:

$$\dot{E_{\chi th}} = \dot{E_{th}} \cdot \left(1 - \frac{T_{amb}}{T_{out}}\right) \tag{3.41}$$

$$\dot{E_{\chi el}} = \dot{E_{el}} \tag{3.42}$$

where $\dot{E_{th}}$ is the rate of thermal energy and $\dot{E_{el}}$ is the rate of electrical energy produced by the PVT system.

The solar exergy output $(\dot{E_{\chi sun}})$ can be expressed through different definitions, summarised by [88]:

$$\dot{E_{\chi sun}} = \left[1 + \frac{1}{3}\left(\frac{T_{amb}}{T_{sun}}\right)^4 - \frac{4T_{amb}}{3T_{sun}}\right] G \tag{3.43}$$

$$\dot{E_{\chi sun}} = \left(1 - \frac{4T_{amb}}{3T_{sun}}\right) G \tag{3.44}$$

$$\dot{E_{\chi}}_{sun} = \left(1 - \frac{T_{amb}}{T_{sun}}\right) G \tag{3.45}$$

where T_{sun} is the solar radiation temperature, typically taken as 6000 K.

3.3 Simulation Methodology

3.3.1 MatLab implementation

By rearranging the energy balance equations, a system of coupled equations is obtained. The system of equations is then solved in MatLAB with the ordinary 'fsolve' function. The coefficients C and D are defined by rearranging the free terms of the energy balance equations above.

$$\begin{cases} C_1 T_g + C_2 T_p - D_1 = 0 \\ C_3 T_g + C_4 T_p + C_5 T_a - D_2 = 0 \\ C_6 T_p + C_7 T_a + C_8 T_f - D_3 = 0 \\ C_9 T_a + C_{10} T_f - D_4 = 0 \end{cases} \tag{3.46}$$

This can be expressed in a matrix form as follows:

$$\begin{bmatrix} C_1 & C_2 & 0 & 0 \\ C_3 & C_4 & C_5 & 0 \\ 0 & C_6 & C_7 & C_8 \\ 0 & 0 & C_9 & C_{11} \end{bmatrix} \times \begin{bmatrix} T_g \\ T_p \\ T_a \\ T_f \end{bmatrix} = \begin{bmatrix} D_1 \\ D_2 \\ D_3 \\ D_4 \end{bmatrix} \tag{3.47}$$

Where

$$C_1 = \frac{M_g c_g}{dt} + h_{g-e,CV} A_g + h_{g-e,RD} A_g + h_{gap} A_g + h_{g-p,RD} A_g \tag{3.48}$$

$$C_2 = -h_{gap} A_g - h_{g-p,RD} A_g \tag{3.49}$$

$$D_1 = \frac{M_g c_g}{dt} T_g + h_{g-e,CV} A_g T_e + h_{g-e,RD} A_g T_{sky} + A_g \alpha_g G_{irr} \tag{3.50}$$

$$C_3 = -h_{gap}A_p - h_{p-g,RD}A_p \tag{3.51}$$

$$C_4 = \frac{M_p c_p}{dt} + h_{gap}A_p + h_{p-g,RD}A_p \tag{3.52}$$

$$C_5 = -h_{p-a,CD}A_p \tag{3.53}$$

$$D_2 = \frac{M_p c_p}{dt}T_p + A_p(\alpha\tau)_p G_{irr}\left(1 - \eta_{EL(T)}\right) \tag{3.54}$$

$$C_6 = -h_{a-p,CD}A_a \tag{3.55}$$

$$C_7 = \frac{M_a c_a}{dt} + h_{a-p,cD}A_a + h_{a-f}A_{ch} + h_{a-e,CD}A_a \tag{3.56}$$

$$C_8 = -h_{a-f}A_{ch} \tag{3.57}$$

$$D_3 = \frac{M_a c_a}{dt}T_a + h_{a-e,CD}A_a T_e \tag{3.58}$$

$$C_9 = -h_{a-f}\frac{\pi DL}{2} \tag{3.59}$$

$$C_{10} = \frac{M_f c_f}{dt} + h_{a-f}\frac{\pi DL}{2} + 2\dot{m}c_f \tag{3.60}$$

$$D_4 = \frac{M_f c_f}{dt}T_f + 2\dot{m}c_f T_{fi} \tag{3.61}$$

The solver solves the equations for each individual timestep and gives a vector solution for $[T_p T_g T_a T_f]$. The results are plotted on a graph and shown in the next section.

3.3.2 Dynamic Simulation with Real Weather Data

The behaviour of the PVT system depends on various parameters. For the simulation, the default values are summarised in the table below.

Length of Collector	2 m	**Tube diameter**	10 mm
Width of Collector	1 m	**Inlet Temperature**	25 ^{o}C
Cell Efficiency	17%	**Mass flow rate**	0.015 kg/m^{2}s
Packing factor	90%	**Solar radiation**	1000 W/m^2
Temperature coefficienct	0.5%/K	**Wind speed**	1 m/s
No. of tubes	10	**Ambient temperature**	25 ^{o}C
Tube spacing	10 cm	**Tilt angle**	30^{o}

TABLE 3.2: Default PVT parameters

The real-time response of the temperatures in the PVT system was evaluated by carrying out a dynamic simulation, that takes into account the variation of meteorological conditions during the day.

The external output of the model consists of the weather data: ambient temperature (T_{amb} [°C]), solar irradiation (G [W/m^2]) and wind speed (W [m/s]). The solar irradiation is an important factor in the performance of a PVT panel. It directly determines the electrical power output and is also contributing to the temperature variation of the PVT layers radiative heat transfer. The ambient temperature is also a contributing factor on the temperatures through convective and conductive heat transfer processes in the solid and liquid layers of the panel. The wind speed is responsible for the variation of the convective heat losses at the surface and at the back of the panel. The total solar irradiation is made up of three components: direct beam irradiation, diffuse irradiation and reflective irradiation. Direct irradiation represents the direct perpendicular radiation beam that reaches the panel, the diffuse irradiation refers to the radiation that is transmitted to the panel by the scattering of the molecules in the atmosphere, and the reflective irradiation is the radiation that has been reflected by the surroundings, and is also known as albedo.

Case study - Bucharest and Strasbourg

The developed numerical model was applied for a PVT panel in two different climate conditions: Bucharest and Strasbourg, which enables a comparison of the performance of the PVT system in both regions. The climate of Romania is temperate continental,

with hot and sunny summers with occasional showers and thunderstorms and cold winters with frequent snow and fog. Bucharest is situated in the south of the country, where the summers are hotter and the winters are milder. France has a temperate climate, characterised by four specific regions. The region where Strasbourg is situated, called Alsace, is defined by a continental climate with cold to mild winters, hot summers, and particularly strong winds. The average summer months temperature in Bucharest is 29.1 ^{o}C, while in Strasburg it is 24.2 ^{o}C. For the winter months, Bucharest has an average of 4^{o}C, and Strasbourg 5.2^{o}C. The monthly summer sun hours are 278.8 and 222.0 for Bucharest and Strasbourg respectively, while the winter sun hours are 72.6 and 54.5.

		Winter	Spring	Summer	Autumn	Total
Temperature	Bucharest	4.0	17.8	29.1	17.4	17.1
[^{o}C]	Strasbourg	5.2	15.2	24.2	14.5	14.8
Monthly	Bucharest	36.9	48.1	64.9	47.9	594
rainfall [mm]	Strasbourg	36.5	52.3	66.9	54.8	632
Monthly	Bucharest	9.3	10.5	9.9	7.5	113
rainy days	Strasbourg	8.4	9.8	10.2	8.9	112
Monthly	Bucharest	72.6	189.7	278.8	163	2121
sun hours	Strasbourg	54.5	160.3	222	108.7	1637

TABLE 3.3: Climate characterisation of Strasbourg and Bucharest (source: WMO - World Meteorological Organization)

The variation of the weather during the day was used as an input into the numerical model in order to assess in real time the temperatures inside the panel. The input is: solar irradiation (G [W/m^2]), ambient temperature (T_{amb} [^{o}C]) and wind speed (W [m/s]). The yearly profile with hourly resolution for each parameter was obtained from Meteonorm Database for both Bucharest, Romania and Strasbourg, France. Figures 3.5 and 3.6 show the weather conditions during a typical summer day in Bucharest and Strasbourg. Figures 3.7 and 3.8 show the weather conditions during a typical winter day in Bucharest and Strasbourg. In all cases, the peak solar irradiation occurs during mid-day, around 12:00-14:00, while the maximum temperature lags behind, occurring around 16:00. Given the fact that the simulations were run for one day, it is important to note the sensitivity of the chosen data on the results of the numerical simulations. This means that the specific day which was chosen from the Meteonorm yearly database is of crucial importance and given the significant day to day variation of the weather, a random day can be misrepresenting the seasonal climate. In this case, the same data was

chosen for both cities, making sure no extreme condition occur and the two weather conditions are comparable at the given time. The representative winter day is 3rd of January and for the summer is 12th of July.

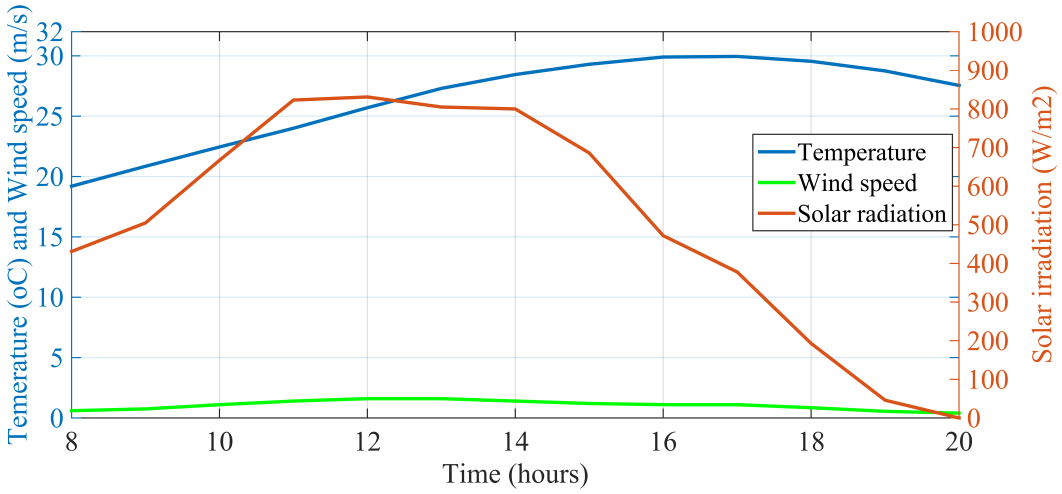

FIGURE 3.5: Ambient temperature during a summer day in Strasbourg from 8 to 20

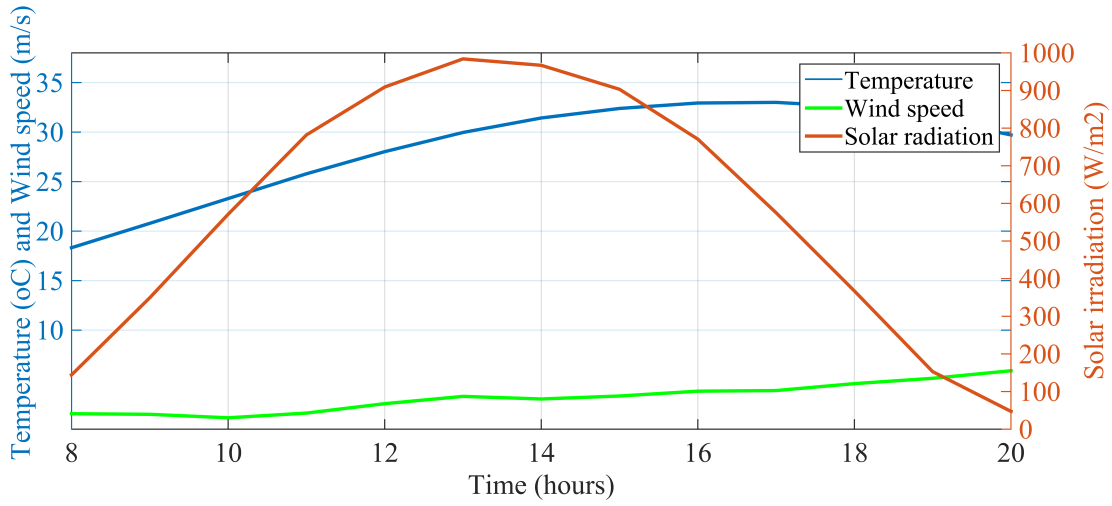

FIGURE 3.6: Ambient temperature during a summer day in Bucharest from 8 to 20

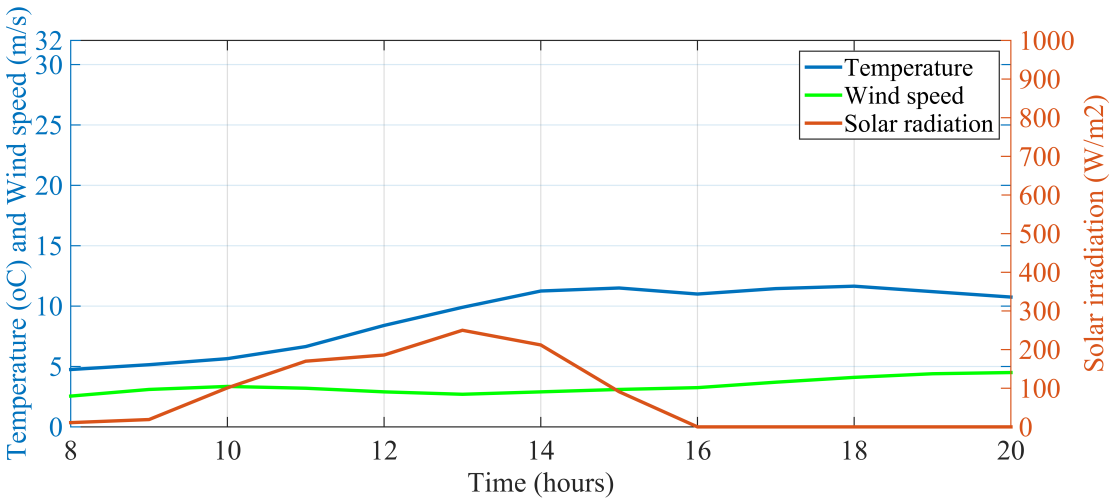

FIGURE 3.7: Ambient temperature during a winter day in Strasbourg from 8 to 20

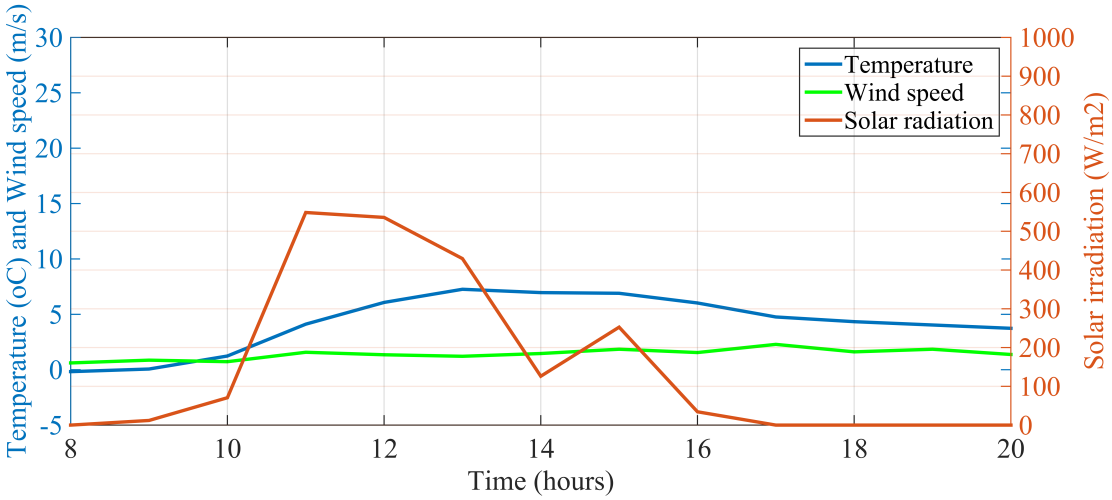

FIGURE 3.8: Ambient temperature during a winter day in Bucharest from 8 to 20

Daily simulations were carried out for a typical summer and winter day in Bucharest, Romania and Strasbourg, France, from 8:00 to 20:00, with the weather data including ambient temperature, wind speed and irradiation, discussed in the previous section.

Given these conditions, the time dependent temperature variance of the system is illustrated in Figures 3.9 and 3.10 for the summer day in Strasbourg and Bucharest, and Figures 3.11 and 3.12 for winter days in Strabourg and Bucharest respectively.

As expected, the layers with the higher thermal conductivity reach the highest temperatures. In all cases, the PV layer is the most heated, reaching 52^{o}C for a summer day in Bucharest. The next layer is the thermal absorber, followed by the fluid. The glass layer is always the coolest. The temperature profile of all the layers follows closely the

profile of the ambient temperature and global irradiation. The effect of the wind speed is not easily noticeable in the simulations. It can also be observed that the working fluid reaches slightly higher temperatures in Bucharest during the summer and in Strasbourg during the winter, due to their specific weather conditions. As a result, assuming that the system would have a water storage tank, it can be expected that the system would have a better thermal efficiency in Bucharest compared to Strasbourg during the summer, and higher in Strasbourg during the winter.

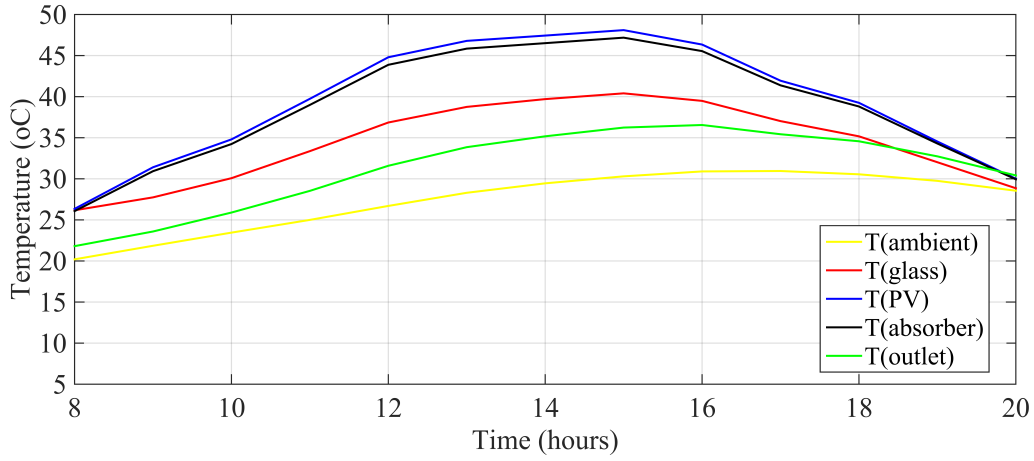

FIGURE 3.9: Time dependent temperature of PVT during a summer day in Strasbourg

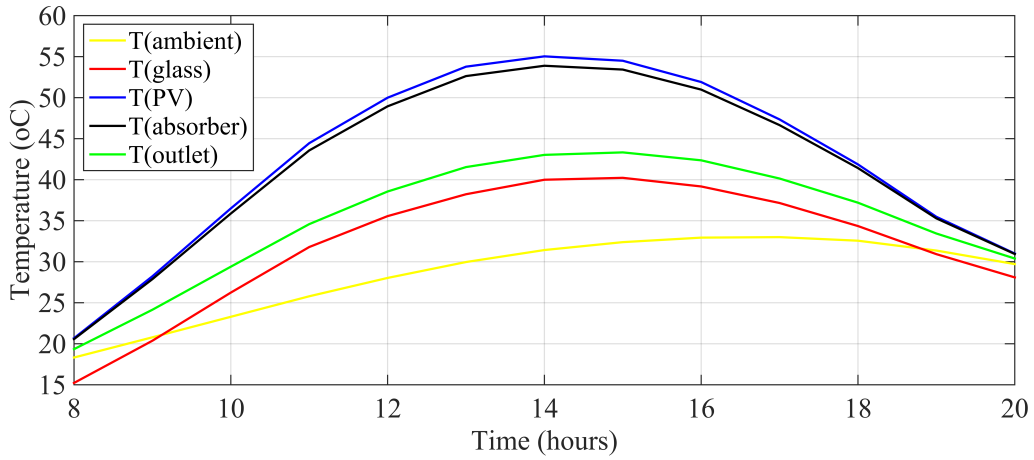

FIGURE 3.10: Time dependent temperature of PVT during a summer day in Bucharest

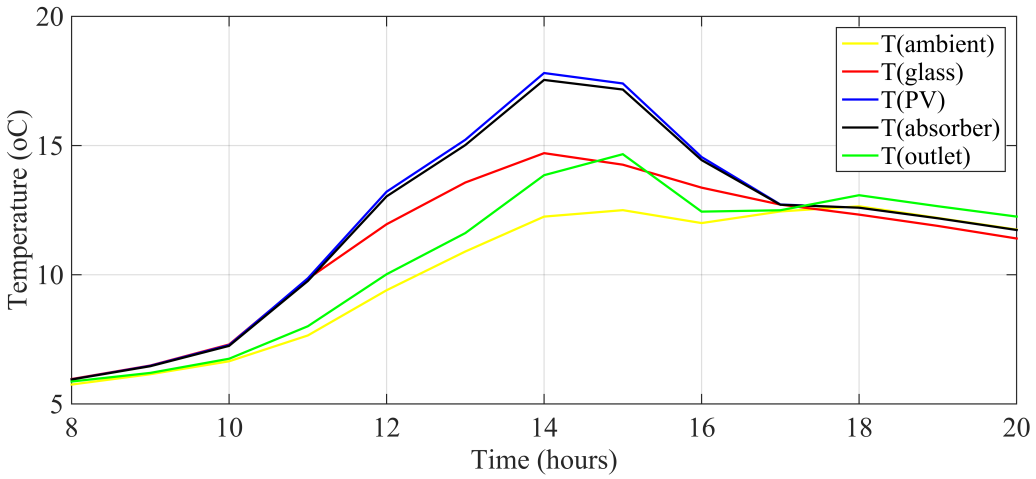

FIGURE 3.11: Time dependent temperature of PVT during a winter day in Strasbourg

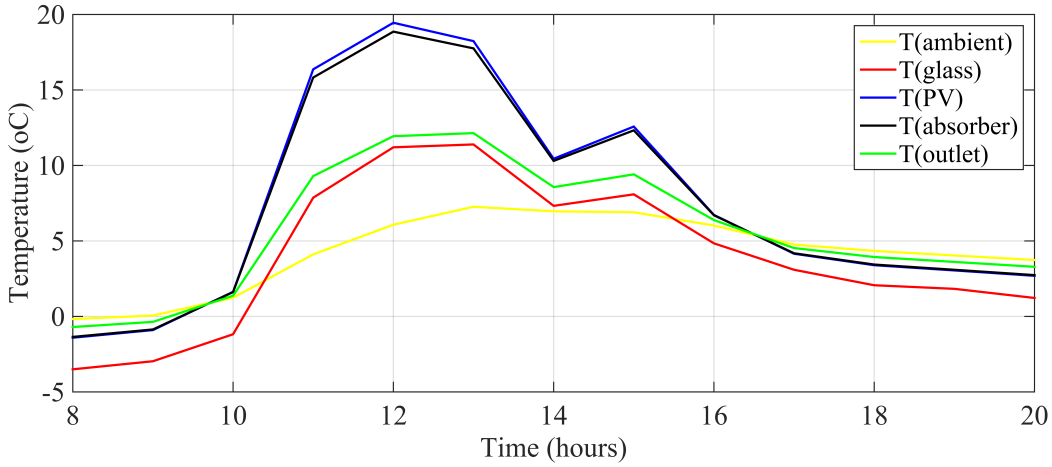

FIGURE 3.12: Time dependent temperature of PVT during a winter day in Strasbourg

3.4 Model Validation

The developed model was validated by comparing the performance results to experimental data found in the literature. To this end, the PVT model described by [89] is recreated using this model, with the configuration and operating conditions used in the experiment. The characteristics of the experimental model are summarised in the table below:

In this case, the performance of the system is be assessed by computing the electrical and thermal efficiencies, according to equations 3.33 and 3.34. These are plotted against the reduced temperature, defined in equation 3.62, to account for the fact that

Size	2 m^2	**Tube diameter**	9 mm
Cell Efficiency	17.3%	**Mass flow rate**	0.02kg/m^2s
Packing factor	80%	**Solar radiation**	1000 W/m^2
Temperature coefficienct	0.405%/K	**Wind speed**	1 m/s
No. of tubes	10	**Ambient temperature**	30 ^oC
Tube spacing	10 cm	**Tilt angle**	30^o

TABLE 3.4: Parameters of validation model [89]

the thermal efficiency is, in fact, dependent on the conditions at which it is calculated (ambient temperature, inlet temperature and global irradiation). The plotted results shown in Figure 3.13 indicate good agreement between the experimental and simulated data, which provides confidence in the numerical model developed for this study.

$$T^* = \frac{T_{in} - T_{amb}}{G} \tag{3.62}$$

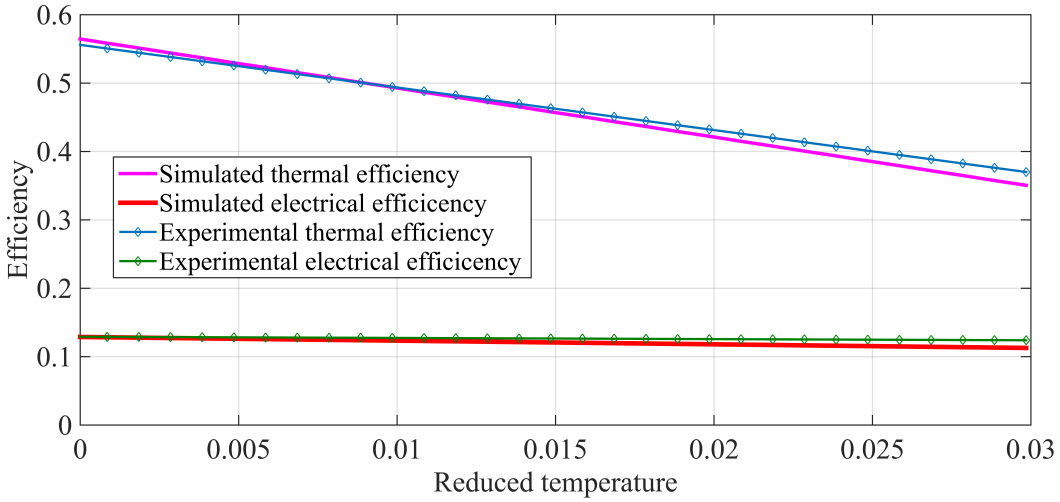

FIGURE 3.13: Comparisons of simulation and experimental [89] results of thermal and electrical efficiencies as a function of the reduced temperature

3.5 Parametric Analysis

A one-factor-at-a-time (OFAT) analysis is carried out to identify the sensibility of the system performance depending on the variation of the certain parameter. This is achieved by varying the parameters according to Table 3.5, while keeping the rest of them to the default values reported in Table 3.2.

The investigated parameters can be categorised into: external parameters (wind speed), electrical parameters (packing factor) and geometrical parameters (thickness of insulation, width of tube).

Wind Speed	1-10 m/s
Packing factor	75-95%
Thickness of insulation	1-10 cm
Flow rate	50-300 l/h
Tube width	5-10 mm

TABLE 3.5: Range of variation of parameters for OFAT sensitivity analysis

3.5.1 Wind Speed

For the parametric study, the performance indicators η_{TH} and η_{EL} are computed at the highest ambient temperature of the summer day against the parameters of interest, with all the rest kept constant. The effect of the two main meteorological conditions, ambient temperature and solar radiation, on the PVT performance are easily observable in the dynamic simulation in Section 4.2. However, the influence of third component, wind speed is not so obvious, therefore this relationship is further analysed by varying its value from 0 to 10 m/s. Increasing the wind speed results in a higher forced convection coefficient, according to Equation 3.4.

The results in Figure 3.14 indicate a 2% decrease in the thermal efficiency, which can be explained by an increased forced convection heat loss from the glass to the ambient. On the other hand, a 0.1% increase in the electrical efficiency can be observed. A higher forced convection leads to a better cooling of the PV cell and a lower operating temperature, which leads to a slightly improved electrical output. However, the effect of high wind speeds on the decrease in thermal performance is much more significant than the beneficial increase in electrical performance. Overall, the global efficiency decreases with higher wind speeds. It is also noticeable that the slope of electrical efficiency decreases gradually and tends towards flattening, which indicates that the operating temperature is close to reaching the STC value of 25^o C, after which cooling no longer has an effect on the electrical output.

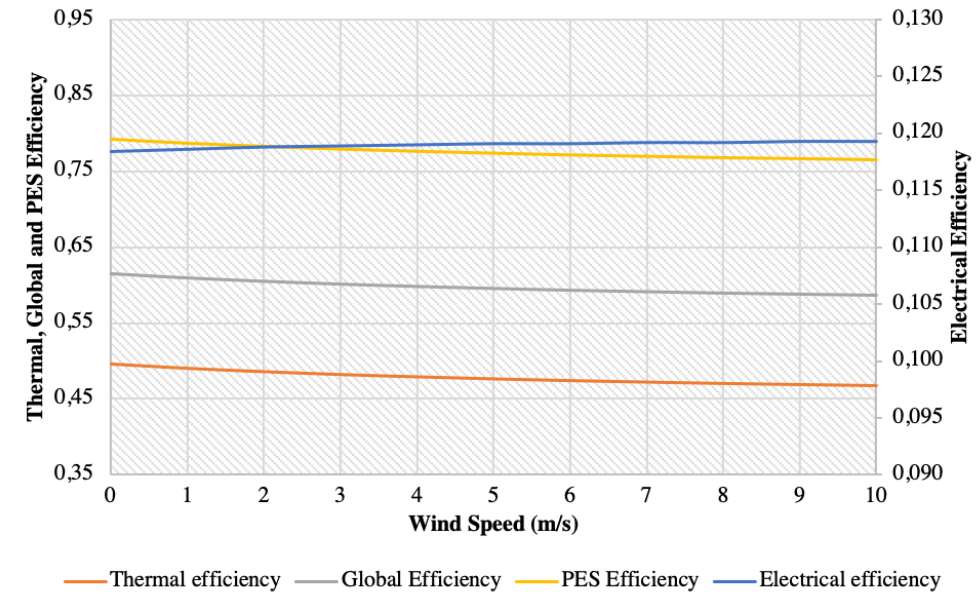

FIGURE 3.14: Variation of thermal and electrical performance as a function of wind speed

3.5.2 Thickness of insulation

Apart from the convective losses caused by the wind, heat losses also take place at the back of the panel through the layer of insulation, and their magnitude is directly influence by the thickness of the layer. The effect of the insulation losses on the system performance can be assessed by a parametric variation of the insulation thickness, from 0.01 to 0.1 m. Figure 3.15 shows a steep effect on both efficiencies at first, followed by a flattened curve, which indicates the fact that that after a certain thickness, the increase in insulation has an insignificant effect on the panel performance. In the case of the electrical performance, this occurs at 0.05 m of insulation, where the PV cells reach the STC temperature. For the thermal performance, the curve is not completely flat even at 0.1%, but the slope decreases gradually. Again, as in the case of wind speed, the effect on the thermal performance is much more significant than on the electrical one, with a variation of 3.5% compared to 0.1%.

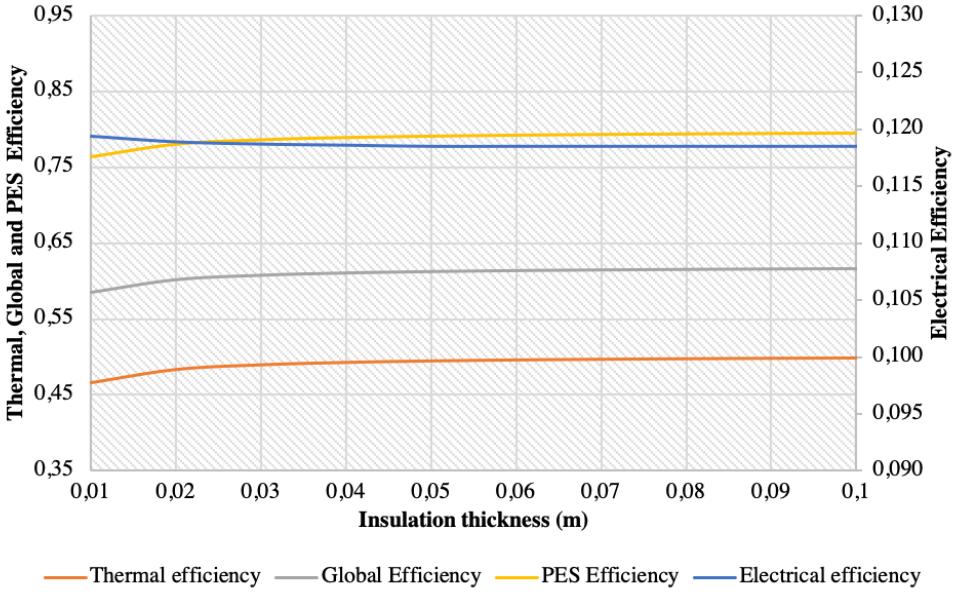

FIGURE 3.15: Variation of thermal and electrical performance as a function of insulation thickness

3.5.3 Diameter of tubes

The width of the absorber channels is varied from 5 to 10 mm for a constant m=0.005 kg/(sm^2).The variation of efficiency is illustrated in Figure 3.16. A wider diameter channel results in a larger cross section area and thus a slower speed of the fluid in the channels, but also a larger area of heat transfer between the absorber and the fluid. A better performance of both components is observed with the increase in channel width. The electrical efficiency increases by 0.6% due to better cooling of the PV, while the significant increase of 20% in the thermal efficiency is explained by a better heat transfer between the absorber an the fluid, and thus an improved thermal energy output. However, there are technical constrains on the fabrication methods of roll bond absorbers that limit the width to 8-10 mm depending on manufacturing method and materials. Overall, the global and PES efficiencies increase with a higher tube thickness.

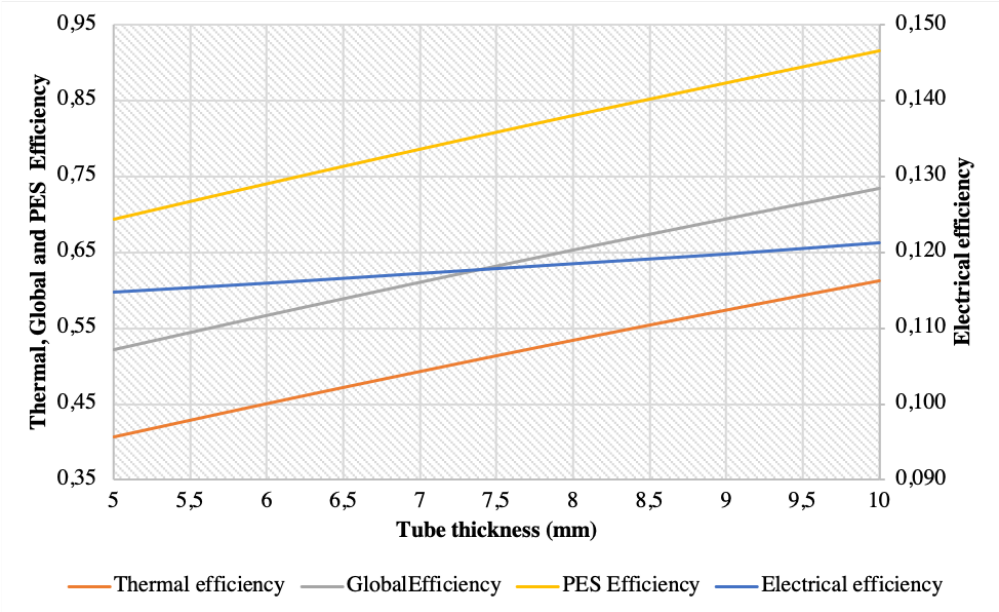

FIGURE 3.16: Variation of thermal and electrical performance as a function of tube width

3.5.4 Packing factor

The effect of the packing factor of the PV cell on the system efficiency is illustrated in Figure 3.17. Typical commercial cells have packing factors of 75% up to 95% for the highest performing ones. It can be observed that the increased packing factor has a significant positive effect on the electrical performance, with more than 2% improvement, due to a larger surface are of the panel being covered with PV cells, and implicitly, a larger amount of incident solar radiation being converted to electricity. The 20% decrease in thermal efficiency with higher packing factors is explained by the fact that a higher fraction of the solar energy is converted to electricity, and thus a smaller fraction remains to be converted into heat. Thus, the variation of the two efficiencies appears equivalent; However, depending on the consumer profile, it might be beneficial to choose a high packing factor for the PVT design, as the electrical energy is more valuable both economically and exergetically than the thermal energy. A high packing factor typically involves increased costs of the PV cells, thus a cost-benefit analysis should be carried out for optimum design. Overall, the global efficiency increases with a higher packing factor.

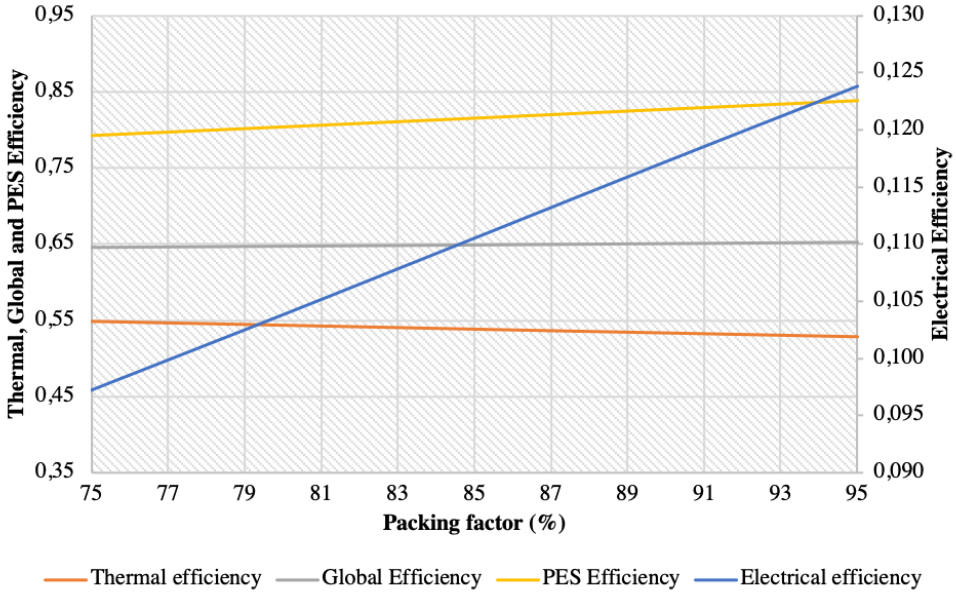

FIGURE 3.17: Variation of thermal and electrical performance as a function of packing factor

3.5.5 Flow rate

Figure 3.18 illustrates the effect of the flow rate on the performance of the collector. As expected, as the flow rate decrease, the thermal efficiency of the collector also decreases. Lower flow rates result in a lower heat transfer coefficient in the channels (caused by the dependence of the Nusselt number on the Reynolds number). Also, low flow rates result in higher temperature and consequently, increased heat losses in the channels. The heat loss coefficient of the absorber layer is dependent on the temperature. If the fluid circulates at a low speed, it collects more heat and its temperature is higher than in the case of high speed circulation, and the heat losses are also higher. On the other hand, the electrical efficiency is slightly improved with lower flow rates due to better heat extraction from the PV cells, and consequently lower operating temperatures. However, the electrical benefit of low flow rates is very small compared to the thermal benefit of high flow rates. In order to maximise the performance of the system, the flow rate should be maximised. However, the curve flattens after a point, and the pumping power increases, so the benefit of the thermal performance is no longer significant with very high flow rates. Overall, the global efficiency increases with high flow rates.

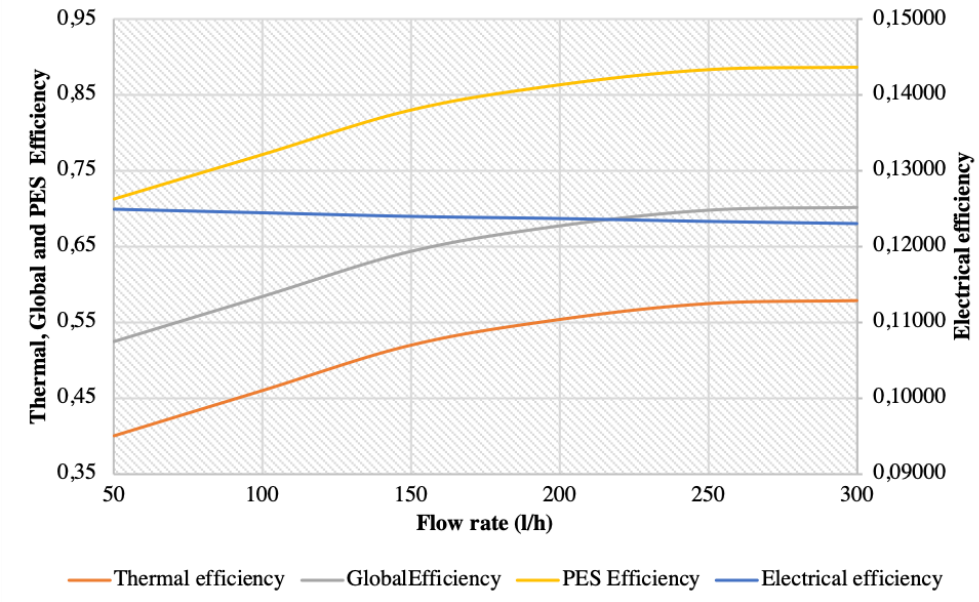

FIGURE 3.18: Variation of thermal and electrical performance as a function of packing factor

3.5.6 Performance maximisation

The PVT panel can be optimised in order to maximise the production of either thermal or electrical energy, depending on the scope and building applications:

- electrical-driven – maximising the electrical efficiency
- thermal-driven - maximising the thermal efficiency
- compromise solution – maximising the global efficiency

The results are summarized in the Table 3.6. In the case of most parameters, the compromise solution coincides with the thermal-driven solution, except for the packing factor.

	Electrical driven solution	**Thermal-driven solution**	**Compromise solution**
Wind speed (m/s)	10	0	10
Insulation thickness (cm)	1	10	10
Packing factor (%)	95	75	95
Tube diameter (mm)	30	30	30
Flow rate (l/h)	50	300	200

TABLE 3.6: Range of variation of parameters for OFAT sensitivity analysis

As a result of this analysis, a number of technical recommendations can be formulated for the efficient operation of PVT collectors. First of all, the roof installation of the panels is important, not only in terms of South-facing positioning (for the Northern

hemisphere) and tilting it to a suitable angle according to the latitude of the location, but also in terms of wind protection. In some cases, space will be limited and there is no flexibility with the mounting, which can lead to high winds and a decrease in global efficiency of the collector. Where there is flexibility in the location, a rose wind is a useful tool for ensuring there is wind protection for the system of collectors, thus improving the overall efficiency. Wind protection is not only beneficial for the efficiency, but also decreases the amount of dust collected and reduces the maintenance costs. In terms of insulation, it was observed that the benefits of increasing its width are significant. However, this can add to the cost of production and can increase the bulkiness and weight of the equipment. Another technical solution is investigating alternative materials for the thermal insulation, with lower coefficient of thermal loss, so that both the thickness and thermal losses can be kept to a minimum. In terms of choosing a packing factor for the PV layer, it is important to keep in mind the end consumer and the applications. Some manufacturers have even started to produce two types of collectors, thermally driven and electrically driven, depending on the needs of the end user. The width of the channels and flow rate can be maximized but keeping in mind that there will be an increase in the pumping power for maintaining the required flow rate.

3.5.7 Parametric analysis conclusions

This section proposed an improved explicit numerical model of a PVT collector based on the heat balance equations between each layer. The model is able to establish the temperatures inside the collector at any given time, depending on the external input: ambient temperature, solar irradiation and wind speed. The model was validated against an experimental prototype from the literature, and a typical behaviour of a PVT panel was illustrated for the case study of Strasbourg France.

The OFAT parametric analyses carried out in this study showed in most cases a compromise between the electrical and thermal performance of the PVT system. In terms of wind speed and insulation, it was observed that the thermal benefits of low wind and high insulation overcome the decrease in electrical efficiency. For optimum design, the insulation thickness should be maximized and the wind speed minimized, which can be achieved by strategic placement of the panels in areas protected from wind. The packing factor was found to be optimum when maximized, as the electrical benefits are

more significant than the thermal ones. The width of the channels in the heat exchanger should also be maximized as far as technologically possible for best performance. The flow rate should also be maximised, but keeping in mind the increased amount of energy used for pumping.

Chapter 4

Transient system simulation

4.1 Introduction

In the past years, residential PVT systems and their applications in different climates has been an interesting topic of research, with multiple state-f-the-art and review papers [28], [90]. Many software tools are available for carrying out system analysis, such as: PVSyst, SolarPro, Ansys, TRSNSY. The simulations carried out in this chapter use the Transient System Simulation Tool TRNSYS.

The first part of the simulation analyses the energy production of a system of PVT collectors connected to a small size domestic household in two similar climate conditions: Strasbourg, France and Bucharest, Romania. As it can be observed from the literature, the continental temperate climate is not the most ideal location for solar energy, most research is focused on hot and arid locations. However, with renewable technologies becoming more accessible, there is an emerging market even in continental or cold climates. France is the lead European country in PVT collectors, and market is fully developed with multiple manufacturers and distributors. On the other hand, in Romania, the market is yet to be matured, with very few distributors of PVT collectors; thus, an interesting comparison can be carried out between the two locations. The explicit TRNSYS model used as a tool to evaluate several performance indicators: first law efficiency, second law efficiency and primary energy saving efficiency is another novelty of this research.

The second part of the simulation looks at a parametric analysis of the a prosumer PVT system, achieved by varying come key parameters. A research gap was identified

in terms of entire system analysis and performance evaluation of a PVT system connected to a building. When carrying out parametric analyses, most models from the literature only looked at numerical models of an isolated PVT collector. A few studies that that considered the entire system were identified but only applied to the conventional solar technologies, solar thermal and photovoltaic panels, but not PVT collectors.

In this given framework, the novelty of this work is the overview of the full energy system to which the PVT collectors are connected, including the thermal energy storage tank and the demand curve of the consumer, as well as a parametric analysis of the most relevant thermal parameters. The parametric analysis is carried out at the level of the system, with focus on the influence that the thermal characteristics have on the electrical output. Similar to any cogeneration system, there is a close relationship between thermal and electrical energy production. For this reason, the influence of the thermal parameters of the system on the electrical performance is an interesting topic of investigation. The consumer demand is also a relevant area of research, as some consumer demand curves are more compatible with the PVT production curve than others.

Therefore, the aim of this is to investigate some of the most important thermal characteristics and their impact on the system electrical energy output. This aim is achieved by developing in TRNSYS a transient model of a simple PVT system of collectors and storage, and performing a OFAT parametric study on some of the most relevant thermal parameters. The results are relevant and useful for designers and planners in order to maximise the electrical efficiency of a PVT system the design stage.

4.2 Software description - TRNSYS

TRNSYS, short for TRaNsient SYStem, is a simulation software used to model thermal systems based on input data for the components available in the software library. TRNSYS was developed more than 4 decades ago by the Solar Energy Lab, University of Wisconsin-Madison. At first, it was mainly used to simulate solar thermal systems in various water heating applications. Subsequently, its application was extended to a wider field, such as thermal analysis of buildings, electrical and HVAC, including several component libraries related to each type of system [91].

The TRNSYS library contains a wide variety of components used in the heating system, such as water heaters, pump, solar collector and fans. Each component is designated as a type that operates on the basis of a set of governing equations or a mathematical model. The user is able create a TRNSYS simulation studio project according to model requirements, and the component characteristics and functioning algorithm are retrieved from the library available in the TRNSYS environment. Governance equations can be used to define each component of the project through a set of equations written as computer code in the Fortran programming language. Each equation is solved iteratively by using the simulation study in the selected time period. Each set of governing equations can be solved iteratively during each time step while running the simulation [91].

The software version used for this project is TRNSYS 18.

4.3 Definition of PVT Panel

The configuration of the PVT collector investigated in these simulations is shown in Figure 4.1 and 4.2. The model is a water-based PVT collector, with direct-flow geometry of the thermal absorber (Figure 4.1), roll bond channels (Figure 4.2) and mono-crystalline-silicon PV cells.

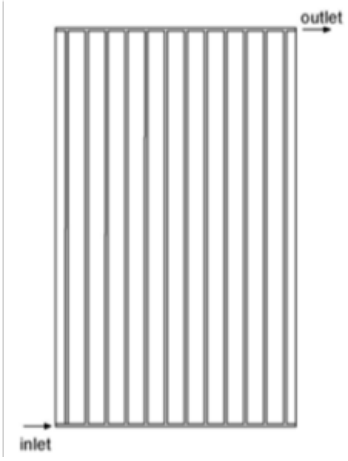

FIGURE 4.1: Diagram of the direct-flow geometry of the collector

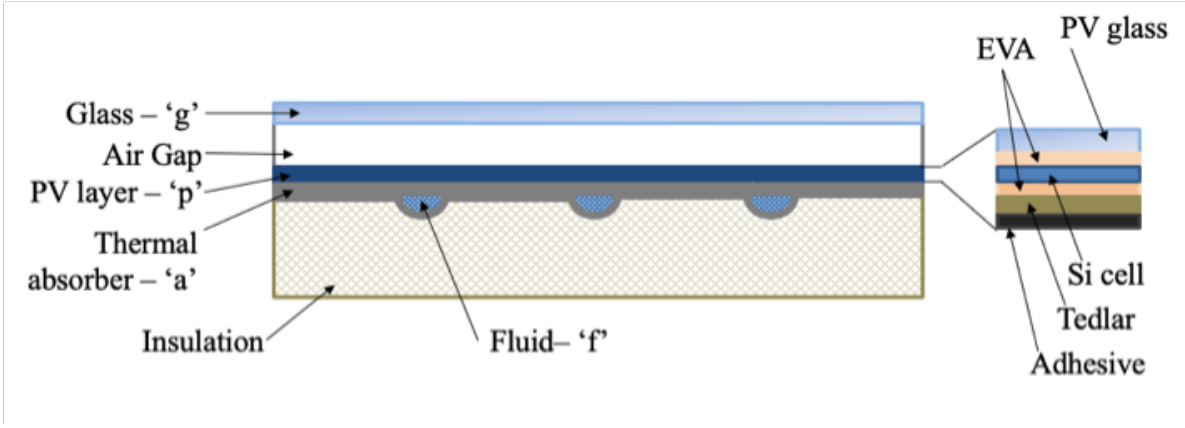

FIGURE 4.2: Diagram of a PVT collector cross section, showing the composing layers

4.4 Simulation and comparison of energy production in two climates: Bucharest and Strasbourg

4.4.1 Description of the PVT system

A schematic diagram of the PVT system used in this simulation is shown in Figure 4.3. The system is made of a PVT panel connected to a thermal storage tank through a coiled heat exchanger, an inlet pump, connection to the end-user, and a battery bank with an inverter/regulator. The system input is the weather data: ambient temperature (T_{amb} [°C])), solar irradiation (G [W/m^2]) and wind speed (W [m/s]). The temperature at the outlet of the PVT panel is T_{out_coll}, the temperature of the cold water that is injected into the tanks is T_{main}, the temperature of the thermal storage tank is T_{tank}, and the temperature at the inlet of the collector is T_{in_coll}, all in [°C]).

The technical characteristics of the PVT collector are shown in Table 4.1.

Parameter	Value	Unit
Collector Area	6	m^2
Thermal Efficiency	70	%
Electrical Efficiency	15	%
Type of fluid	Water + Glycol	-
Thermal loss coefficient	20	%
Slope	30	^{o}
Temperature coefficient of PV cells	-0.5	%/^{o}C
Packing Factor	80	%

TABLE 4.1: Characteristics of the PVT panel

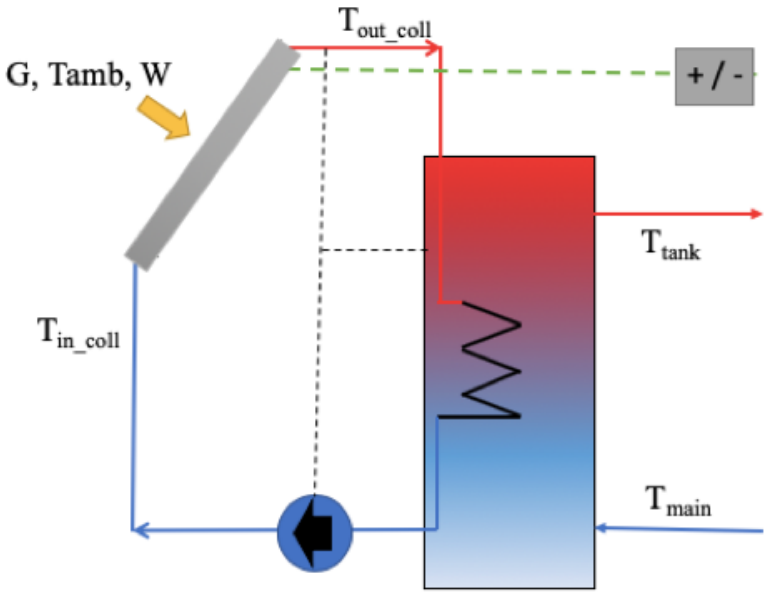

FIGURE 4.3: Simplified diagram of a PVT system coupled with a storage tank

4.4.2 Meteorological data

The output of the PVT system depends on the weather parameters: solar radiation, ambient temperature and wind speed. The solar radiation has the highest impact on the output of a PVT collector, as it determines the electrical energy production, but also impacts the temperature of the layers through the process of radiative heat transfer. The temperatures of the component layers of the PVT collector also depend on the ambient temperature, through the process of conductive and convective heat transfer that occur in the liquid and solid layers of the collector, but also on the wind speed, which determines the convective heat losses at the back and on the surface of the collector. A typical yearly profile of each weather parameter is taken from the Meteonorm Database.

The total solar radiation is made up of three different components: diffuse radiation, direct beam radiation and reflected radiation. Diffuse radiation refers to the radiation that has been scattered through the molecules of the atmosphere, direct radiation refers to the incident beam radiation directly on the surface of the panel, and reflected radiation is the radiation reflected by the surroundings, and is also referred to as albedo.

The weather conditions of Bucharest, Romania and Strasbourg, France are used in parallel for the simulations, in order to obtain a comparison of the system performance in the two locations. The weather parameters are summarised in Table 4.2:

		Winter	Spring	Summer	Autumn	Total
Temperature	Bucharest	4.0	17.8	29.1	17.4	17.1
[^{o}C]	Strasbourg	5.2	15.2	24.2	14.5	14.8
Monthly	Bucharest	36.9	48.1	64.9	47.9	594
rainfall [mm]	Strasbourg	36.5	52.3	66.9	54.8	632
Monthly	Bucharest	9.3	10.5	9.9	7.5	113
rainy days	Strasbourg	8.4	9.8	10.2	8.9	112
Monthly	Bucharest	72.6	189.7	278.8	163	2121
sun hours	Strasbourg	54.5	160.3	222	108.7	1637

TABLE 4.2: Climate characterisation of Bucharest and Strasbourg (source: WMO.com)

A daily comparison of meteorological conditions of the two cities is illustrated in Figures 4.4 to 4.9. Figure 4.4 and 4.5 illustrate the total solar radiation for a typical summer and winter week in Bucharest and Strasbourg. The two locations have average values between 700-900 W/m^2 during the summer days. The ambient temperature variation for the two locations is shown in Figure 4.6 and 4.7. It can be noticed that summer temperatures are slightly lower in Strasbourg compared to Bucharest, while the French winters have higher temperatures. Figure 4.8 and 4.9 illustrate the wind speed variation during the summer and winter weeks. On average, it is observed that the wind is stronger in Strasbourg overall, while in Bucharest there are some isolated peaks. Overall, the temperature and wind characteristics predict that the PVT system will perform better in Bucharest, while the solar radiation falls in a similar range for both locations.

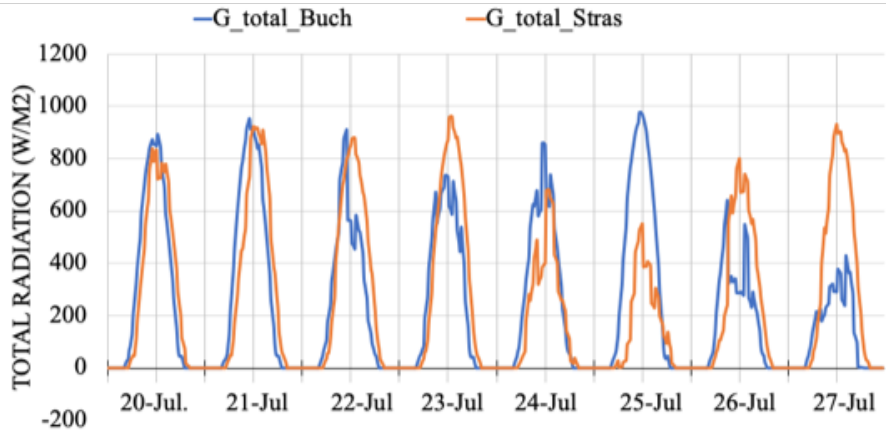

FIGURE 4.4: Solar radiation during summer

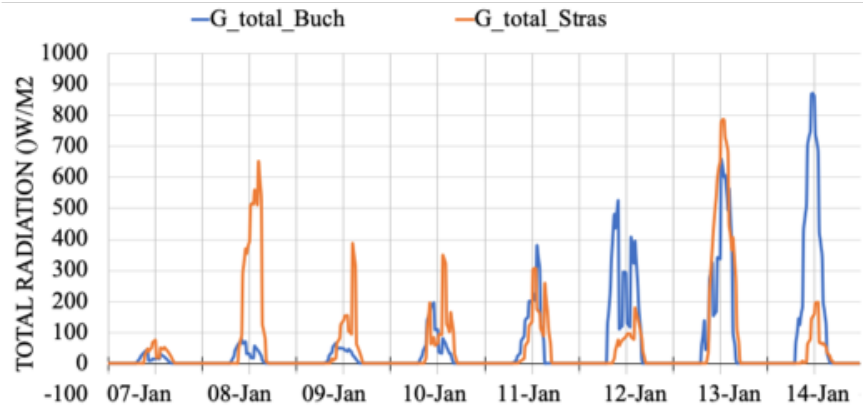

FIGURE 4.5: Solar radiation during winter

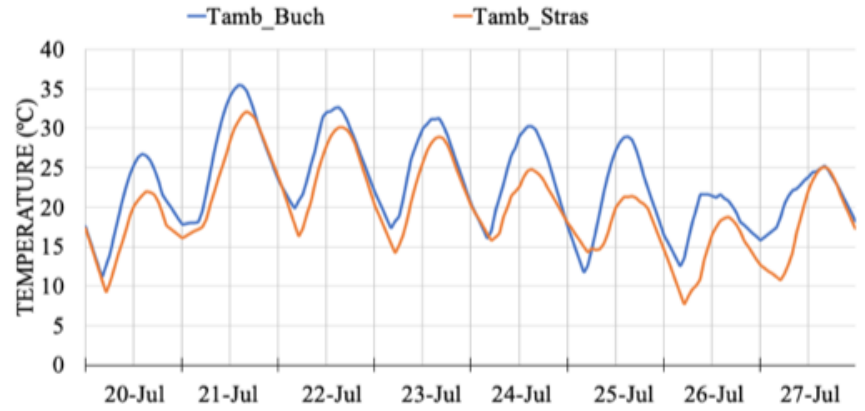

FIGURE 4.6: Ambient temperature during summer

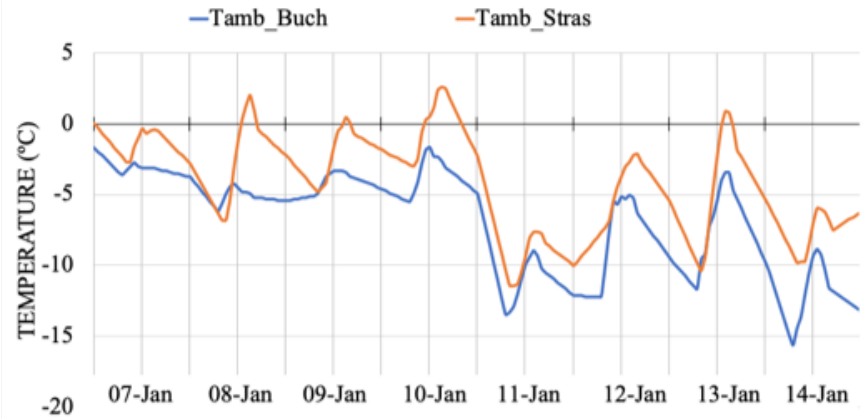

FIGURE 4.7: Ambient temperature during winter

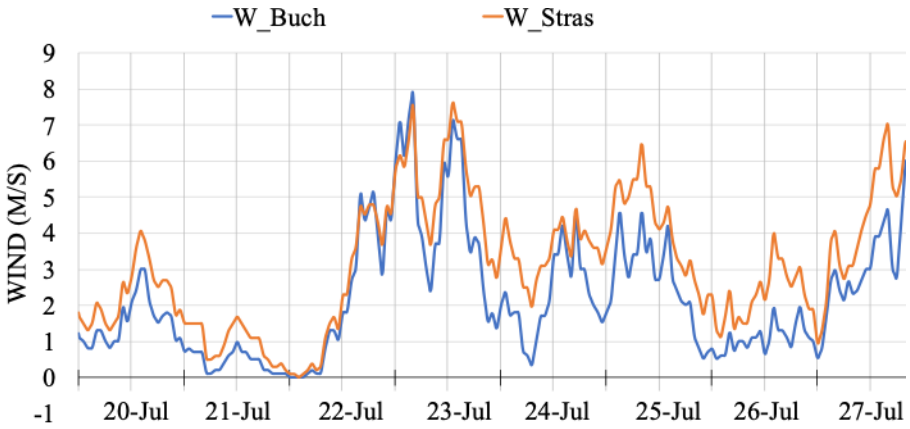

FIGURE 4.8: Wind speed during the summer

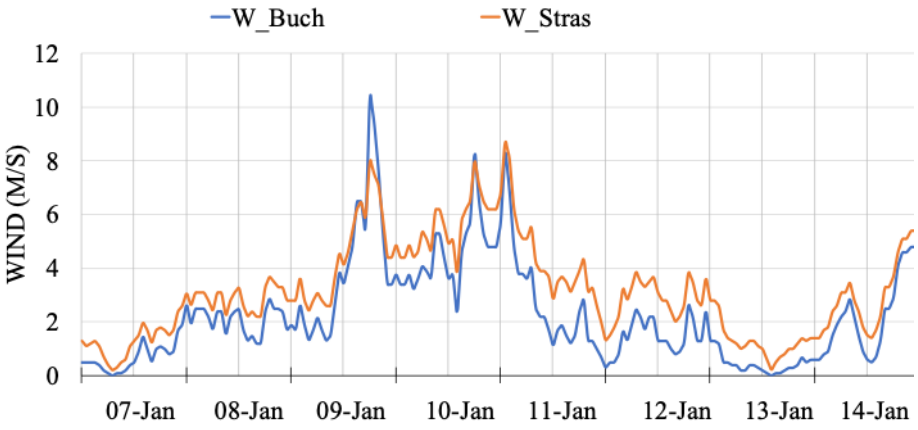

FIGURE 4.9: Wind speed during the winter

4.4.3 Domestic hot water and electricity demand

A realistic profile of a typical household domestic hot water demand is necessary for carrying out an accurate simulation. The daily profile of DHW depends on several parameters: ambient condition, seasonal variations, appliances, the number of inhabitants, the average daily and the yearly demand of water [44].

DHW-calc is a software developed for the IEA-SHC Task 26, that can generate realistic domestic hot water profiles for European countries for any time step and period of time [92], [93], and this sogtware was used to generate the DHW demand curve for this study. This software has been successfully used and validated in several research papers [44], [93], [94]. The user can configure several parameters, such as flow rates, holidays, the total average daily water volume, probability distribution, etc. Figure 4.10 shows an example of a three day profile with a one hour time-step resolution for an average consumption of 200 l/day. The profile generated by DHW-calc takes into account variations for holidays, weekdays and weekends. The profile is included in the y DHW Load function of TRNSYS, shown in Figure 4.11.

The electrical energy demand curve was generated from a forcing function in TRNSYS and by taking into account weekday and weekend variation, as well as holidays. The electricity demand also includes own services, i.e the circulation pump electrical power consumption. The system includes a battery bank. The excess electricity is injected into the local grid if the battery is fully charged, and when the battery load is less than the demand, electricity is purchased back from the national grid.

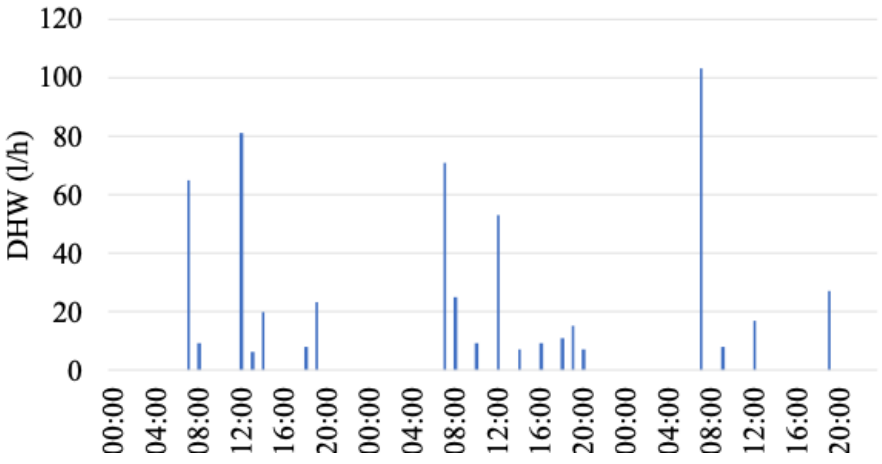

FIGURE 4.10: DHW profile over a period of 3 days (generated with DHW-calc)

The same DHW and electricity demand profiles were used for both simulations, in Bucharest and Strasbourg. The profiles are suitable for both locations as the DHW profile is applicable for any European country, and the electricity demand can also assumed to be similar. As a result, a comparison based only on the input whether data can be carried out.

4.4.4 TRNSYS model

A TRNSYS model was developed to simulate the system in Figure 4.11, and it includes: PVT pannels (Type 50), Meteorological Data (Type 15), Single Speed Pump (Type 114), Stratified Storage Tank with a volume of 100l (Type 4), a Battery Bank (Type 47) with Inverter/Charge controller (Type 48) and Controllers (Type 2). The simulation assumes that no heat losses occur on the pipes, that there is no surroundings partial shading or dust and that the optical properties of materials are constant. The flow of liquid is shown in blue, the flow of electricity with purple arrows, and the dotted arrows are for the control circuit and demand.

The main components of the model are described below:

- Type 15 is a tool reads meteorological data either from the built-in database or from a spreadsheet provided by the user and processes it to deliver the input parameters for the simulation (solar radiation, temperature, wind speed).
- The thermal storage tank (Type 4) models a tank that can be modelled to be stratified by defining the number of thermal nodes N. If N is equal to 1, the tank is modelled as fully-mixed with no stratification.
- Type 114 models a pump with a constant mass flow rate of the thermal agent.
- The pump control strategy defined by a Type 2 component is based on the temperature of the thermal agent in the storage tank and the DHW demand. The pump circulates water from the tank when there is available energy to be collected, and the water is drawn ti the thermal load and refilled when it reaches a low volume.
- Type 48 is a component that models both the inverter that converts the DC power to AC and the regulator of the system which distributes DC power from the solar

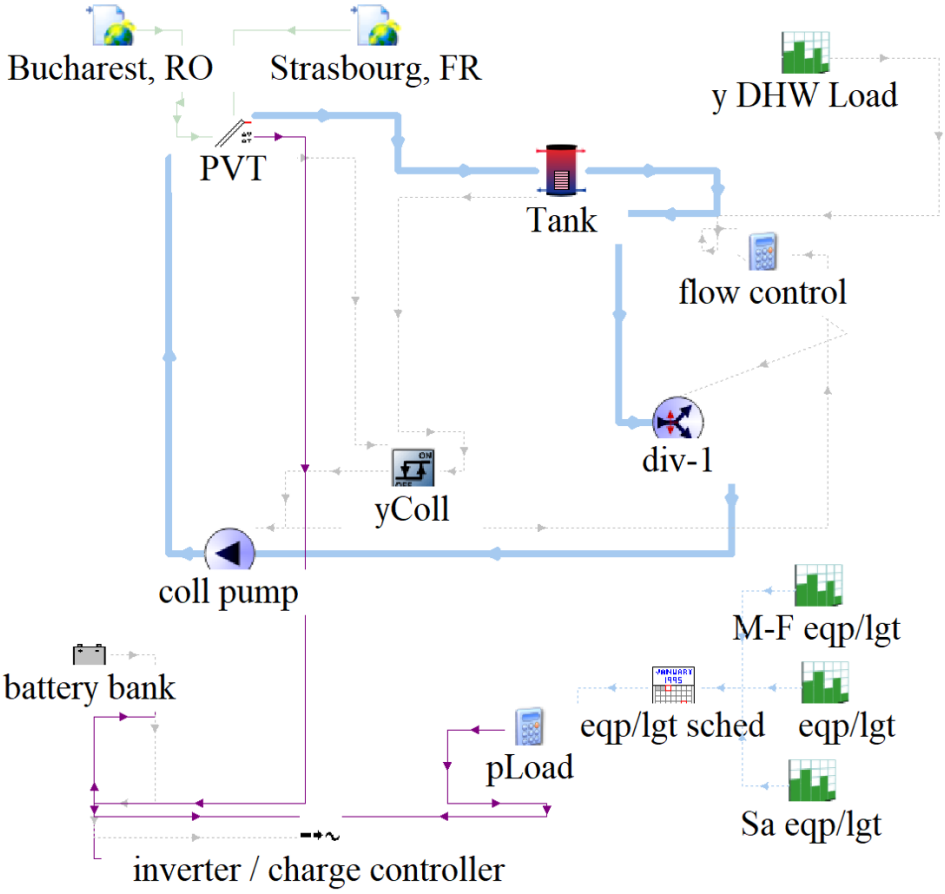

FIGURE 4.11: Components of the TRNSYS model

cell array to and from a battery. The electrical controller decides whether to use the electrical power for meeting the demand or for charging the battery.

- Type 47 is a component that models the battery bank of the system based on a lead-acid type of battery and can output data on the rate of charge or discharge and the instantaneous state of charge.

- The numerical model behind the PVT collector (Type 50) was developed using the Hottel-Whillier-Bliss equations and based on the work of [13]. Starting from the steady state energy balance of a system:

$$\frac{d^2T}{dx^2} = \frac{1}{k\delta}[U_L(T - T_a) - S + q_e] \tag{4.1}$$

where T [^{o}C] is the temperature of the element dx, k is the thermal conductivity [W/mK], δ is the element thickness [m], U_L is the thermal loss coefficient [W/m^{2}K], T_a is the ambient temperature [^{o}C], S is the total absorbed solar energy [W] and q_e is the electrical power [W]. The thermal energy output of the PVT collector is defined as:

$$Q_u = A_c F_R[S - U_L(T_{f,i} - T_a)] \tag{4.2}$$

where A_c is the collector area [m^2], F_R is the heat removal factor [-] and $T_{f,i}$ is the temperature of the fluid at the inlet of the collector [^{o}C]. The electrical power output of the system can be defined as:

$$Q_e = \frac{A_c S \eta_a}{\alpha}\left\{1 - \frac{\eta_r \beta_r}{\eta_a}\left[F_R(T_{f,i} - T_a) + \frac{S}{U_L}(1 - F_R)\right]\right\} \tag{4.3}$$

where η_a is the efficiency of the cell at ambient temperature [%], α is the effective absorbance of the cell [-], η_r is the reference cell efficiency [%] and β_r is the temperature coefficient of the cell [%/K].

The temperature at the outlet of the collector can be approximated as:

$$T_{f,o} = T_{f,i} + \frac{Q_u A_c}{(V_{flow}\rho c_f)} \tag{4.4}$$

where V_{flow} is the volumetric flow rate at the inlet of the collector [m^3/s], ρ is the density of the fluid [kg/m^3] and c_f is the heat capacity of the collector fluid [J/(kgK)].

This methodology is used to model a simplified version of a full numerical dynamic model that can be defined for a PVT collector based on the heat transfer processes in each layer [44], [60] where a system of ordinary differential equations is solved simultaneously to find the temperatures at any time step of the simulation. The detailed models are used for more complex applications, such as layer analysis and optical, geometrical or thermo-physical sizing and optimization. The TRNSYS Type 50 model was validated and proved accurate for a quantitative analysis of the daily, weekly and annual energy production.

The PVT component requires a set of input parameters specific to the constructive configuration and properties of the collector. These can be found in the manufacturer's specifications and refer to: number of glass covers, plate absorbance, collector fin efficiency, collector plate emittance, loss coefficient, optical efficiency, temperature coefficient, packing factor and STC temperature. As a result, the module can be adjusted to replicate any product available on the market.

4.4.5 System Performance

The energy performance of the system can be defined in terms of thermal, electrical and global efficiencies (η_{TH}, η_{EL}, $\eta_{overall}$). The definitions for each performance parameter parameter have been previously discussed in Section 3.3.2.

4.4.6 Simulation Results

Weekly Simulations

The simulations were run with a 15-minute time step for representative one week periods of summer and winter (7 Jan-13 Jan and 20 Jul- 26 Jul) and for both weather conditions of Strasbourg and Bucharest. Additionally, an annual simulation was run for determining the weekly electrical and thermal energy system output.

The weekly curves of electrical power output for the summer and winter periods are shown in Figures 4.12 and 4.13 respectively. The curve variation follows closely the

solar radiation variation. The ambient temperature also impacts the electrical power: as the collector operating temperature increases, the efficiency of the photovoltaic cells decreases.

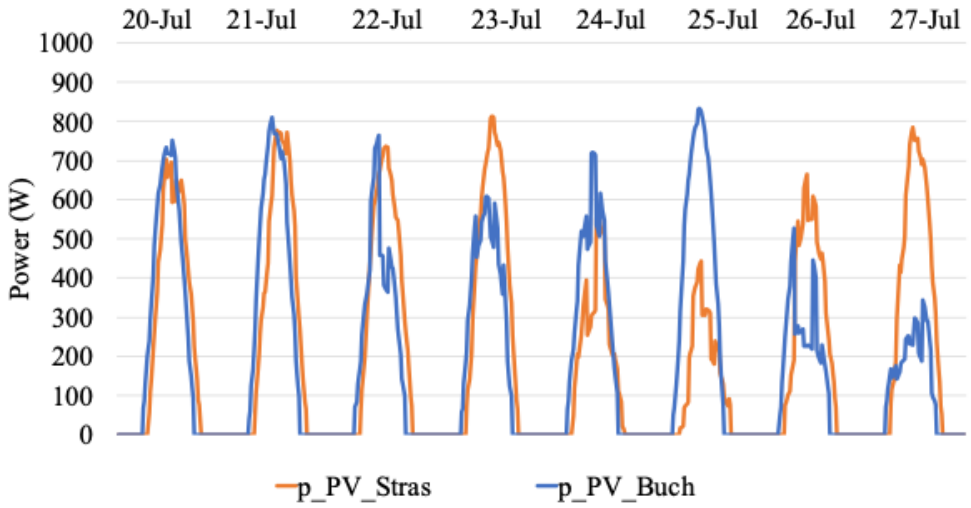

FIGURE 4.12: Instantaneous electricity produced during the summer period

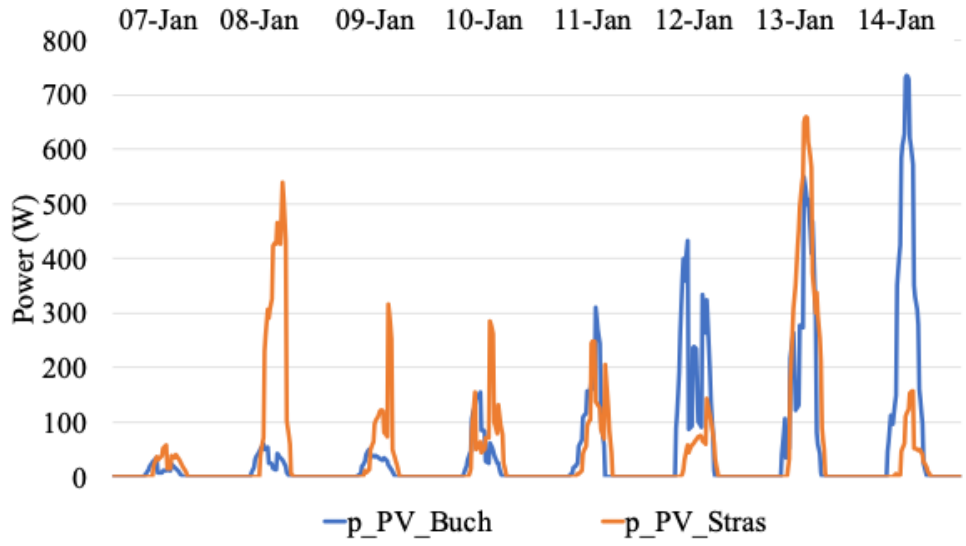

FIGURE 4.13: Instantaneous electricity produced during the winter period

Figures 4.14 and 4.15 show the variation of the temperature at the collector outlet (T_{out_coll}) and the thermal storage tank temperature (T_{tank}) for summer and winter in Strasbourg and Bucharest. During winter, the tank reaches a maximum of 15°C, while during the summer the maximum value is 30°C.

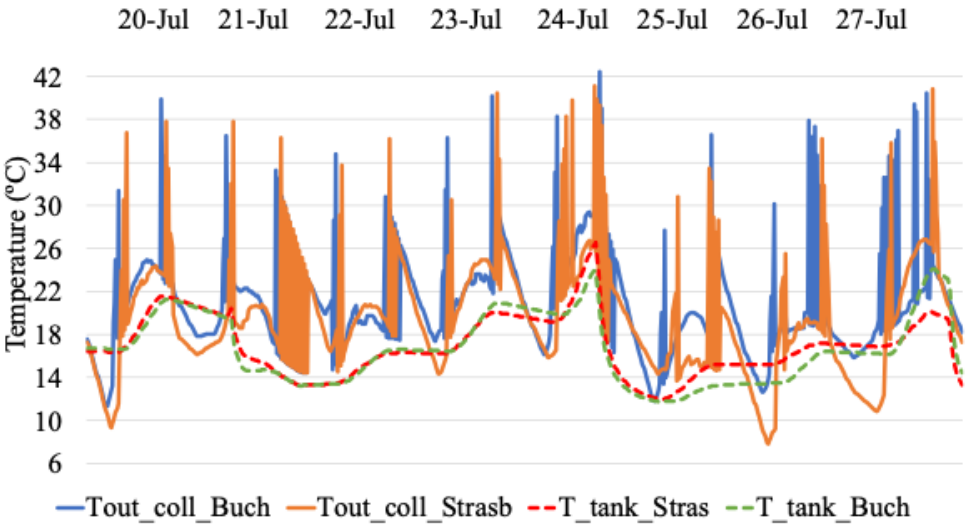

FIGURE 4.14: Temperature of the storage tank during summer

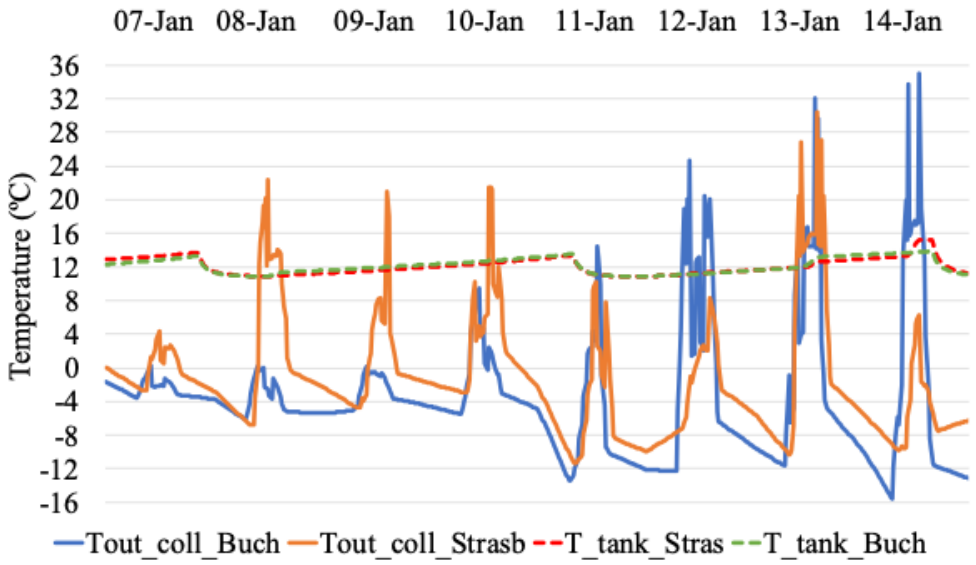

FIGURE 4.15: Temperature of the storage tank during winter

Annual Simulations

The weekly thermal and electrical energy productions are illustrated in Figure 4.16 for the period of one year. The total annual energy produced by the system in the two locations is shown in Table 4.3. Assuming an annual energy consumption of 2000 kWh and a thermal energy for domestic hot water of 6000 kWhTH, the table also shows the ratio of coverage for the household demand. It is observed that the system performs slightly better in the weather conditions of Bucharest, where it reaches a coverage ratio of over 50% of the annual consumption.

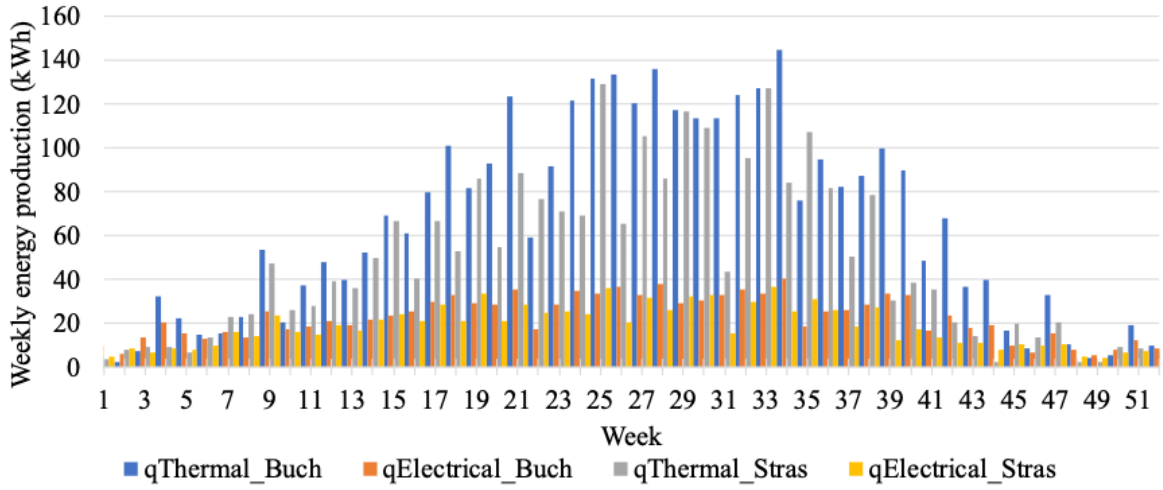

FIGURE 4.16: Weekly energy production for one year

Energy	Total Annual Output	Percentage of total consumption
Thermal energy in Bucharest	3340,80 kWh_{TH}	55,68%
Thermal energy in Strasbourg	2491,96 kWh_{TH}	41,53%
Electrical energy in Bucharest	1173,24 kWh_{EL}	58,66%
Electrical energy in Strasbourg	962,52 kWh_{EL}	48,13%

TABLE 4.3: Total annual energy output for Bucharest and Strasbourg

The results reveal that a 6 m^2 PVT system performs well in both locations, with a 10-12% better performance in Bucharest. The meteorological conditions of Bucharest are more suitable (higher ambient temperature and solar radiation) during the summer but less suitable during winter. From the overall performance a slight advantage of PVT systems in Bucharest compared to Strasbourg can be observed.

Another area of investigation is the system efficiency in terms of thermal, electrical and global performance. As previously discussed, the performance of the system can be assessed in various ways: first law efficiency, primary energy saving efficiency and second law efficiency. The thermal efficiency was calculated by subtracting the electrical power from the surface incident irradiation. The weekly efficiency of the system is obtained by taking into account the total weekly energy production (Figure 4.16) and the total incident energy on the surface of the panel during the week.

Figure 4.17 shows the weekly electrical and modified thermal efficiency of the system. It is noticed that, due to the increase in the operating cell temperature, the electrical efficiency drops during the summer for both cases, while the thermal efficiency reaches its peak during the summer weeks, with up to 64% in Bucharest and 55% in Strasbourg.

The global performance indicators described in Section 3.3.2 were calculated and are shown in Figure 4.18. It can be observed that the trend-line of the second law efficiency follows closely the trend-line of the electrical efficiency shown in Figure 4.17. The contribution of the thermal efficiency is minimal due to the fact that the difference between the logarithmic mean temperature of the fluid and the ambient temperature is very small, and as a result the Lorentz efficiency is close to zero. The first law efficiency is simply the sum of the electrical and thermal efficiency from Figure 4.17. Generally, it was observed that the system operates with a better performance in Bucharest. The efficiency calculated by the PES method is higher than the efficiency calculated with the first law method, reaching up to 90% in Bucharest. Due to the fact that the average efficiency of

producing electrical power is higher in Strasbourg than in Bucharest (0.601 compared to 0.532), the difference between the two cities in terms of PES increases further compared to the first law efficiency, which can be noticed in the Figure. The overall trend follows closely the the thermal efficiency, with high values during the summer period and low values during winter. The inverse variation of the electrical efficiency is insignificant and does not affect the general trend.

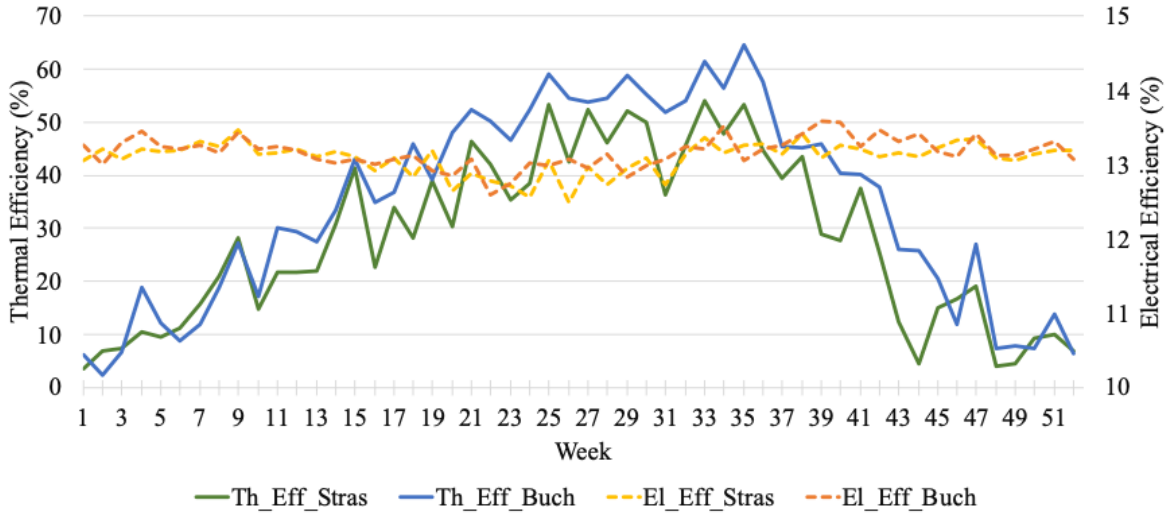

FIGURE 4.17: Weekly electrical and thermal efficiency over one year

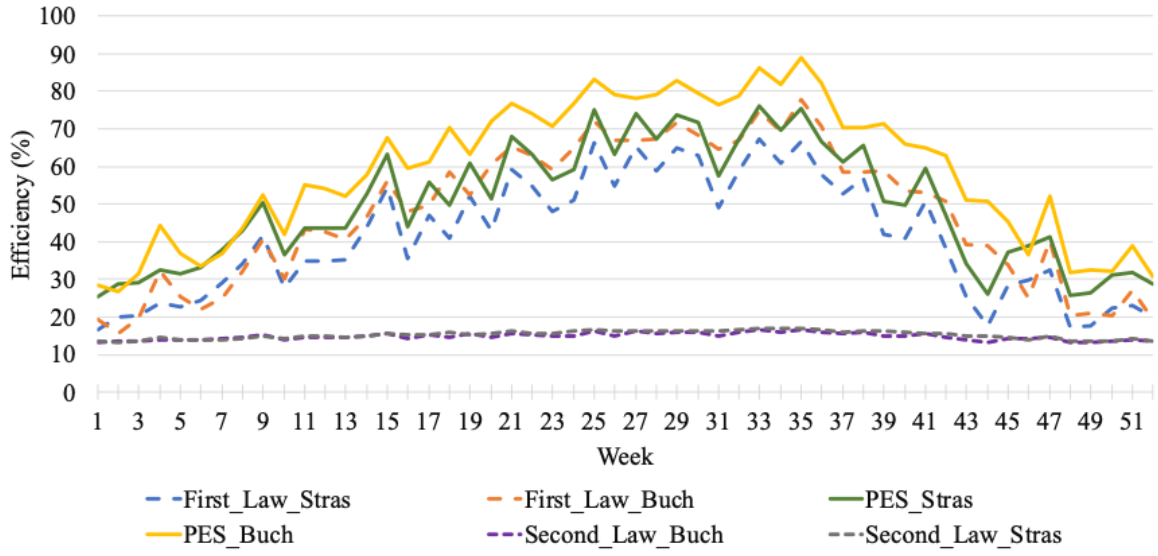

FIGURE 4.18: Overall efficiency for a week

4.4.7 Discussion of results

The system presented in this study integrates a PVT system into a typical domestic household applied in two locations with different meteorological characteristics. According to the weather data, the two locations, Strasbourg and Bucharest, have somehow similar overall meteorological patterns with cold winters and hot summers. However, there are some small differences in terms of average ambient temperature, wind speed and total irradiation which would predict that Bucharest is a more suitable location for achieving the best PVT performance. The simulations were run for typical one week summer and winter times in order to assess the power output, the temperature in the thermal storage tank and the temperature of the fluid at the outlet of the panel, and also for a one year period in order to assess the global annual performance. As expected, the electrical performance follows closely the trend of the solar radiation with only little influence from the wind speed and ambient temperature.

Overall, the yearly energy production of electricity and heat, both supported by back-up solutions (auxiliary heater and battery bank respectively) indicates that the energy demand of an average single family house could be covered to about 50% over one year, with a slightly better performance in the Bucharest climate compared to Strasbourg. This was expected due to the slightly better meteorological conditions.

There are multiple methods of assessing the overall performance of a system and there is an open debate over which is the most accurate method. The first law efficiency is the most widely used and simple method, where there is no distinction made between the thermal and electrical power. The Primary Energy Saving (PES) efficiency considers the regional differences in energy the efficiency and methods of production, and it can be useful to compare two different locations, as is the case of this research. Finally, the second law efficiency takes very little into account the thermal energy generated by the system, because it assumes that it will be used to produce electricity. The thermal energy is used directly for water heating purposes in the case of PVT systems, which means that the first law efficiency does not describe accurately the performance of the system according to this operational mode.

The main limitations of this simulation and the results obtained from it are: the simplicity of the PVT model compared to a full 3d numerical model, the fact that all

the libraries in TRNSYS are pre-defined and customisation options are limited, the consumer profiles can vary significantly according to the specific end user behaviour and the system location.

Generally, it can be concluded that a small scale PVT system is a promising solution for maximal solar energy harvesting. Residential prosumers are the main target market of this technology, which is quickly developing in the Western European countries, but is currently lagging in the East, except for China. More public awareness and demonstrative projects providing proof of concept are required to accelerate the integration this technology on the wide market.

4.5 Parametric analysis of a PVT system coupled with a DHW tank

Chapter 3 carried out a parametric analysis of an independent PVT panel, based on the variation of certain isolated parameters. Another interesting type of parametric analysis is at the level of the entire system, which will be carried out in this section. First, the relationship between the temperature at the outlet of the thermal storage tank and the electrical efficiency of an individual PVT panel is defined with a numerical model. Next, the full system is modelled, followed by an OFAT parametric analysis based on the main thermal characteristics. Finally, the results are discussed in terms of percentage of variation and annual electrical energy production.

4.5.1 Numerical model of a PVT collector

For establishing the relation between the temperature at the outlet of the heat exchanger of the tank and the electrical efficiency, two intermediate relationships are evaluated: first, the relationship between the electrical efficiency η_{el} and the operating temperature of the cell T_c (Equation 4.5); then, the relationship between the operating temperature of the cell T_c (Equation 4.6) and the PVT colelctor inlet temperature T_{inPVT}. A simplifying assumption of negligible heat losses on the pipes from the outlet of the tank to the inlet of the PVT collector was made. Consequently, the temperature at the outlet of the tank heat exchanger T_{tank} can be replaced with the temperature at the PVT panel inlet (Equation 4.7).

$$f\left(T_c\right) = \eta_{el} \tag{4.5}$$

$$f\left(T_{inPVT}\right) = T_c \tag{4.6}$$

$$T_{inPVT} = T_{tank} \tag{4.7}$$

From the three equations above, the relationship between the electrical efficiency and the temperature at the outlet of the thermal storage tank heat exchanger can be defined:

$$f\left(T_{tank}\right) = \eta_{el} \tag{4.8}$$

Next, the equations are expanded based on a thermal numerical model [95], [96] and based on the same cross-sectional scheme previously used in Figure 4.2. Equation 4.9 shows the relationship between the electrical efficiency and the cell operating temperature [95].

$$\eta_{el} = \eta_{ref}\left[1 - \beta_r\left(T_c - T_r\right)\right] \tag{4.9}$$

The temperature of the cell can be written as [95]:

$$T_c = \frac{\tau_G\left[\alpha_c\beta_c + \alpha_T\left(1 - \beta_c\right)\right] I(t) - \eta_c I(t)\beta_c + U_t T_a + U_T T_{bs}}{U_t + U_T} \tag{4.10}$$

Where τ_G is the glass transmissivity, α_c is the cell absorptivity, β_c is the packing factor, α_T is the Tedlar layer absorptivity, $I(t)$ is the incident solar radiation, η_c is the efficiency of the cell, U_t is the overall heat transfer coefficient through glass from the solar cell to the exterior, T_a is the ambient temperature, U_T is the conductive heat transfer coefficient from the solar cell to the water. T_{bs} (the temperature on the back surface of the panel) is defined as [95]:

$$T_{bs} = \frac{h_{p1}(\alpha\tau)_{eff} I(t) + U_{tT} T_a + h_T T_w}{U_{tT} + h_T} \tag{4.11}$$

Where h_{p1} and h_{p2} are penalty factors, U_{tT} is the overall heat transfer coefficient through the solar cell from glass to Tedlar, h_T is the heat transfer coefficient of the Tedlar, T_w is the temperature of the water.

From the equations above, the dependence of the electrical efficiency on the temperature in the tank can be calculated. The simulation was carried out for a variation of temperature at the outlet of the tank heat exchanger from 1^oC to 25^oC and the results are illustrated in Figure 4.19. As expected, as the temperature in the tank increases, there is also an increase in the temperature of the cell and a drop in the electrical efficiency.

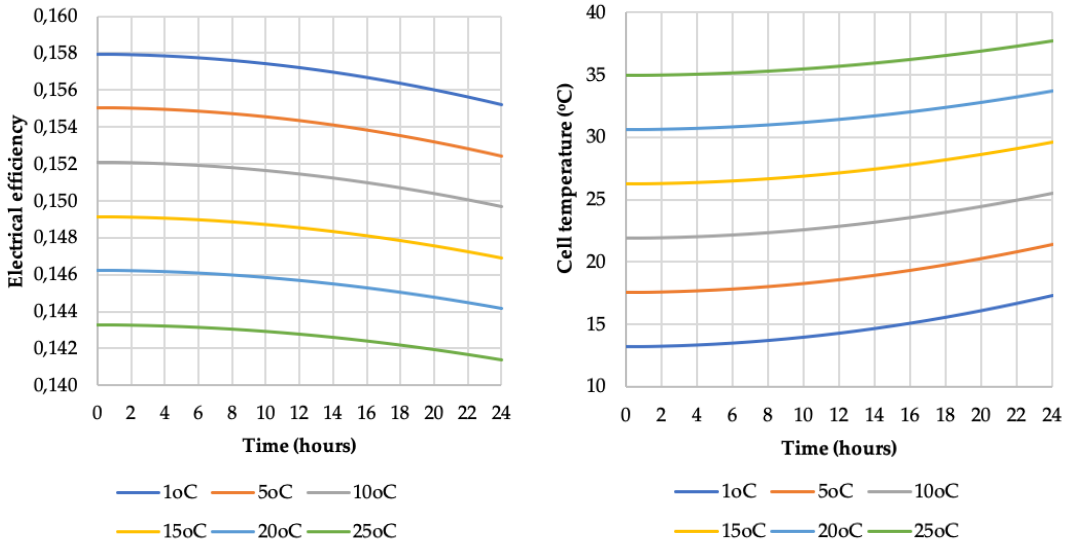

(A) (B)

FIGURE 4.19: Variation over a one day period of (A) electrical efficiency; (B) cell temperature

However, the shortcoming of this analysis is the fact that the water temperature at the outlet of the heat exchanger of the tanks is not a parameter that can be set by design, but is in turn dependent on various other parameters related to the tank. This simplified model only considers a limited number of factors regarding the collector, while the interaction with the parameters of the system is not considered. Thus, a system simulation will be carried out using TRNSYS, with PVT collectors connected to a thermal storage tank. in the next section.

4.5.2 Transient model of PVT collectors coupled with a storage tank

The same PVT system as in Figure 4.3 was replicated for this simulation, consisting of a PVT collector connected to a water storage tank with a coiled heat exchanger, a circulation pump, an inverter/regulator for the electrical energy, an inlet for the cold water main, and outlet to the consumer.

The components of the TRNSYS model include:

- PVT panel Type 50d – modelled after DualSun Spring Hybrid collector - This component is a hybrid model that adds a PV module to the flat-plate solar thermal collector. It models a hybrid collector and incorporates the work developed by Florschuetz [13] [97].

- Coiled Water Storage Tank Type 534 – the tank was modelled after a commercial boiler Viessman Vitocell 340-M – It is a constant volume storage tank with immersed heat exchangers. This component models a cylindrical tank with a vertical configuration. The fluid in the storage tank interacts with the fluid in the immersed heat exchanger, with the environment (through thermal losses from the top, bottom and edges) and with the flow streams at the inlet and outlet of the storage tank [97].

- Controller Type 2b - The on/off differential controller generates a control function which can have a value of 1 or 0. The value of the control signal is chosen as a function of the difference between upper and lower temperatures Th and Tl, compared with two dead band temperature differences DTh and DTl. The new value of the control function depends on the value of the input control function at the previous time-step. The controller is normally used with the input control signal connected to the output control signal, providing a hysteresis effect [97].

- Circulation pump Type114 - A single (constant) speed pump that is able to maintain a constant fluid outlet mass flow rate. It sets the downstream flow rate based on its rated flow rate parameter and the current value of its control signal input [97].

- Inverter/Regulator 48d - Models both the regulator and inverter, operates in Mode 1: Peak-power tracking collector, monitoring state of charge [97].

- Output online and offline printer Type 65c - The online graphics component is used to display selected system variables while the simulation is progressing. Data sent to the online plotter is automatically printed, once per time step to a user defined external file [97].

- Forcing function for defining the demand curve Type 14h – This is a repeated pattern. The pattern of the forcing function is established by a set of discrete data points input by the user which indicate the value of the function at various times in a cycle. Linear interpolation is done for generating a continuous function from the discrete data [97].

- Weather data Type 15- It reads data from the Meteonorm database at regular time intervals, interpolating the data at the required time-step and transmits it to other TRNSYS components [97].

A screenshot of the TRNSYS model is shown in Figure 4.20.

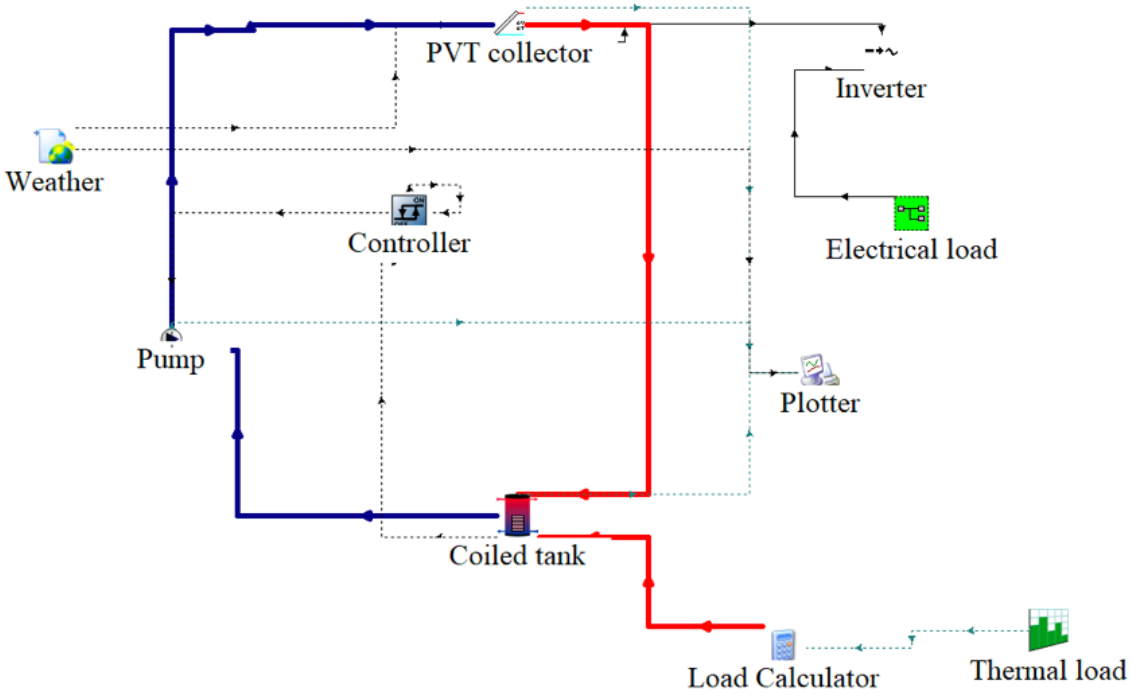

FIGURE 4.20: TRNSYS System

4.5.3 Parametric analysis of the system

The parametric analysis is done by performing a one factor at a time (OFAT) variation. The aim of this analysis is to identify the level of impact that each of the investigated thermal characteristics has on the electrical efficiency of the collector. The 'default' parameters are summarised in Table 4.4. The area of PVT collectors is equivalent to that of a system made up of two PVT panels connected in series.

Prarameter	Notation	Value
Ambient Temperature	T_a	25^oC
Solar Radiation	G	1000 W/m^2
Wind speed	v_w	0 m/s
Reference electrical efficiency of cell	η_c	16%
Pump flow rate	$\dot{m_{pump}}$	200 l/h
PVT area	A	3 m2
Tank volume	V_{tank}	250 l
Temperature coefficient	β_r	-0.5%
Tank outlet flow rate	$\dot{m_{out}}$	5 l/h
Tank inlet temperature	T_{in}	7 oC

TABLE 4.4: Default parameters for PVT system analysis

Parameters	Range	Variation
Tank inlet temperature	1-25 oC	5 oC
Tank outlet flow rate	1-30 l/h	5 l
Tank volume	100-600 l	100 l
Demand curve	refer to Fig. 4.26	refer to Fig. 4.26

TABLE 4.5: Range of variation of parameters for OFAT analysis

One of the parameters is varies according to Table 4.5, while the rest are kept constant to 'default' values shown above. The simulations are carried out for 24 hours.

4.5.4 OFAT parametric analysis

The result of the OFAT parametric analysis will be described and discussed in this section.

Tank inlet temperature

The tank inlet temperature depends on the temperature of the cold water main, which can vary depending on the location from 1^oC to 25^oC, with a most common value of 7^oC [98]. In this study, the cold water temperature was varied from 1 to 25^oC in order to evaluate the magnitude of the effect it has on the electrical efficiency of the collector. It's expected that colder water will lead to better cooling of the collector and better electrical cell efficiency.

Figure 4.21 illustrates graphically the results of the simulation in terms of cell temperature and electrical efficiency. In the initial state, before the temperature rises, the electrical efficiency of the PVT collector has a default value of 16%. However, there is no electricity production before the start of the solar radiation, so this value is only

theoretical. As the temperature in the cell begins to rise above the standard test conditions of 25^{o}C and the solar radiation starts, the electrical energy production begins and the temperature of the cell rises. The results indicate a small and proportional decrease in the electrical efficiency with higher tank inlet temperatures, with a variation of only 0.2%. That being said, the inlet temperature from the cold-water main is a constant in any particular location, so this analysis is only applicable when comparing equivalent systems in different locations.

As a comparison and in order to ensure the theoretical constant parameter simulation would also work for realistic weather conditions, the same simulation was run for a typical summer day in Bucharest, Romania. In this case, the solar radiation and temperature were no longer kept constant according to Table 4.4, but varied according to Figure 4.22. The results are shown in Figure 4.23. It can be observed that the same proportional difference as in the OFAT analysis is kept between consecutive steps, but the efficiency drops even lower, to 15.7%. This is caused by the fact that the cell temperature reaches values of 60^{o}C due to radiation and temperature being higher that the standard test conditions at noon. The peak occurs at maximum radiation around midday, with an additional spike around 16 due to the peak ambient temperature. The rest of the simulation results are run for constant STC conditions.

Tank volume

The default volume of the modelled tank is 600l. For the parametric variation, the tank volume takes values from 100l to 600l with increments of 100l. The results of the simulations are illustrated in Figure 4.24. In this case, the difference between the steps is not proportional, as it was with the inlet temperature. With the smallest tank size, a steep decrease in efficiency occurs, followed by a flat curve that goes down to 13.5%. As the tank size increases, the efficiency also increases as the temperature in the tank is lower, and also the shape of the curve changes to a constant slope. The difference between the highest and lowest step is more significant than in the previous simulation, with a value of about 0.7%. With the smallest tank size of 100l, the curve flattens to a value of 13.5% for electrical efficiency, after this point there is no further decrease.

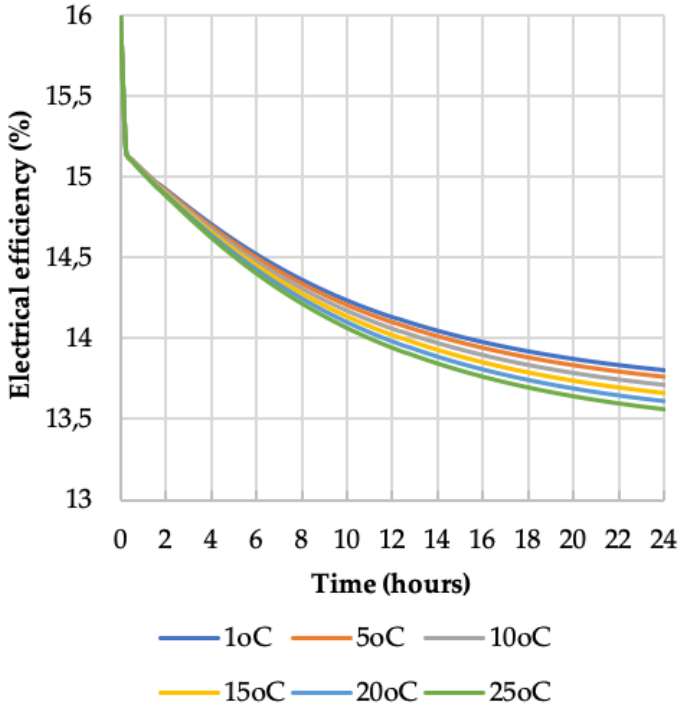

(A)

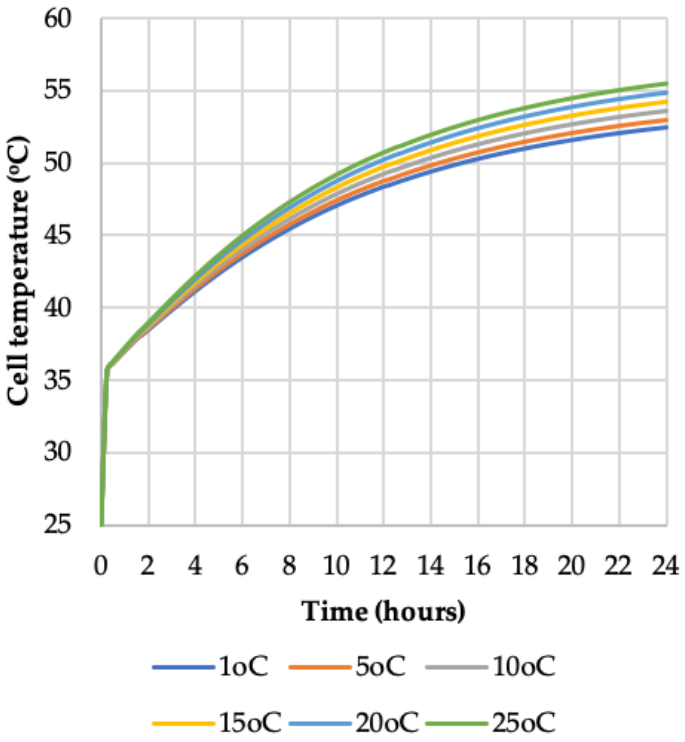

(B)

FIGURE 4.21: Evolution of the (A) electrical efficiency; (B) cell temperature; as a function of the temperature at the inlet of the tank

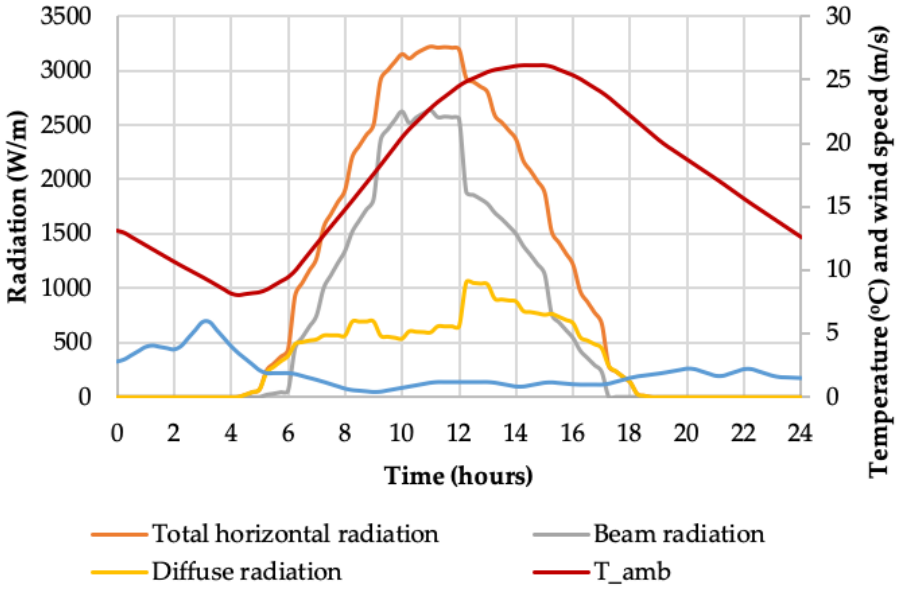

FIGURE 4.22: Meteorological data for a typical summer day in Bucharest, Romania (obtained from Meteonorn database)

Flow rate to consumer

The flow rate at the outlet of the tank represents to the rate of consumer demand. The simulation was run for volumetric rates of 0 to 20l/h. This is the equivalent of 0 to 480 l/day.

The results in Figure 4.25 show that the higher the water draw, the better the electrical efficiency. This is due to the fact that hot water in the tank is replaced with cold water from the main at a higher rate and the cell is better cooled. The difference between the minimum and maximum simulation step is 1.1%. With a lower flow rate, the curve is steeper and the stabilisation point is further along in time.

Various demand curves

The daily profile of hot water depends on various parameters: he number of end-users, type of building, appliances, seasonal variations, ambient condition, the total daily hot water demand and the yearly demand [31].

The default household DHW demand was obtained using the DHW-calc software, which can generate realistic domestic hot water profiles for European countries for any required period of time and timestep [92], [99].

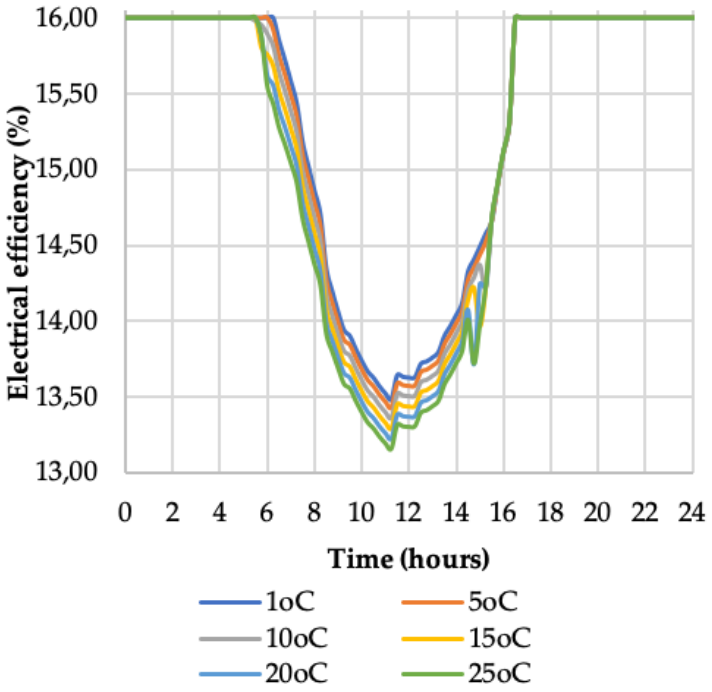

(A)

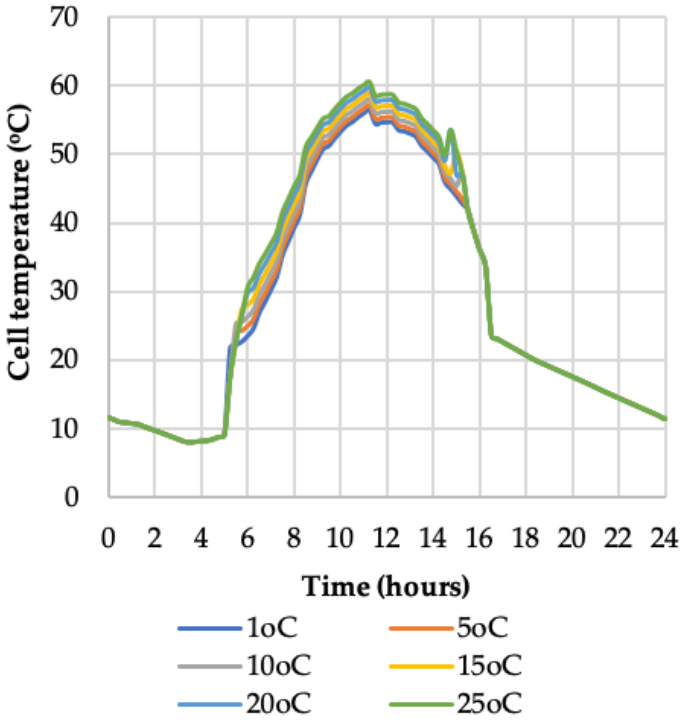

(B)

FIGURE 4.23: Evolution of the (A) electrical efficiency; (B) cell temperature; during a typical summer day in Bucharest, Romania

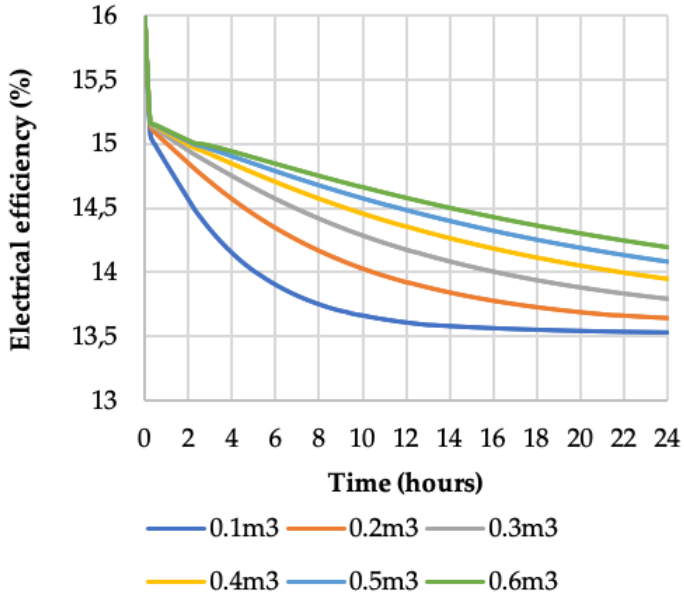

(A)

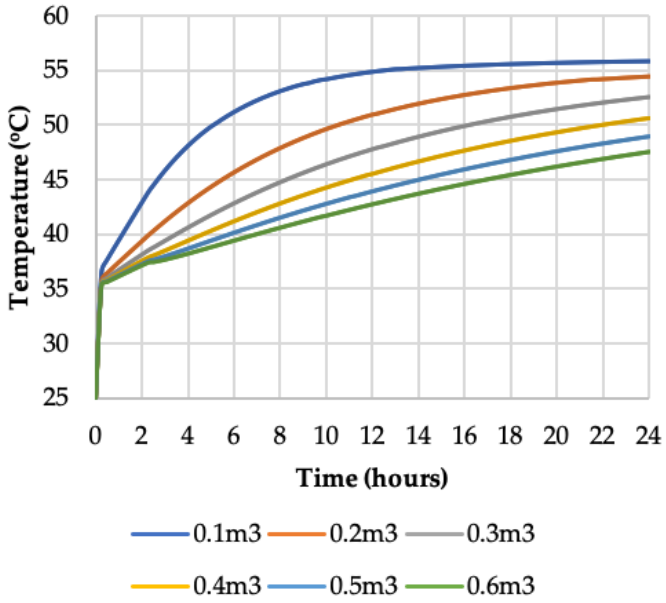

(B)

FIGURE 4.24: Evolution of the (A) electrical efficiency; (B) cell temperature; as a function of the tank volume

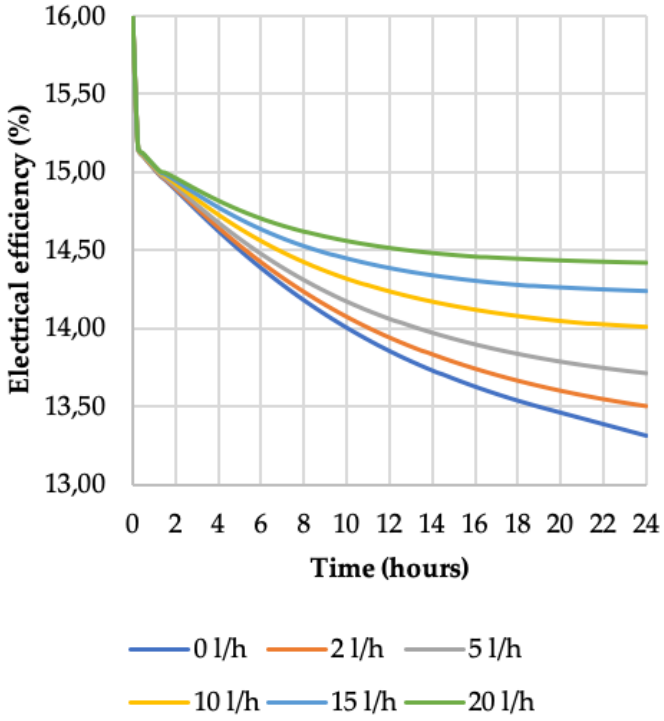

(A)

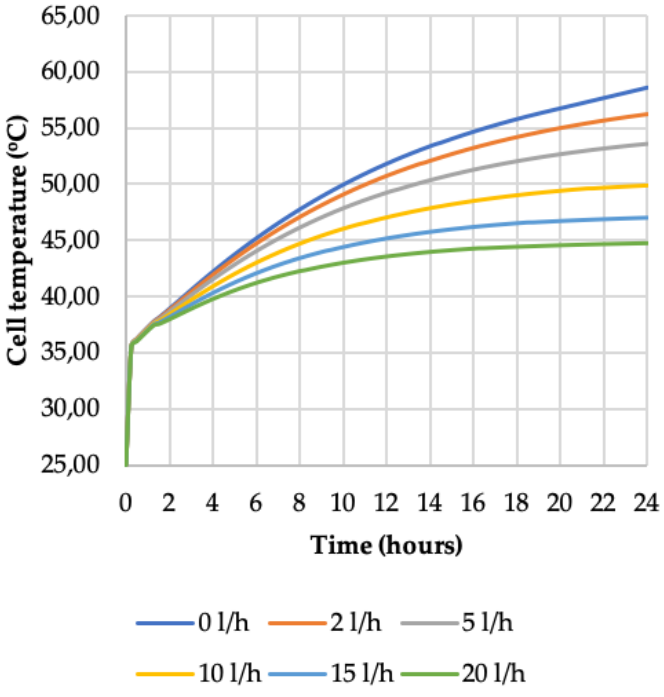

(B)

FIGURE 4.25: Evolution of the (A) electrical efficiency; (B) cell temperature; as a function of the flow rate to the consumer

Type of building	Location of measured data	Reference
Home	Europe	[92], [99]
Hotel	Japan	[100]
Kindergarten	Estonia	[103]
School	Estonia	[103]
Office	Estonia	[103]

TABLE 4.6: Demand data summary for various types of consumers

The hot water demand of the hotel was taken from a study with real measurement of the demand of one double room with two occupants in a city hotel, located in downtown Kyoto city [100]. The curve is shown in Figure 4.26. The demand of a hotel is particular compared to the household, as we can observe that the peak demand occurs later in the evening, as typically hotel guests are out late. The measurements are taken in Kyoto, Japan, which has a temperate humid climate, different from the temperate continental climate of Bucharest. This means that the amount of water draw is also different, since ambient conditions are an important factor in the amount of water demand [101], [102]. However, since all the demand curves were scaled down to match each other at 200 l/day, the important factor here is not the total volume, but the daily distribution, which is typical to hotel guests in big cities (out during the day, up late in the night).

Other considered profiles are of a kindergarten and school. They show similar curves with slight variations, both peaking at midday when there is the maximum water draw for lunchtime. The data was collected from a study [103] where the gym was excluded from the school campus, as it would considerably impact the curve.

The demand curve of the office building was adapted from a small office building in Estonia [103]. The curve peaks at midday, with an additional period of consumption at the end of the office hours.

The demand data is summarized in Table 4.6.

For the parametric study on the demand curve, an average total water draw of 200 l was considered for the daily usage, varying only the daily curve distribution according to the source data. In the case of larger users, such as hotels or office buildings, this is an assumption that scales down the size of the user to an equivalent home. The demand curves are illustrated in Figure 4.26 for a typical weekday (Monday-Friday, scaled down from the data to reach an area under each curve of 200l/day.

The results of the 24h simulations are shown in Figure 4.27. It's interesting to observe

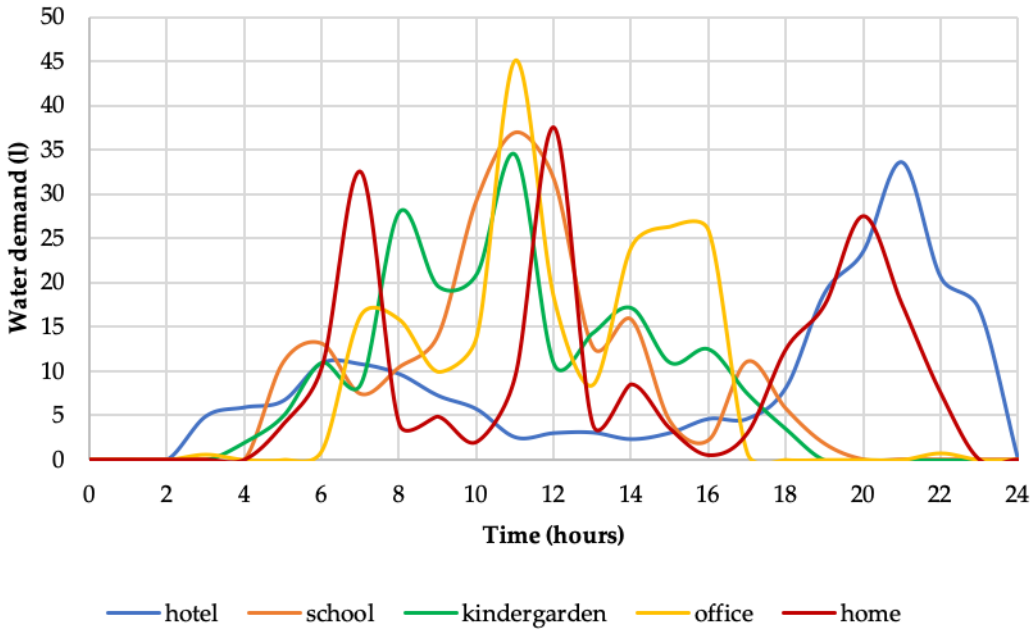

FIGURE 4.26: DHW demand curves for various buildings

that the peak efficiency occurs during the peak demand of each curve. A variation of more than 1% is observed between the peak and minimum electrical efficiency overall, and about 0.5% at a particular time.

Power versus PVT inlet temperature

An interesting aspect to observe is the variation of the instantaneous power as a function of the temperature of the coolant at the inlet of the PVT panel, shown in Figure 4.28. This was carried out with all the parameters kept constant to the default values.

As expected, the electrical power (P_{el}) decreases with higher inlet temperatures. For this particular modelled panel, the approximate slope of the curve is -2.14. The instantaneous thermal power extracted from the PVT panel (P_{thPVT}), calculated at the outlet of the panel, as a function of the temperature difference between the inlet and the cell, also decreases as the temperature at the inlet of the panel increases, with a slope of -16.28. That is due to the fact that the difference in the temperature decreases. However, if we look at the net instantaneous power delivered to the tank, calculated as the rate at which energy is removed from the tank through the specified outlet port minus the rate at which energy is added to the tank through the corresponding inlet port, it can be observed that it increases with a slope of +12.14. This means that the total amount of

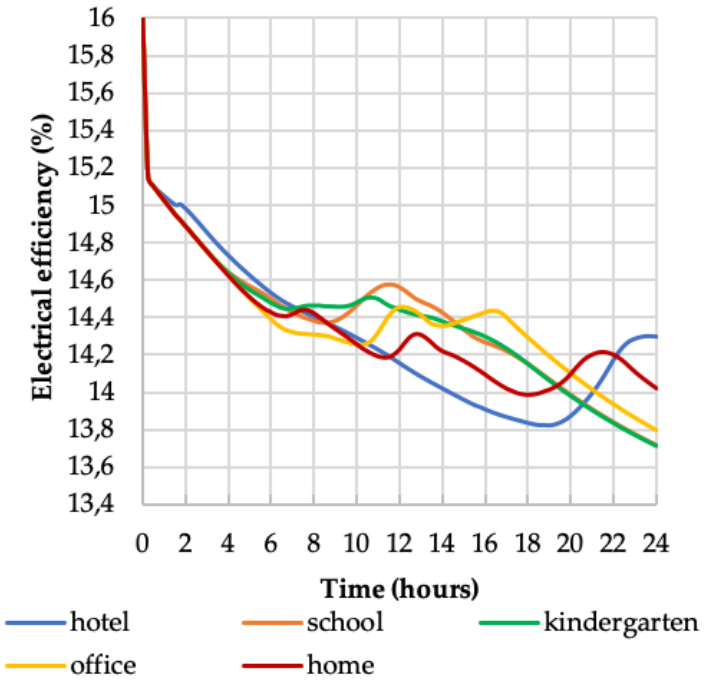

(A)

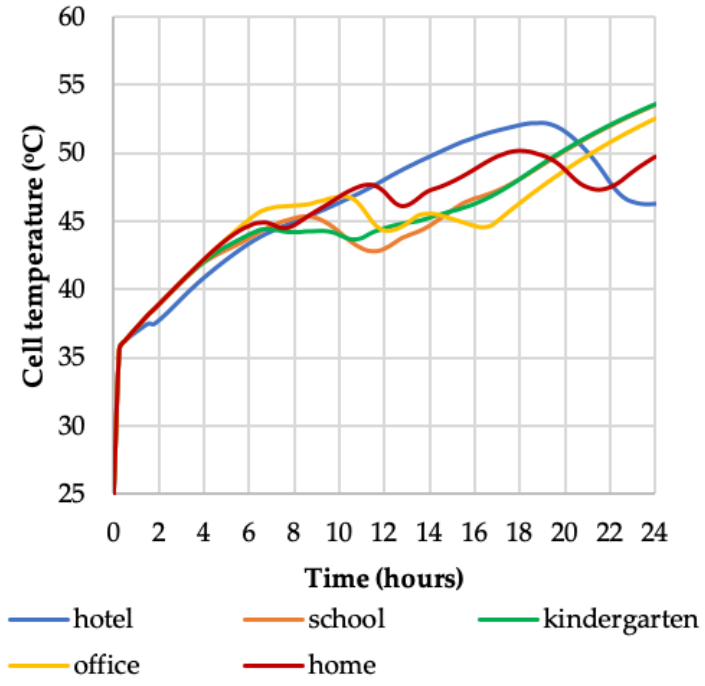

(B)

FIGURE 4.27: The variation of the (A) electrical efficiency; (B) cell temperature; as a function of the consumer demand curve

energy produced by the system is increasing, keeping in mind that the outlet flow rate to the consumer is constant during the simulation.

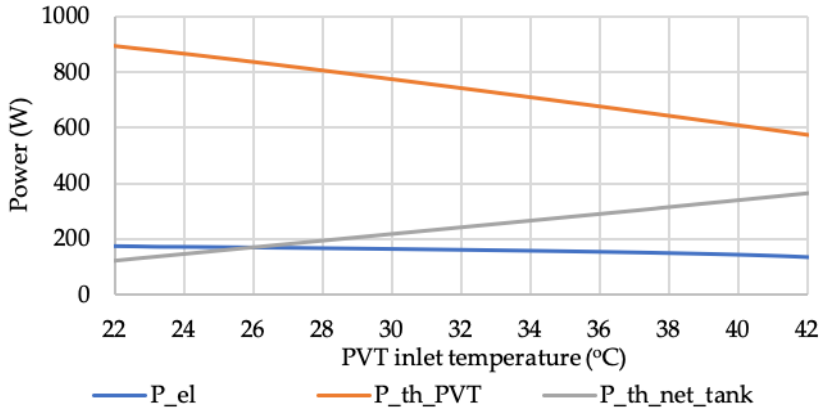

FIGURE 4.28: Instantaneous power versus PVT inlet temperature

4.5.5 Discussion of results

The parametric analysis showed that the flow rate at the outlet of the tank has the most impact on the electrical efficiency, and secondly ranked is the volume of the tank, as illustrated in Figure 4.29. This indicates the fact that the consumer demand is a critical factor in the efficient performance of a PVT system. If the system is not sized suitable to the consumer, it can occur that there is not sufficient hot water draw from the tank and the temperature increases, with a big impact on the electrical performance of the system. In reality, his situation occurs in some buildings: for example, in schools and other educational units, during holidays the water demand drops significantly and as a consequence the electrical efficiency also drops significantly. Mitigation measures should be put in place for these situations, such as additional cooling by ventilation, over-designing the size of the tank or additional cooling of the tank by removing an amount of hot water. Further research will look at the effects and overall energy impact of these various measures. The curve of the consumer demand is also important; dwellings that require higher volumes of water during midday, when the peak solar radiation occurs, are more suitable for a PVT system, such as school, kindergarten, office buildings. However, as stated previously, in these cases the annual demand is not constant due to holidays. Homes and hotels have a peak consumption later in the day, but their demand is more or less constant during the year.

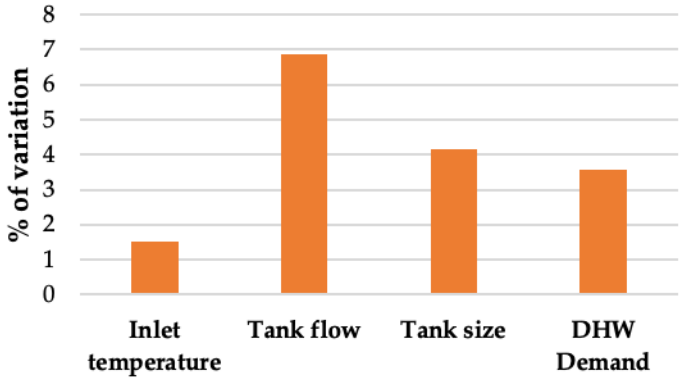

FIGURE 4.29: Ranking of the thermal parameters as a function of their impact on the electrical efficiency

Parameter	Variation	% variation from total	Annual variation in terms of electrical energy (kWh)
Tank inlet temperature	0,242	1,514	17,76
Tank outlet flow rate	1,099	6,871	80,62
Tank volume	0,664	4,153	48,72
Demand curve	0,574	3,588	42,09

TABLE 4.7: Results summary of the OFAT analysis

Table 4.7 summarises the maximum variation between the minimum and maximum steps of the OFAT simulation. The variation from the total refers to the maximum electrical efficiency that can be achieved by the chosen PV cell. The annual variation in terms of energy refers to a total of annual energy produced by a residential PVT system of 1173,24 kWh_{EL} [104].

This section modelled the temperature interactions in a simple PVT panel and in a PVT system connected to a DHW storage tank. Next, an OFAT parametric analysis was carried out to investigate the impact on the electrical efficiency of various thermal characteristics: size of DHW tank, flow rate to the consumer, cold water main inlet temperature, consumer demand curve. The analysis was done by keeping all the other parameters constant and varying only the investigated parameter.

The results show that the variation of the outlet flow to the consumer has the highest impact on the electrical efficiency, of about 6.8%. The next highest impact factor is the size of the tank with a variation of 4.7%. The cold-water main temperature showed a variation of only 1.5%. Matching the profile of the consumer is also an important aspect, as it was observed that the peak electrical efficiency occurs during peak consumer demand. Finally, the instantaneous variation of the thermal and electrical power of the

system was analysed as a function of the temperature at the inlet of the photovoltaic-thermal panel. The results of this analysis indicate that the net instantaneous power delivered to the tank increases at a rate of 12.14% with the increase of temperature of the PVT inlet fluid.

The main conclusions of this research can be summarised as:

- The lower the cold-water temperature of the main, the better the cell electrical efficiency;
- The bigger the water storage tank, the better the cell electrical efficiency;
- The higher the consumer water demand, the better the cell electrical efficiency;
- When there is a peak in the hot water demand from the consumer, the electrical efficiency of the cell also peaks;
- The biggest impact on the electrical efficiency is the water draw to the consumer;
- With increasing temperature of the fluid at the inlet of the PVT panel, the instantaneous electrical power decreases, the instantaneous thermal power also decreases, but the net instantaneous thermal power added to the tank increases.

Chapter 5

Experimental analysis

The introduction of small scale decentralized solar energy is an essential contributor to the energy mix of the future. On site-production of renewable heat and electricity is beneficial for multiple reasons: less pollution, less heat/electrical losses due to transportation, increased reliance of the system. A hybrid solar based system, comprising of solar thermal (ST) panels, photovoltaic (PV) panels and photovoltaic-thermal (PVT) panels was implemented for a kindergarten in Bucharest, Romania. The aims of this installation are:

- to provide DHW to the building;
- academic research;
- teaching purposes - the installation will be use in laboratory classes for the students of the Faculty of Power Engineering.

This chapter will begin by describing the thermal and electrical system set-up, as well as the meteorological data collectors. The individual equipment employed for this project and its technical characteristics are also described. Next, an overview and analysis of the collected data will be carried out for a determined period of time. The raw collected data is processed and the efficiencies as well as the total amount of energy produced can be computed and assessed.

From this, the performance of the PVT panels can be evaluated and assessed, as well as its suitability for this particular type of end-user. The implementation of this demonstrative system was efficient in reducing the energy consumption of the end-user, and it also provides a useful resource for academic and teaching purposes.

5.1 Experimental set-up

5.1.1 Building description

The hybrid pilot project was designed and implemented in 2020 at University Politehnica of Bucharest (UPB), Splaiul Independentei no. 313, District 6, Bucharest. The beneficiary and end-used is the kindergarten building located in the UPB campus. The 1.5 storey building was built in 2016 and is formed of 6 classrooms, 6 sleep rooms, toilets and one large common area. The photographs in Figure 5.1 shows the interior and exterior of the building.

(A) (B)

FIGURE 5.1: Photographs of the UBP Kindergarten A)Interior B)Exterior

The rooftop on which the panels are located has the geographical coordinates 44^o 26′ 18.5316" N and 26^o 2′ 35.8116" E. According to Figure 5.2, the building is located on the S-N direction with a deviation of 15^o to the V-E direction. The terrace has the dimensions of 40 m x 40 m The solar panels are placed parallel to the south side of the terrace, while the boiler and other installations are located inside the building, in a designated service room.

5.1.2 System overview

The technical design of this installation followed the technical regulations in force:

FIGURE 5.2: Satellite view of the UPB Kindergarten building

- Law 10/1995 on quality in constructions;
- Norm I 9 - 2015 for the design and execution of sanitary installations;
- Norm for fire safety of constructions - indicative P 118 - 99;
- National standards regarding the design of sanitary installations: -1478- Internal water supply for civil and industrial constructions;
- European regulations used for the design of solar installations:
  - Roof mounting:
    * DIN 18338 Roofing and sealing operations
    * DIN 18339 Tinsmith work
    * DIN 18451 Scaffolding works
    * DIN 1055 Maximum loads for construction
  - Connection of solar thermal installations:
    * DIN En 12975-1 Solar thermal installations and their components - panels

    - DIN En 12976-1 Solar thermal installations and their components - installations manufactured in accordance with customer requirements
    - DIN 4757-1 Solar heating systems, with water or water mixtures as thermal agent, requirements for a technically safe execution
  - Installation and execution of water heating devices:
    - DIN 1988 Technical rules for hot systems of domestic and sanitary hot water
    - DIN 4753-1 Water heaters and water heaters maintenance: requirements, marking, structure and verification
    - DIN 18380 Heating systems and domestic hot water systems
    - DIN 18381 Installation works for gas and water supply for wastewater drainage in buildings
    - DIN 18421 Insulation of technological installations
    - DVGW W 881 Domestic hot water and pipe preparation installations; Technical measures to reduce the formation of bacteria.
  - Electrical connection:
    - DIN 18328 Installations for cables and electrical installations in buildings

The system is a six-panel hybrid installation formed of three types of collectors:

- two photovoltaic (PV) panels
- two solar thermal (ST) panels
- two hybrid photovoltaic-thermal (PVT) panels

Along with it, there is a state of the art meteorological station for collecting live weather data. It comprises of:

- solar radiation sensor
- ambient temperature sensor
- wind direction transmitter
- wind speed sensor

Figures 5.3 and 5.4 show overview photographs of the panels and the meteorological station.

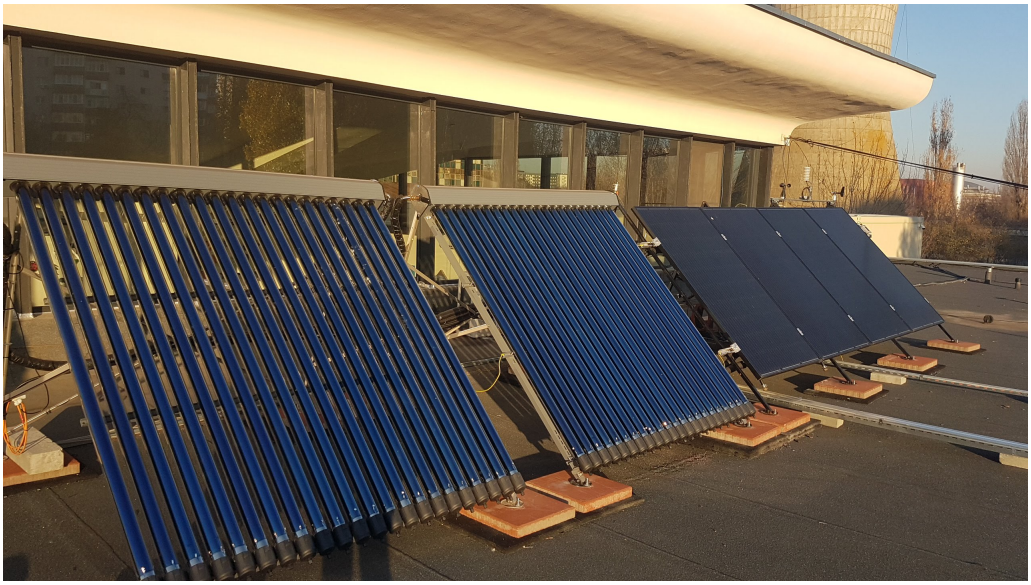

FIGURE 5.3: Photography of the installed panels

FIGURE 5.4: Photography of the meteorological station

5.1.3 System description

The new system for preparing domestic hot water complements the existing District System connection. The solar system for producing electricity is connected to the General Electric Panel through an inverter and a battery system is also installed.

No.	Ttpe fo equipment	Parameters
1.	PV Panel	Pel= 280...310Wp
2.	PVT Panel	Pel= 280...310 Wp, Pt= 700...850W
3.	Solar Thermal Panel	Pt= 700...850W
4.	Solar Regulator MPPT	Cell voltage: 24V Max. charging current: 10A Nominal PV power: 24V-290W Max. voltage: 75V
5.	PV invertor	Input voltage: 24V Output voltage: 230V Nominal output power : 1500W
6.	Batteries	Tensiune celula baterie: 2V OpzV cell
7.	Thermal Storage	Volume 500L
8.	Plate heat exchanger	Pt= 35...50kW
9.	Meteo station	Temperature, solar radiation, wind speed and direction

TABLE 5.1: Experimental system main components

The entire system is designed and executed in order to prepare DHW and electricity, but also for the analysis of the production data according to the external parameters, the internal consumptions and the operation scenario of the system. The data obtained by monitoring the thermal, electrical parameters, the production of hot water and electricity, the consumption of hot water and electricity is displayed in a dispatcher, but also in the UPB Kindergarten on a live monitor.

The main components of the installation are shown in Figure 5.5, with the legend shown in Figure 5.6. The full technical drawing of the scheme can be found in Appendix A.

The positions in the diagram of the following construction elements are presented: panels, boilers, heat exchangers, pumps, valves, connecting elements and fittings. All the elements, together with the measurement and control system of the installation will be presented in detail in the following sections. The main components are summarised in Table 5.1. The legend of the ducts is shown in Figure 5.6, and the nomenclature of the elements is explained in Table 5.2.

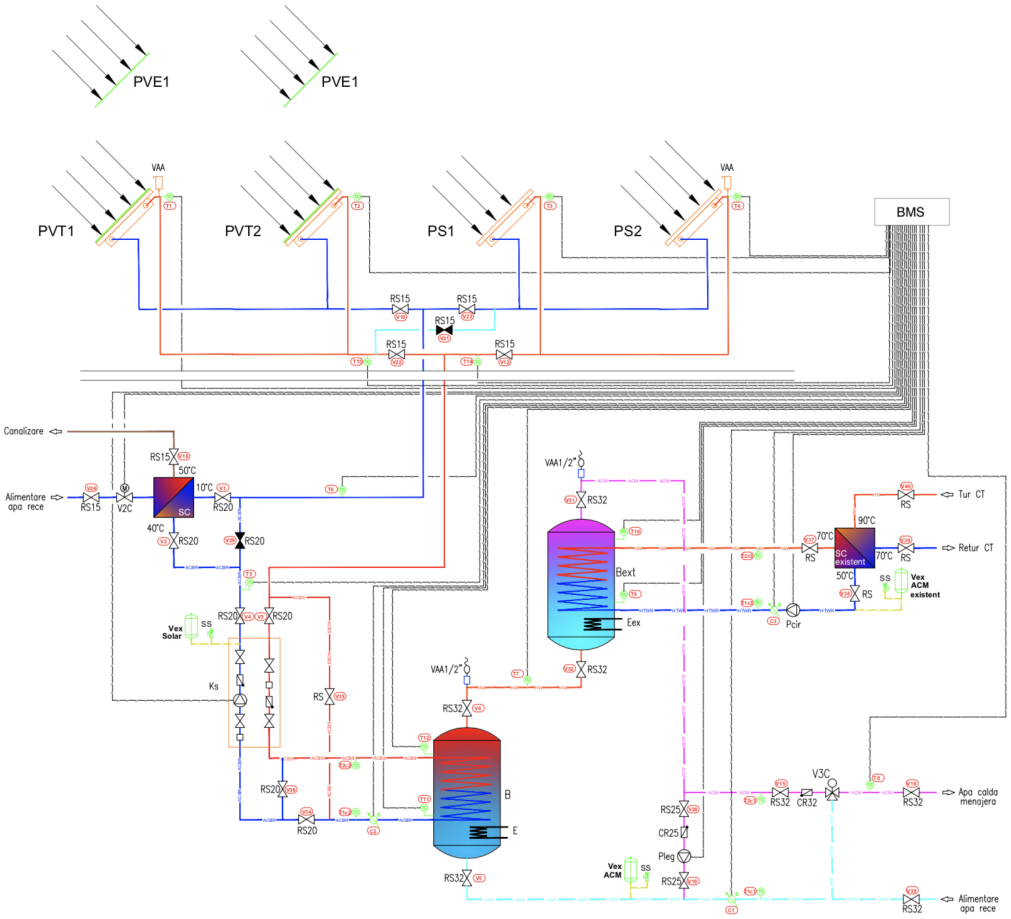

FIGURE 5.5: Thermo-mechanical diagram of the hybrid installation

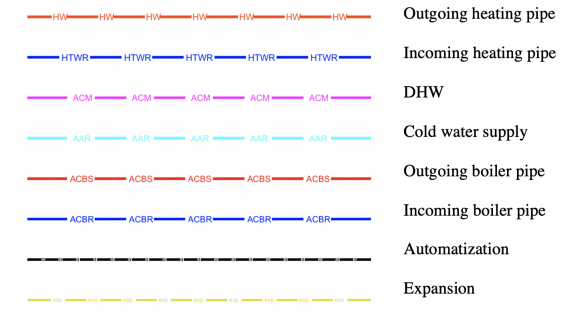

FIGURE 5.6: Legend for the thermo-mechanical scheme

Component name	Component description
PS	Solar thermal panel
PVT	Photovoltaic Thermal Panel
PVE	Photovoltaic Panel
Pcir	Circulation pump for boiler heating Q=5 m2/h, H=2.5mCA
Pleg	Circulation pump against legionela Q=2 m2/s, H=2.5 mCA
Ks	Solar Kit for water circulation
SC	Danfoss plate heat exchanger
SCext	Existing plate heat exchanger
B	Vertical boiler DHW V=500l
Bext	Existing vertical boiler DHW V=500l
SS	Safety valve 3 bar
Vex acm	Expansion vase closed with membrane for DHW
Vex acm ext	Existing expansion vase closed with membrane V=200l
Vext solar	Expansion vase closed with membrane for solar circuit
V3C	Mechanical three way valve
V2C	Variable two way valve 0-10 V
E	Electrical resistance P=2.3 kW
Eex	Existing electrical resistance P=9 kW
RS	Sectioning valve
CS	Reversing flap
VAA	Venting valve
TC	Temperature sensor
C	Thermal energy meter

TABLE 5.2: Nomenclature of thermo-mechanical scheme

General functioning principles

The functioning regime of the system is very interesting, as it can be easily changed and adapted to multiple configurations and operation scenarios. The main features of the system are described below:

- By default, the 4 thermal panels are connected in parallel, as seen in Figure 5.5. By closing the sectioning valves V23 and V22 and opening V21, the two PVT panels are now in series with the two ST panels. This is useful in order to investigate the performance of various configurations;
- The configuration of the serpentine exchanger in the thermal storage tank can also be modified by changing the configuration of the valves (open /close);
- There is an anti-legionella filter in order to ensure that bacteria is removed from the DHW;
- When there is no thermal consumer and the no heat is drawn from the tank, there is the possibility of cooling the water in order to ensure the panels do not overheat;
- There is a thermal energy back up system, consisting of electrical resistances in both boilers and connection to district heating;
- The electrical energy produced is stored in battery, used for own services or injected into the grid, depending on the electrical requirements. The decision is taken by an automatisation system.

Solar thermal collectors

The chosen solar thermal collectors are evacuated tube collectors (ETC). ETC's are typically designed with two parallel rows of glass tubes. Each inner glass tube contains a metal heat pipe attached to an absorber fin. The air between the two glass tubes is evacuated to form a vacuum, which reduces conductive and convective heat loss [105]. A schematic diagram of ETC's is shown in Figure 5.7. Figure 5.8 shows the ST panels before installation and Figure 5.9 the roof-mounted ST panels. The main technical characteristics of the panel are summarised in Table 5.3. The full technical description can be found in Appendix B.

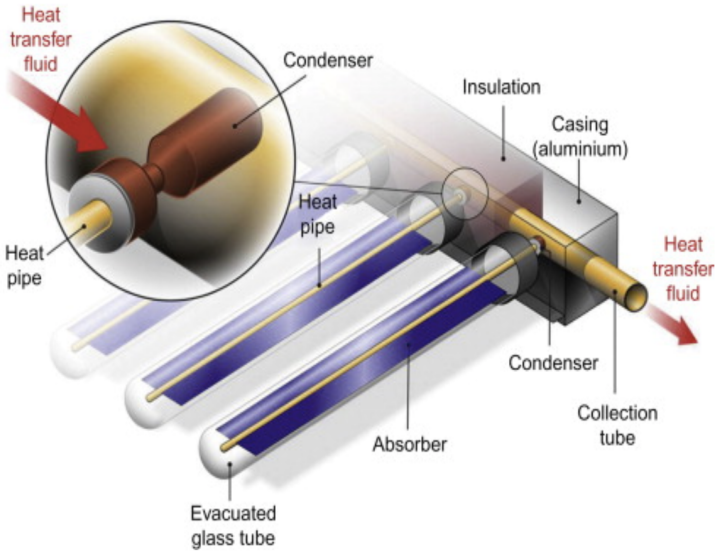

FIGURE 5.7: Schematic diagram of an evacuated tube collector [105]

FIGURE 5.8: Photography of the solar thermal panels before installing the evacuated tubes

Module name	WESTECH B58-22	**Volume capacity (l)**	2.2
No. of tubes	22	**Weight (kg)**	79
Width (mm)	1920	**Collector material**	Al/Cu/Glass
Length (mm)	2000	**Max. operating pressure**	8 bar
Total area (m2)	1.635	**Pressure drop @ 100l\h**	78 Pa
Absorbtion area (m2)	1.79	**Tilt angle**	45

TABLE 5.3: ECT technical data

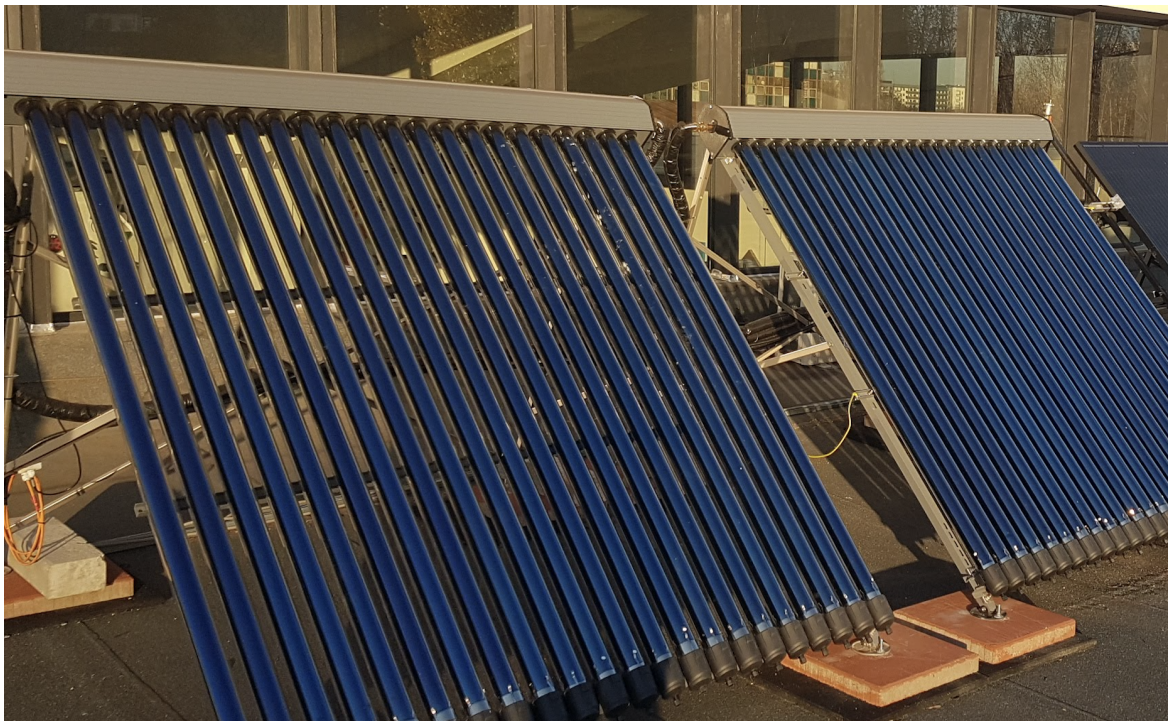

FIGURE 5.9: Photography of the solar thermal panels after installation

Photovoltaic panels

A number of two flat high efficiency mono-crystalline silicon PV panels were used for the installation. The panels use the Passivated Emitter and Rear Cell (PERC) technology, which has become an industry standard for the latest generation PV panels [106]. Figure 5.10 shows the roof-mounted PV panels, they are the two highlighted in red. The main technical characteristics of the panel are summarised in Table 5.4. The full technical description can be found in Appendix B.

Module name	Dual Sun FLASH	**Tempetrature (oC)**	-40 to +85
Cell type	PERC Mono-C	**Max. voltage**	1000 VDC
Width (mm)	991	**Nominal Power (W)**	300
Length (mm)	1650	**Efficiency (%)**	18.3
Total area (m2)	1.635	**Temperature coeff. (%)**	-0.39
Weight (kg)	18.5	**NOCT (oC)**	45 +-2

TABLE 5.4: PV technical data

FIGURE 5.10: Photography of the photovoltaic panels panels installed on the roof

PVT panels

The PVT panels are from the same manufacturer as the PV panels, the French-based company named Dual Sun. This is useful as the two modules can be easily compared in terms of overall efficiency. The PVT panel is composed of high efficiency mono-crystalline cells cooled by water circulation on the backside of the panel, with anti-reflective glass that helps with high performance even in diffuse light. The chosen PVT panel is insulated. Both PV and PVT panels have the same electrical characteristics and design. The front and back of the PVT panel is shown in Figure 5.11, and the cross section in Figure 5.12. Figure 5.13 shows the roof-mounted PVT panels, they are the two highlighted in green. The main technical characteristics of the panel are summarised in Table 5.5. The full technical description can be found in Appendix B.

Module name	Dual Sun SPRING	**NOCT (oC)**	45 +-2
Cell type	PERC Mono-C	**Volume of liquid (l)**	5
Width (mm)	991	**Max. operating pressure (bar)**	1.5
Length (mm)	1650	**Optical efficiency a0 (%)**	58.2
Total area (m2)	3.76	**Maximum temperature (oC)**	75.6
Weight (kg)	25.1	**Heat loss coefficient (W/K/m2)**	10.8
Op. temperature (oC)	-40 to +85	**Pressure loss (Pa) @ 100l/h**	47
Electrical Efficiency (%)	18.3	**Temperature coeff. (%)**	-0.39

TABLE 5.5: PVT technical data

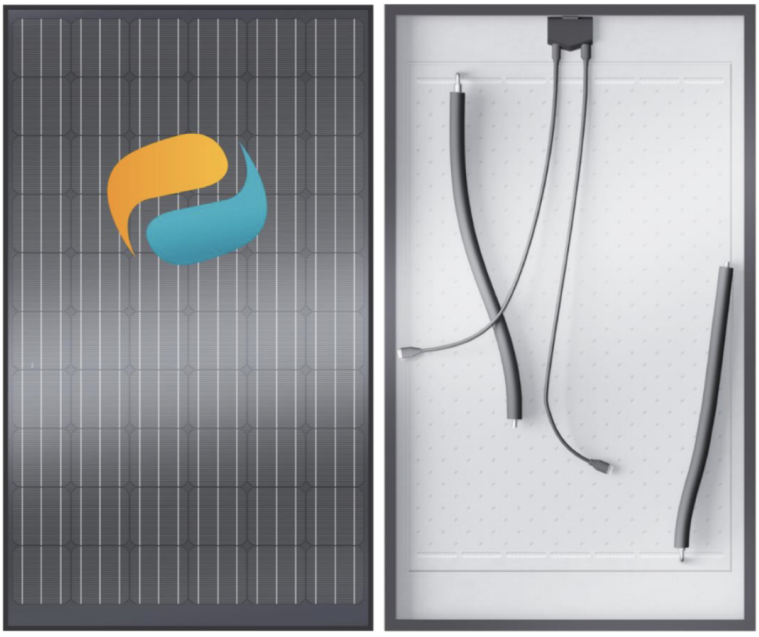

FIGURE 5.11: Front and back of the Dual Sun PVT collector [72]

FIGURE 5.12: Cross section of the Dual Sun PVT collector [72]

FIGURE 5.13: Photography of the PVT panels panels installed on the roof

Figure 5.14 shows the power output as a function of the temperature of the water in the panels, by various applications: water-water heat pump, pool heating and domestic hot water production.

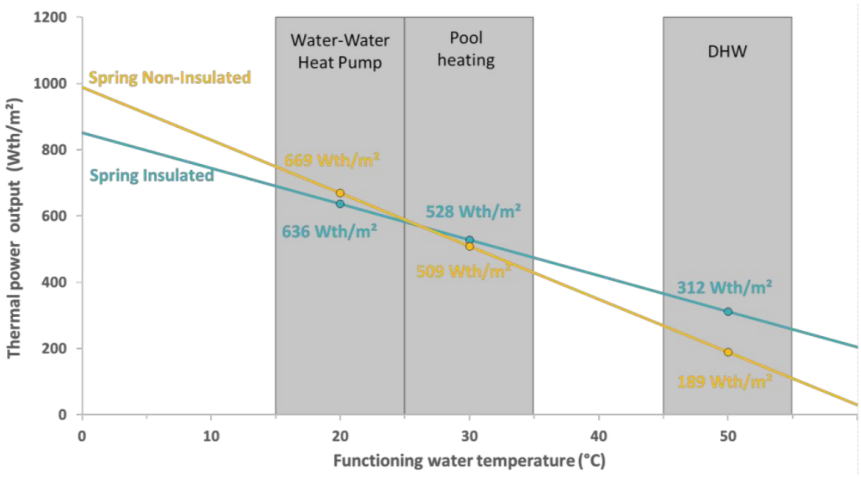

FIGURE 5.14: Power output as a function of the water temperature for Dual Sun Spring PVT panel

Boiler

A double serpentine boiler from Thermic Energy with a 500l volume capacity was installed as the heat exchanger between the solar energy system and the DHW main. A cross section of the two serpentine heat exchangers is shown in Figure 5.15. This boiler is illustrated in Figure 5.5 in the lower side of the diagram. Figure 5.16 shows the installed boiler, and its main technical characteristics are summarised in Table 5.6.

FIGURE 5.15: Cross section of the water storage tank

FIGURE 5.16: Photography of the newly installed boiler

Product name	**Thermic Energy WP-TWS-2W 500**
Volume	500 l
Heating surface of bottom serpentine	1.5 m2
Heating surface of top serpentine	4.6 m2
Draw-off capacity top / bottom	2400 / 1200 l\h
Bottom heat exchanger volume	8.21 l
Top heat exchanger volume	25.17 l
Insulation	75 mm
Stand by heat loss	58 Wh
Max. pressure (heat exchanger / water)	16 / 10 bar
Max. temperature (heat exchanger / water)	130 / 95 oC
Diameter	810 mm
Height	17000 mm

TABLE 5.6: Boler technical data

There was an existing boiler installed in the system, shown in Figure 5.5 in the right hand side of the diagram, connected to the district heating system. The new boiler is connected to the old one, hot water from the new boiler is circulated towards the existing boiler, and from there towards the DHW consumer. Both boilers have back-up electrical resistances for heating the water. The existing boiler is also connected through a heat exchanger to the district heating system of the University Campus.

Pumps

The recirculation pump between the two boilers is a Wilow standard pump, suitable for domestic hot water, with manual selection of three rated speeds and a rated flow rate of 2.06 m^3/h and a height of pumping of 2.66m. The three rated speeds are shown in Figure 5.17 in terms of height of pumping and used electrical power.

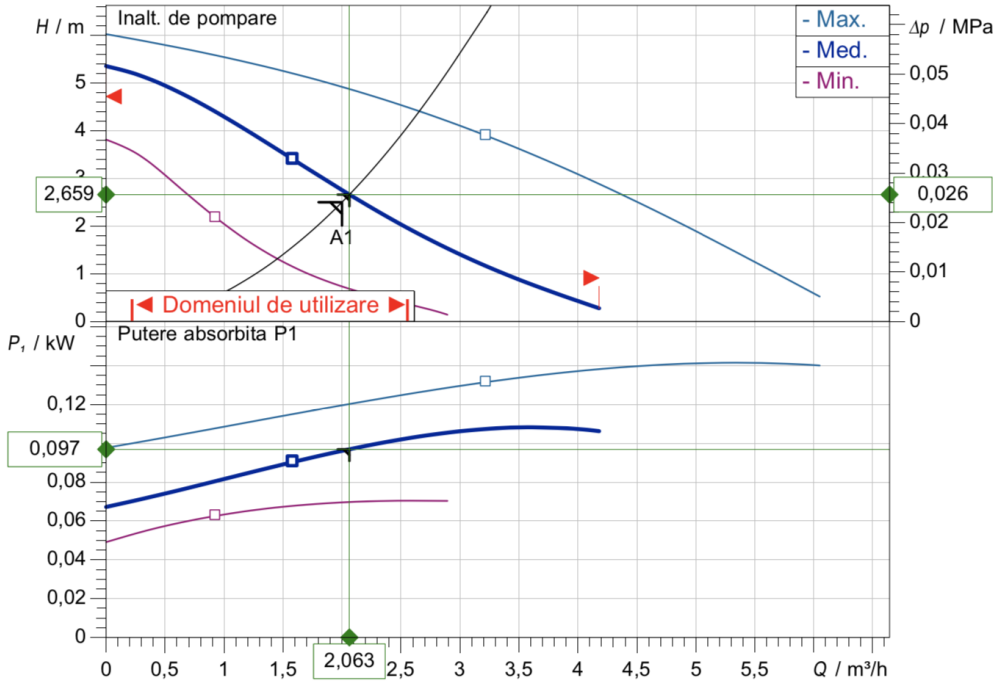

FIGURE 5.17: Minimum, medium and high pump flow rate as a function of the height of pumping (above) and used electrical power (below)

Meteorological station

The meteorological station is composed of:

- Digital Silicon Irradiance Sensor which measures up to 1500 W/m^2, and has a range of operating temperatures from -35 to 80 ^{o}C. It has an uncertainty of +-5 W/m^2;
- Ambient Temperature Sensor with casing protection from sun/ rain. It has an uncertainty of 1K and a measuring range from -40 to 90^{o}C;
- Wind direction transmitter for the acquisition of the horizontal wind direction. It has a measuring range from 0 to 360^o and an uncertainty of +-5^o;
- Wind speed Sensor, type cup star anemometer. It has a measuring range from 0.9 to 40m/s and an uncertainty of 5%.

The components are shown in Figure 5.18.

(A) (B) (C) (D)

FIGURE 5.18: Meteorological station components A)Irradiance Sensor B)Ambient Temperature Sensor C)Wind direction transmitter D)Wind speed Sensor

Heat exchangers

There are two plate heat exchangers in the system:

- An existing heat exchanger between the existing boiler and the district heating system;
- A new Micro plate heat exchanger from Danfoss, connected to the cold water main, used for cooling down the system of panels in case of overheating. Under normal operating conditions, this heat exchanger is bypassed with a shut-off valve.

Monitoring and control

The monitoring and control system covers the following functions of the experimental installation: data acquisition in the process; installation control; operational safety of the installation. All the component are illustrated in the thermo-mechanical scheme of the installation, in Figure 5.5 and Appendix A. The system consists of the following components:

- 21 temperature sensors for recording the live temperature on various points along the circuit;
- shut-off valves, two way valves and three way valves for manual reconfiguration of the flows, bypass and safety;
- three thermal energy meters for monitoring the amount of heat output from the boilers and input from the district heating;
- the meteorological station for recording ambient temperature, radiation, wind speed and direction, discussed in the previous section;
- venting valves for removing the air from the installation;
- independent pressure regulating and balancing valve.

5.1.4 Data collection

The live data is collected in multiple points for various sensors, and is all directed towards the BST system. A screenshot of the user interface is shown in Figure 5.19. The temperature sensors are displayed on the interface in multiple points: on the back of the panels, on the ducts, in the boiler, in the pumps. On the right hand side there are some additional parameters: power, meteorological parameters, battery state.

In the user interface, C1 represents the amount of energy sent to the DHW consumer, C3 represents the amount of energy that comes from the local DH system and C3 shows the amount fo energy input into the new boiler from the panels.

This section shows the experimental results obtained by using the hybrid solar installation described in the previous section. Sampling was done at fixed intervals of 5 minutes. A total of 288 readings were performed for each day. The data collection

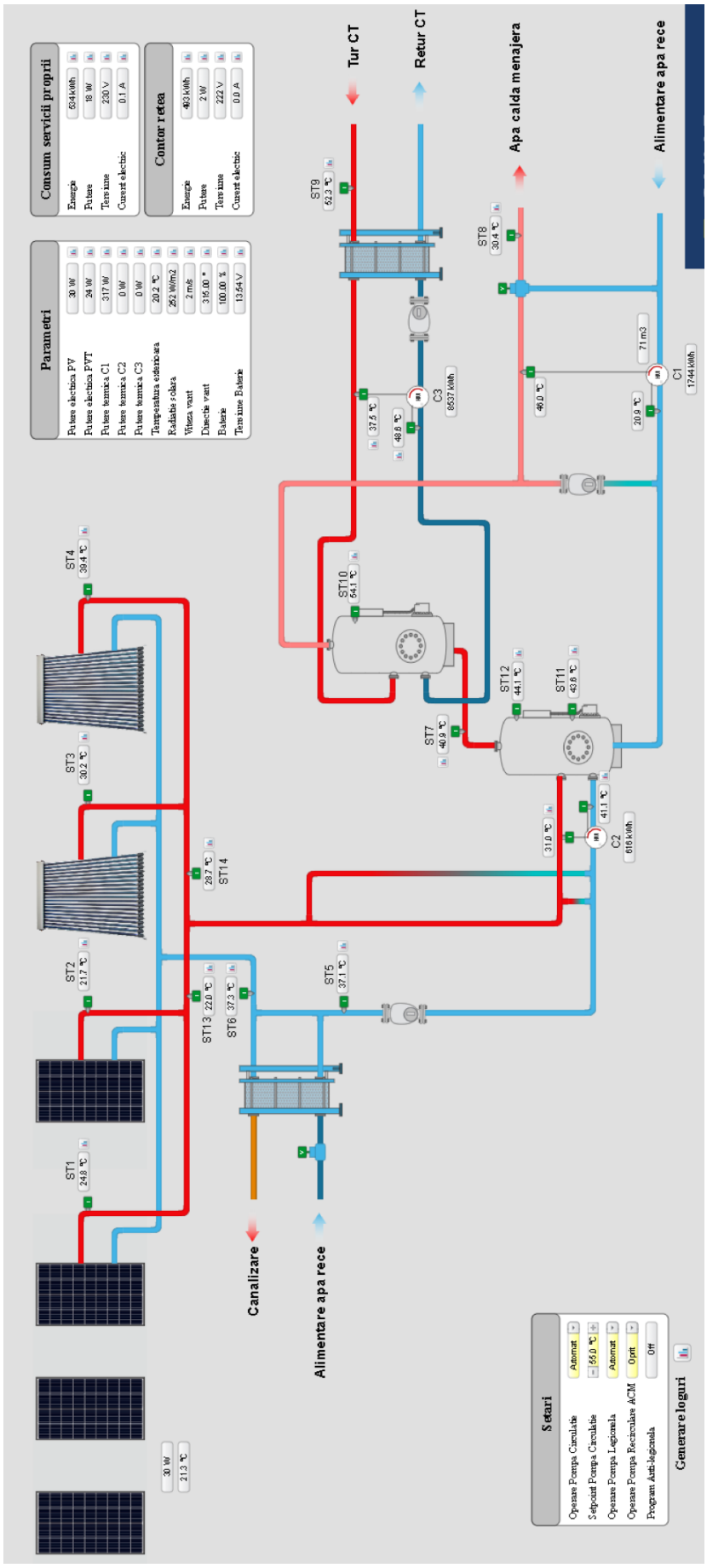

FIGURE 5.19: BST system user interface

system was installed and tested on 11th of May 2020, but it only started collected full system measurements in all the points on 8h of February 2021.

5.2 Analysis of collected data

Daily analyses were carried out for each day, from 00:00 to 23:59. A number of representative days were chosen to be illustrated graphically. When choosing a representative day for the graphical analysis, a few factors have to be taken into account:

- the solar radiation is within average limits for the specific time of the year (excluding extreme weather conditions);
- the ambient temperature is within average limits for the specific time of the year (excluding extreme weather conditions);
- the thermal consumer is existent - there is activity being carried out in the kindergarten building. Due to the 2020-2021 pandemic, most educational institutions were closed, and this period overlaped with the time when the measurements were taken. Some days were identified when activities were carried out in the building and there was a minimum of DHW consumption.

Four types of days where chosen for the analysis:

- spring cloudy day - referd to as **day A**
- spring sunny day - referred to as **day B**
- summer cloudy day -referred to as **day C**
- summer sunny day - referred to as **day D**

These representative days will be analysed in terms of:

- meteorological parameters
- classified curves of solar radiation
- temperature evolution at the back of the panels
- demand curves

- temperature of the thermal agent at the inlet and outlet of the panels
- energy and power production

5.2.1 Meteorological parameters

The meteorological station data for days A-D is shown in Figures 5.20 - 5.23.

During day A, the wind speed reaches two isolated peaks of 4 m/s, with an average of 0.32 m/s. The ambient temperature during night time goes below 0 (-1.9^{o}C), and reaches a maximum of 10 ^{o}C during noon. The solar radiation, shown on the secondary axis on the right, also peaks at noon with values close to 1200 W/m^2. The high variation in the meteorological parameters indicate that this was a cloudy day, which is typical for the Romanian spring season.

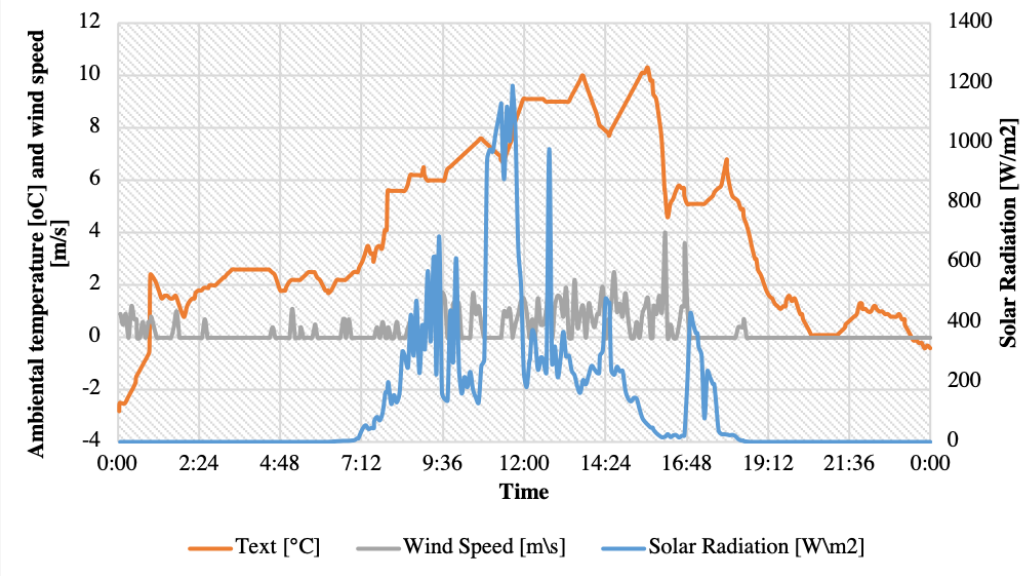

FIGURE 5.20: Meteorological data for Day A

Day B is show in Figure 5.21. This day has higher ambient temperature and more constant solar radiation (less cloudy) compared to the day previously analysed. The wind speed reaches up 4 m/s, with an average of 0.37 m/s. The ambient temperature during night time stays positive, with a minimum of 1^{o}C, and during the day it reaches a maximum of 22 ^{o}C at noon. The solar radiation, shown on the secondary axis on the right, also peaks at noon with values close to 1050 w/m^2. There is little variation in the temperature and radiation, which means this was a clear day, non-cloudy.

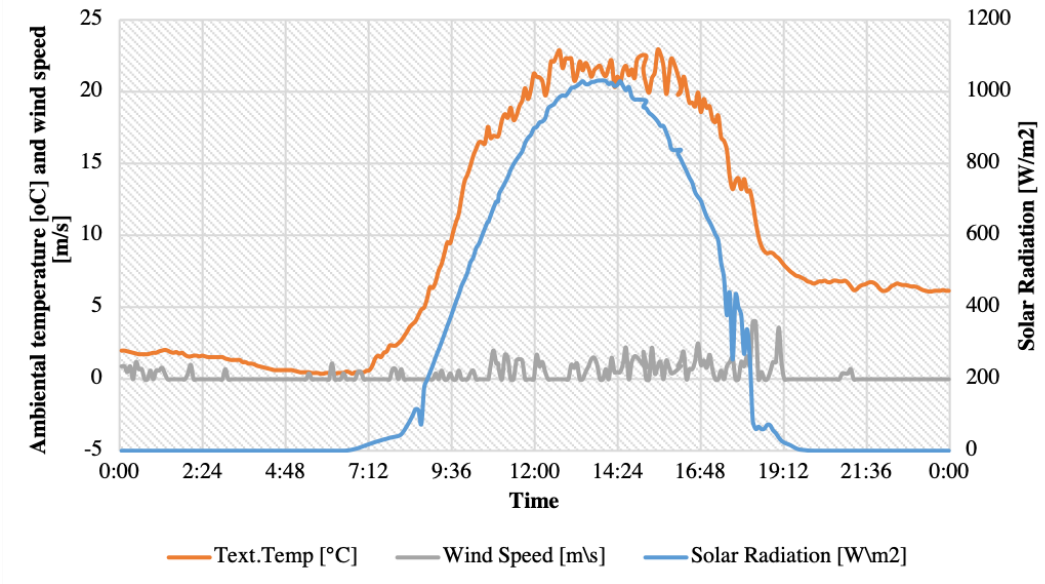

FIGURE 5.21: Meteorological data for Day B

Day C is shown in Figure 5.22. During this day there is a high irregularity in the weather parameters, typical to a cloudy day. The ambient temperature starts to increase from 06:00 AM to a peak of 25 ^{o}C in the late morning, around 9:30 AM, followed by a decrease during midday down to 17 ^{o}C. In the afternoon there is a second peak of 24 ^{o}C, correlated with the dispersion of clouds and the apparition of the sun. The solar radiation has low values in the first half of the day due to the presence of clouds, with a peak of around 950 W/mm^2 for a brief period between 14:30 and 16:30 PM. The wind speed reaches an isolated peak in the afternoon of 4.1 m/s, with an average value of 0.45 m/s during the rest of the day.

Day D is shown in Figure 5.23. A curve that peaks during midday can be observed in this figure for both ambient temperature and solar radiation, consistent with a clear day. The ambient temperature reaches a peak of 35 ^{o}C, typical for a hot summer day. The local variation of the data can be attributed to the error of measurements, but they do not affect the general trend-line of the curve. The solar radiation also follows an ascendent curve that peaks at 13:00 PM, and starts decreasing in the second half of the day, until the total disappearance of the sun around 20:30 PM. This day is characterised by low winds, with no isolated peaks and an average speed of 0.36 m/s.

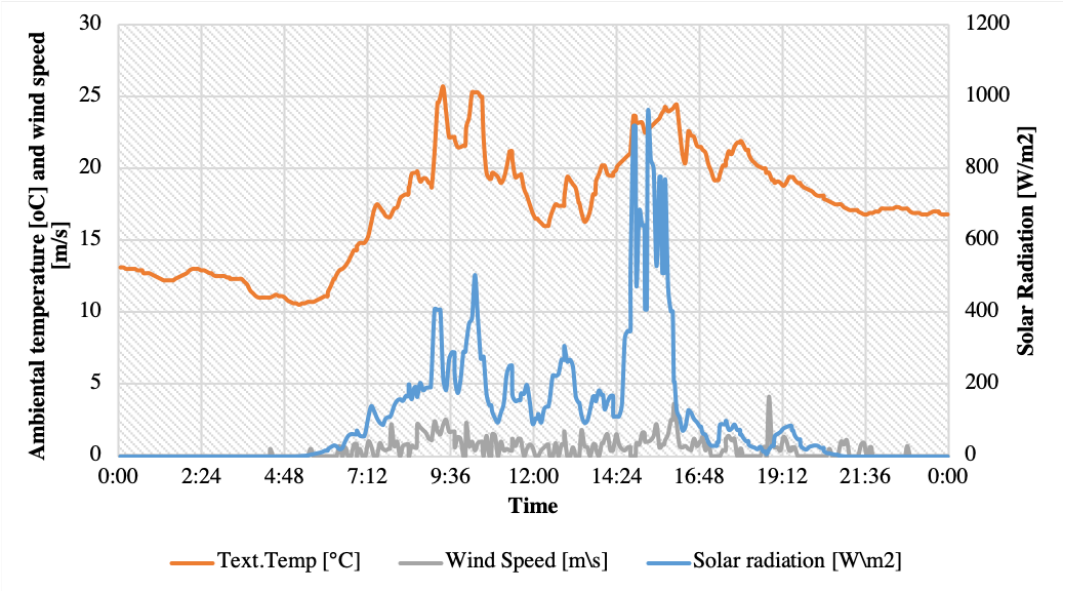

FIGURE 5.22: Meteorological data for Day C

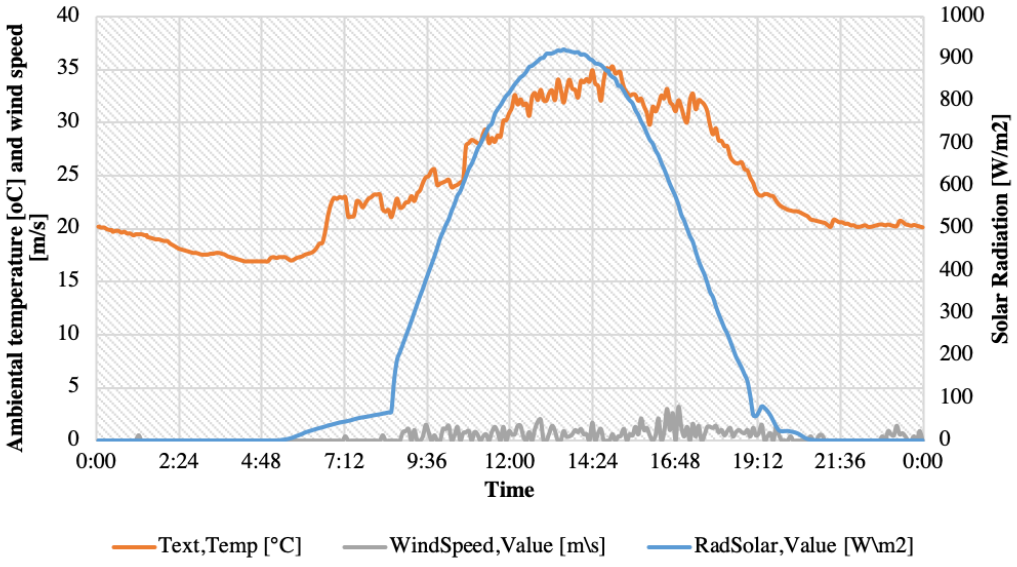

FIGURE 5.23: Meteorological data for Day D

5.2.2 Classified curves of solar radiation

The classified curve for the solar intensity for day A is shown in Figure 5.24. The total number of hours with solar radiation is around 13, and the maximum radiation reaches 1200 W/m^2, with an average of 300 W/m^2 over the 13 radiation hours. By multiplying the average value with the period of sun radiation, the total amount of energy that can be collected during the day per m^2 can be obtained, and that is 3.9 kWh/m^2/day.

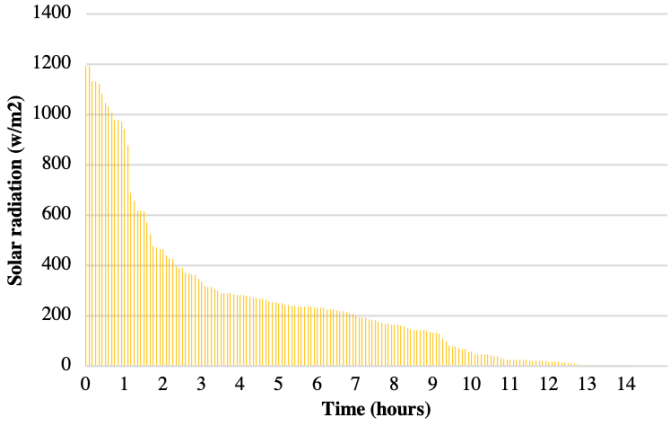

FIGURE 5.24: Classified curve of solar radiation for Day A

The classified curve for the solar intensity on day B is shown in Figure 5.25. The total number of hours with solar radiation is 13.5, and the maximum radiation reaches 1031 W/m^2, with an average of 550 W/m^2 over the 13.5 radiation hours. By multiplying the average value with the period of sun radiation, the total amount of energy that can be collected during the day per m^2 can be obtained, and that is 7.15 kWh/m^2/day.

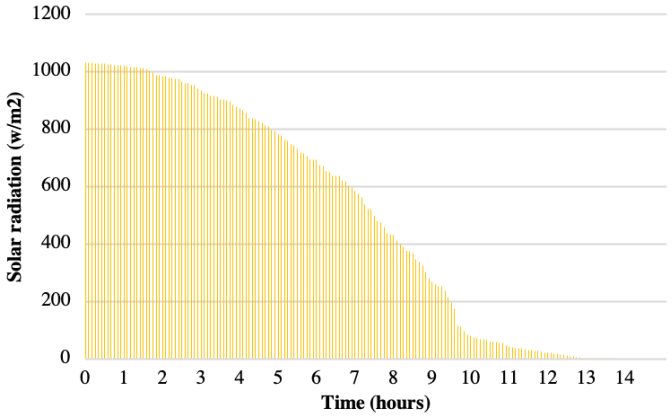

FIGURE 5.25: Classified curve of solar radiation for Day B

The classified curve for the solar intensity on day C is shown in Figure 5.26. The

total number of hours with solar radiation is 15.7, and the maximum radiation reaches 950 W/m^2, with an average of 170 W/m^2 over the 15.7 hours of solar radiation. By multiplying the average value with the period of sun radiation, the total amount of energy that can be collected during the day per m^2 can be obtained, and that is 2.67 kWh/m^2/day.

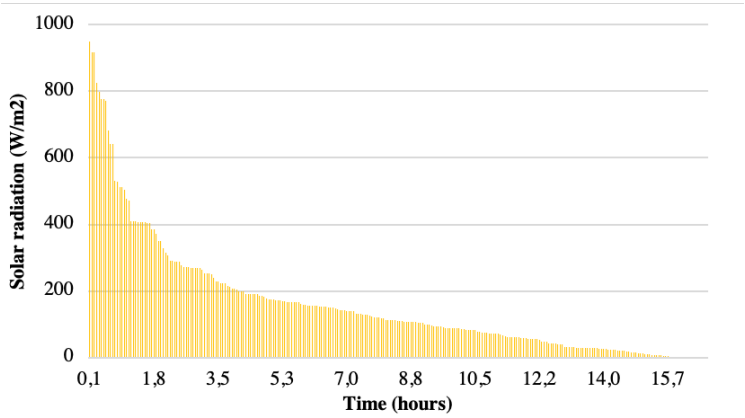

FIGURE 5.26: Classified curve of solar radiation for Day C

The classified curve for the solar intensity on day D is shown in .Figure 5.27. The total number of hours with solar radiation is 16, and the maximum radiation reaches 921 W/m^2, with an average of 445 W/m^2 over the 16 hours of solar radiation. By multiplying the average value with the period of sun radiation, the total amount of energy that can be collected during the day per m^2 can be obtained, and that is 7.12 kWh/m^2/day.

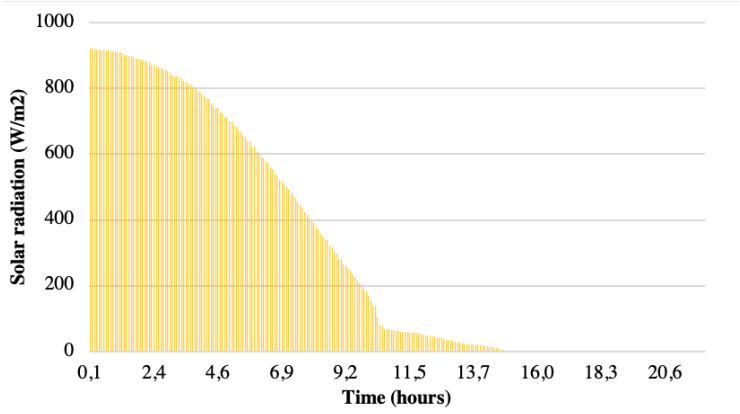

FIGURE 5.27: Classified curve of solar radiation for Day D

5.2.3 Temperature at the back of the panels

The temperature variation on each panel is recorded by a temperature sensor placed on the back of the panel. The evolution of this temperature during day A is shown in Figure 5.28, where PV temp refers to the temperature on the back of the PV panels, ST1 and ST2 refer to the PVT panels, and ST3 and ST4 refer to the solar thermal panels. Comparing Figure 5.20 with Figure 5.28, it can be observed that the temperature on the back of the panels follows closely the intensity of the solar radiation. The highest peak temperature is reached by the PV panel, but overall, during the rest of the time, ST4, which represents the second solar thermal panel, has the highest temperatures. The PVT panels have similar temperatures as the PV panel, sometimes higher, sometimes lower. If the the thermal agent that flows into the PVT panels is not cooled down in the tank (which can occur if there is not sufficient circulation towards the thermal consumer), then the temperature increases slightly above the PV temperature.

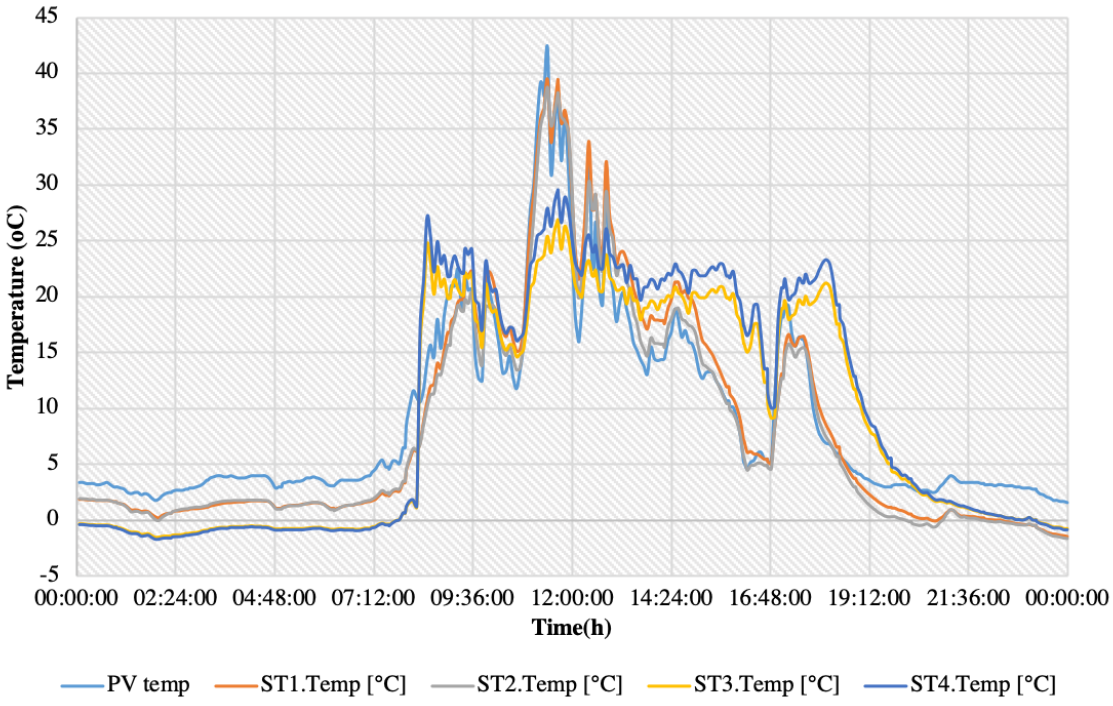

FIGURE 5.28: Variation of the temperature on the back of the panels for Day A

The evolution of the temperatures on the back of the panels for day B is shown in Figure 5.29. Here there is very little water draw to the consumer, so heat accumulated in the tank, which leads to the temperature in the PVT panels to increase above the PV

panels.

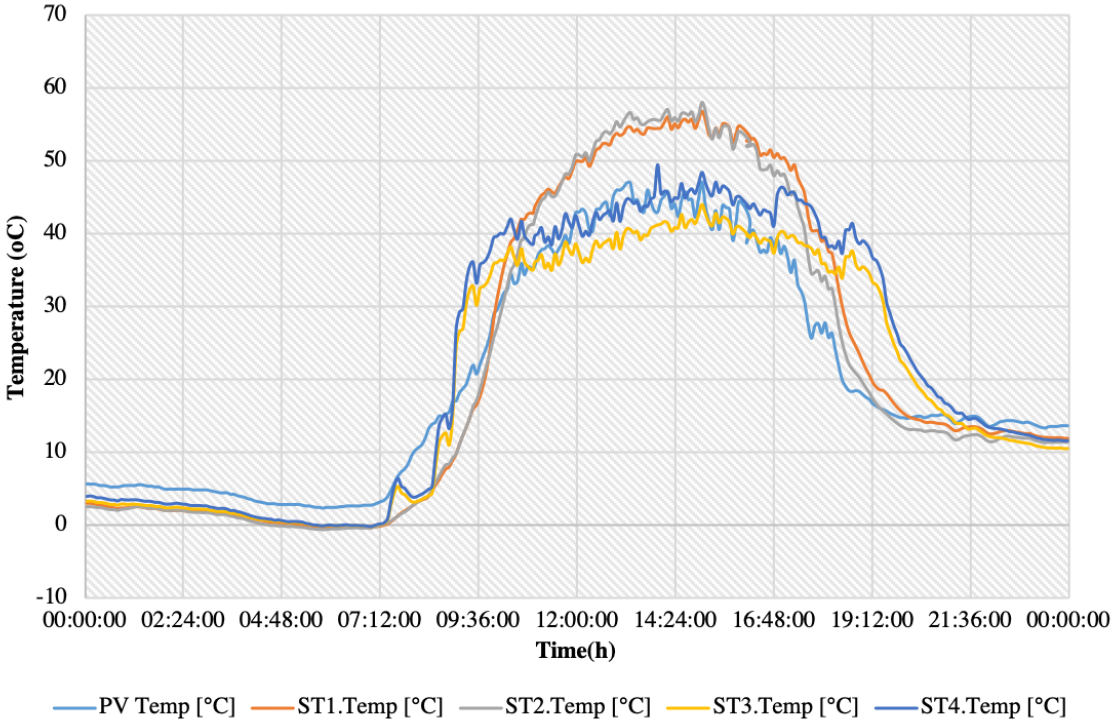

FIGURE 5.29: Variation of the temperature on the back of the panels for Day B

The evolution of the temperatures on the back of the panels for day C is shown in Figure 5.30. During this day, the PVT collector ST2 reaches the peak temperature. Overall, the two solar thermal collectors have the highest temperatures. The two PVT panels function at similar temperatures as the PV panel, with very small differences.

The evolution of the temperatures on the back of the panels for day D is shown in Figure 5.31. During this day, the solar thermal collector ST4 reaches the peak temperature in the second part of the day. Overall, the two solar thermal collectors higher temperatures compared to the PVT panels. The two PVT panels function at similar temperatures as the PV panel in the first half of the day, with very small differences. In the second part of the day the temperature of the PVT panels increases above the temperature of the PV panel. Again, the fact that the PVT collectors are not cooled down sufficiently can be attributed to the accumulation of thermal energy in the tank.

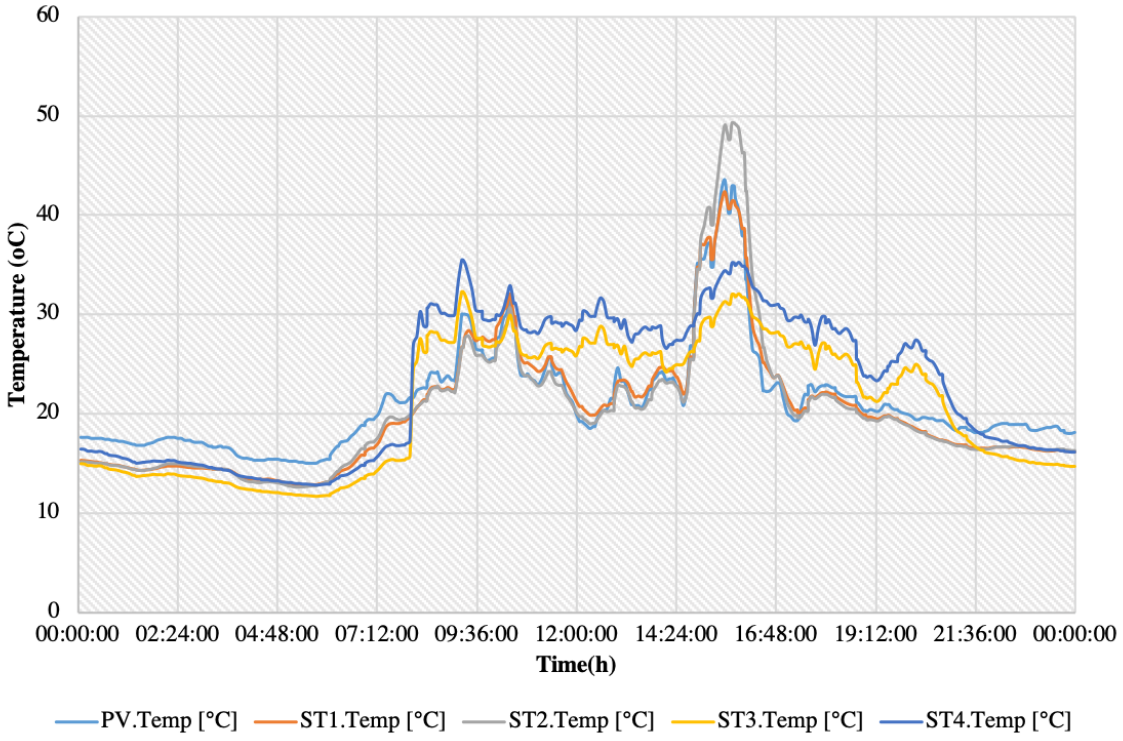

FIGURE 5.30: Variation of the temperature on the back of the panels for Day C

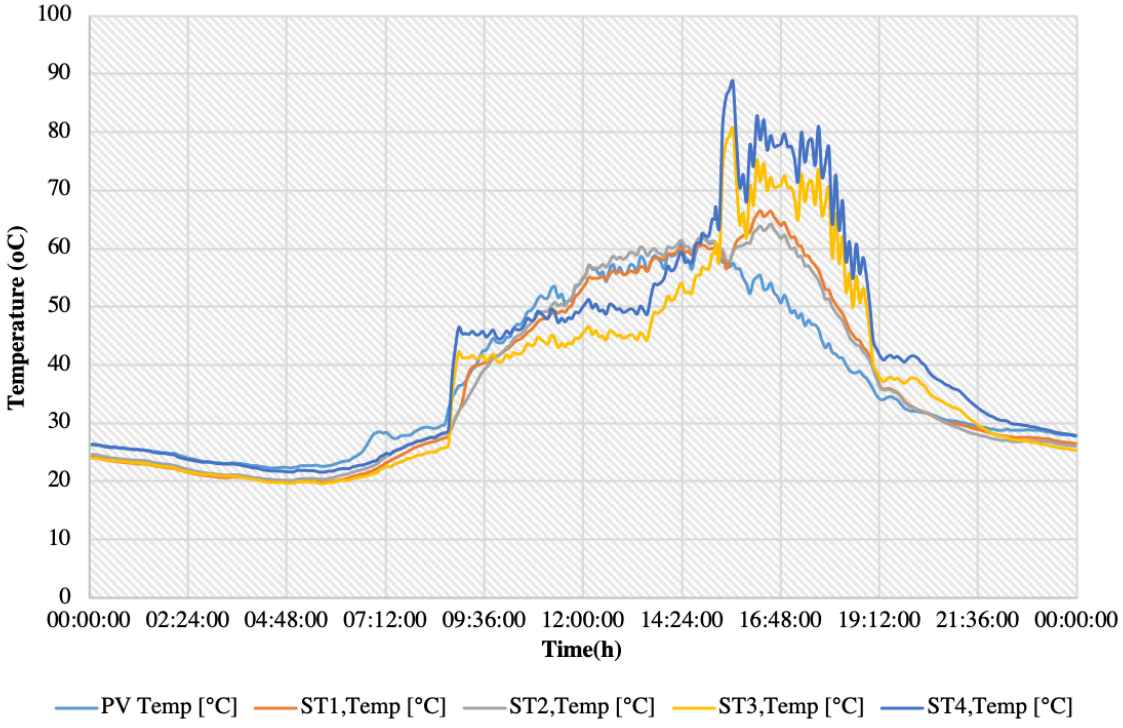

FIGURE 5.31: Variation of the temperature on the back of the panels for Day D

5.2.4 Consumer flow rate

The flow rate of the of the consumer demand for day A is shown in Figure 5.32 in l/h. As previously mentioned, during the time of the measurements the kindergarten was sometimes closed for regular activities, so the demand is not typical for the activities with children, but particular to administrative duties and building maintenance. The total water draw for this day was 500l.

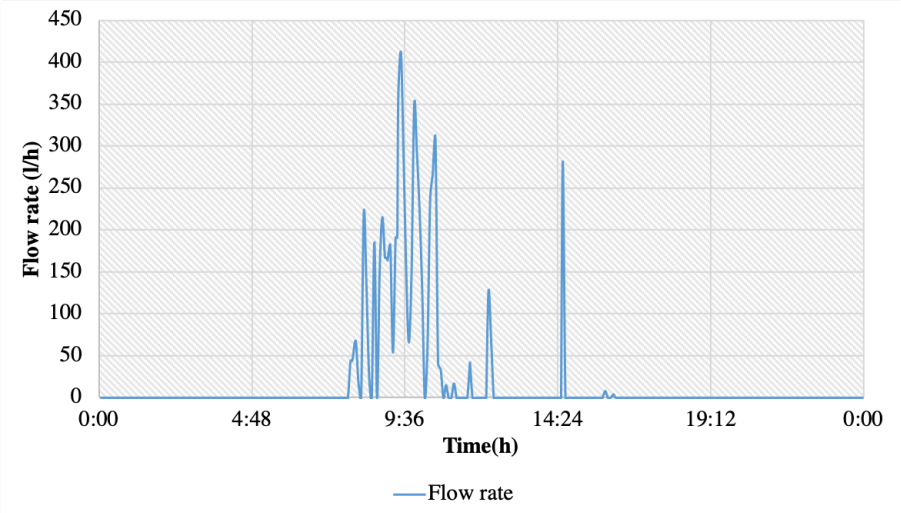

FIGURE 5.32: Demand curve for the kindergarten for Day A

The flow rate of the of the consumer demand on day B is shown in Figure 5.33 in l/h. The total water draw for this day was low, only 170l.

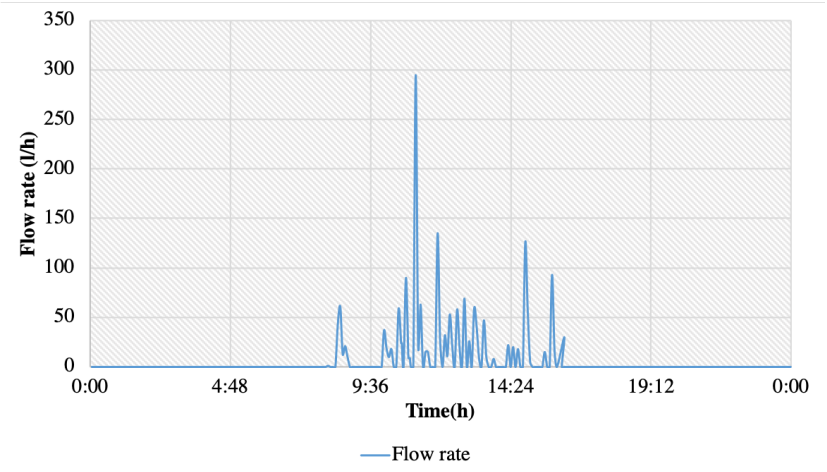

FIGURE 5.33: Demand curve for the kindergarten for Day B

The flow rate of the of the consumer demand on day C is shown in Figure 5.34 in l/h. The total water draw for this day was the highest of all days, 1060l.

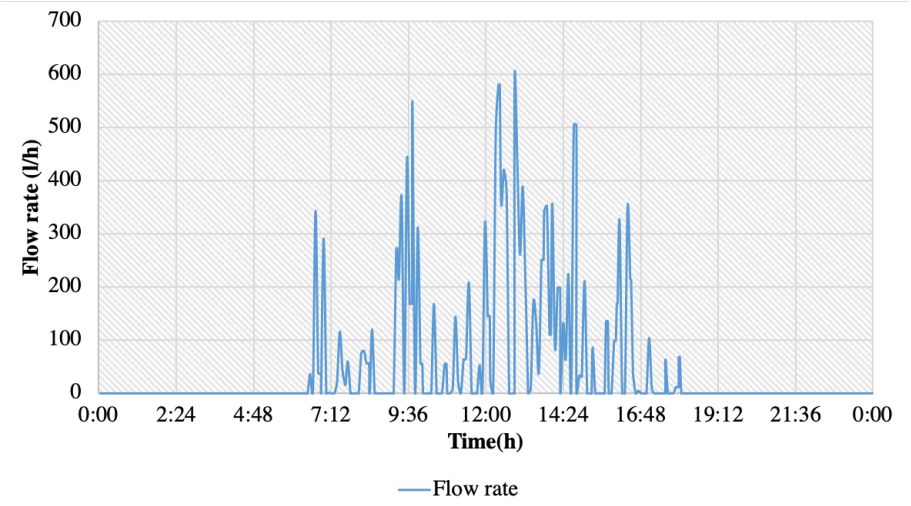

FIGURE 5.34: Demand curve for the kindergarten for Day C

The flow rate of the of the consumer demand on day D is is shown in Figure 5.35 in l/h. The total water draw for this day was high, with a value of 970l.

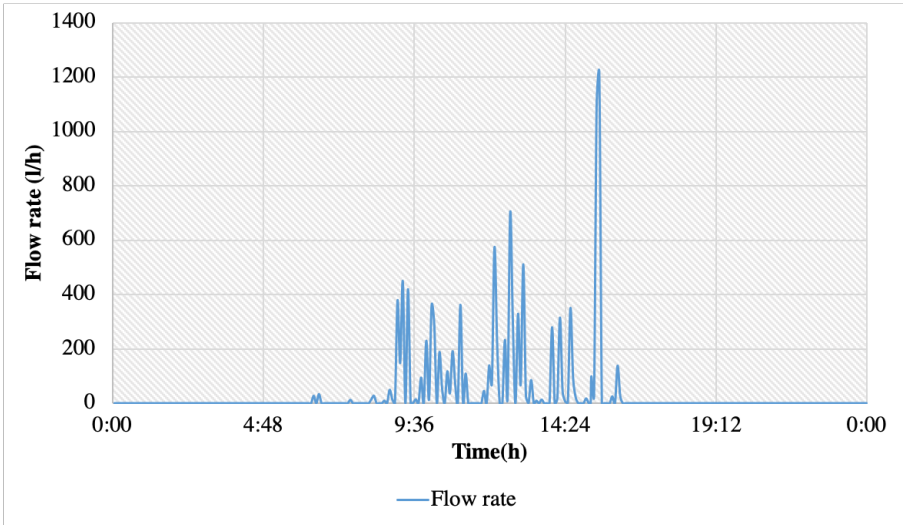

FIGURE 5.35: Demand curve for the kindergarten for Day D

5.2.5 Temperature of the thermal agent at the inlet and outlet of the panels

Next, the temperature at the inlet and outlet of the set of panels is analysed. In this particular day, the panels were configured as follows: the two PVT panels in parallel, the two ST panels in parallel, and the two sets of panels in series.

Two temperatures are considered here:

- the temperature at the inlet of the PVT panels, on the common pipe, before it splits in parallel - ST13;

- the temperature at the outlet of the ST panels, on the main pipe, after the parallel pipes rejoin - ST14.

The temperature of the thermal agent at the inlet and outlet of the set of panels is shown in Figures 5.36-5.39 for Day A-D respectively.

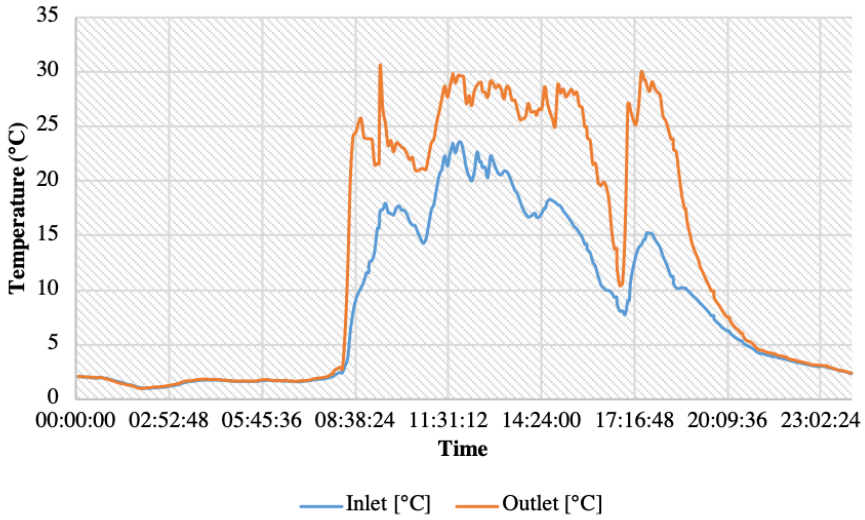

FIGURE 5.36: Temperature of the thermal agent at the inlet and outlet of the panels for Day A

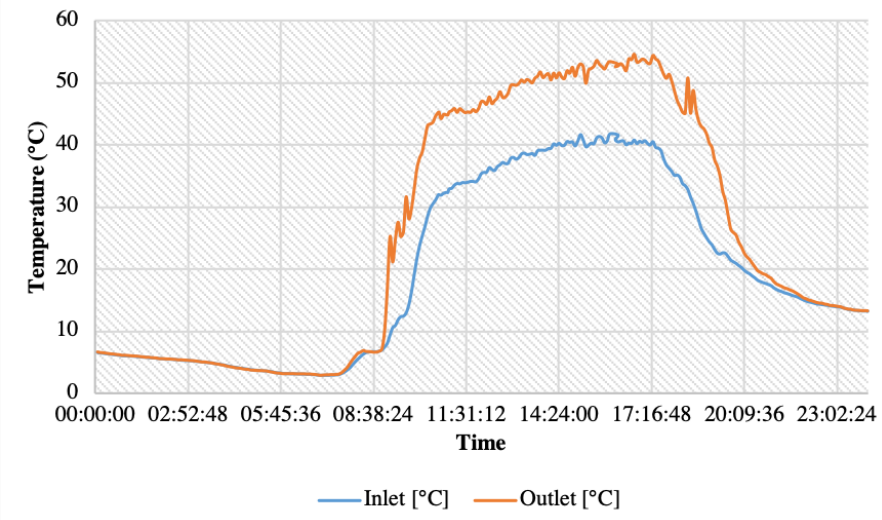

FIGURE 5.37: Temperature of the thermal agent at the inlet and outlet of the panels for Day B

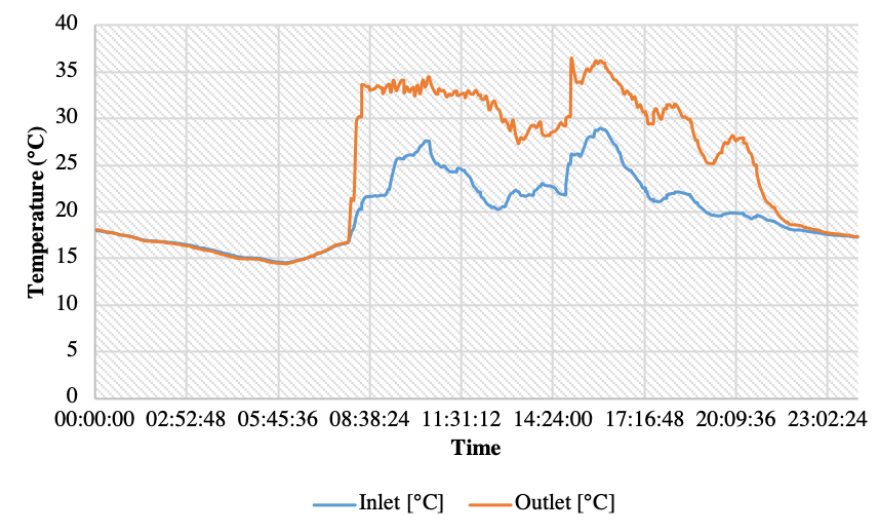

FIGURE 5.38: Temperature of the thermal agent at the inlet and outlet of the panels for Day C

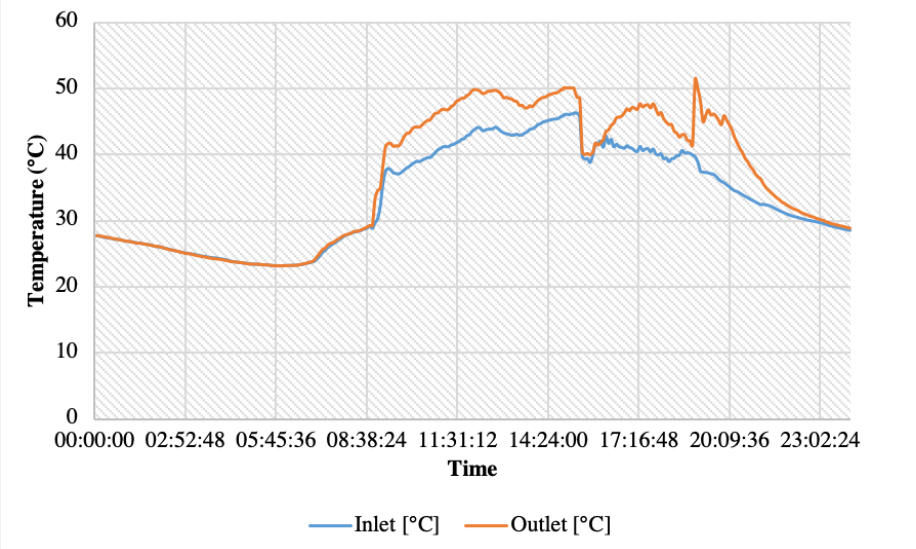

FIGURE 5.39: Temperature of the thermal agent at the inlet and outlet of the panels for Day D

An interesting aspect to analyse is the temperature difference between inlet and outlet for the four days. This is illustrated in Figure 5.40. It can be observed that the highest temperature increase occurs during day B, which is defined by high solar radiation, average ambient temperatures and low water draw. The lowest increase occurs during day D, defined by high temperatures, high solar intensity and high water draw. This is due to the fact that during this day the thermal energy accumulates in the tank the temperature increases significantly and the water draw is not sufficient to cool it down. During this day, delta T drops down to 0 around 15.50 PM, simultaneous with the high water draw from Figure 5.35. This is due to the fact that there is a sudden large water draw and the tank is refilled with cold water from the main, loses its thermal stratification. During day A and day C the temperature increase is variable, in line with the high variation of meteorological conditions. The period of heat accumulation starts around 8-8.30 AM, depending on the particular day, and it continues until late in the day, around 9.30-10 PM.

It's important to note that this analysis is not based on a single variable parameter, but on multiple factors that influence the outcome, therefore the implications and relationships between the parameters are not straight-forward.

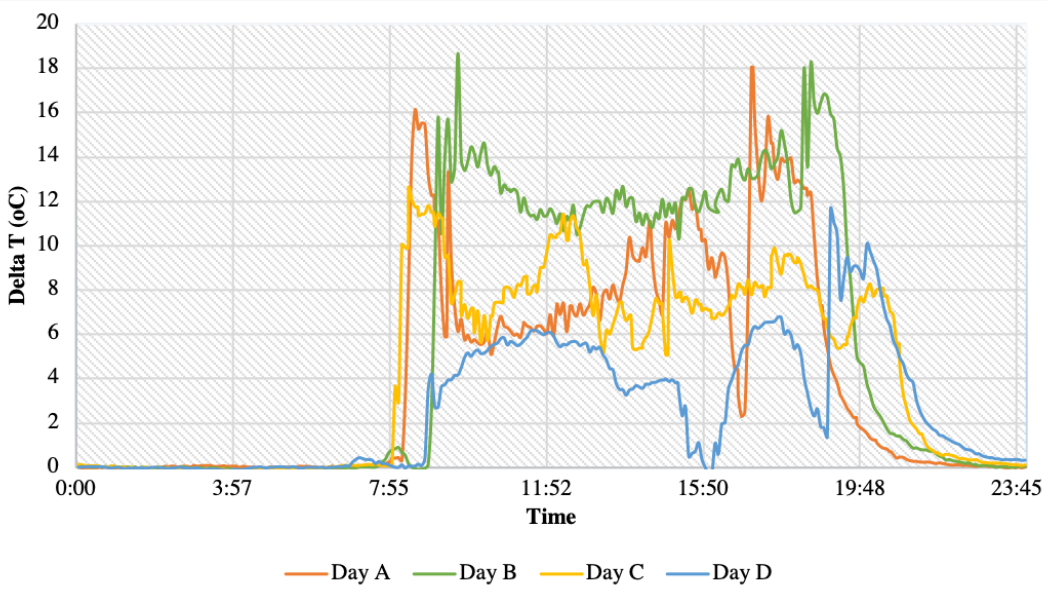

FIGURE 5.40: Evolution of the temperature difference between inlet and outlet during the four days

5.2.6 Daily energy and power output

The instantaneous thermal and electrical powers measured during the four days are shown in Figure 5.41 and 5.43. The electrical power measurements refer here to the PVT collectors, excluding the separate PV panels. It is interesting to observe the relationship between them, and how the increase of one generally means a decrease in the other. This occurs due to the fact that the PV cells are overheated and their efficiency decreases.

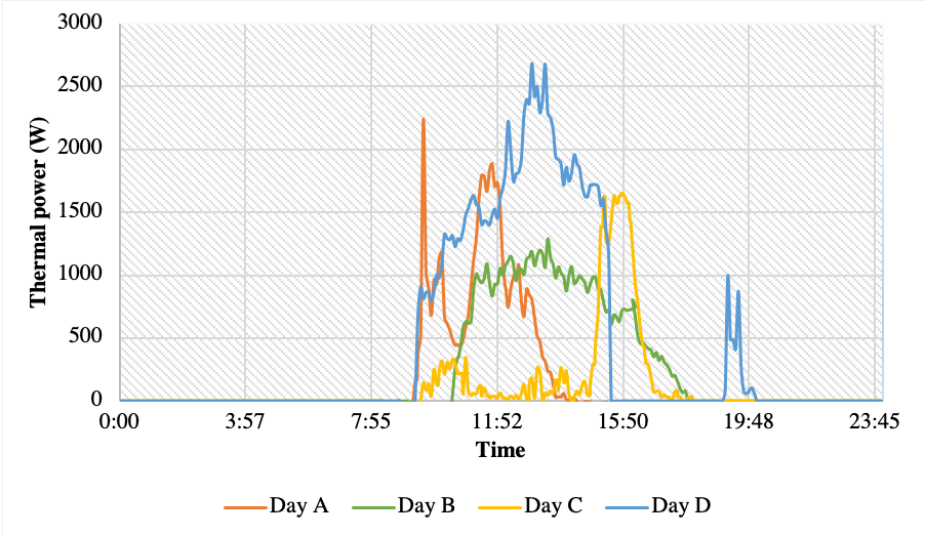

FIGURE 5.41: Instantaneous thermal power measured by the meter during the four days

The classified curve of the instantaneous thermal power is shown in Figure 5.42. The highest values for the thermal power are recorded during Day D, with a period of power production of 7.3 hours. Day C has a period of 1.5 hours of high power, followed by a steep decrease for the rest of the power production period, due to the intermittence of solar radiation and variability of ambient temperature. Day A shows a similar steep decrease, for the same reasons. Day B has a curve similar in shape with day D, but with lower values.

The classified curve of the instantaneous electrical power is shown in Figure 5.44. During the clear days, the electrical power curve has a steeper decrease compared to the cloudy days. The highest electrical power is produced during day D, which is the summer clear day, followed closely by the spring cloudy day, day A. Although is seems counter-intuitive, the spring day has a high power production to the cells operating at lower temperatures.

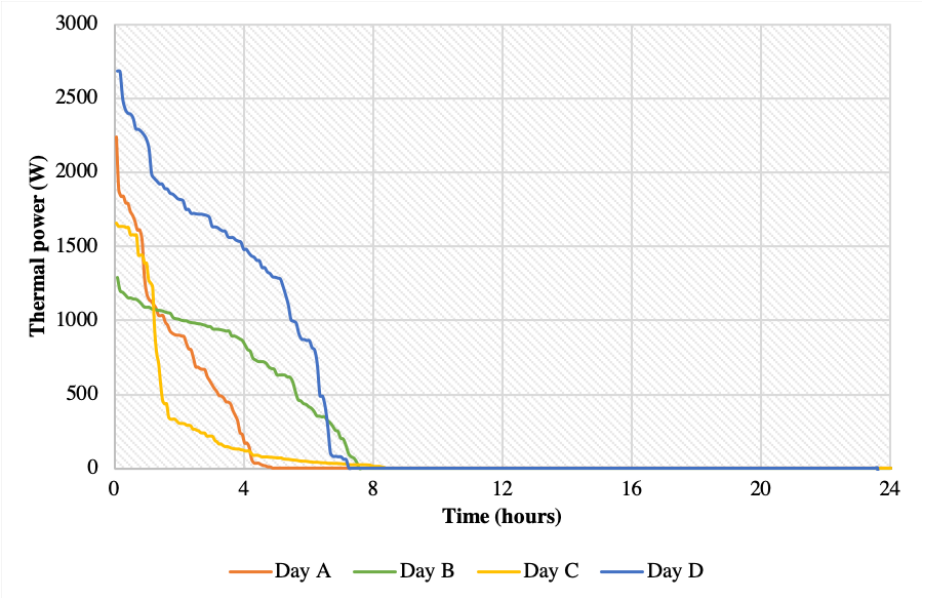

FIGURE 5.42: Classified curve of the instantaneous thermal power during the four days

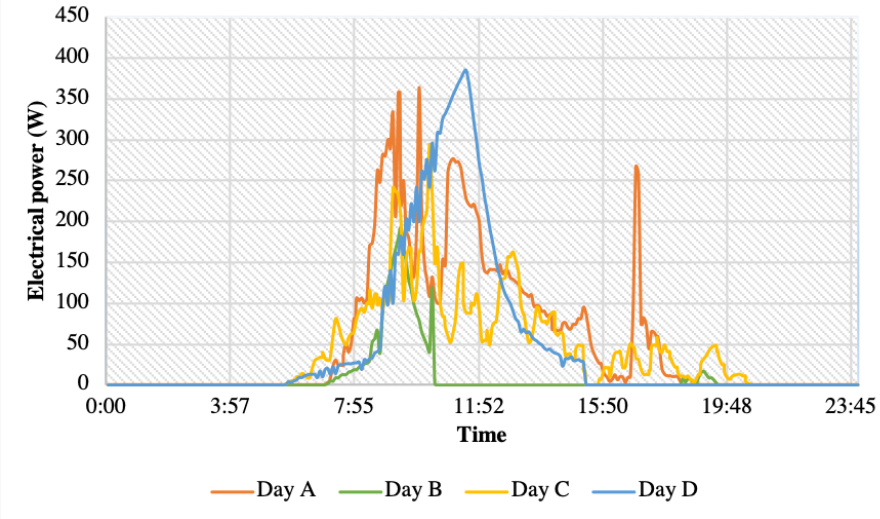

FIGURE 5.43: Instantaneous electrical power given by the two PVT panels measured by the meter during the four days

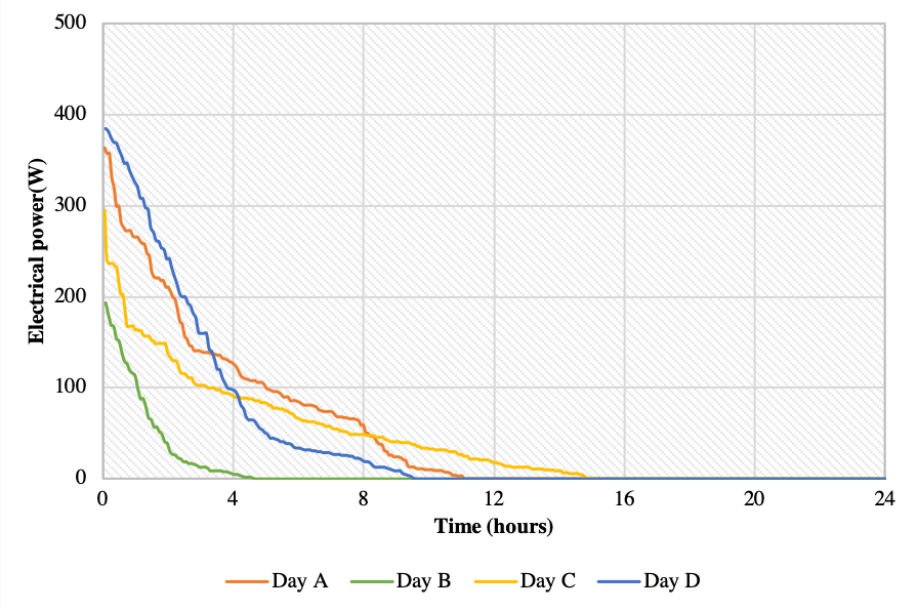

FIGURE 5.44: Classified curve of the instantaneous electrical power during the four days

The thermal efficiency of the system can be computed from Equation 5.1.

$$\eta_{th} = \frac{(T_{out} - T_{in}) \cdot c_{pwater} \cdot \dot{m}}{G \cdot A} \tag{5.1}$$

where T_{out} and T_{in} are the inlet and outlet temperatures respectively, c_{pwater} is the thermal capacity of water, $\dot{m}$ is the flow rate through the panels and G is the solar radiation and A is the total area of the collectors.

For a more accurate analysis, the thermal efficiency is generally plotted against the reduced temperature T', in order to account for the temperature difference between the ambient and the fluid, which is an important factor in determining the thermal efficiency. The reduced temperature is defined as:

$$T' = \frac{T_{av} - T_{amb}}{G} \tag{5.2}$$

where T_{av} is the average value between the inlet and outlet of the collectors, T_{amb} is the ambient temperature and G is the solar radiation.

The instantaneous operational points of the thermal system over the four days are shown in Figure 5.45. It is observed that all the real operating points of the solar collectors cannot lead to the construction of clear operating characteristics due to the very large dispersion of the obtained data. In the figures representing the operating points

on clear days (B and D) the dispersion of the points is smaller than on cloudy days (A and C). However, due to the transient phenomenon, it is still yet possible to build a functioning feature of solar energy system.

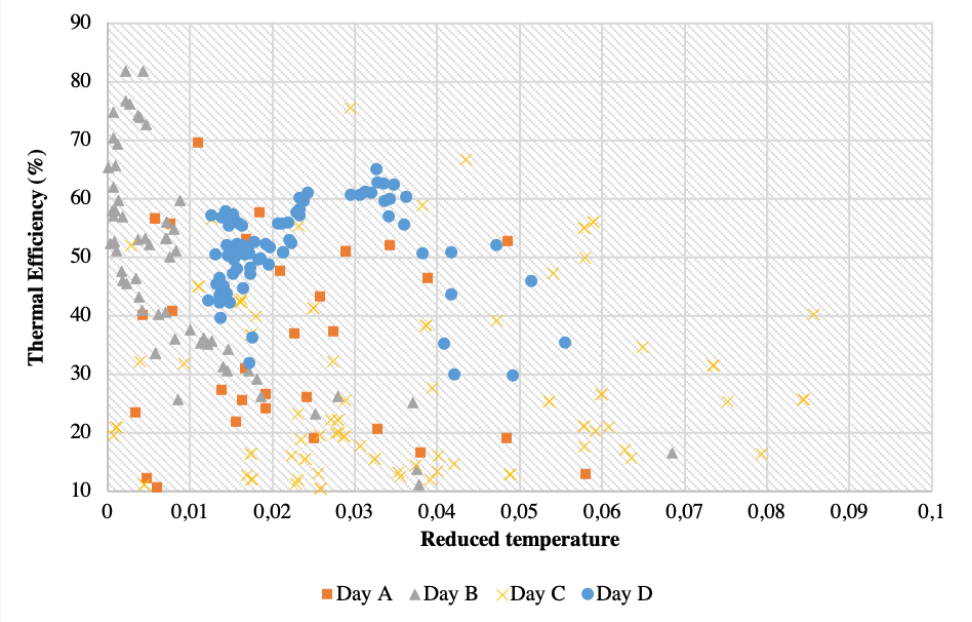

FIGURE 5.45: Instantaneous operational points over the four days - thermal efficiency plotted against reduced temperature

5.2.7 Comparison of the representative days

The results of each of the analysed days are summarised in Table 5.7. The highest values are highlighted with red, the average values are in yellow and the lowest in green. A number of conclusions can be drawn from here:

- Although day B has significantly lower ambient temperature compared to day D, the maximum temperature at the outlet of the panels is similar for both days. Both days have high solar intensity and similar available energy. This can suggest the fact that the intensity of the solar radiation is a factor of much higher impact on the temperature of the collectors than the ambient temperature.

- During the two days of high solar intensity (day B and day D), the total hours of electrical energy production are lower compared to the other two days. Although counter-intuitive, this shows that the overheating of the PV cells has a significant impact on the power production capability of the collectors.

- The total electrical energy collected has the highest value during the spring cloudy day, due to the fact that the cells are sufficiently cooled down and the efficiency of the collector does not decrease as much as in the warmer days.
- On the other hand, the period of thermal energy production is the longest during the sunny clear day (day D), and the shortest during the spring cloudy day (day A).
- The highest thermal energy production occurs during the two clear days.
- The functioning of thermal and electrical components of the system show trends that suggest an inversely proportional relationship - when the thermal energy production peaks, the electrical energy production drops.
- PVT collectors are energy productive during both seasons - spring and summer, producing high outputs of either electrical or thermal energy, as opposed to individual collectors (ST or PV) which would only be highly productive during one season.

	Day A	Day B	Day C	Day D
Maximum ambient temperature (^{o}C)	10.3	22	25.7	35
Average ambient temperature (^{o}C)	3.9	9.3	17.4	16,8
Maximum solar radiation (W/m^2)	1190.9	1031.9	949.1	921.9
Average solar radiation (W/m^2)	130.4	300	112.6	278.3
Maximum wind speed (m/s)	4	4	4.1	3,1
Average wind speed (m/s)	0.32	0.37	0.45	0.35
Hours of solar radiation	13	13.5	15.7	16
Total energy that can be collected (kWh/m^2/day)	3.9	7.15	2.67	7.12
Total water draw (l)	500	170	1060	970
Maximum outlet temperature (^{o}C)	30.5	54.7	36.3	53
Hours of thermal power production	4.7	7.5	8.3	9.5
Hours of electrical power production	11	4.6	15	7.3
Total thermal energy collected (kWh)	3.89	5.71	2.78	10.9
Total electrical energy collected (kWh)	1.24	0.23	1.01	0.95

TABLE 5.7: Summary of experimental results for the four analysed days

5.2.8 Monthly energy output

Data was collected over four months, from 1st of April to 30th of July. During this period, the instantaneous power was measured at each time step. From here, the monthly

energy output was calculated, and the results are shown in Figure 5.46. By dividing the monthly energy output to the area for each type of collector, the specific energy was obtained, shown in Figure 5.47.

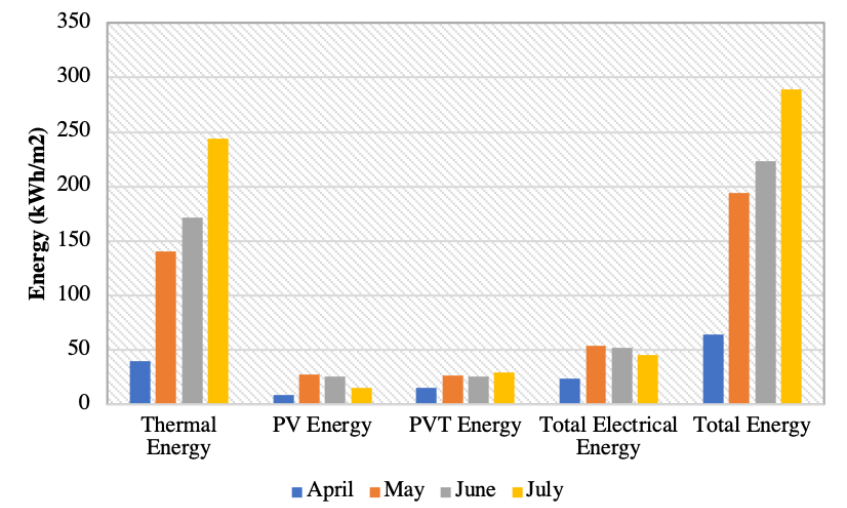

FIGURE 5.46: Thermal and electrical energy collected over four months

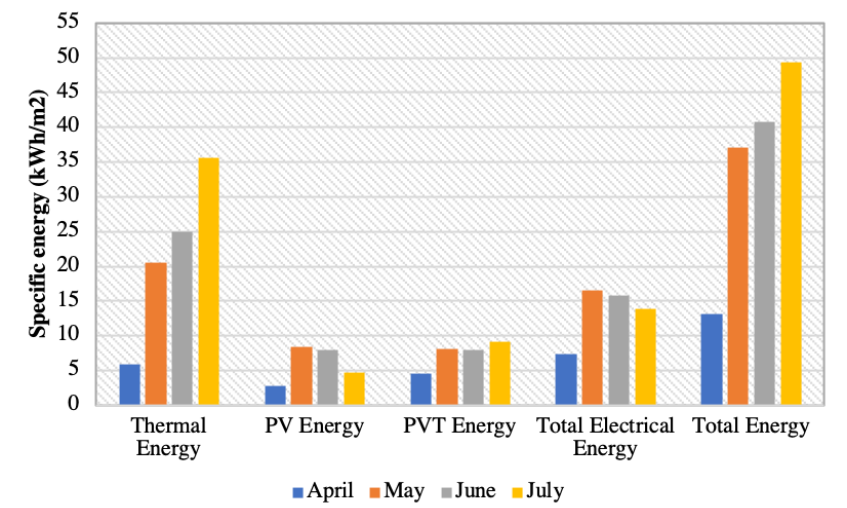

FIGURE 5.47: Specific thermal and electrical energy collected over four months

It can be observed that, overall, the energy produced by the PVT panels exceeds the PV collectors. This occurs due to the better cooling of the PV cells and operation at lower temperatures. This effect is especially noticeable during July, when the panels tend to overheat. The energy collected by the PV collectors peaks in May, while for the PVT collectors it peaks in July. This indicates the fact that PVT collectors are more suitable for high temperature operating conditions compared to the traditional PV collectors.

The thermal energy collected increases as the month approach the summer season, with the lowest output in April and the highest output in July. The total energy collected by the system has an ascending trend as the months reach the peak summer in July.

5.2.9 Comparison of PV and PVT panels

The electrical efficiency can be defined in two ways, either by comparing the total power produced to the available solar radiation (Equation 5.3) or by using the temperature coefficient (Equation 5.4).

$$\eta_{el} = \frac{P_{el}}{G \cdot A} \tag{5.3}$$

$$\eta_{el} = \eta_0 \left[1 - \beta_{\mathrm{PV}} \left(T_{\mathrm{PV}} - T_0\right)\right] \tag{5.4}$$

The first method is based upon the measurements of the instantaneous power and the measurements of solar radiation. The second method is based on the measurements of the temperature sensors placed at the back of the panels. This can lead to inaccuracy because the sensors are not located directly on the PV cell, and the temperature on the back of the panel, where the area is shaded, is lower than the actual PV cell operating temperature. This effect will be observed in the results shown in the next figures, showing the evolution over a day of the power and electrical efficiency of the PV and PVT collectors, as well as the intensity of solar radiation for reference.

Figure 5.48 shows the electrical performance during day A. It can be observed that the efficiency calculated based on the temperature sensors (Figure 5.48A) shows higher values than the efficiency in Figure 5.48B calculated by the measured power showed in Figure 5.48C. The measured power efficiency shows more dips during the day compared to the temperature efficiency. This is a cloudy spring day, with low ambient temperature and variable solar radiation. Power production peaks before the peak of solar radiation, due to lower operating temperatures. When the solar radiation peaks, the power production increases, but not higher than the previous peak. Comparing the PVT and PVT, it can be observed that the PVT perform slightly better in terms of power production and the efficiency calculated based on it.

Figure 5.49 shows the electrical performance during day B. Again, the efficiency calculated based on the temperature sensors shows higher values than the efficiency calculated by the measured power. When the solar radiation peaks, the efficiencies drop. Also, the power intensity decreases as the solar radiation intensifies. The PVT power and efficiency decrease more rapidly than the PV. This is due to the heat accumulated in the tank and insufficient water consumption by the end-used in order to dissipate this heat.

Figure 5.50 shows the electrical performance during day C, with the same difference between the two methods of calculating the electrical efficiency as discussed in the paragraphs above. The same trend can be observed, with dips in the efficiency when the solar radiation peaks. During this day, the PV power is slightly higher than the PVT power.

Figure 5.51 shows the electrical performance during day D, with the same difference between the two methods of calculating the electrical efficiency as discussed before. Due to high accumulation of thermal energy in the tank, the PVT power drops significantly compared to the PV panel.

As a result of this comparison, a few interesting facts can be observed. First, the electrical efficiency calculated as a function of the temperature recorded at the back of the panels is not entirely accurate. Also, the electrical efficiency shows dips when the solar radiation peaks in intensity. When comparing the two type of collectors, PVT performs better in the days when there is no excess of heat accumulation in the tank (either because the heat is dissipated appropriately to the consumer, or the meteorological conditions do not lead to overheating). On the other hand, the PV performs slightly better during the days when the tank thermal energy is not dissipated, and instead of cooling the cells of the PVT, the thermal agents adds thermal energy. This accentuates again the importance of a suitable consumer for the system. Another solution would be to eliminate the extra heat to a cold source, but this would mean that energy is lost, and the overall efficiency of the system would decrease.

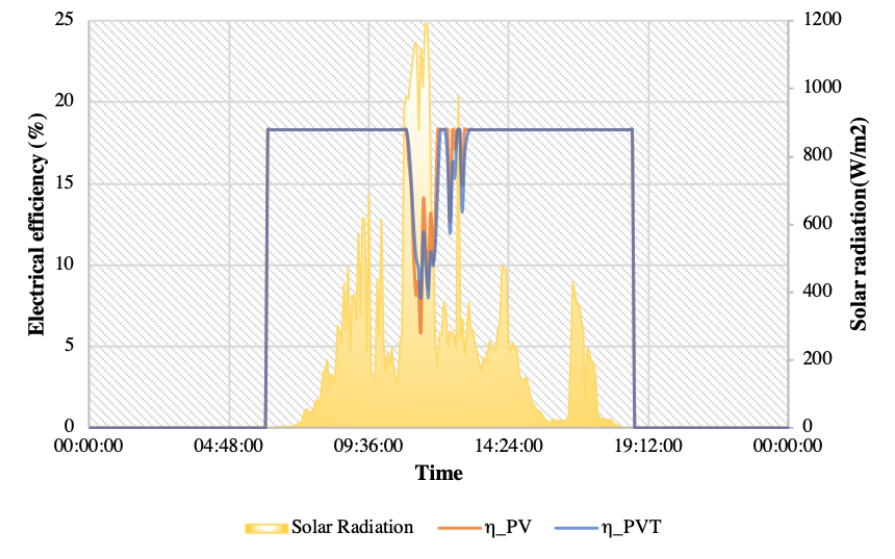

(A)

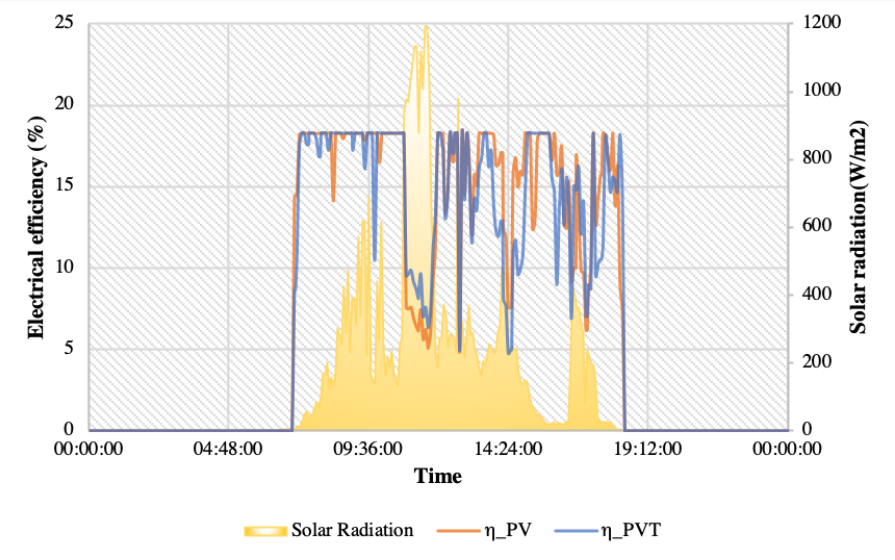

(B)

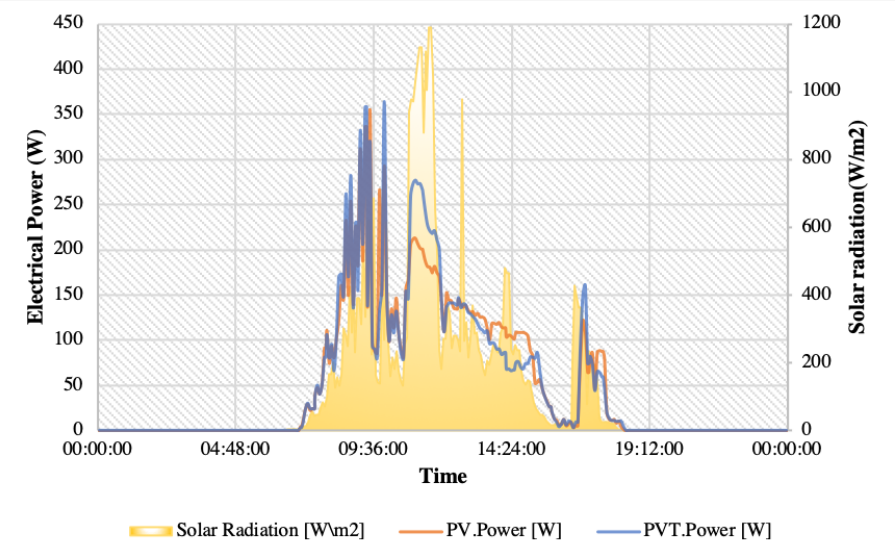

(C)

FIGURE 5.48: Electrical parameters during Day A - A)Theoretical electrical efficiency calculated with equation 5.4 B)Measured electrical efficiency calculated with equation 5.3 C)Instantaneous electrical power

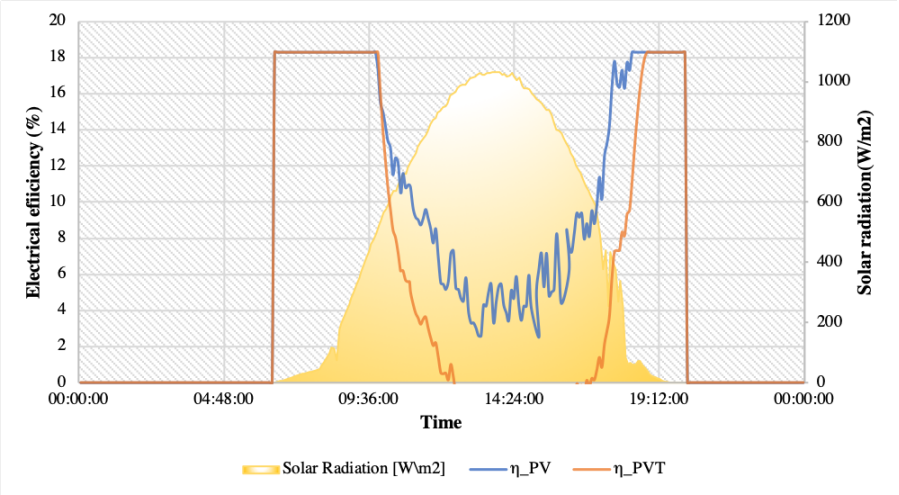

(A)

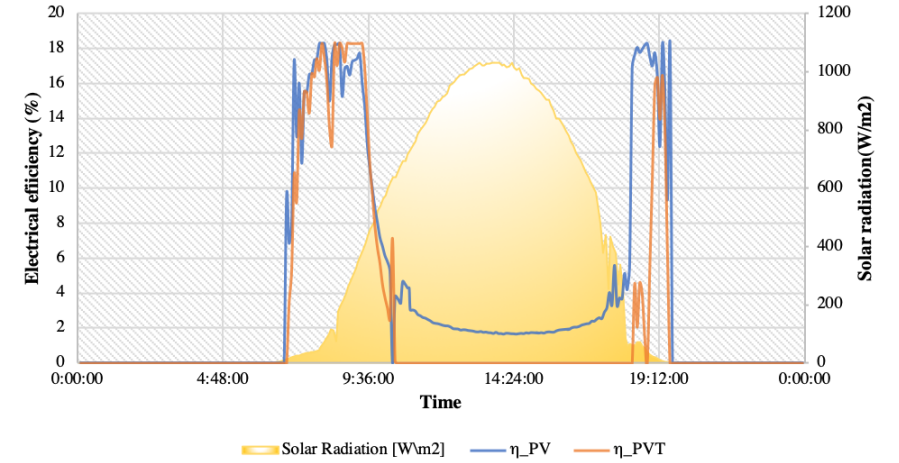

(B)

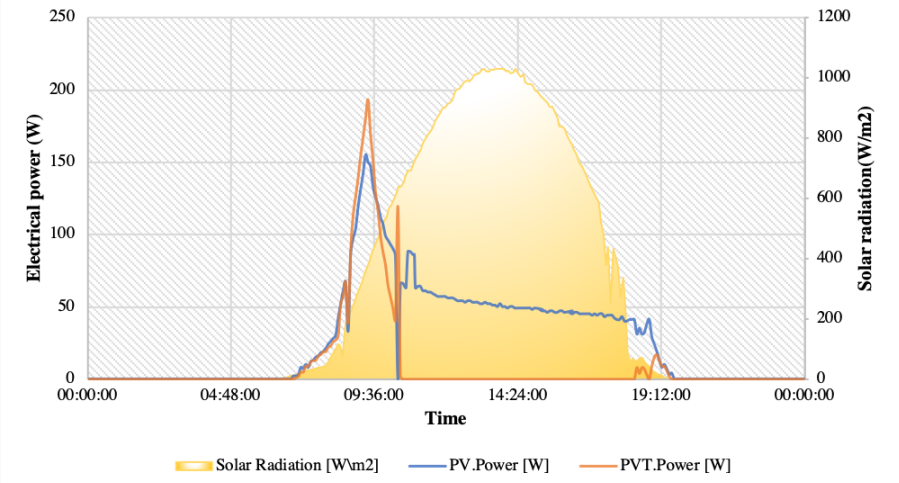

(C)

FIGURE 5.49: Electrical parameters during Day B - A)Theoretical electrical efficiency calculated with equation 5.4 B)Measured electrical efficiency calculated with equation 5.3 C)Instantaneous electrical power

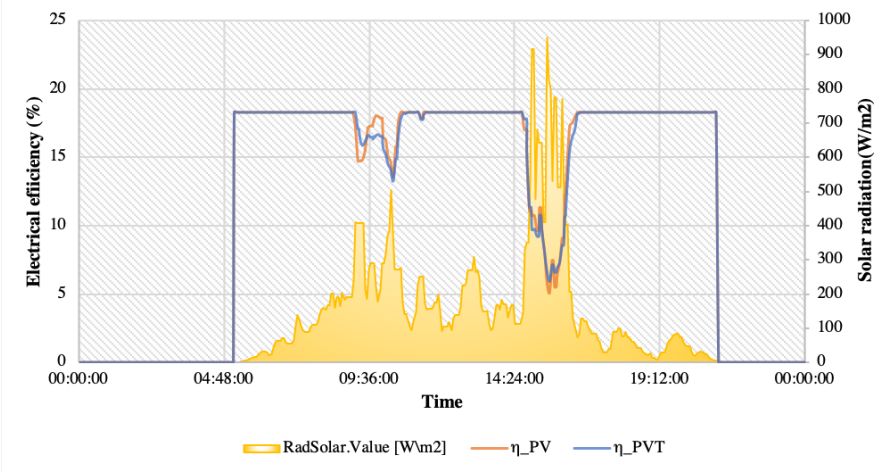

(A)

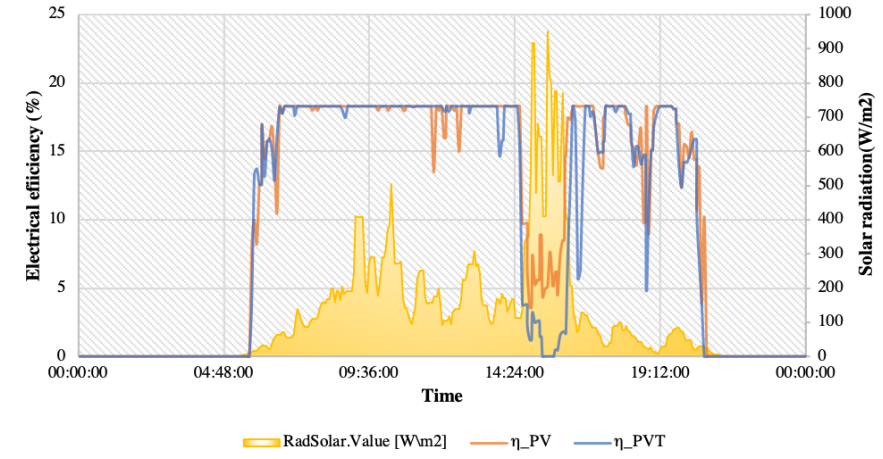

(B)

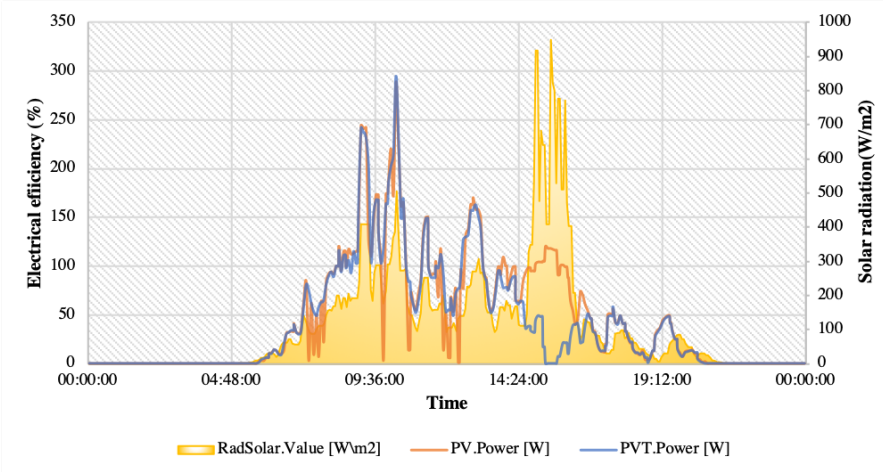

(C)

FIGURE 5.50: Electrical parameters during Day C - A)Theoretical electrical efficiency calculated with equation 5.4 B)Measured electrical efficiency calculated with equation 5.3 C)Instantaneous electrical power

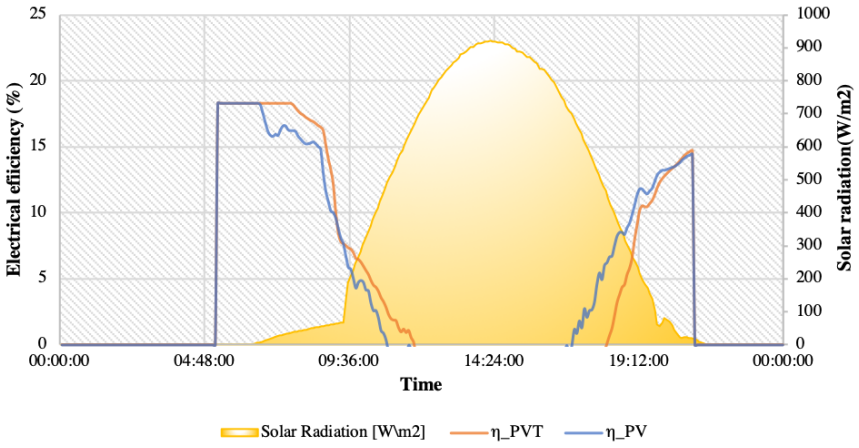

(A)

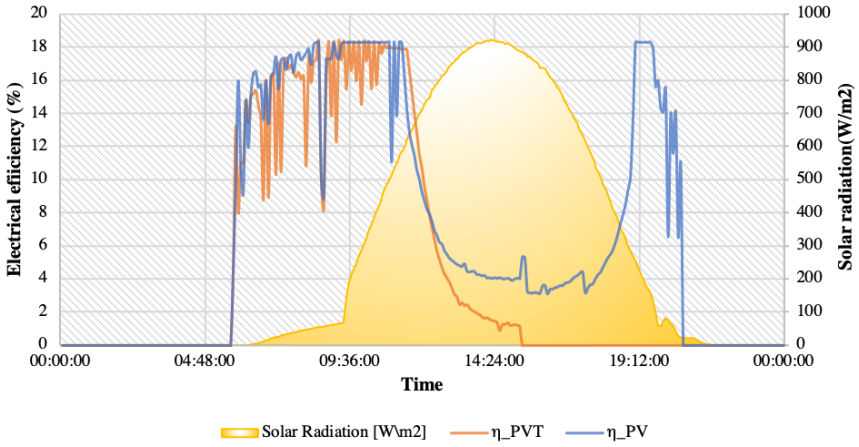

(B)

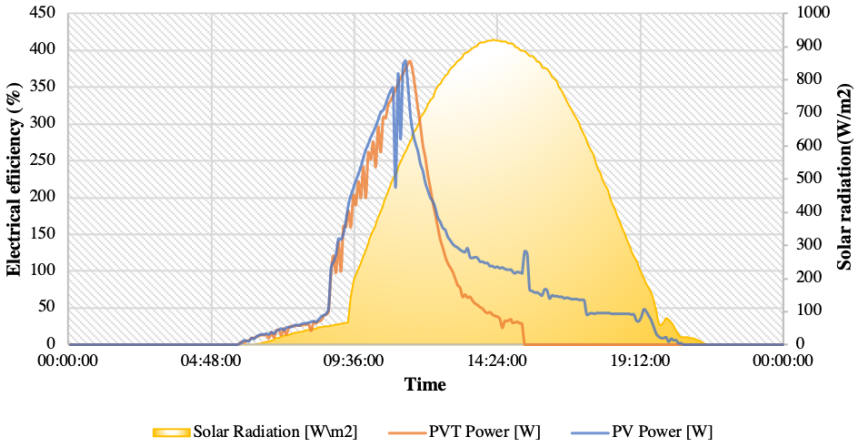

(C)

FIGURE 5.51: Electrical parameters during Day D - A)Theoretical electrical efficiency calculated with equation 5.4 B)Measured electrical efficiency calculated with equation 5.3 C)Instantaneous electrical power

5.3 Summary of experimental data

In this chapter, a hybrid demo installation has been analysed, comprising of six energy collectors: two photovoltaic panels, two solar thermal panels and two PVT panels. The installation is located within the UPB campus and the end used is a kindergarten. Meteorological data is collected with a meteorological station, and the system parameters are recorded by multiple sensors, flowmeters and energy meters and exported in the BST system.

The daily analysis of four representative days (spring cloudy day, spring clear day, summer cloudy day, summer clear day) showed that the best thermal performance of the system occurs on the warm clear days, while the best electrical performance occurs during the colder cloudy days. There is a tradeoff between the electrical and thermal production of the system. In order to improve the electrical efficiency during the very hot days, a sufficient dissipation of heat from the tank is necessary, otherwise the thermal energy accumulates and the calls are no longer cooled down. Overall, the PVT collector produced more energy over the analysed four month period.

From the comparison of PV and PVT panels it was concluded that PVT performs better in the days when there is no excess of heat accumulation in the tank; on the other hand, the PV performs slightly better during the days when the tank thermal energy is not dissipated. As a technical recommendation, PVT collectors are only appropriate in systems that have a nearby source of heat dissipation, either to a consumer or in thermal storage.

Chapter 6

Techno-Economic Evaluation

6.1 PVT market evaluation

PVT collectors were modelled, tested and proved particularly efficient in hot and tropical climates [60], [107]. Currently, there is an emerging worldwide focus on the research and development of PVT collectors. The International Energy Agency (IEA) has implemented the research project Task 35 PV-Thermal Solar Systems [108], which aimed to accelerate the development and adoption of competitive high-quality and commercial collectors and to contribute towards introducing international standards of performance, monitoring and testing of PVT collectors. Another research project has been implemented since May 2018, Task 60-PVT Systems: Application of PVT Collectors and New Solutions in HVAC Systems, part of the Solar Heating and Cooling Program, with thirteen countries involved. This project investigates innovative PVT technologies with focus on HVAC solutions [109].

Overall, Task 60 project of the IEA has identified and surveyed a total of 24 manufacturers worldwide. Their distribution is shown in Figure 6.1.

In Europe, 98 types of modules were identified, with 54 modules available on the market, 32 modules stopped from production and 6 modules under research and development. The identified modules are glazed, unglazed, or concentrated (Figure 6.2). Most of the market available modules are unglazed (Figure 6.3a) [110].

The current leader in solar thermal energy, China, which holds 86% of the global energy production market and an installed capacity of 64% of the total, also shows interest in PVT technology, especially in systems connected to geothermal pumps [71], and has the potential to become the main solar technology incorporated in new constructions

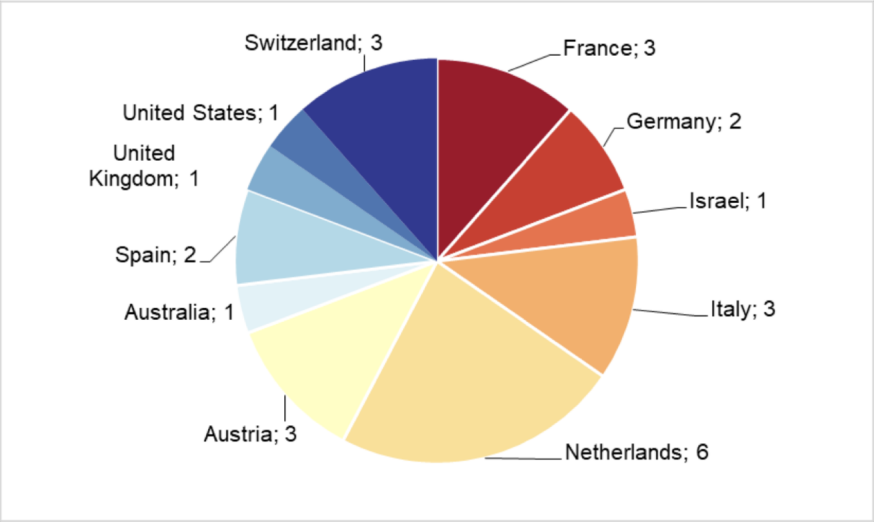

FIGURE 6.1: PVT manufacturers by country [110]

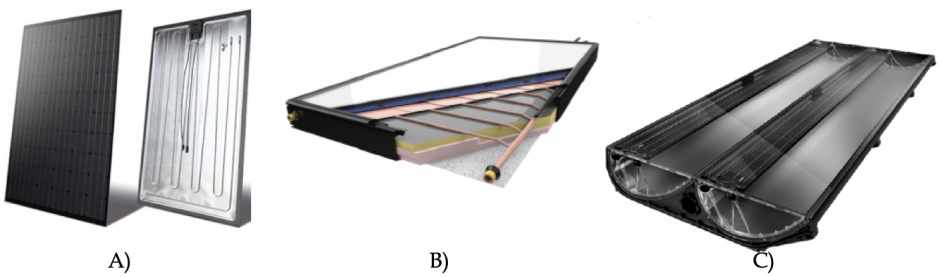

FIGURE 6.2: Examples of commercial modules A)glazed B)unglazed C)concentrated [110]

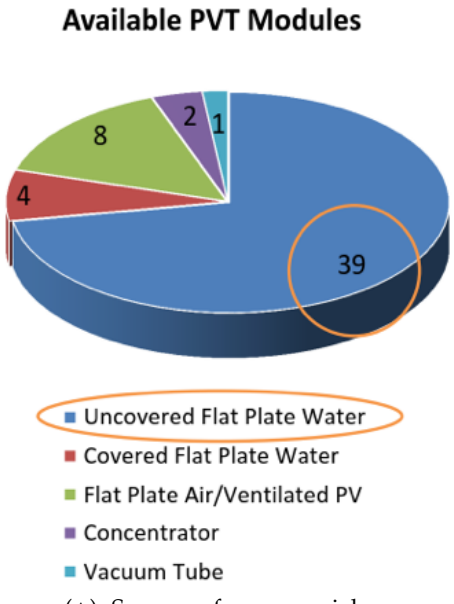

(A) Survey of commercial PVT modules [110]

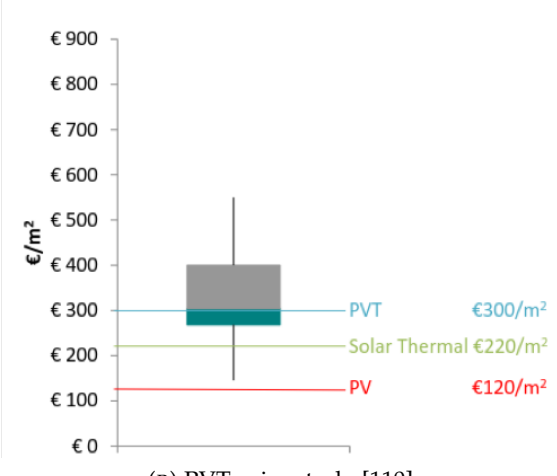

(B) PVT price study [110]

[111].

A price study was also performed as part of Task 35, identifying an average cost of 300€/m^2 for unglazed modules with thermal water agent, higher compared to 120€/m^2 for PV and 220€/m^2 for thermal collectors. These average prices indicate that, even in the current commercial stage, the installation of a PVT system is more economical than the use of two separate PV and solar thermal panels.

Another important economic aspect, besides the price of the modules, is represented by the subsidy schemes. The 'Feed in Tariffs' (FiT) scheme is widely used in Europe and is a flat-rate subsidy system for injecting excess electricity into the grid. Figure 6.3 below illustrates the major impact that the tariff rate has on the net present value (NPV) after 20 years, and the investment payback period of a PVT project.

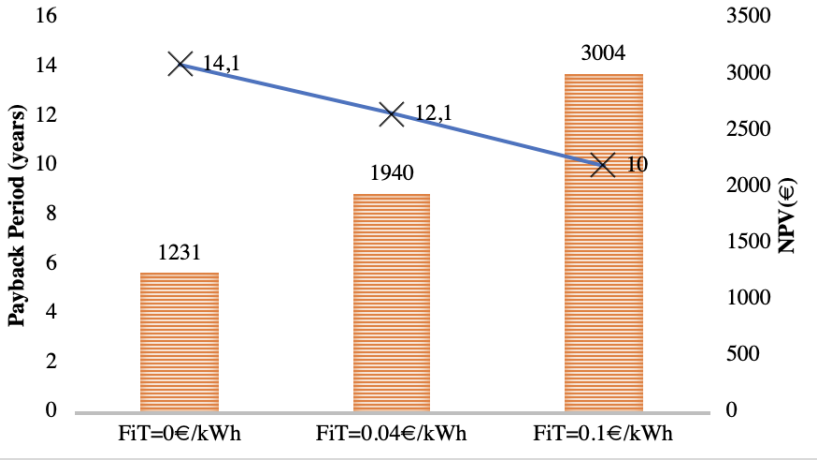

FIGURE 6.3: Example of the effect of Feed in Tarrifs on the NPV and Payback Period [112]

Due to their novelty, PVT collectors have only been included in the annual energy survey carried out by Solar Heat Worldwide since 2019. A survey carried out by SHC Task 60 identified in 2019 a total installed PVT collector area of 1 166 888 m^2 (606 MW_{th}, 208 MW_{peak}), with 567 MW_{th} and 194 MW_{peak} of the total installed capacity. A significant share is in Europe (675 427 m^2) followed by Asia excluding China (281 104 m^2) and China (133 942 m^2).

France is the leader of the EU market with an installed collector area of 484 587 m^2 followed by Germany with 112 326 m^2 and the Netherlands with 32 127 m^2. In Switzerland, Italy and Spain collector areas range between 10 000 m^2 and 15 000 m^2, and less than 10 000 m^2 in the rest of the European countries. In Romania there is no

centralised data on the installed capacity of PVT collectors [6]. The distribution is shown in Figure 6.4.

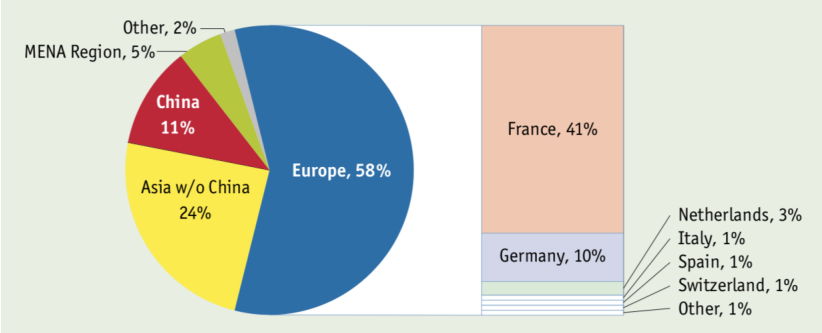

FIGURE 6.4: Distribution of the total installed PVT area by location in 2019 (reproduced from [6])

The same survey carried out on 31 PVT manufacturers indicated a 9% global growth in PVT sales in 2018 and 2019, and a +14% growth in Europe [6]. The trends are shown in Figure 6.5.

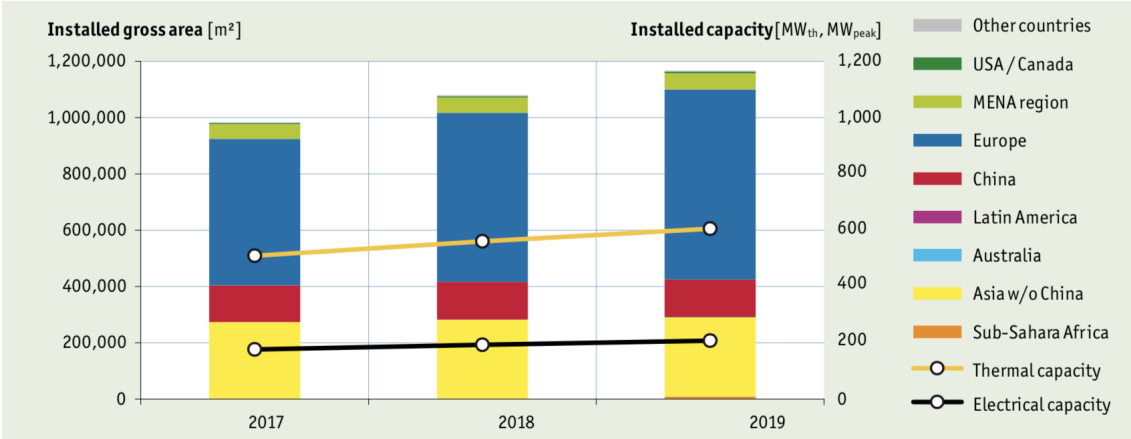

FIGURE 6.5: PVT market growth from 2017 to 2019 (reproduced from [6])

In terms of typology, the most common types are uncovered liquid based PVT collectors, with 55% of the total thermal installed capacity, followed by air-based PVT collectors with 43%, covered liquid based collectors with only 2%, and a very minor installed capacity of concentrated PVT and evacuated tube PVT [6].

The main applications identified for PVT collectors are: domestic hot water production (small or large scale), swimming pool heating, solar air heating, solar district heating and combined systems. Their distribution as a function of the type of collector is shown in Figure 6.6.

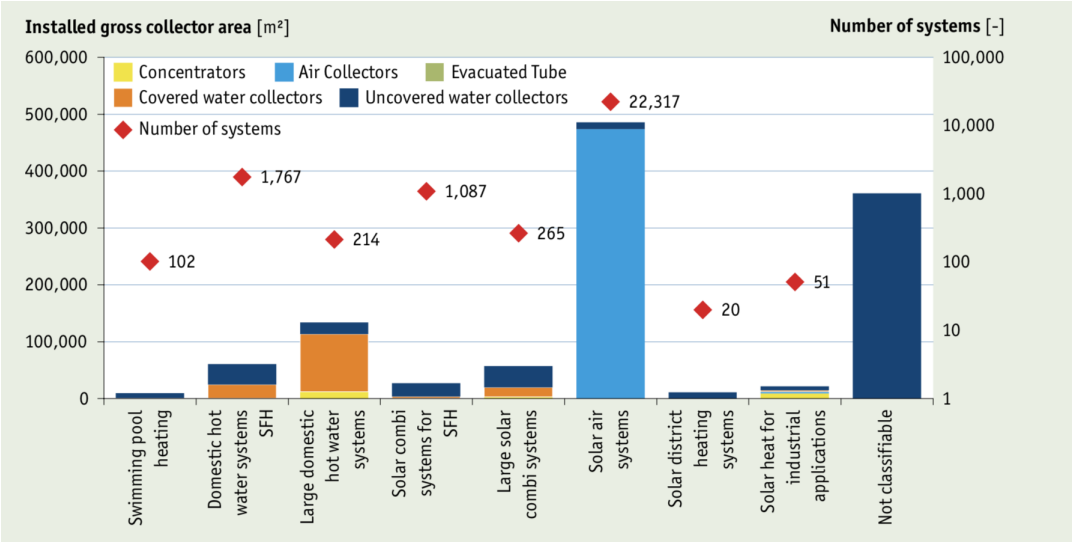

FIGURE 6.6: PVT systems applications and installed areas in 2019 (reproduced from [6])

French and Romanian Market

This project is a collaboration between Romania and France, thus it is important to establish how the two markets compare and what is the future potential for development. Both the French and Romanian markets have interesting positions regarding the adoption of PVT technologies.

In Romania, the solar energy market is growing, with 110 MWth of solar thermal capacity installed at the end of 2017 and 1.37 GW of PV energy [30]. However, the PVT market has not yet emerged, with only very few distributors identified on the market, and no centralaside data on the amount of PVT collector area installed, which provides great opportunity of further exploiting the PVT technology.

In France, the PV market is growing even more, with 875 MW of new installations in 2017, reaching to a cumulative capacity of 8.04 GW. The solar thermal market capacity is not as impressive as the PV, but still significantly higher than in Romania: 1.64 GWth in 2018 [113]. PVT panels have been introduced on the French marked since 2013, with one of the largest European producers, DualSun [110] (Figure 6.7). France is the European leader in the total installed PVT collector area, with 484 587 m^2, which represents an impressive 41% of the total European market [6]. The consumers are already familiar with the technology and are more willing to adopt it in their environmentally-friendly projects than in Romania.

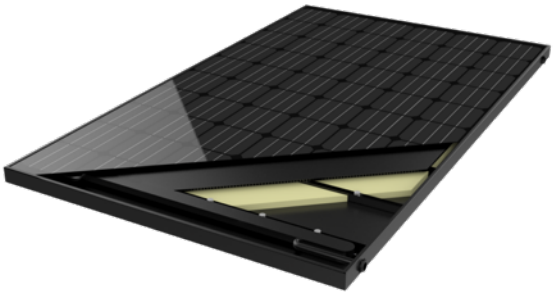

FIGURE 6.7: A typical PVT panel produced by DualSun manufacturer [110]

6.2 Available subsidies

Renewable energy has been encouraged by government subsidies and funding schemes in order to enhance their market penetration. Subsidy schemes are common for photovoltaic and solar thermal systems, but for PVT's the situation is unclear and yet to be defined in many European countries. There are three possible situations:

- PVT systems have a separate and well defined own subsidy scheme;
- PVT systems are included in the PV or ST schemes;
- No scheme is available / PVT are clearly excluded from funding schemes.

A survey was carried out by SHC Task 60 in 7 European countries with the leading PVT markets in order to investigate the type of subsidies available [114]. The results are summarised in Table 6.1. In Austria, there is one PV subsidy scheme that explicitly excludes PVT collectors, and 7 solar thermal schemes, 2 of which allow for inclusion of PVT panels. In France, all 3 PV subsidy schemes allow for PVT, and none of the 3 solar thermal include the PVT collectors. In Germany, the one subsidy scheme available also includes PVT panels, while the one solar thermal does not. In Italy there are two PV schemes, both of which allow PVT panels, and 4 solar thermal schemes, out of which only half include PVT panels. In Netherlands all 3 PV schemes include PVT, while none of the 2 ST do. In Switzerland both PV schemes include PVT collectors, and the one solar thermal scheme excludes them. Finally, in UK there is no information on the PV schemes, and out of the two available ST schemes only one allows for PVT collectors to

Country	PV schemes			ST schemes			Number of specific PVT schemes
	Total	PVT included	Rate	Total	PVT included	Rate	
Austria	1	0	0%	7	2	29%	0
France	3	3	100%	3	0	0%	0
Germany	1	1	100%	1	0	0%	1
Italy	2	2	100%	4	2	50%	0
Netherlands	3	3	100%	2	0	0%	0
Switzerland	2	2	100%	1	0	0%	0
UK	-	-	-	2	1	50%	0

TABLE 6.1: Available subsidy schemes in EU countries for PV, ST and PVT (adapted from [114])

be included. In terms of standalone PVT schemes, the only country that has one in place is Germany, since 2019.

The main conclusions of this investigation are:

- Many of the schemes do not indicate specifically if PVT are accepted and require further clarifications;
- In general, the PV schemes have higher acceptance of PVT in their funding than solar thermal schemes;
- The type of PVT collector (air-based, liquid-based, covered, uncovered) is also a criteria of exclusion in some cases;
- There is only one standalone PVT subsidy scheme;
- Further clarification and standardisation is necessary in all the investigated countries, and also in the rest of Europe.

In terms of monetarily quantifying the subsidy contributions, the survey concluded that they are difficult to compare in different countries due to the the currency and manner of being offered - feed in tariff, percentage of tax relief or ceiling amount.

Therefore, the two aspects of major financial importance for the commercial development of PVT systems are:

- Decreasing the price of modules and energy storage systems (including transport, installation, maintenance).
- Implementation of subsidy schemes such as Feed in Tariffs, with an optimal tariff for the purchase of electricity.

6.3 Economic analysis of PVT panels compared to traditional technologies

Currently on the solar energy market there are three available options for the consumers:

- Photovoltaic panels (PV) for the production of electrical energy;
- Solar Thermal panels (ST) for the production of thermal energy;
- Photovoltaic Solar panels (PVT) for the simultaneous production of electrical and thermal energy.

An interesting analysis is to compare the three options from a financial point of view, applied to a real small-size household consumer. This section carries out a technical and economical analysis and comparison between multiple possible configurations of solar energy systems for a prosumer with a relatively low annual energy consumption (6MWh/year) in various scenarios of subsidies. The results show that in the absence of a subsidy scheme, the traditional PV panels are more beneficial due to their lower costs compared to novel PVT collectors. On the other hand, if there is the possibility of selling the excess electricity to the grid in exchange for some financial bonus, the investment in PVT, although currently high, becomes justified, and the profitability increases by 50% compared to standard PV. Finally, an overview of the pros and cons of the PVT technology was carried out, in the form of a strength-weakness-opportunity-threat (SWOT) analysis.

6.3.1 Methodology for the technical-economical analysis

The following methodology was followed for carrying out the technical-economical comparison between PT, PV and PVT for a small-sized residential consumer (6 MWh/year):

- Determine the annual thermal and electrical energy production for each technological solution in order to cover or partially cover the consumer demand;
- Determine the initial investment for each of the solutions;
- Determine the payback period (PP) and the net present value (NPV) of the investments.

The analysis was carried out based on the following premises:

- The consumer is a domestical building with an annual energy demand of 6 MWh: 2 MWh of electrical energy and 4 MWh of thermal energy for heating and domestic hot water. From the total energy demand 40% is electrical energy and 60% is thermal energy, which is provided by on-site central heating;
- The available roof area that is oriented towards South has the dimensions of 8m x 6m;
- The PV cells in the PVT collectors operate at 9% higher efficiency than the cells in the individual PV collector (η_{elPV}=0.91 x η_{elPVT});
- The the thermal efficiency of the PVT collector is 30% less that the thermal efficiency of the ST collector (η_{tPVT}=0.7 x η_{tST} [39];
- All the collectors (PVT, PV and ST) have equivalent sizes and a total of 24 panels can be installed in the area available on South side of the roof;
- The average annual solar radiation (Hi) in Romania is 1350 kWh/m^2/year;
- Auxiliary energy storage equipment (boilers, batteries) is not included in the financial calculation.

6.3.2 Proposed technical solutions

Based on the aforementioned premises, the nominal parameters and costs of equipment were collected from the manufacturers' data and are summarised in Table 6.2.

Type	Nominal electrical power (We)	Nominal thermal power (Wt)	η_{el} (%)	η_{th} (%)	Dimension (cmxcmxcm)	Price (€)
ST	-	900	-	90	165x100x 0.4	150
PV	240	-	14	-	165x100x 0.4	210
PVT	260	630	15.3	63	165x100x 0.4	450

TABLE 6.2: Nominal characteristics of installed equipments

For this particular consumer, the analysis considered 4 configurations of installation of the solar energy systems on the available roof space. The configurations are shown in Figure 6.8 and summarised below:

- Solution 1 - 50% of the roof is covered with PVT panels, 50% of the roof is empty;

- Solution 2 - 50% of the roof is covered with PV panels, 50% of the roof is covered with ST panels;
- Solution 3 - 50% of the roof is covered with PV panels, 50% of the roof is empty;
- Solution 4 - 100% of the roof is covered with PVT panels;

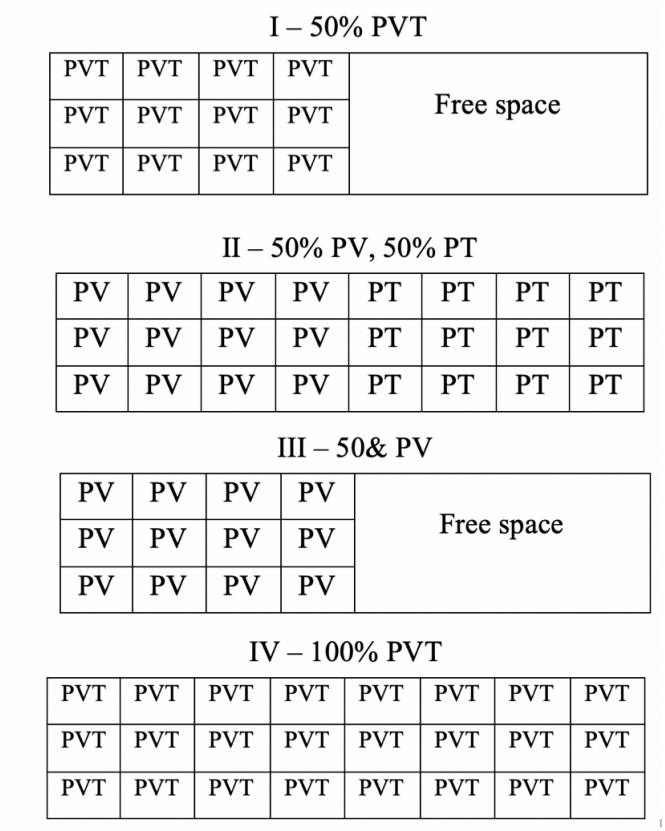

FIGURE 6.8: Configuration of 4 technical solutions

6.3.3 Investment analysis

The annual thermal and electrical energy output is estimated in Table 6.3 for each configuration. It's important to note that during winter time the solar thermal collectors in both ST and PVT were considered to only operate at 20% capacity, and the remaining thermal energy demand during winter (for both hot water and heating) is a deficit that is met by the central heating system.

The systems can be compared in terms of payback period and net present value. The payback period represents the time it takes for the investment to be paid off from the income it generates, while the NPV is the total cost of the system over its lifetime and is

Solution	Electrical output (kWhe/year)	Thermal output (kWht/year)	Total investment (€)	Unit cost €/kWhel	Unit cost €/kWhel
I	3207	4010	5400	1.684	1.347
II	2916	6600	4320	1.481	0.655
III	2916	-	2520	0.864	-
IV	6415	8020	10800	1.684	1.347

TABLE 6.3: Operating characteristics of the proposed configurations

calculated as the sum of the capital cost F_c and the annual present value o for each year of operation N.

$$\text{Payback Period } = \frac{\text{Initial Investment}}{\text{Net Cash Flow per Period}} \tag{6.1}$$

$$NPV_N = F_c + \sum_{N=1}^{N} \frac{(1+i)^{N-1}}{(1+d)^N} \tag{6.2}$$

With an average electricity price of 0.13€/kWh [115], the payback period and the NPV of the investment were computed at a discount rate of 8% over the 20 years lifetime of the equipment. First, the option of selling the excess energy to the electrical grid was excluded. Then, a subsidy scheme of ‚Feed in Tariffs' (FiTs) was considered for selling the electricity to the grid. The first option, with no subsidy, was considered because until recently the small 'prosumers' were not able to sell the excess electricity back to the grid. This is a new scheme in Romania which was only proposed at the end of 2017 and implemented in 2019.

The NPV and payback period of the non-subsidised scenario were first calculated. Next, the 'Feed in Tariffs' scheme was considered as a form of governmental subsidy. This scheme is widely used across Europe and consists in offering any renewable energy producer a fixed financial reward for selling their excess electrical energy to the national grid. In Romania, this scheme is in early stages, and was introduced in 2019. During the initial proposal the subsidy tariff was 0.04€/kWh [116], 70% less than the EU average, and it was contested by the public and NGOs. In this analysis, two tariff scenarios were considered, one with the initial proposal of 0.04€/kWh, and a second one with a tariff of 0.1€/kWh, closer to the European average of 0.157€/kWh. The results of the analysis are shown in the Figures 6.9 and 6.10.

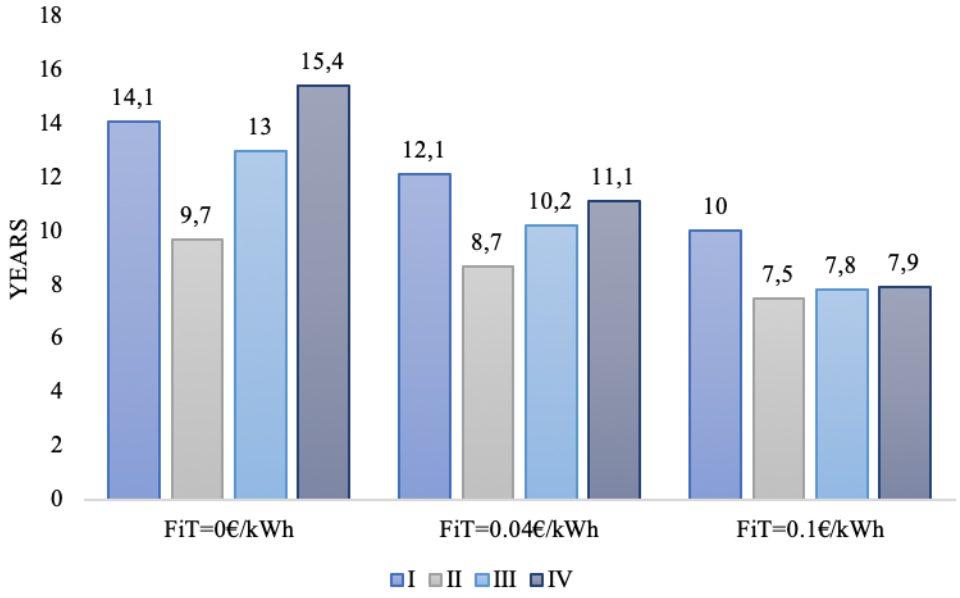

FIGURE 6.9: Payback period for the 4 solutions

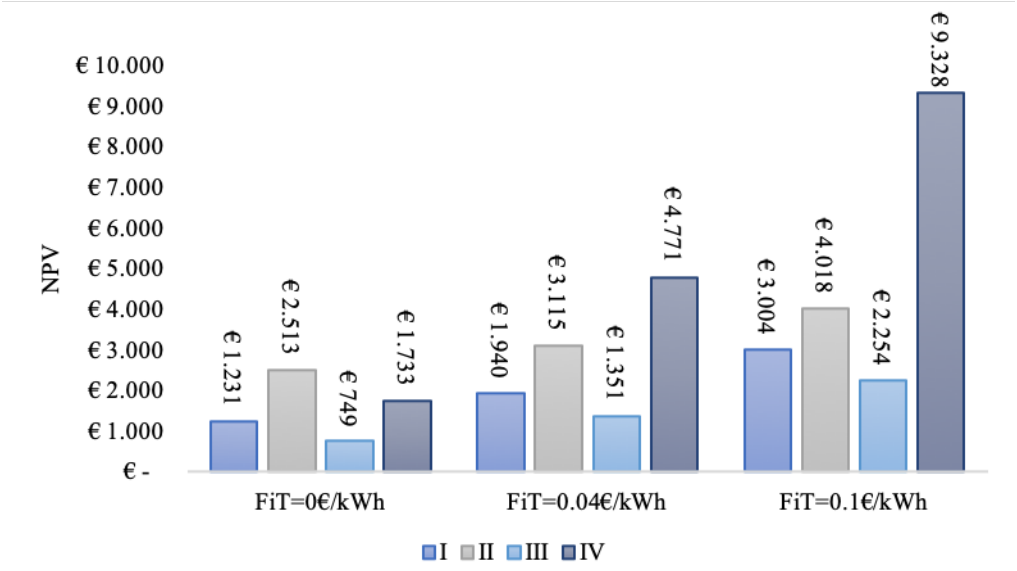

FIGURE 6.10: Net Present Value after 20 years for the 4 solutions

The conclusions of this analysis are:

- In every subsidy scenario, the fastest payback period is for configuration II (50% PV, 50% ST);
- In the non-subsidised scenario, the most profitable is configuration II with 12 PV and 12 ST, both in terms of the payback time (9.7 years) and the NPV (2,513€);
- For the low subsidy scenario (0.04€/kWh) the shortest payback time is also for configuration II (8.7 years), but the most profitable NPV is €4,771 and is achieved by configuration IV (24 PVT);
- In the high subsidy scenario (0.1€/kWh) the payback period of configurations II, III and IV are similar, with values between 7.5 and 8 years. However, the highest NPV is achieved by configuration IV, as it appears to be increasing exponentially with the increase in subsidy;
- Systems with a significantly higher capacity compared to the consumer demand are only feasible with a proper tariff scheme in place, which allows for the excess electricity to be sold to the national grid. Otherwise, the excess electricity doesn't bring financial profits and the high initial investment is not justified.

6.3.4 SWOT Analysis

It was observed, from the economical analysis, that the investment in PVT collectors is not financially profitable at small scale due to the current high price of PVT compared to the standard PV and ST collectors. However, for a larger installed capacity and with a proper subsidy scheme in place, the co-generation solution becomes profitable, the investment is recovered shortly, and the NPV during the lifetime of the equipment is high. Thus, it can be concluded that, in the current market conditions, PVT collectors are only profitable at larger scales and only with subsidy schemes in place. Furthermore, if the available space is limited, the investment in PVT is also justified against standard PV and ST for maximisation of the solar conversion.

A common method of analysing the feasibility of a technology is the SWOT analysis. Figure 6.11 illustrates a SWOT analysis carried out for the PVT technology. Here it can

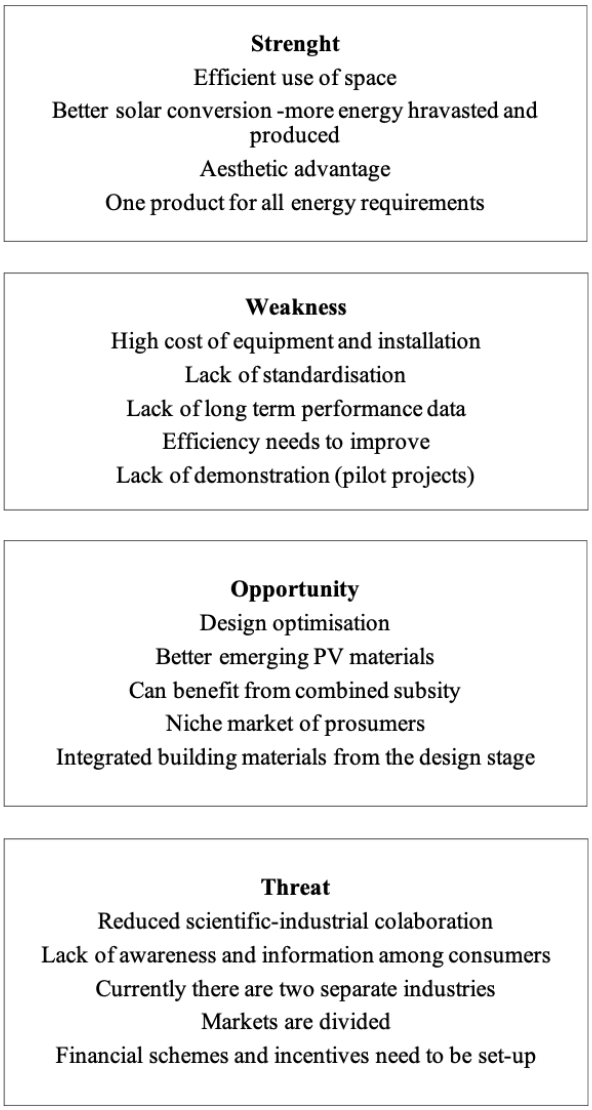

FIGURE 6.11: PVT SWOT analysis

be observed that the strong points are significant, but there are also multiple internal and external barriers and threats regarding the technology and the trends of the market.

Chapter 7

Conclusions and Further Work

This project carried out a comprehensive analysis of PVT collectors in various functioning regimes. The general advantages of solar energy (free fuel, no noise, no emissions, safe operation) are enhanced by another set of benefits provided by the integration of PV and solar thermal collectors (better PV efficiency due to lower operating temperature, better use of space, more solar conversion, on site production for both types energy requirements).

Although generally speaking, the demand curve of the consumer matches the functioning hours of the PVT collectors, solar energy still has a random character, both predictable (day-night cycle) and unpredictable (given by nebulosity). Currently, the use of hybrid photovoltaic solar thermal collectors is conditioned by the combination of the solar source with another back up source or external storage systems.

PVT collectors are still a novel technology, not yet fully penetrated on the market, with little reliable performance data available for designers and planners. In terms of technology and economy, the two separate industries (PV and solar thermal) need to converge more, and an interdisciplinary effort from industry and academia is required in order to accelerate the development of PVT collectors and reach a competitive market price that it is accessible to the large mass of prosumers.

7.1 Main Findings of this Thesis

In the first section, the review of the available literature gathered and synthesised information about the functioning principles of PVT panels, their applications, their strengths and weaknesses. It also investigated the latest research on the topic, and identified areas that require further examination: an explicit numerical model that can be easily adapted

for any panel configuration and functioning regime; a parametric analysis of the entire PVT system, not just the standalone panel, the impact of the consumer demand on the efficiency of the PVT system and panel, real experimental data on PVT system performances. These areas were addressed in the rest of this research.

The second section proposed an improved explicit numerical model of a PVT collector based on the heat balance equations between each layer. The model is able to establish the temperatures inside the collector at any given time, depending on the external input: ambient temperature, solar irradiation and wind speed. The model was validated against an experimental prototype from the literature, and a typical behaviour of a PVT panel was illustrated for the case study of Strasbourg France. The OFAT parametric analyses carried out in this study showed in most cases a compromise between the electrical and thermal performance of the PVT system. In terms of wind speed and insulation, it was observed that the thermal benefits of low wind and high insulation overcome the decrease in electrical efficiency. For optimum design, the insulation thickness should be maximized and the wind speed minimized, which can be achieved by strategic placement of the panels in areas protected from wind. The packing factor was found to be optimum when maximized, as the electrical benefits are more significant than the thermal ones. The width of the channels in the heat exchanger should also be maximized as far as technologically possible for best performance. The flow rate should also be maximised, but keeping in mind the increased amount of energy used for pumping. A number of technical recommendations have been proposed based on this analysis.

A transient analysis of a PVT system connected to a real consumer showed that half of the yearly demand of electrical and thermal energy could be provided by a simple and inexpensive PVT combined with back-up solutions (such as auxiliary heater and a battery bank). Overall, small scale PVT technology appears to be a promising solution for maximum solar energy conversion, especially in the residential and urban sectors.

The parametric analysis of the PVT system showed a number of interesting facts. First of all, the best cell efficiency os achieved at the lowest cold-water main temperature. Also, the larger the thermal storage tank, the better the electrical efficiency is, but there is a loss in the quality of thermal energy. The higher the consumer water demand, the better the cell electrical efficiency, as a result of the fact that the cells are cooled down

faster. At the peak consumer hot water demand there is also a peak in the electrical efficiency of the cell. The most significant impact on the electrical efficiency is the flow rate to the consumer, which means that a suitable fit of consumer to the system is essential for performance maximisation. When the temperature of the fluid at the inlet of the PVT panel increases, there is a decrease in the instantaneous electrical power, the instantaneous thermal power also decreases, but the net instantaneous thermal power delivered to the tank increases. These conclusions are useful for designing highly efficiency small scale renewable energy systems and providing maximum performance for a given consumer.

The experimental analysis indicates that there is a tradeoff between the electrical and thermal production of the system. The functioning of thermal and electrical components of the system show trends that suggest an inversely proportional relationship - when the thermal energy production peaks, the electrical energy production drops.. Overall, the PVT collector produced more energy over the analysed four month period.

From the comparison of PV and PVT panels it was concluded that PVT performs better in the days when there is no excess of heat accumulation in the tank; on the other hand, the PV performs slightly better during the days when the tank thermal energy is not dissipated. As a technical recommendation, PVT collectors are only appropriate in systems that have a nearby source of heat dissipation, either to a consumer or in thermal storage. PVT collectors are energy productive during both seasons - spring and summer, producing high outputs of either electrical or thermal energy, as opposed to individual collectors (ST or PV) which would only be highly productive during only one of the two seasons.

Finally, the economic overview of the PVT market and the available subsidies revealed the fact that there is still a lack of standardisation at a European level, and lack of clarity regarding the classification of PVT collectors in the solar energy technologies. In terms of economical evaluation, subsidies are an important parameter for establishing the benefits of the investment. Three scenarios were investigated, with high, medium and no subsidy, and the results showed a payback period of the investment between 7 and 15 years, which is comparable to the traditional solar technologies.

7.2 Directions for further research

As a result of this project, several areas of that could benefit from further research have been identified. An important area is the combination and hybridisation of various renewable energy technologies, among which PVT collectors, for providing the reliable and self sufficient energy systems of the future. These technologies include - solar, biomass, heat pumps, for providing heat, electricity and also cooling. In many urban areas, interior cooling and air conditioning is a major source of energy consumption, thus solar trigeneration is an important area of research.

Further investigation into the PVT materials and coatings for maximising the thermal efficiency without affecting the electrical output would also be beneficial for pushing the technology forward on the market and demonstrating its potential.

An experimental prototype tailored according to the results of this research is planned to be developed at INSA Strasbourg ICube laboratory, where it will be tested in the indoor laboratory (Figure 7.1).

(A) (B) (C)

FIGURE 7.1: Components of indoor laboratory A)Solar simulator B)Flux meter C)Infrared camera

Further research will be carried out on the experimental stand at University Politehnica of Bucharest. The system can be truncated by changing the valve configuration and the PVT, solar thermal, and PV panels can function individually instead of in series / in parallel. This can be investigated in terms of system performance and identifying the most suitable configuration for the given end-user.

Multiple demonstrative projects are taking shape involving the novel PVT technologies. An interesting project carried out by UPB is the evaluation of PVT technologies as part of an upgrade of the District Heating System of Bucharest. This project investigates the possibility and benefits of the integrating PVT panels at the thermal points

of the district heating of Bucharest, Romania. This will lead to the modernisation of the system, to increasing its self-reliability, and ultimately reducing the pollution caused by fossil fuels. One other important benefit of introducing the renewable energy source directly at the distribution point is the reduction of transportation losses; in this case from the date provided by the distributor, the losses are quite significant, up to 37%. The next stages of this project are an in depth technical-economic analysis and sizing of the system for its potential implementation. Sizing the three technological solutions is currently in work and the results will be soon published.

Appendix A

Appendix A - Thermo-mechanical scheme of experimental installation

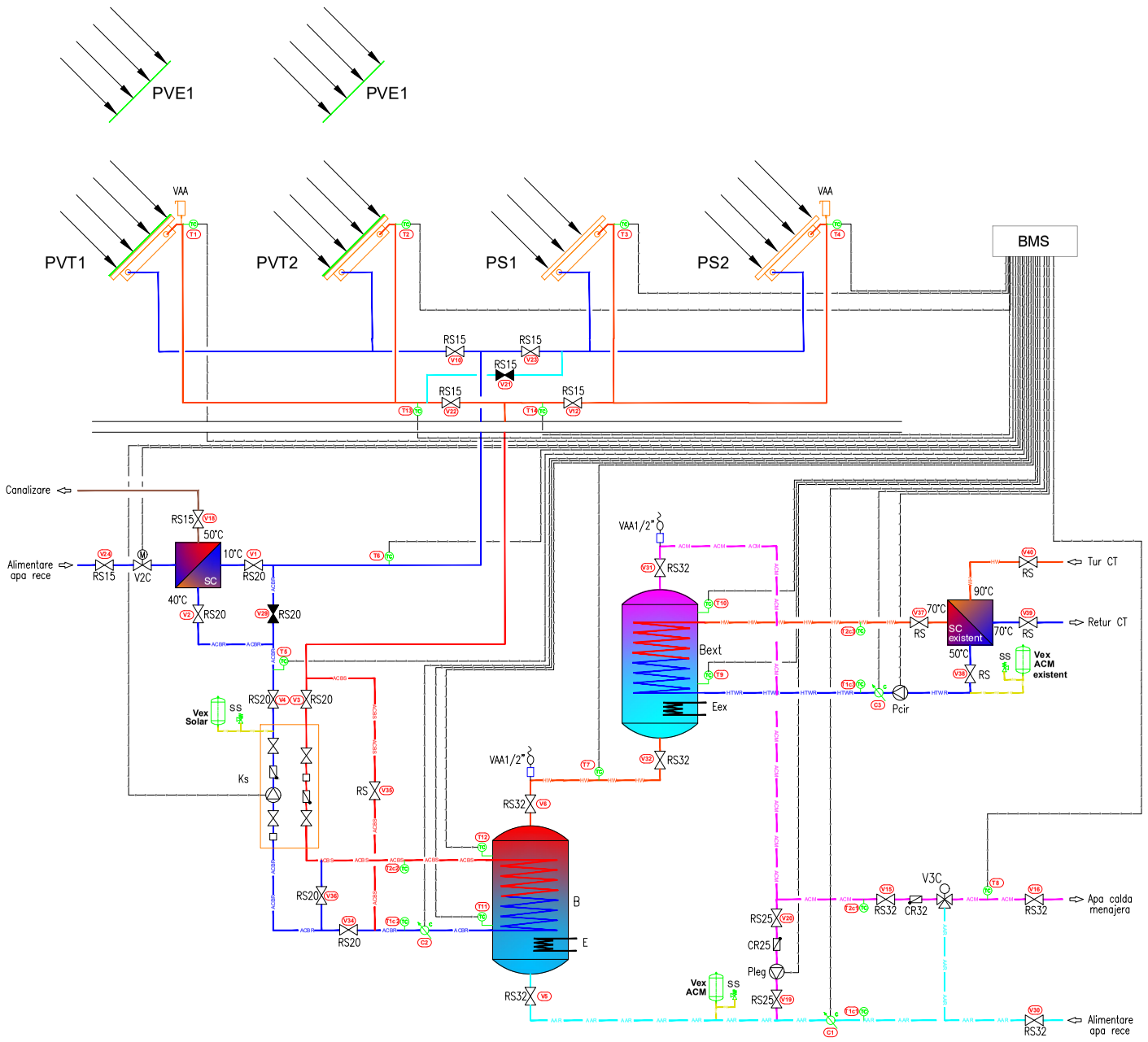

LEGENDA

1. PS - Panou Solar
2. PVT - Panou Hibrid Solar Fotovoltaic
3. PVE - Panou Foto voltaic
4. Pcir - Pompa circulatie Incalzire boiler Q= 5,0mc/h ; H=2,5mCA
5. Pleg - Pompa circulatie anti legionela Q= 2,0 mc/h ; H=2,5 mCA
6. Ks - Kit Solar circulatie apa
7. SC - Schimbator de Caldura Danfoss in placi Tprimar=70/60°C; Tsecundar= 15/22°C; Q=2kW
8. SCext - Schimbator de caldura existent in placi Tprimar=90/70°C; Tsecundar= 70/50°C; Q=200kW
9. B - Boiler vertical ACM V=500litri
10. Bext - Boiler existent vertical ACM V=500litri
11. SS - Supapa de siguranta instalatie 3 bar
12. Vex acm - Vas de expansiune inchis cu membrana
13. Vex acm existent - Vas de expansiune inchis cu membrana V=200litri
14. Vex solar - Vas de expansiune inchis cu membrana
15. V3C - Vana cu trei cai mecanica
16. V2C - Vana cu doua cai modulanta 0 -10 V
17. E - Rezistenta electrica P=2,3 kW
18. Eex - Rezistenta electrica existenta P = 9 kW
19. RS - Robinet de sectionare
20. Cs - Clapeta de sens
21. VAA - Ventil de aerisire
22. TC - Senzor de temperatura
23. C - Contor energie termica

CONDUCTA _TUR INCALZIRE
CONDUCTA _RETUR INCALZIRE
CONDUCTA _ACM
CONDUCTA _ALIMENTARE APA RECE
CONDUCTA _TUR BOILER
CONDUCTA _RETUR BOILER
CONDUCTA _AUTOMATIZARE
CONDUCTA _EXPANSIUNE

ENGIE BUILDING SOLUTIONS S.R.L.
RO 032126 BUCURESTI, Str. Ilioara ,nr.60, etaj 1
Tel :(+4021)311.04.33 (+4021)311.04.32

Denumire proiect: **Universitatea Politehnica Bucuresti**	Proiect nr.: XXXX-H-01		Faza: PT
	Desen nr.: XXXX-H-01		Scara: %
Instalatie: Incalzire	Desenat: LA		Data: 31.07.2020
	Proiectat: LA		Data: 31.07.2020
Plan: Centrala Termica	Verificat: CA		Data: 31.07.2020

Appendix B

Appendix B - Technical sheet for the PV, PV and ST collectors

TECHNICAL DATA

PHYSICAL DATA	
Length	1650 mm
Width	991 mm
Frame width	35 mm
Weight	18,5 kg
Number of cells	60
Cell type	PERC Monocrystalline
Connectors	MC4 / MC4 compatible
Junction box	IP67 – 3 diodes
Maximum load	5400 Pa (snow) / 2400 Pa (wind)
Frame colour	Anodised aluminium / White

OPERATIONAL CHARACTERISTICS	
Temperature	-40°C to +85°C
Maximum system voltage	1000 VDC
Reverse current load	20 A
NOCT	45 ± 2°C
Application class	Class II

PHOTOVOLTAIC CHARACTERISTICS STC Conditions (AM 1,5 – 1000 W/m² - 25°C)	
Nominal power (P_{mpp} / W)	300
Power output tolerance	0 / +5W
Module efficiency (%)	18,3
Rated voltage (V_{mpp} / V)	32,7
Rated current (I_{mpp} / A)	9,18
Open circuit voltage (V_{oc} / V)	39,1
Short circuit current (I_{sc} / A)	9,68

Tolérance de mesure de puissance: +/- 3%

TEMPERATURE COEFFICIENTS	
Voltage temperature coefficient (μV_{oc})	-0,30 %/°C
Current temperature coefficient (μI_{sc})	0,06 %/°C
Power temperature coefficient (μP_{mpp})	-0,39 %/°C

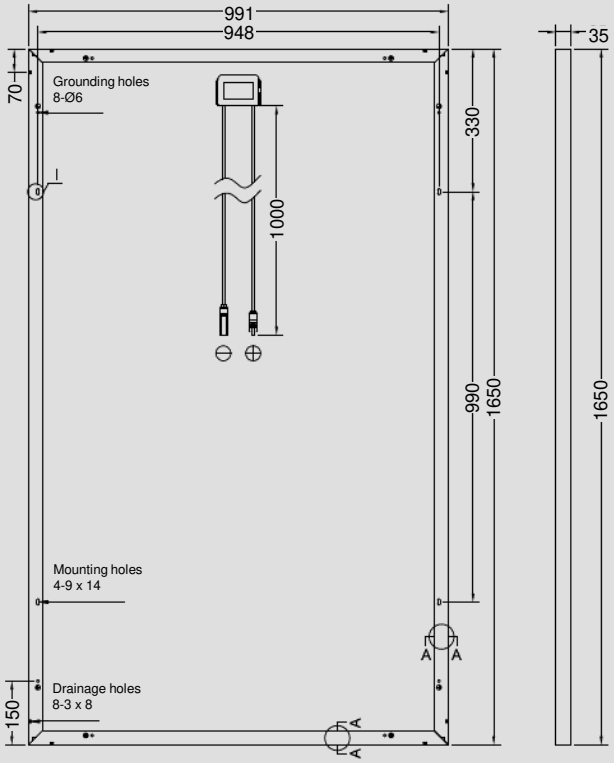

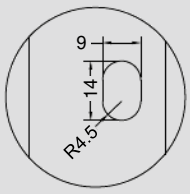

DETAIL I

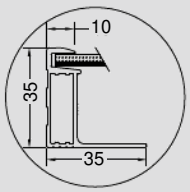

SECTION A-A

List of Flash compatible mounting systems available on DualSun website – Professional Area

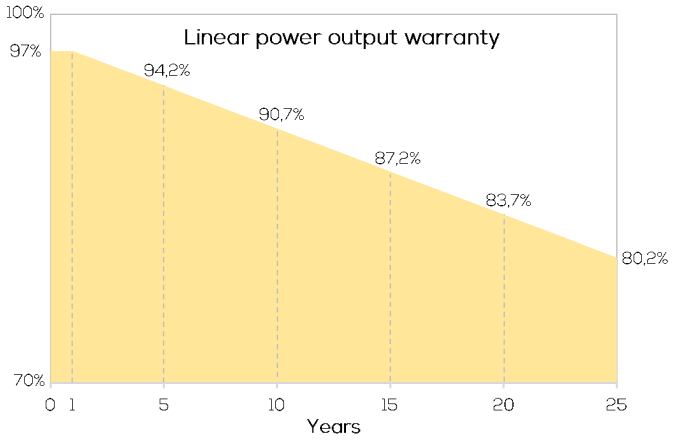

www.dualsun.com
contact@dualsun.com
2 rue Marc Donadille – 13013 Marseille - France

TECHNICAL DATA

GENERAL DATA		
Length	1650 mm	
Width	991 mm	
Frame width	35 mm	
Frame color / Backsheet	Black / Black	
Maximum load	5400 Pa (snow) / 2400 Pa (wind)	
	Spring NI*	Spring I*
Weight empty / filled	24,3 / 29,3 kg	25,1 / 30,1 kg

* NI = Non-Insulated, I = Insulated

PHOTOVOLTAIC DATA		
Number of cells per module	60	
Cell type	PERC Monocrystalline	
Nominal power (P_{mpp})	300 Wp	310 Wp
Module efficiency	18,3 %	19,1 %
Rated voltage (V_{mpp})	32,6 V	33,2 V
Rated current (I_{mpp})	9,19 A	9,31 A
Open circuit voltage (V_{oc})	39,9 V	40,3 V
Short circuit current (I_{sc})	9,77 A	9,88 A
Power output tolerance	0 / +5W	
Maximum system voltage	1000 V DC	
Reverse current load	20 A	
NOCT	45 ± 2°C	
Connectors	MC4 / MC4 compatible	
Application class	Classe II	
Voltage temperature coefficient (μV_{oc})	-0,29 %/°C	
Current temperature coefficient (μI_{sc})	0,05 %/°C	
Power temperature coefficient (μP_{mpp})	-0,39 %/°C	

Power measurement tolerance : +/- 3%

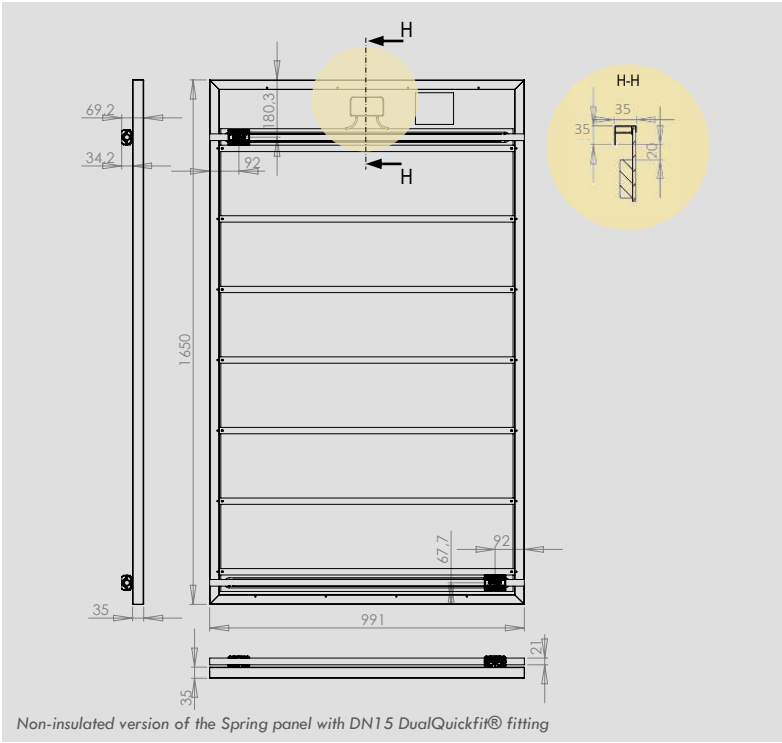

Non-insulated version of the Spring panel with DN15 DualQuickfit® fitting

THERMAL DATA			
Gross area	1,635 m²		
Volume of heat transfer liquid	5 L		
Maximum operating pressure	1,5 bar		
Pressure loss per panel (Pa | *mmWS*)	Portrait	Landscape	
	59 | *6*	167 | *17*	at 32 L/h
	461 | *47*	961 | *98*	at 100 L/h
Hydraulic input/output	DualQuickfit® fittings		
	Non-Insulated	Insulated	
Maximum temperature	70 °C	75,6 °C	
Optical efficiency a_0	58,9 % *	58,2 % *	
Heat loss coefficient a_1	16,0 W/K/m² *	10,8 W/K/m² *	
Heat loss coefficient a_2	0 W/(m²,K²) *		

* The a_0, a_1 et a_2 coefficients are the measured values from testing during EN 9806:2017 certification at KIWA for unglazed collectors with a **windspeed u = 1m/s : $a_0 = n_0 - c_6{}^*u'$; $a_1 = c_1 + c_3{}^*u'$; $u' = u - 3$.**

Power output as a function of the temperature of the water in the panel (by application)

Power values are calculated using a0 and a1 coefficients (windspeed=1m/s) in STC conditions (Text = 25°C, G = 1000 W/m²)

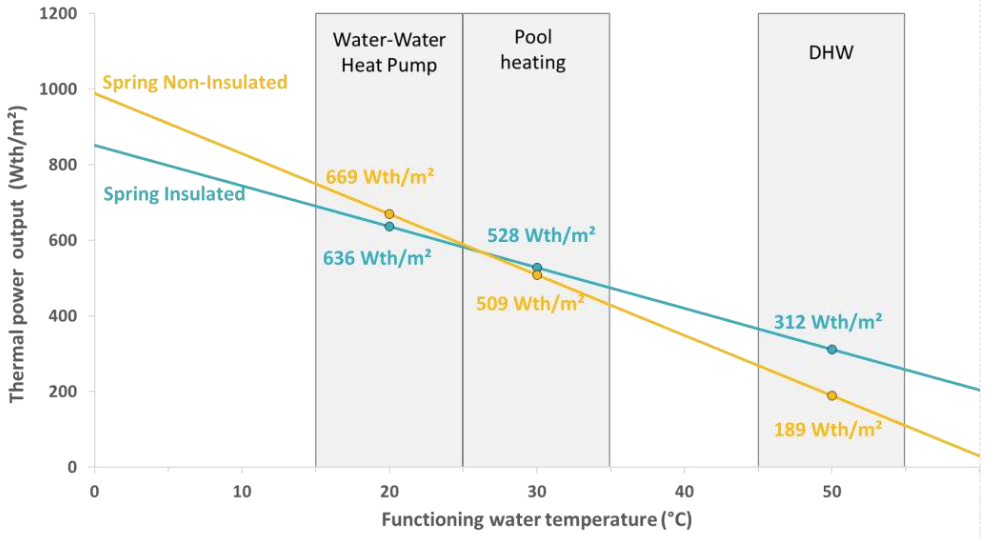

www.dualsun.com
contact@dualsun.com
2 rue Marc Donadille - 13013 Marseille - France

Date tehnice B58

Colector solar	**B58-10**	**B58-12**	**B58-15**	**B58-18**
Număr de tuburi	10	12	15	18
Lățime (mm)	960	1120	1360	1600
Înălțime (mm)	2000	2000	2000	2000
Suprafața totală (m^2)	1.85	2.07	2.54	3.32
Suprafața zonei de deschidere (m^2)	0.94	1.28	1.41	1.70
Suprafața zonei de absorbție (m^2)	0.8	0.96	1.2	1.46
Capacitatea colectorului (l)	1.0	1.2	1.5	1.8
Greutatea (kg)	36	43	50	63

Colector solar	**B58-20**	**B58-22**	**B58-24**	**B58-25**
Numărde tuburi	20	22	24	25
Lățime (mm)	1760	1920	2080	2160
Înălțime (mm)	2000	2000	2000	2000
Suprafața totală (m^2)	3.32	3.76	3.98	.11
Suprafața zonei de deschidere (m^2)	1.88	2.07	2.25	2.35
Suprafața zonei de absorbție (m^2)	1.6	1.79	1.2	2.0
Capacitatea colectorului (l)	2.0	2.2	2.4	2.5
Greutatea (kg)	72	79	89	92

Colector solar	**B58-30**
Numărde tuburi	30
Lățime (mm)	2560
Înălțime (mm)	2000
Suprafața totală (m^2)	5.05
Suprafața zonei de deschidere (m^2)	2.80
Suprafața zonei de absorbție (m^2)	2.40
Capacitatea colectorului (l)	3.0
Greutatea (kg)	110

Rama	Oțel inoxidabil	Conexiune la tub	Cupru de 22 mm
Colectorul solar	Al/Cu/Sticlă	Presiune maximă de operare	6 bari
Izolarea	Vată minerală bazaltică		

Presiunea maximă de operare: 8 bari

Căderea de presiune la 100 l/oră: 78 Pa

Încărcarea cu zăpadă și rezistența la vânt:
Încărcarea cu zăpadă este de 2400 Pa, conform EN 12975.
Rezistența la vânt este de 130 km/h.
Rezistența la grindină: până la bucăți cu diametrul de 25 mm.
Unghiul de înclinare: minimum 20°, maximum 90°.

Bibliography

[1] Curtea de Conturi Europeană, "Raportul special nr. 8/2019: Energia eoliană și solară pentru producerea de energie electrică", 2020. DOI: 10.2865/343610. [Online]. Available: eca.europa.eu.

[2] Agenția Europeană de Mediu. (2017). Eea greenhouse gas – data viewer, [Online]. Available: https://www.eea.europa.eu/data-and-maps/data/data-viewers/greenhouse-gases-viewer/ (visited on 12/10/2020).

[3] European Comission. (2019). Communication from the commission to the european parliament, the council, the european economic and social committee and the committee of the regions -a policy framework for climate and energy in the period from 2020 to 2030, [Online]. Available: http://publications.europa.eu/resource/cellar/88484dd0-8947-11e3-9b7d-01aa75ed71a1.0001.04/DOC_1 (visited on 12/10/2020).

[4] E. Comission. (2019). Communication from the commission to the european parliament, the council, the european economic and social committee and the committee of the regions a roadmap for moving to a competitive low carbon economy in 2050, [Online]. Available: http://publications.europa.eu/resource/cellar/5db26ecc-ba4e-4de2-ae08-dba649109d18.0002.02/DOC_1 (visited on 12/15/2020).

[5] IThe European Renewable Energy Council, *Renewable Energy in Europe, 2nd Ed.* EarthScan, 2015.

[6] W. Weiss and M. Spork-Dur, "Solar heat worldwide - global market development and trends in 2019 | detailed market figures 2018", 2020. [Online]. Available: https://www.iea-shc.org/solar-heat-worldwide-2020.

[7] W. Poortinga, S. Fisher, G. Bohm, L. Steg, L. Whitmarsh, and C. Ogunbode, *European attitudes to climate change and energy: Topline results from Round 8 of the European Social Survey*, English, ser. ESS Topline Results Series. University of London, 2018.

[8] International Renewable Energy Agency, "Renewable power generation costs in 2019", 2020. [Online]. Available: https://www.irena.org/publications/2020/Jun/Renewable-Power-Costs-in-2019.

[9] Solar Power Europe, "Eu market outlook for solar power 2019-2023", 2019. [Online]. Available: https://www.solarpowereurope.org/eu-market-outlook-for-solar-power-2019-2023.

[10] O. Isabella, A. Smets, R. Van Swaaij, M. Zeman, and J. Klaus, *Solar Energy - Fundamentals, Technology, and Systems*. Delft University of Technology, 2014.

[11] E. Radziemska, "Performance Analysis of a Photovoltaic-Thermal Integrated System", *International Journal of Photoenergy*, vol. 2009, R. N. Bhattacharya, Ed., p. 732 093, 2009, ISSN: 1110-662X. DOI: 10.1155/2009/732093. [Online]. Available: https://doi.org/10.1155/2009/732093.

[12] S. Dubey, J. N. Sarvaiya, and B. Seshadri, "Temperature dependent photovoltaic (pv) efficiency and its effect on pv production in the world – a review", *Energy Procedia*, vol. 33, pp. 311 –321, 2013, PV Asia Pacific Conference 2012, ISSN: 1876-6102. DOI: https://doi.org/10.1016/j.egypro.2013.05.072. [Online]. Available: http://www.sciencedirect.com/science/article/pii/S1876610213000829.

[13] L. Florschuetz, "Extension of the hottel-whillier model to the analysis of combined photovoltaic/thermal flat plate collectors", *Solar Energy*, vol. 22, no. 4, pp. 361 –366, 1979, ISSN: 0038-092X. DOI: https://doi.org/10.1016/0038-092X(79)90190-7. [Online]. Available: http://www.sciencedirect.com/science/article/pii/0038092X79901907.

[14] J. K. Kaldellis, M. Kapsali, and K. A. Kavadias, "Temperature and wind speed impact on the efficiency of pv installations. experience obtained from outdoor measurements in greece", *Renewable Energy*, vol. 66, pp. 612 –624, 2014.

[15] P. Singh and N. Ravindra, "Temperature dependence of solar cell performance - an analysis", *Solar Energy Materials and Solar Cells*, vol. 101, pp. 36 –45, 2012, ISSN: 0927-0248. DOI: https://doi.org/10.1016/j.solmat.2012.02.019. [Online]. Available: http://www.sciencedirect.com/science/article/pii/S0927024812000931.

[16] S. Chander, A. Purohit, A. Sharma, S. Nehra, and M. Dhaka, "Impact of temperature on performance of series and parallel connected mono-crystalline silicon solar cells", *Energy Reports*, vol. 1, pp. 175 –180, 2015, ISSN: 2352-4847. DOI: https://doi.org/10.1016/j.egyr.2015.09.001. [Online]. Available: http://www.sciencedirect.com/science/article/pii/S2352484715000293.

[17] E. Radziemska, "The effect of temperature on the power drop in crystalline silicon solar cells", *Renewable Energy*, vol. 28, no. 1, pp. 1 –12, 2003, ISSN: 0960-1481. DOI: https://doi.org/10.1016/S0960-1481(02)00015-0. [Online]. Available: http://www.sciencedirect.com/science/article/pii/S0960148102000150.

[18] D. Meneses-Rodriguez, P. P. Horley, J. Gonzalez-Hernández, Y. V. Vorobiev, and P. N. Gorley, "Photovoltaic solar cells performance at elevated temperatures", *Solar Energy*, vol. 78, no. 2, pp. 243 –250, 2005, ISES Solar World Congress 2003.

[19] P. Dash and N. Gupta, "Effect of temperature on power output from different commercially available photovoltaic modules", *Int. Journal of Engineering Research and Applications*, 2015.

[20] K. Ray and J. Lienhard, "Photovoltaic cell efficiency at elevated temperatures", 2010.

[21] R. Pierret and G. Neudeck, *Advanced Semiconductor Fundamentals, Volume VI of Modular Series on Solid State Devices*. Pearson Education, 1982.

[22] S. Kurtz, U. Packard, K. Berger, K. Kato, T. Friesen, H. Liu, and M. Van Iseghem, "Performance and reliability of photovoltcaic systems–subtask 3.2: Review of failures of photovoltaic modules", International Energy Agency (IEA), Photovoltaic Power Systems Programme, Technical report, 2014.

[23] L. El Chaar, L. lamont, and N. El Zein, "Review of photovoltaic technologies", *Renewable and Sustainable Energy Reviews*, vol. 15, no. 5, pp. 2165 –2175, 2011,

ISSN: 1364-0321. DOI: https://doi.org/10.1016/j.rser.2011.01.004. [Online]. Available: http://www.sciencedirect.com/science/article/pii/S1364032111000050.

[24] BRE National Solar Centre, "Evidence gathering – low carbon heating technologies - hybrid solar photovoltaic thermal panels", Delta-ee, 2016.

[25] J. Duffie and W. Beckman, *Solar Engineering of Thermal Processes*. Wiley, 2006.

[26] M. Lämmle, "Thermal management of pvt collectors - development and modelling of highly efficient glazed, flat plate pvt collectors with low-emissivity coatings and overheating protection", PhD thesis, Fraunhofer Institute for Solar Energy Systems ISE, 2018. [Online]. Available: https://www.researchgate.net/publication/327882787.

[27] R. Daghigh, M. Ruslan, and K. Sopian, "Advances in liquid based photovoltaic/thermal (pv/t) collectors", *Renewable and Sustainable Energy Reviews*, vol. 15, no. 8, pp. 4156–4170, 2011, ISSN: 1364-0321. DOI: https://doi.org/10.1016/j.rser.2011.07.028. [Online]. Available: http://www.sciencedirect.com/science/article/pii/S1364032111002681.

[28] N. Aste, C. del Pero, and F. Leonforte, "Water flat plate PV-thermal collectors: A review", *Solar Energy*, vol. 102, pp. 98–115, 2014, ISSN: 0038092X. DOI: 10.1016/j.solener.2014.01.025.

[29] S Vorrath. (2017). Reneweconomy- anu team cracks solar thermal efficiency of 97% – a world record., [Online]. Available: http://reneweconomy.com.au/anu-team-cracks-solar-thermal-efficiency-of-97-a-world-record-34199/ (visited on 10/29/2020).

[30] W. Weiss, M. Spörk-Dür, and F. Mauthner, "Solar heat worldwide. iea solar heating and cooling programme", IEA, AEE - Institute for Sustainable Technologies, 2017. [Online]. Available: http://www.iea-shc.org/data/sites/1/publications/Solar-Heat-Worldwide-2017.pdf.

[31] I. Guarracino, "Hybrid photovoltaic-thermal solar systems for combined heating", PhD thesis, Imperial College London, 2017. DOI: 10.1016/j.enconman.2017.03.024.

[32] T. Sathe and A. Dhoble, "A review on recent advancements in photovoltaic thermal techniques", *Renewable and Sustainable Energy Reviews*, vol. 76, pp. 645 –672, Sep. 2017. DOI: 10.1016/j.rser.2017.03.075.

[33] M. Alghoul, B. Azmi, and M. Wahab, "Review of materials for solar thermal collectors", *Anti-Corrosion Methods and Materials*, vol. 52, pp. 199–206, Aug. 2005. DOI: 10.1108/00035590510603210.

[34] IEA Solar Heating and Cooling Technology Collaboration Programme, "Existing pvt systems and solutions", International Energy Agency, SHC Task 60/Report A1, 2020.

[35] Fraunhofer Institute for Solar Energy Systems, "Photovoltaics report", Fraunhofer Institute, 2020. [Online]. Available: https://www.ise.fraunhofer.de/content/dam/ise/de/documents/publications/studies/Photovoltaics-Report.pdf.

[36] NREL. (2020). Best research-cell efficiency chart, [Online]. Available: https://www.nrel.gov/pv/cell-efficiency.html (visited on 10/29/2020).

[37] Our World in Data. (2020). Installed solar energy capacity - cumulative installed solar capacity, measured in gigawatts (gw)., [Online]. Available: https://ourworldindata.org/grapher/installed-solar-pv-capacity (visited on 10/29/2020).

[38] H. Zondag, "Flat-plate pv-thermal collectors and systems: A review", *Renewable and Sustainable Energy Reviews*, vol. 12, no. 4, pp. 891 –959, 2008, ISSN: 1364-0321. DOI: https://doi.org/10.1016/j.rser.2005.12.012. [Online]. Available: http://www.sciencedirect.com/science/article/pii/S1364032107000020.

[39] S. H. Euh, J.-B. Lee, Y. Choi, and D.-H. Kim, "The performance and efficiency analysis of a pvt system compared with a pv module and a solar collector", *Journal of the Korean Solar Energy Society*, vol. 32, Apr. 2012. DOI: 10.7836/kses.2012.32.2.001.

[40] A. Ramos, I. Guarracino, and A. Mellor, "Solar-thermal and hybrid photovoltaic-thermal systems for renewable heating", Imperial College, London, UK, Grantham Institute Briefing paper No 22, 2017.

[41] S. Nižetić, D. Čoko, A. Yadav, and F. Grubišić-Čabo, "Water spray cooling technique applied on a photovoltaic panel: The performance response", *Energy Conversion and Management*, vol. 108, pp. 287 –296, 2016, ISSN: 0196-8904. DOI: https://doi.org/10.1016/j.enconman.2015.10.079. [Online]. Available: http://www.sciencedirect.com/science/article/pii/S0196890415010018.

[42] M. Herrando and C. N. Markides, "Hybrid pv and solar-thermal systems for domestic heat and power provision in the uk: Techno-economic considerations", *Applied Energy*, vol. 161, pp. 512 –532, 2016, ISSN: 0306-2619. DOI: https://doi.org/10.1016/j.apenergy.2015.09.025. [Online]. Available: http://www.sciencedirect.com/science/article/pii/S0306261915010958.

[43] M. Herrando, C. N. Markides, and K. Hellgardt, "A uk-based assessment of hybrid pv and solar-thermal systems for domestic heating and power: System performance", *Applied Energy*, vol. 122, pp. 288 –309, 2014, ISSN: 0306-2619. DOI: https://doi.org/10.1016/j.apenergy.2014.01.061. [Online]. Available: http://www.sciencedirect.com/science/article/pii/S0306261914000907.

[44] I. Guarracino, A. Mellor, N. J. Ekins-Daukes, and C. N. Markides, "Dynamic coupled thermal-and-electrical modelling of sheet-and-tube hybrid photovoltaic/thermal (PVT) collectors", *Applied Thermal Engineering*, vol. 101, pp. 778–795, 2016, ISSN: 13594311. DOI: 10.1016/j.applthermaleng.2016.02.056.

[45] C. Lamnatou and D. Chemisana, "Photovoltaic/thermal (pvt) systems: A review with emphasis on environmental issues", *Renewable Energy*, vol. 105, pp. 270 –287, 2017, ISSN: 0960-1481. DOI: https://doi.org/10.1016/j.renene.2016.12.009. [Online]. Available: http://www.sciencedirect.com/science/article/pii/S0960148116310588.

[46] E. C. Kern Jr. and M. C. Russell, "Combined photovoltaic and thermal hybrid collector systems", *Photovoltaic Specialists Conference, 13th, Washington, D.C., June 5-8*, Jan. 1978. [Online]. Available: https://www.osti.gov/biblio/6352146.

[47] A. Ibrahim, M. Othman, M. Ruslan, M. Alghoul, M. Yahya, and Zaharim, "Performance of photovoltaic thermal collector (pvt) with different absorbers design", *WSEAS Transactions on Environment and Development*, vol. 5, Mar. 2009.

[48] N. Aste, F. Leonforte, and C. Del Pero, "Design, modeling and performance monitoring of a photovoltaic-thermal (PVT) water collector", *Solar Energy*, vol. 112, pp. 85–99, 2015, ISSN: 0038092X. DOI: 10.1016/j.solener.2014.11.025.

[49] M. Hermann, K. Lunz, H. Keyl, L. Koch, and G. Stryi-Hipp, *Fluid flow investigations of bionic absorbers made from aluminum and steel*. EuroSun 2010 Conference 28 September - 1 October 2010.

[50] H. Zhiwei, Y. Hwang, V. Aute, and R. Radermacher, *Review of Fractal Heat Exchangers Review of Fractal Heat Exchangers*. International Refrigeration and Air Conditioning Conference 2016.

[51] Z. Huang, Y. Hwang, and R. Radermacher, "Review of nature-inspired heat exchanger technology", *International Journal of Refrigeration*, vol. 78, pp. 1 –17, 2017, ISSN: 0140-7007. DOI: https://doi.org/10.1016/j.ijrefrig.2017.03.006. [Online]. Available: http://www.sciencedirect.com/science/article/pii/S0140700717301019.

[52] K. Yaji, T. Yamada, S. Kubo, K. Izui, and S. Nishiwaki, "A topology optimization method for a coupled thermal–fluid problem using level set boundary expressions", *International Journal of Heat and Mass Transfer*, vol. 81, pp. 878 –888, 2015, ISSN: 0017-9310. DOI: https://doi.org/10.1016/j.ijheatmasstransfer.2014.11.005. [Online]. Available: http://www.sciencedirect.com/science/article/pii/S0017931014009776.

[53] D. Pence, "The simplicity of fractal-like flow networks for effective heat and mass transport", *Experimental Thermal and Fluid Science*, vol. 34, no. 4, pp. 474 –486, 2010, ECI International Conference on Heat Transfer and Fluid Flow in Microscale, ISSN: 0894-1777. DOI: https://doi.org/10.1016/j.expthermflusci.2009.02.004. [Online]. Available: http://www.sciencedirect.com/science/article/pii/S0894177709000338.

[54] E. Comission. (2020). Internal market, industry, entrepreneurship and smes, [Online]. Available: https://ec.europa.eu/growth/sectors/raw-materials/specific-interest/critical_en/ (visited on 10/29/2020).

[55] R. Santbergen, C. Rindt, H. Zondag, and R. van Zolingen, "Detailed analysis of the energy yield of systems with covered sheet-and-tube pvt collectors", *Solar Energy*, vol. 84, no. 5, pp. 867 –878, 2010, ISSN: 0038-092X. DOI: https://doi.org/10.1016/j.solener.2010.02.014. [Online]. Available: http://www.sciencedirect.com/science/article/pii/S0038092X10001015.

[56] P. Charalambous, S. Kalogirou, G. Maidment, and K. Yiakoumetti, "Optimization of the photovoltaic thermal (pv/t) collector absorber", *Solar Energy*, vol. 85, no. 5, pp. 871 –880, 2011, ISSN: 0038-092X. DOI: https://doi.org/10.1016/j.solener.2011.02.003. [Online]. Available: http://www.sciencedirect.com/science/article/pii/S0038092X11000314.

[57] P. Dupeyrat, C. Ménézo, M. Rommel, and H.-M. Henning, "Efficient single glazed flat plate photovoltaic–thermal hybrid collector for domestic hot water system", *Solar Energy*, vol. 85, no. 7, pp. 1457 –1468, 2011, ISSN: 0038-092X. DOI: https://doi.org/10.1016/j.solener.2011.04.002. [Online]. Available: http://www.sciencedirect.com/science/article/pii/S0038092X11001125.

[58] I. Singh, D. Singh, and M. Singh, "Thermal modeling and performance evaluation of photovoltaic thermal (pv/t) systems: A parametric study", *International Journal of Green Energy*, vol. 16, pp. 1–7, Mar. 2019. DOI: 10.1080/15435075.2019.1584103.

[59] T. T. Chow, "Performance analysis of photovoltaic-thermal collector by explicit dynamic model", *Solar Energy*, vol. 75, pp. 143–152, 2003, ISSN: 0038092X. DOI: 10.1016/j.solener.2003.07.001.

[60] O. Rejeb, H. Dhaou, and A. Jemni, "Parameters effect analysis of a photovoltaic thermal collector: Case study for climatic conditions of Monastir, Tunisia", *Energy Conversion and Management*, vol. 89, no. February 2019, pp. 409–419, 2015, ISSN: 01968904. DOI: 10.1016/j.enconman.2014.10.018. [Online]. Available: http://dx.doi.org/10.1016/j.enconman.2014.10.018.

[61] T. Ma, J. Zhao, and Z. Li, "Mathematical modelling and sensitivity analysis of solar photovoltaic panel integrated with phase change material", *Applied Energy*, vol. 228, pp. 1147 –1158, 2018, ISSN: 0306-2619. DOI: https://doi.org/10.1016/

j.apenergy.2018.06.145. [Online]. Available: http://www.sciencedirect.com/science/article/pii/S0306261918310158.

[62] S. Kallio and M. Siroux, "Energy analysis and exergy optimization of photovoltaic-thermal collector", *Energies*, vol. 13, Oct. 2020. DOI: 10.3390/en13195106.

[63] P. Ijumba and A. Sebitosi, "Evaluating the impact of consumer behaviour on the performance of domestic solar water heating systems in south africa", *Journal of Energy in Southern Africa*, vol. 21, pp. 25–34, Feb. 2010. DOI: 10.17159/2413-3051/2010/v21i1a3247.

[64] A. Arsalis and A. N. Alexandrou, "Parametric study and cost analysis of a solar-heating-and-cooling system for detached single-family households in hot climates", *Solar Energy*, vol. 117, pp. 59 –73, 2015, ISSN: 0038-092X. DOI: https://doi.org/10.1016/j.solener.2015.04.024. [Online]. Available: http://www.sciencedirect.com/science/article/pii/S0038092X15002121.

[65] L. Nhut, W. Raza, and Y. Park, "A parametric study of a solar-assisted house heating system with a seasonal underground thermal energy storage tank", *Sustainability*, vol. 12, p. 8686, Oct. 2020. DOI: 10.3390/su12208686.

[66] S. Tzinnis, E. Bellos, and C. Tzivanidis, *Parametric Analysis of a Solar Cooling System Designed for Athens Climate*. IConference: EinB2016 – 5th International Conference "ENERGY in BUILDINGS 2016.

[67] K. R. Khalilpour and A. Vassallo, "Technoeconomic parametric analysis of pv-battery systems", *Renewable Energy*, vol. 97, pp. 757 –768, 2016, ISSN: 0960-1481. DOI: https://doi.org/10.1016/j.renene.2016.06.010. [Online]. Available: http://www.sciencedirect.com/science/article/pii/S0960148116305225.

[68] N. T. Raj, S. Iniyan, and R. Goic, "A review of renewable energy based cogeneration technologies", *Renewable and Sustainable Energy Reviews*, vol. 15, no. 8, pp. 3640 –3648, 2011, ISSN: 1364-0321. DOI: https://doi.org/10.1016/j.rser.2011.06.003. [Online]. Available: http://www.sciencedirect.com/science/article/pii/S1364032111002346.

[69] M. E. A. Slimani, M. Amirat, I. Kurucz, S. Bahria, A. Hamidat, and W. B. Chaouch, "A detailed thermal-electrical model of three photovoltaic/thermal (pv/t) hybrid air collectors and photovoltaic (pv) module: Comparative study under algiers climatic conditions", *Energy Conversion and Management*, vol. 133, pp. 458 –476, 2017, ISSN: 0196-8904. DOI: https://doi.org/10.1016/j.enconman.2016.10.066. [Online]. Available: http://www.sciencedirect.com/science/article/pii/S0196890416309487.

[70] H. Onovwiona and V. Ugursal, "Residential cogeneration systems: Review of the current technology", *Renewable and Sustainable Energy Reviews*, vol. 10, no. 5, pp. 389 –431, 2006, ISSN: 1364-0321. DOI: https://doi.org/10.1016/j.rser.2004.07.005. [Online]. Available: http://www.sciencedirect.com/science/article/pii/S1364032104001340.

[71] C. Good, J. Chen, Y. Dai, and A. G. Hestnes, "Hybrid photovoltaic-thermal systems in buildings – a review", *Energy Procedia*, vol. 70, pp. 683 –690, 2015, International Conference on Solar Heating and Cooling for Buildings and Industry, SHC 2014, ISSN: 1876-6102. DOI: https://doi.org/10.1016/j.egypro.2015.02.176. [Online]. Available: http://www.sciencedirect.com/science/article/pii/S1876610215002982.

[72] L. Brottier, "Optimisation biénergie d'un panneau solaire multifonctionnel : Du capteur aux installations in situ", PhD thesis, Université Paris-Saclay, 2019.

[73] M. Debbarma, K. Sudhakar, and P. Baredar, "Comparison of bipv and bipvt: A review", *Resource-Efficient Technologies*, vol. 3, no. 3, pp. 263 –271, 2017, ISSN: 2405-6537. DOI: https://doi.org/10.1016/j.reffit.2016.11.013. [Online]. Available: http://www.sciencedirect.com/science/article/pii/S240565371630207X.

[74] J.-H. Kim, S.-H. Park, J.-G. Kang, and J.-T. Kim, "Experimental performance of heating system with building-integrated pvt (bipvt) collector", *Energy Procedia*, vol. 48, pp. 1374 –1384, 2014, Proceedings of the 2nd International Conference on Solar Heating and Cooling for Buildings and Industry (SHC 2013), ISSN: 1876-6102. DOI: https://doi.org/10.1016/j.egypro.2014.02.155. [Online]. Available: http://www.sciencedirect.com/science/article/pii/S1876610214004172.

[75] H. Zhang, C. Dai, K. Cheng, Y. Lei, and Y. Yang, "Research hotspots and evolution of energy prosumer: A literature review and bibliometric analysis", *Mathematical Problems in Engineering*, 2020, International Conference on Solar Heating and Cooling for Buildings and Industry, SHC 2014. DOI: https://doi.org/10.1155/2020/5703101.

[76] R. Kamel, A. Fung, and P. Dash, "Solar systems and their integration with heat pumps: A review", *Energy and Buildings*, vol. 87, pp. 395–412, Jan. 2015. DOI: 10.1016/j.enbuild.2014.11.030.

[77] G. Xu, S. Deng, X. Zhang, L. Yang, and Y. Zhang, "Simulation of a photovoltaic/thermal heat pump system having a modified collector/evaporator", *Solar Energy*, vol. 83, no. 11, pp. 1967 –1976, 2009, ISSN: 0038-092X. DOI: https://doi.org/10.1016/j.solener.2009.07.008. [Online]. Available: http://www.sciencedirect.com/science/article/pii/S0038092X09001765.

[78] N. Sommerfeldt and H. Madani, "Review of solar pv/thermal plus ground source heat pump systems for european multi-family houses", Jan. 2016, pp. 1–12. DOI: 10.18086/eurosun.2016.08.15.

[79] J. Salpakari and P. Lund, "Optimal and rule-based control strategies for energy flexibility in buildings with pv", *Applied Energy*, vol. 161, pp. 425 –436, 2016, ISSN: 0306-2619. DOI: https://doi.org/10.1016/j.apenergy.2015.10.036. [Online]. Available: http://www.sciencedirect.com/science/article/pii/S0306261915012635.

[80] J. Freeman, I. Guarracino, S. Kalogirou, and C. Markides, "A small-scale solar organic rankine cycle combined heat and power system with integrated thermal energy storage", *Applied Thermal Engineering*, vol. 127, pp. 1543 –1554, 2017, ISSN: 1359-4311. DOI: https://doi.org/10.1016/j.applthermaleng.2017.07.163. [Online]. Available: http://www.sciencedirect.com/science/article/pii/S1359431117348287.

[81] H. Pierrick, M. Christophe, G. Leon, and D. Patrick, "Dynamic numerical model of a high efficiency PV-T collector integrated into a domestic hot water system", *Solar Energy*, vol. 111, pp. 68–81, 2015, ISSN: 0038092X. DOI: 10.1016/j.solener.2014.10.031.

[82] S. Armstrong and W. G. Hurley, "A thermal model for photovoltaic panels under varying atmospheric conditions", *Applied Thermal Engineering*, vol. 30, no. 11-12, pp. 1488–1495, 2010, ISSN: 13594311. DOI: 10.1016/j.applthermaleng.2010.03.012. [Online]. Available: http://dx.doi.org/10.1016/j.applthermaleng.2010.03.012.

[83] K. Touafek, A. Khelifa, and M. Adouane, "Theoretical and experimental study of sheet and tubes hybrid PVT collector", *Energy Conversion and Management*, vol. 80, pp. 71–77, 2014, ISSN: 01968904. DOI: 10.1016/j.enconman.2014.01.021. [Online]. Available: http://dx.doi.org/10.1016/j.enconman.2014.01.021.

[84] K. G. T. Hollands, T. E. Unny, G. D. Raithby, and L. Konicek, "Free Convective Heat Transfer Across Inclined Air Layers", *Journal of Heat Transfer*, vol. 98, no. 2, p. 189, 1976, ISSN: 00221481. DOI: 10.1115/1.3450517.

[85] F. Incropera, *Fundamentals of heat and mass transfer*. John Wiley and Sons, 2011.

[86] P. Bombarda, G. Di Marcoberardino, A. Lucchini, S. Leva, G. Manzolini, L. Molinaroli, F. Pedranzini, and R. Simonetti, "Thermal and electric performances of roll-bond flat plate applied to conventional PV modules for heat recovery", *Applied Thermal Engineering*, vol. 105, pp. 304–313, 2016, ISSN: 13594311. DOI: 10.1016/j.applthermaleng.2016.05.172. [Online]. Available: http://dx.doi.org/10.1016/j.applthermaleng.2016.05.172.

[87] B. Huang, T. Lin, W. Hung, and F. Sun, "Performance evaluation of solar photovoltaic/thermal systems", *Solar Energy*, vol. 70, no. 5, pp. 443–448, 2001, ISSN: 0038-092X. DOI: 10.1016/S0038-092X(00)00153-5. [Online]. Available: https://www.sciencedirect.com/science/article/pii/S0038092X00001535.

[88] T. T. Chow, "Performance analysis of photovoltaic-thermal collector by explicit dynamic model", *Solar Energy*, vol. 75, pp. 143–152, 2008, ISSN: 0038092X. DOI: 10.1016/j.solener.2003.07.001.

[89] S. Bhattarai, J. H. Oh, S. H. Euh, G. Krishna Kafle, and D. Hyun Kim, "Simulation and model validation of sheet and tube type photovoltaic thermal solar system and conventional solar collecting system in transient states", *Solar Energy Materials and Solar Cells*, vol. 103, pp. 184–193, 2012, ISSN: 09270248. DOI:

10.1016/j.solmat.2012.04.017. [Online]. Available: http://dx.doi.org/10.1016/j.solmat.2012.04.017.

[90] A. Kumar, P. Baredar, and U. Qureshi, "Historical and recent development of photovoltaic thermal (pvt) technologies", *Renewable and Sustainable Energy Reviews*, vol. 42, pp. 1428 –1436, 2015, ISSN: 1364-0321. DOI: https://doi.org/10.1016/j.rser.2014.11.044. [Online]. Available: http://www.sciencedirect.com/science/article/pii/S1364032114009757.

[91] Solar Energy Laboratory, "Version 16. input: Output—parameter reference—a transient system simulation program user's manual", University of Wisconsin, Madison, U.S.A, 2006.

[92] U. Jordan and K. Vajen, "Dhwcalc: Program to generate domestic hot water profiles with statistical means for user defined conditions", *Proc. ISES Solar World Congress, Orlando (US)*, Jan. 2005.

[93] N. Pflugradt and U. Muntwyler, "Synthesizing residential load profiles using behavior simulation", *Energy Procedia*, vol. 122, pp. 655 –660, 2017, CISBAT 2017 International ConferenceFuture Buildings & Districts – Energy Efficiency from Nano to Urban Scale, ISSN: 1876-6102. DOI: https://doi.org/10.1016/j.egypro.2017.07.365. [Online]. Available: http://www.sciencedirect.com/science/article/pii/S1876610217329697.

[94] N. Kelly, A. Samuel, and P. Tuohy, "The effect of hot water use patterns on heating load and demand shifting opportunities", *Proceedings of BS2015*, vol. 122, pp. 655 –660, 2015, 14th Conference of International Building Performance Simulation Association, Hyderabad, India, Dec. 7-9, 2015.

[95] A. Tiwari and M. Sodha, "Performance evaluation of hybrid pv/thermal water/air heating system: A parametric study", *Renewable Energy*, vol. 31, no. 15, pp. 2460–2474, 2006, ISSN: 0960-1481. DOI: https://doi.org/10.1016/j.renene.2005.12.002. [Online]. Available: https://www.sciencedirect.com/science/article/pii/S0960148105003575.

[96] M. Alobaid, B. Hughes, D. O'Connor, J. K. Calautit, and A. Heyes, "Improving thermal and electrical efficiency in photovoltaic thermal systems for sustainable cooling system integration", *Journal of Sustainable Development of Energy, Water*

and Environment Systems, vol. 6, pp. 305–322, Jun. 2018. DOI: 10.13044/j.sdewes.d5.0187.

[97] Solar Energy Laboratory, "Trnsys 17 - a transient system simulation program - volume 4 mathematical reference", University of Wisconsin, Madison, U.S.A, 2014.

[98] C. Agudelo-Vera, S. Avvedimento, J. Boxall, E. Creaco, H. Kater, A. Di Nardo, A. Djukic, I. Douterelo, K. Fish, P. Rey, N. Jacimovic, H. Jacobs, Z. Kapelan, F. Martinez-Solano, C. Montoya-Pachongo, O. Piller, C. Quintiliani, J. Ručka, L. Tuhovčák, and E. Blokker, "Drinking water temperature around the globe: Understanding, policies, challenges and opportunities", *Water*, vol. 2020, p. 1049, Apr. 2020. DOI: 10.3390/w12041049.

[99] U. Jordan, K. Vajen, F. Physik, and F. Solar, "Realistic domestic hot-water profiles in different time scales", *IEA SHACP Task 26*, Jan. 2001.

[100] A. TANAKA, S. MURAKAWA, Y. KOSHIKAWA, and H. TAKATA, "Calculation of hot water supply demands and instruments capacity for the guest rooms in a city hotel", *Journal of Environmental Engineering (transactions of Aij)*, vol. 73, pp. 69–75, Jan. 2008. DOI: 10.3130/aije.73.69.

[101] A. Souza, F. Aristone, I. Sabbah, D. Da, S. Santos, A. Paola, S. Lima, and G. Lima, "Climatic variations and consumption of urban water", *Atmospheric and Climate Sciences*, vol. 5, pp. 292–301, Aug. 2015. DOI: 10.4236/acs.2015.53022.

[102] S. Becken, "Water equity – contrasting tourism water use with that of the local community", *Water Resources and Industry*, vol. 7-8, pp. 9–22, 2014, ISSN: 2212-3717. DOI: https://doi.org/10.1016/j.wri.2014.09.002. [Online]. Available: https://www.sciencedirect.com/science/article/pii/S2212371714000341.

[103] T.-A. Koiv, H. Voll, and A. Hani, "Domestic hot water consumption in educational premises, apartment and office buildings", *WSEAS Transactions on Environment and Development*, vol. 6, Jan. 2010.

[104] M. Barbu, G. Darie, and M. Siroux, "Analysis of a residential photovoltaic-thermal (pvt) system in two similar climate conditions", *Energies*, vol. 12, no. 19, 2019,

ISSN: 1996-1073. [Online]. Available: https://www.mdpi.com/1996-1073/12/19/3595.

[105] Z. Wang, Z. Huang, S. Zheng, and X. Zhao, "6 - solar water heaters", in *A Comprehensive Guide to Solar Energy Systems*, T. M. Letcher and V. M. Fthenakis, Eds., Academic Press, 2018, pp. 111–125, ISBN: 978-0-12-811479-7. DOI: https://doi.org/10.1016/B978-0-12-811479-7.00006-3. [Online]. Available: https://www.sciencedirect.com/science/article/pii/B9780128114797000063.

[106] N. Balaji, D. Lai, V. Shanmugam, P. K. Basu, A. Khanna, S. Duttagupta, and A. G. Aberle, "Pathways for efficiency improvements of industrial perc silicon solar cells", *Solar Energy*, vol. 214, pp. 101–109, 2021, ISSN: 0038-092X. DOI: https://doi.org/10.1016/j.solener.2020.11.025. [Online]. Available: https://www.sciencedirect.com/science/article/pii/S0038092X20311804.

[107] T. Nualboonrueng, P. Tuenpusa, Y. Ueda, and A. Akisawa, "Field experiments of pv-thermal collectors for residential application in bangkok", *Energies*, vol. 5, no. 4, pp. 1229–1244, 2012, ISSN: 1996-1073. DOI: 10.3390/en5041229. [Online]. Available: https://www.mdpi.com/1996-1073/5/4/1229.

[108] I. E. Agency. (2018). Ea shc task 35, [Online]. Available: http://task35.iea-shc.org (visited on 10/29/2020).

[109] J. Hadorn. (2017). French pvt market is picking up, [Online]. Available: http://www.iea-shc.org/article?NewsID=205 (visited on 10/29/2020).

[110] S. IEA, *Task 60 - pvt systems: Application of pvt collectors and new solutions in hvac systems*, http://task60.iea-shc.org, 2019, (accessed: 01.09.2019).

[111] X. Fang and D. Li, "Solar photovoltaic and thermal technology and applications in china", *Renewable and Sustainable Energy Reviews*, vol. 23, pp. 330 –340, 2013, ISSN: 1364-0321. DOI: https://doi.org/10.1016/j.rser.2013.03.010. [Online]. Available: http://www.sciencedirect.com/science/article/pii/S136403211300169X.

[112] M. Barbu, R. Patrascu, G. Darie, and D Tutică, "A technical-economical analysis of the implementation of hybrid solar energy systems in small energy prosumer applications", *Quality - Access to Success*, vol. 20, pp. 134–138, 2019.

[113] IEA Solar Heating and Cooling Technology Collaboration Programme, "France country report 2018", International Energy Agency, SHC Task 60/Report A1, 2019. [Online]. Available: http://www.iea-shc.org/country-report-france.

[114] A. Resch, "2020 subsidies for pvt collectors in selected countries -shc task 60/report d6", Solar Heating and Cooling Programme - International Energy Agency, 2020. DOI: 10.18777/ieashc-task60-2020-0005. [Online]. Available: https://task60.iea-shc.org/Data/Sites/1/publications/IEA-SHC-Task60-D6-Subsidies-PVT.pdf.

[115] Statista.com. (2017). Romania: Electricity prices for households 2010-2017 | statistic, [Online]. Available: www.statista.com/statistics/418113/electricity-prices-for-households-in-romania/ (visited on 10/29/2020).

[116] ANRE, "Proiect de ordin pentru aprobarea preturilor de vanzare a energiei electrice produsa in centrale electrice din surse regenerabile cu putere electrica instalata sub 100 kw apartinand persoanelor fizice catre operatorii de distributie concesionari." autoritatea naţională de reglementare în domeniul energiei.", Bucharest, Romania, 2017.